



# **Investigating the use of bio-derived lignosulfonate admixtures in alkali activated cements**

By

Gaone Koma

Supervisors:

Professor John L. Provis

Dr. Hajime Kinoshita

A thesis submitted in total fulfilment of the requirements for the  
degree of

**Doctor of Philosophy**

Department of Materials Science and Engineering

The University of Sheffield

September 2022



## Abstract

Alkali activated cements have been successfully developed as viable alternatives to conventional Portland cement, attracting a lot of interest in both academic research and industry. This study aims to study the fresh state performance of alkali activated cements and the potential that bio-derived admixtures have in improving their properties. The main challenge faced when using these admixtures is lack of detailed understanding of their behaviour in these cements and their interactions with the precursor particles, to bring about the observed fresh state properties.

This study investigated the behaviour of lignosulfonates in aqueous solutions, increasing pH and ionic strength to determine their chemical stability. The chemical treatment of these admixtures was done with solutions that simulate the activating solution environment of the alkali activated cements. The activator plays a crucial role not only in activating the precursors but also providing an environment in which admixtures must dissolve and interact with the cement particles to induce dispersion. Therefore, it is important to understand how the admixtures behave in such chemical environments presented by alkali activated cements.

In exploring the fresh state behaviour of alkali activated cements, pastes were produced from mix designs formulated and optimised from low calcium fly ash and high calcium ground granulated blast furnace slag, activated with sodium silicate solution. It was demonstrated that an optimum dosage can be achieved for the dispersion efficiency of lignosulfonate admixtures. The effectiveness of the admixtures was determined by the type of lignosulfonate, dosage and cement system it was added to, highlighting that compatibility plays an essential role in admixture selection.

The working mechanisms of lignosulfonate admixtures in alkali activated cements were elucidated. This was achieved through zeta potential and adsorption measurement studies. It was demonstrated that lignosulfonates work primarily through electrostatic interactions, and that these interactions are greatly influenced by the chemical environment and the surface chemistry of the precursor particles.

This study established the potential of lignosulfonates for use as admixtures in alkali activated cements. The understanding gained from this study about the chemical action and stability of lignosulfonates in alkaline media, their interactions in cement systems and effect on the properties of these cements filled gaps in the literature and challenged some long-standing conclusions on these materials.

## Acknowledgements

Firstly, I would like to extend my sincerest gratitude to my supervisor, Professor John L. Provis for introducing me to the field and instilling in me a curiosity about the world of cement and concrete. I am grateful for his continued guidance and support throughout my PhD.

This work is dedicated to my mother, Marea Koma in appreciation for teaching me how to find my way in this world. I wish to thank my family, Kamogelo and Olekotse Koma, for being my light, for believing in me and trusting me to follow my own path even when it meant being away from them. To the rest of my extended family and my chosen family found in close friends, thank you.

A special thanks to Dr Sam Ghazizadeh, a friend and supervisor for his help and guidance, though a short lived team, some parts of this work would not be possible without him. A massive thank you to my colleagues, the cements team (past and present) at Sheffield for all their help in the lab, and fruitful discussions that helped in this research. I have learned a lot from all of you and am proud to have been a part of such a great team. I have found lifelong friends in some of you, and for that I am truly grateful.

I would like to acknowledge the Top Achievers Programme ran by the Botswana Government for sponsoring the entirety of my academic journey, including my PhD studies. I would like to thank the MIDAS Facility at the University of Sheffield, for providing the equipment used in this study, and the Chemical and Biological Engineering department for allowing me access to their facilities to conduct some of my experiments. Thank you to Borregaard for their generosity in supplying the admixtures.

# Contents

<b>Abstract</b> .....	I
<b>Acknowledgements</b> .....	III
<b>List of Figures</b> .....	VII
<b>List of Tables</b> .....	XIV
<b>Chapter 1 INTRODUCTION</b> .....	1
1.1 Research background .....	1
1.1 Aim and objectives.....	3
1.2 Thesis structure .....	3
<b>Chapter 2 LITERATURE REVIEW</b> .....	6
2.1 Alkali activated cements and admixtures.....	6
2.1.1 Fresh state behaviour of alkali activated cements.....	9
2.1.2 Reaction kinetic studies .....	16
2.1.3 Reaction and phase assemblage of activated FA and BFS cements .....	21
2.1.4 Mechanical properties development .....	24
2.2 Lignosulfonate admixtures.....	28
2.2.1 Structure and composition .....	28
2.2.2 Chemical action of lignosulfonates in alkaline media .....	31
2.2.3 Conformational effects of lignosulfonates in alkaline media.....	36
2.3 Interaction of admixtures with cement at the solid-liquid interface.....	39
2.3.1 Theory and background .....	39
2.3.2 Zeta potential of cements .....	44
2.3.3 Admixture adsorption behaviour in cements .....	48
2.3.4 Admixture working mechanism.....	50
2.4 Conclusions .....	54
<b>Chapter 3 MATERIALS AND EXPERIMENTAL METHODS</b> .....	56
3.1 Materials.....	56
3.1.1 Precursors.....	56
3.1.2 Activator .....	59
3.1.3 Admixtures.....	59
3.1.4 Sample preparation and mixing procedure .....	60
3.2 Analytical Techniques.....	61
3.2.1 Workability (minislump).....	62
3.2.2 Rheology .....	63
3.2.3 Isothermal Calorimetry .....	66

3.2.4	Compressive strength testing .....	68
3.2.5	Vicat setting time .....	70
3.2.6	Scanning electron microscopy .....	72
3.2.7	Thermogravimetric Analysis.....	72
3.2.8	Fourier Transform Infrared spectroscopy (FTIR) .....	72
3.2.9	Nuclear Magnetic Resonance (NMR).....	74
3.2.10	X-ray photoelectron spectroscopy (XPS).....	75
3.3	Experimental plan outline .....	77
<b>Chapter 4 CHEMICAL ACTION OF LIGNOSULFONATE ADMIXTURES IN ALKALINE MEDIA.....</b>		<b>78</b>
4.1	Introduction .....	78
4.2	Materials.....	80
4.3	Analytical techniques and procedures.....	81
4.3.1	Titration.....	82
4.3.2	Chemical treatment and characterisation .....	85
4.4	Results & Discussion .....	89
4.4.1	Titration.....	89
4.4.2	Fourier Transform Infrared Spectroscopy (FTIR) .....	96
4.4.3	<sup>13</sup> C Nuclear Magnetic Resonance spectrometry (NMR).....	104
4.4.4	X-ray photoelectron spectroscopy (XPS).....	108
4.5	Conclusions .....	121
<b>Chapter 5 THE EFFECT OF LS ADMIXTURES ON THE FRESH STATE BEHAVIOUR AND MECHANICAL PROPERTIES OF ALKALI ACTIVATED CEMENTS .....</b>		<b>123</b>
5.1	Introduction .....	123
5.2	Materials.....	124
5.3	Analytical techniques and procedures.....	124
5.4	Effect of lignosulfonates on the properties of alkali activated blast furnace slag... 125	
5.4.1	Workability .....	125
5.4.2	Rheology .....	129
5.4.3	Setting time .....	137
5.4.4	Compressive strength.....	139
5.4.5	Isothermal Calorimetry .....	143
5.4.6	The fate of lignosulfonates in alkali activated slag pastes .....	145
5.5	Effect of lignosulfonates on the properties of alkali activated fly ash .....	150
5.5.1	Workability .....	150
5.5.2	Rheology .....	153

5.5.3	Setting time .....	157
5.5.4	Compressive strength.....	160
5.5.5	Isothermal Calorimetry .....	164
5.5.6	The fate of lignosulfonates in alkali activated fly ash pastes .....	166
5.6	Conclusions .....	169
<b>Chapter 6 ALKALI ACTIVATED CEMENT - LIGNOSULFONATE ADMIXTURE INTERACTIONS.....</b>		<b>171</b>
6.1	Introduction .....	171
6.2	Materials.....	173
6.3	Analytical techniques and procedures.....	173
6.3.1	Zeta potential measurements.....	173
6.3.2	Adsorption measurements.....	175
6.4	Results & Discussion .....	180
6.4.1	Zeta potential ( $\zeta$ ) a function of pH.....	180
6.4.2	Zeta potential ( $\zeta$ ) as a function of order of addition.....	184
6.4.3	Effect of silicate ions on $\zeta$ .....	187
6.4.4	Zeta potential ( $\zeta$ ) as a function of ionic strength.....	190
6.4.5	Adsorption studies.....	194
6.5	Conclusions .....	199
<b>Chapter 7 CONCLUSIONS AND FUTURE WORK.....</b>		<b>202</b>
7.1	Conclusions .....	202
7.1.1	The chemical stability of LS in alkaline media.....	202
7.1.2	Effect of LS on the performance of alkali activated cements .....	203
7.1.3	Interaction of lignosulfonates with slag and fly ash.....	204
7.2	Future work .....	206
<b>References.....</b>		<b>208</b>

## List of Figures

Figure 2.1 Fresh state alkali activated material.....	10
Figure 2.2 Rheological models conventionally applied to the description of the shear stress – shear rate relationship of cementitious pastes. Adapted from (Malvern Instruments Limited, 2016). .....	12
Figure 2.3 Viscosity of sodium silicate solutions as a function of modulus and Na <sub>2</sub> O concentration. Used with permission of Annual Reviews, Inc, (Provis & Bernal, 2014),permission conveyed through Copyright Clearance Center, Inc.....	14
Figure 2.4 Thixotropic behaviour of alkali activated slag. Immediately after stopping mixing, the pastes underwent pre-shearing followed by cycles at 5, 10, 15, 20 and 25 minutes. Adapted from Palacios et al., 2008. ....	15
Figure 2.5 Isothermal calorimetry curves for slag metasilicate activated slag pastes, as a function of the water content. Adapted from Bernal et al., 2015. ....	17
Figure 2.6 Thermal power and cumulative hydration of cements with additions of lignosulfonate admixture. Adapted with permission (Danner et al., 2015) Copyright Elsevier 2015.....	18
Figure 2.7 Effect of admixtures on setting time of Portland cement at w/c = 0.27. Adapted with permission (Uchikawa et al., 1995) Copyright Elsevier 1995. ....	20
Figure 2.8 Alkali activation reaction route for low and high calcium precursors. Used with permission of Annual Reviews, Inc, (Provis & Bernal, 2014), permission conveyed through Copyright Clearance Center, Inc.....	23
Figure 2.9 Proposed structure of the (a) interunit linkages and (b) lignin polymer. Adapted from Ruwoldt, 2020.....	29
Figure 2.10 Sulfonation process of lignin to obtain lignosulfonate. Adapted from Eraghi Kazzaz et al., 2019. ....	30
Figure 2.11 Simplified structure of a lignosulfonate. Adapted with permission (Gelardi et al., 2015) Copyright Elsevier 2015. ....	31
Figure 2.12 Nucleophilic substitution of the methoxyl group in highly alkaline media.....	34
Figure 2.13 Reaction of the phenolic hydroxyls in (a) water and (b) sodium hydroxide. ....	35
Figure 2.14 Some of the proposed conformations of lignosulfonates in solution, (a) microgel, (b) branched polyelectrolyte, (c) oblate ellipsoid model and possible $\pi$ - $\pi$ stacking Adapted from Ruwoldt, 2020. ....	38
Figure 2.15 Schematic showing the formation of an electric double layer around a negatively charged particle suspended in an electrolyte solution. Reproduced with permission (Park & Seo, 2011) Copyright Elsevier 2011. ....	40

Figure 2.16 Potential energy as a function of distance between interacting particles. Reproduced with permission (Park & Seo, 2011) Copyright Elsevier 2011.....	41
Figure 2.17 Effect of pH on measured zeta potential values of fly ash, slag and slag cement (a Portland and BFS blend). Reproduced with permission (Nagele & Schneider, 1989) Copyright Elsevier 1989. ....	47
Figure 2.18 Adsorption isotherms of lignosulfonates of different compositions onto a MgO surface in NaOH solution. Reproduced with permission (Houst et al., 2008) Copyright Elsevier 2008. ....	49
Figure 2.19 Schematic of the electrostatic and steric repulsive forces induced by the adsorption of dispersant admixtures onto cement particle surfaces. Adapted with permission (Lei et al., 2022) Copyright Elsevier 2022. ....	51
Figure 2.20 Schematic of the adsorption of lignosulfonate on slag particles (Luukkonen et al., 2019) © <b>copyright 2019</b> Reprinted by permission of Informa UK Limited, trading as Taylor & Taylor & Francis Group.....	52
Figure 3.1 Particle size distribution of the ground granulated blast furnace slag and fly ash obtained by laser diffraction using a Malvern Mastersizer 3000.....	57
Figure 3.2 Scanning electron micrographs of (a) fly ash and (b) GGBFS.....	58
Figure 3.3 X-ray diffractograms of the starting materials fly ash and ground granulated blast furnace slag. ....	58
Figure 3.4 High speed mixing of the waterglass slag activated paste.....	61
Figure 3.5 Downscaled Abrams cone. ....	62
Figure 3.6 The upward and downward ramp of the rheology test. ....	65
Figure 3.7 Schematic of the isothermal calorimetry setup (a), examples of the alkali activated fly ash and alkali activated slag pastes after testing (b).....	67
Figure 3.8 The 300 kN Shimadzu at start of sample testing and untested and crushed samples. ....	69
Figure 3.9 3000 kN cube crusher and the test setup. ....	69
Figure 3.10 Vicat instrument and the experiment sheet showing the penetration depths over time. ....	71
Figure 3.11 Schematic of the photoemission and Auger process adapted from Wren et al., 2011.....	76
Figure 3.12 An experimental plan to achieve the main objectives of the study. ....	77
Figure 4.1 Lignosulfonate powders as received.....	80
Figure 4.2 Procedure followed for the chemical treatment and washing process of the lignosulfonates. ....	85
Figure 4.3 Schematic of the ion exchange process between the resin and the solution with lignosulfonate dissolved.....	87
Figure 4.4 The forward and backward titration curves of the DP1717 (high Mw, low sugar) sample. 90	
Figure 4.5 The forward and backward titration curves of the DP1718 (low Mw, low sugar) sample..	92

Figure 4.6 The forward and backwards titration curves of DP1765 (high Mw, high sugar) sample. ...	93
Figure 4.7 The forward and backward titration curves of the DP4426 (low Mw, high sugar) sample. 95	95
Figure 4.8 Colour change of lignosulfonates in NaOH solution (Dilling & Sarjeant, 1984).....	96
Figure 4.9 The FTIR spectra of the lignosulfonates as received; DP1717 (high Mw, low sugar), DP1718 (low Mw, low sugar), DP1765 (high Mw, high sugar) and DP4426 (low Mw, high sugar). .	98
Figure 4.10 The FTIR spectra of the DP1717 sample before and after treatment with increasing concentrations of NaOH. The same amount of resin was used to ion exchange (IE) all samples. ....	100
Figure 4.11 The FTIR spectra of the DP1717 sample before and after treatment with increasing concentrations of NaOH. The amount of resin used was varied according to the NaOH concentration. ....	101
Figure 4.12 The FTIR spectra of the DP1718 sample before and after treatment with increasing concentrations of NaOH. ....	102
Figure 4.13 The FTIR spectra of the DP4426 sample before and after treatment with increasing concentrations of NaOH. ....	103
Figure 4.14 The FTIR spectra of the DP1765 sample before and after treatment with increasing concentrations of NaOH. ....	103
Figure 4.15 Typical structural unit of a lignosulfonate polymer, where the R can be any of: H, alkyl or aryl groups. R <sup>1</sup> can also be unsubstituted. Various linkage units can be represented by varying the substitutions. Adapted from (Gierer, 1986) and (Danner et al., 2015). ....	105
Figure 4.16 <sup>13</sup> C CP MAS NMR spectra of the control samples, DP1717 and DP1718 before chemical treatment. DP1717- high Mw, low sugar, DP1718 – low Mw, low sugar. ....	106
Figure 4.17 The NMR spectra of the DP1717 sample before and after treatment with increasing concentrations of NaOH. ....	107
Figure 4.18 The NMR spectra of the DP1718 sample before and after treatment with increasing concentrations of NaOH. ....	108
Figure 4.19 Wide angle scan of the DP1717 control sample, with 3 spectra overlaid. ....	109
Figure 4.20 Wide angle scan of the DP1717 sample before and after treatment with increasing concentrations of sodium hydroxide solution. ....	110
Figure 4.21 C 1s and S 2p XPS data for the lignosulfonate DP1717 after treatment with increasing concentrations of NaOH. ....	112
Figure 4.22 Deconvoluted C 1s and S 2p spectra of the DP1717 sample, (a) control and (b) 10 M NaOH treated sample. ....	113
Figure 4.23 Wide angle XPS scans of the DP1718 sample before and after treatment with increasing concentrations of NaOH solution. ....	114

Figure 4.24 C 1s and S 2p spectra of the DP1718 sample before and after treatment with increasing concentrations of NaOH solution.....	115
Figure 4.25 Deconvoluted C 1s and S 2p spectra of the DP1718 LS sample. ....	116
Figure 4.26 Wide angle scan of the DP4426 before and after treatment with increasing concentrations of NaOH solution.....	117
Figure 4.27 C 1s and S 2p spectra of the DP4426 before and after treatment with increasing concentrations of NaOH solution.....	117
Figure 4.28 Deconvoluted C 1s and S 2p spectra for the control (left) and 10 M treated (right) samples.....	118
Figure 4.29 Wide angle XPS scans of the DP1765 sample before and after treatment with increasing NaOH concentration. ....	119
Figure 4.30 C 1s and S 2p spectra of DP1765 before and after treatment with increasing concentrations of NaOH solution.....	120
Figure 4.31 Deconvoluted C 1s and S 2p spectra of DP1765 for the control (a) and the 10 M treated (b) sample.....	121
Figure 5.1 The relative slumps of AAS pastes with additions of DP1717 (low sugar, high Mw) and DP1718 (low sugar, low Mw) lignosulfonates. Error bars represent the standard error of the mean.	126
Figure 5.2 Relative slumps of AAS paste with 0.3 and 3 wt.% additions of four types of lignosulfonates; DP1717 - high Mw, low sugar, DP1718 - low Mw, low sugar, DP1765 - high Mw, high sugar, DP4426 – low Mw, high sugar. Error bars represent the standard error of the mean. ....	127
Figure 5.3 The relative slumps of the AAS pastes when different orders of addition of LS (DP1718) were followed. Error bars represent the standard error of the mean. ....	128
Figure 5.4 The shear stress vs shear rate curves of the AAS control paste without any LS over time after stopping mixing. ....	130
Figure 5.5 Rheometric flow curve of the AAS paste with additions of LS at selected levels. ....	131
Figure 5.6 The shear stress vs shear rate curves of the AAS pastes with increasing dosages of DP1717 LS. Experimental data are the markers, and the solid lines are the model fit. ....	133
Figure 5.7 Rheological data from additions of different types of LSs at 20 minutes since stop of mixing. DP1718 – low Mw, low sugar, DP1717 – high Mw, low sugar, DP1765 – high Mw, high sugar, DP4426 – low Mw, high sugar.....	135
Figure 5.8 Rheological data when different modes of DP1718 LS addition were followed at a dosage of 0.3 wt.%. (a) DA and (b) SA as a function of time after the end of AAS paste mixing.....	136
Figure 5.9 Rheological data for the AAS + DP1718 sample without LS, DA and SA, tested 20 minutes after stopping mixing. ....	136
Figure 5.10 The initial and final setting times of the AAS pastes with increasing dosages of the low sugar, high Mw DP1717 and low sugar, low Mw DP1718. ....	138

Figure 5.11 The initial and final setting times of the AAS pastes with increasing dosages of the high Mw, high sugar DP1765 and low Mw, high sugar DP4426. ....	139
Figure 5.12 The compressive strengths of the AAS pastes after 7 and 28 days of curing at 20 °C with increasing additions of lignosulfonates. (a) DP1717 – high Mw, low sugar and (b) DP1718 – low Mw, low sugar. Error bars represent the standard error of the mean. ....	140
Figure 5.13 Compressive strengths of the AAS hardened pastes with additions of four types of lignosulfonates, measured at 7 days of curing. DP1717 – high Mw, low sugar, DP1718 – low Mw, low sugar, DP1765 – high Mw, high sugar, DP4426 – low Mw, high sugar. Error bars represent the standard error of the mean. ....	141
Figure 5.14 The cubes of the AAS pastes after 7 days of curing. (a) control, (b) LS added at 0.3 wt.% and (c) LS added at 3 wt.%. ....	142
Figure 5.15 The heat evolution for AAS pastes with the four types of lignosulfonates: (a) DP1718, (b) DP1717, (c) DP4426 and (d) DP1765. ....	145
Figure 5.16 The FTIR spectra of the AAS pastes with and without DP1718 LS additions after 7 and 28 days of curing at 20 °C. ....	147
Figure 5.17 Thermogravimetric analysis of the AAS pastes after 7 and 28 days of curing at 20 °C, with and without addition of DP1718 LS at 0.3 wt.% dosage. ....	148
Figure 5.18 The scanning electron micrographs of the AAS pastes with and without 3 wt.% addition of LS after 7 days of curing. Top row: low magnification; bottom row: higher magnification. ....	149
Figure 5.19 The relative slumps of AAFA pastes with increasing additions of DP1717 (low sugar, high Mw) and DP1718 (low sugar, low Mw) lignosulfonates. Error bars represent the standard error of the mean. ....	151
Figure 5.20 Relative slumps of AAFA with 0.3 and 3 wt.% additions of four types of lignosulfonates; DP1717- high Mw, low sugar, DP1718 - low Mw, low sugar, DP1765 - high Mw, high sugar, DP4426 - low Mw, high sugar. Error bars represent the standard error of the mean. ....	152
Figure 5.21 The shear stress vs shear rate curves of the AAFA control paste as a function of time after stopping mixing. ....	153
Figure 5.22 Rheometric flow curve of the AAFA paste with 0.3 and 3.0 wt.% additions of LS. ....	154
Figure 5.23 The shear stress vs shear rate curves of the pastes with the highest LS dosage (3 wt.% of DP1717) since stopping mixing. ....	155
Figure 5.24 The shear stress vs shear rate curves of the pastes with increasing dosage of the DP1717 LS. Experimental data are the markers, solid lines are the model fit. ....	156
Table 5.2 The Herschel-Bulkley model parameters fitted to the curves shown in Figure 5.25. ....	156
Figure 5.26 Effect of different types of lignosulfonates on the rheology of the AAFA pastes. DP1717 - low sugar, high Mw, DP1718 - low sugar, low Mw, DP1765 - high sugar, high Mw, DP4426 - high sugar, low Mw. ....	157

Figure 5.27 AAFA paste during setting time testing. ....	158
Figure 5.28 The initial and final setting times of the AAFA activated pastes with increasing dosages of the low sugar samples DP1717 (high Mw) and DP1718 (low Mw). ....	159
Figure 5.29 The initial and final setting times of AAFA pastes for the high sugar sample DP1765 (high Mw) and DP4426 (low Mw). ....	159
Figure 5.30 The 50 mm paste cubes cured for 28 days before and after compressive testing strength testing, (a) AAFA_control, (b) AAFA + 3.0 wt.% LS. ....	161
Figure 5.31 The compressive strength of AAFA hardened pastes after 7 and 28 days of curing at 20 °C. Error bars represent the standard error of the mean. ....	162
Figure 5.32 The compressive strength of AAFA pastes at (a) 7 days and (b) 28 days of curing at 20 °C. Error bars represent the standard error of the mean. ....	163
Figure 5.33 The heat evolution of AAFA pastes with addition of the four types of lignosulfonates, (a) DP1717, (b) DP4426, (c) DP1718, and (d) DP1765. ....	165
Figure 5.34 FTIR spectra of the AAFA paste after 7 and 28 days of curing with increasing additions of DP1717 LS. ....	166
Figure 5.35 The thermogravimetric analysis of the AAFA paste after (a) 7 days and (b) 28 days of curing at 20 °C, with and without DP1717 LS addition. ....	167
Figure 5.36 The scanning electron micrographs of the AAFA pastes with and without 3 wt.% additions of LS after 7 days of curing, and elemental maps corresponding to the higher-resolution image shown. ....	168
Figure 6.1 A schematic of the Ocean Optics UV-Vis setup. ....	176
Figure 6.2 UV-Vis spectra of DP1718 and DP1717 dissolved in water. ....	177
Figure 6.3 Calibration curves for (a) DP1718, (b) DP1717 and (c) DP1765. ....	178
Figure 6.4 Zeta potential profile of slag in dispersions of increasing pH adjusted by NaOH with different types of LS: DP1718 (low Mw, low sugar), DP1717 (high Mw, low sugar), DP1765 (high Mw, high sugar), DP4426 (low Mw, high sugar). ....	181
Figure 6.5 Zeta potential of fly ash in increasing pH adjusted by NaOH and with addition of the DP1765 (high Mw, high sugar) sample. ....	184
Figure 6.6 Zeta potential profiles of slag dispersions with DP1718 LS added at different stages. ....	186
Figure 6.7 Zeta potentials of slag, pH adjusted with NaOH, a constant amount of silicate (0.6 wt.% of the slag) and DP1718 LS added. ....	188
Figure 6.8 Zeta potentials of fly ash, pH adjusted with NaOH, a constant amount of silicate (0.6 wt.% of the slag) and DP1765 added. ....	189
Figure 6.9 Zeta potential of slag in NaOH + Waterglass without any LS (control), and then with the silicate loaded first, and another with the LS (DP1718) loaded before the silicate. ....	190

Figure 6.10 Zeta potential as a function of ionic strength adjusted with NaCl, and with addition of LS. .....	191
Figure 6.11 Schematic showing the effect of ionic strength on LS in solution. Adapted from (Ruwoldt et al., 2020). .....	192
Figure 6.12 Zeta potentials of LS (DP1718) as a function of increasing ionic strengths. The pink band represents the error margins. ....	193
Figure 6.13 The adsorbed amount of LS DP1717 and DP1718 onto slag in an increasing pH environment (adjusted with NaOH solution). ....	195
Figure 6.14 The adsorbed amounts of DP1718 when simultaneously added (SA) and addition is delayed (DA) in increasing pH environment. ....	196
Figure 6.15 The amount of DP1718 adsorbed when there is competitive adsorption of anionic silicates and LS admixture. The sample at pH 7 serves as a control, where the BFS was only dissolved in water without addition of NaOH solution nor silicate. ....	197
Figure 6.16 FTIR spectra of the slag solid filtrates after LS adsorption in NaOH, as a function of increasing pH. ....	198
Figure 6.17 Illustration of the working mechanism of LS added when slag is dissolved in (a) water and (b) pH 14 NaOH solution. ....	200

## List of Tables

Table 2.1 Summary of the use of admixtures in alkali activated cements.....	26
Table 3.1 Chemical composition of the precursors determined by XRF. LOI corresponds to the loss on ignition measured in air at 1000 °C . .....	56
Table 3.2 Summary of the mix ratios, defined on a mass basis.....	60
Table 4.1 Composition of the lignosulfonate powders as received. ....	80
Table 4.2 The FTIR peak assignments of the lignosulfonates as received (Boeriu et al., 2004), (Rodríguez-Lucena et al., 2009), (Yan et al., 2018). ....	98
Table 4.3 Composition of the control and 10 M NaOH treated LS samples. ....	111
Table 5.1 The Herschel-Bulkley model parameters fitted to the curves in Figure 5.6. ....	133
Table 5.2 The Herschel-Bulkley model parameters fitted to the curves shown in Figure 5.24. ....	156

# Chapter 1 INTRODUCTION

## 1.1 Research background

The current high production capacity of the cement industry globally, and its continued increase into the future as societies continue to expand their infrastructure, has given rise to a substantial contribution of approximately 8% to the world's anthropogenic carbon emissions (Miller et al., 2018). Portland cement has been used for close to two centuries with an increasing global production estimated at 4.4 billion tonnes in 2021 (Garside, 2022). Although this process has been largely optimised, the most efficient cement production is around 0.913 tonnes of CO<sub>2</sub> equivalent per tonne of cement which is still quite high (Dunster, 2020). The production and use of Portland cement have generated environmental concerns related to the quarrying of raw materials, immense energy consumption and high carbon emissions (Criado et al., 2009). The general increase in global CO<sub>2</sub> emissions from cement production has been the main driving factor towards mitigating their impact and transitioning towards more environmentally friendly alternative methods of production (Andrew, 2017).

Alkali activated materials have been successfully developed as viable alternatives; these materials utilise waste and are less energy-intensive in terms of production methods than conventional Portland cement. Wastes mainly from industrial manufacturing and mining processes are valorised through this technology to yield high performing, high mechanical strength, and durable structural materials; provided they are adequately designed and cured (Provis & van Deventer, 2014). Through this technology, the environmental impact due to the disposal of these wastes in landfills or water sources is also mitigated (Bernal et al., 2016; M. Palacios et al., 2009). This proposed alternative does not aim to completely replace Portland cement, nor does it present a one-size-fits-all alternative, but rather offers opportunities where

it can be designed to fit a specific purpose (Provis, 2018). This means designing mixtures using the right available materials, at the right time and place, and for the right application.

The future of alkali activated cement, though promising is uncertain, there is still a growing need to further improve the properties of alkali activated materials and make them more commercially competitive against Portland cement than they currently are (Provis, 2018). Great strides have been made on the material development of these materials, with limitations on the industrial processing and delivery still a matter of concern. However, further research and development of key performance areas of these materials would encourage their acceptance and uptake in the industry. One way in which their advancement can be achieved is through the use of admixtures; these are additives that enhance material properties, resulting in improved workability, rheology and setting (Puertas et al., 2005). Despite the widespread use and commercialisation of admixtures in the cement industry, there is limited research and development of admixtures specifically designed for alkali activated materials. Admixtures designed for Portland cement systems have been in use for decades, but there is limited understanding of their surface chemistry and how these admixtures work in alkali activated cement systems. This gap limits the development of new tailored admixtures to improve the properties of cement which requires the knowledge of mechanisms that govern their interactions.

The increasing awareness of environmental issues has generated interest in utilising more sustainable biomass such as lignin which has a wide range of applications; the current study drives sustainability even further by exploring the utilisation of these renewable biomass derivatives as additives in non-Portland cements. These earlier generation admixtures remain competitive in the market because of their lower cost and often good performance. This study seeks to close knowledge gaps by providing the first comprehensive assessment of various kinds of bio-derived admixtures.

## **1.1 Aim and objectives**

This study aims to evaluate the behaviour of admixtures, specifically bio-derived lignosulfonates in alkali activated cement, considering their interaction with the activator as well as the precursor during activation. The study investigates 1<sup>st</sup> generation admixtures and aims to fill the gap in the understanding of their interaction with alkali activated cements by evaluating the key elements of their performance in these systems. The research objectives are outlined as follows:

- To investigate the physical and chemical effects of highly alkaline solutions that simulate the environment presented by the activator during alkali activation on different types of lignosulfonate admixtures.
- To explore the efficacy of lignosulfonates with varying molecular weights and sugar contents when used in fly ash and ground granulated blast furnace slag activated systems, assessing the proposed working mechanisms and compatibility with the activated cement systems.
- To explore the surface chemistry of fly ash and ground granulated blast furnace slag at the interface with lignosulfonate admixtures i.e., to elucidate their working mechanisms whether electrostatic, electro-steric, or both.

## **1.2 Thesis structure**

There are 7 chapters included in this thesis. An extensive literature review on the alkali activation process, the fresh state behaviour, mechanical properties, and how these properties

are affected by the addition of admixtures is presented in Chapter 2. This chapter explores the possible interactions between cement and polymeric admixtures, and what understanding has been established on their working mechanisms by previous researchers. Lignosulfonate admixtures are evaluated in greater detail, and their stability in cement environments and dispersion efficiency is also addressed. Correlations between the structure of the admixture and their efficiency in improving the properties of the fresh state cement are drawn.

Chapter 3 provides details of the experimental plan outlined to achieve the project objectives. The characterised starting materials, mix designs and sample preparation processes are presented. A summary of the analytical techniques and equipment setup is also provided.

Chapter 4 presents a detailed description of changes or structural breakdowns that may occur due to the interaction of lignosulfonates with alkaline activating solutions, to elucidate their stability in these environments. Increasing pH and ionic strength environments are simulated to monitor these changes. The lignosulfonate samples are treated and then fully characterised using a range of analytical techniques: titration, FTIR, solid-state NMR and XPS, observing closely any changes to the main functional groups of the macromolecule.

Chapter 5 evaluates the effect of different types of lignosulfonates on low calcium fly-ash and high-calcium ground granulated blast furnace slag activated cement. The fresh state behaviour and mechanical strength paste properties of the optimised mix designs are presented and compared with pastes with increasing additions of lignosulfonate. This chapter presents results from the following studies: workability through slump tests, rheology, setting time, hydration kinetics through isothermal calorimetry and compressive strength. These analyses provide information on the effect of the presence of lignosulfonates in these systems, whether physical or chemical, positive, or adverse.

Chapter 6 assesses the interaction between the cement precursors and admixtures, exploring the surface chemistry at their interphase by zeta potential and adsorption measurements. The zeta potentials and adsorption measurements are used to examine the colloidal interactions and influence of ions in solution to elucidate the working mechanisms of the lignosulfonate admixtures. The adsorption measurements were achieved by UV-Vis spectroscopy.

Finally, Chapter 7 offers conclusions drawn from the chemical stability studies, investigations on the effect on alkali activated paste properties, and the elucidated working mechanisms for these cement systems. Work that should be considered for study in the future is highlighted.

## Chapter 2 LITERATURE REVIEW

### 2.1 Alkali activated cements and admixtures

Alkali activation technology utilises industrial waste and by products in the production of sustainable cements that are 60% less energy intensive and have up to 70% less global warming potential compared to conventional Portland cement (Puertas et al., 2014). In this process, siliceous and aluminous materials are transformed into compact cementitious binders by reaction with an alkaline activator to yield high performing products (Palomo et al., 1999). The starting materials (precursors) have varying compositions and characteristic chemistries which result in products with a range of properties; the most utilised precursors being blast furnace slag, coal fly ash, calcined clays and natural pozzolans (Bernal & Provis, 2014). An alkaline activator is required as most of these precursors show little to no cementing properties when only mixed with water, unlike Portland cement (Shi & Day, 1995). Several activating solutions have been successfully used with the most common being waterglass  $(\text{Na,K})_2 \cdot n\text{SiO}_2 \cdot m\text{H}_2\text{O}$ , alkali metal hydroxides, and alkali metal carbonates (Provis & van Deventer, 2014). The role of the alkaline activator is to induce dissolution of the precursors and facilitate processes that form an aluminosilicate binding gel made up of a three-dimensional network of aluminium and silicon atoms cross-linked by oxygen atoms, that then polymerise over time to form a compact cementitious binder (Criado et al., 2009). The main CO<sub>2</sub> savings are from the avoidance of using calcium carbonate (limestone) as a precursor and the high temperature processing of the cement constituents in a kiln required for Portland cement (Provis & Bernal, 2014). Much of the CO<sub>2</sub> emissions attributed to alkali activated cements (AACs) are associated with the alkaline activator, particularly when waterglass is used (Provis, 2018). Each precursor requires

the correct activator to yield good performance, however, limited information is available on the optimal matching of the precursor and the activator (Provis, 2018).

Alkali activated cements have been in development for over a century and gaining particular interest in Western Europe, Soviet Union and China (Provis & van Deventer, 2014). In the early 1960s, alkali activation contributed towards solving an ecological problem in providing a pathway for the use of the slag by-product (Fernández-Jiménez et al., 1999). There is evidence of industrial application of AACs used in pre-casting and in situ with large scale applications being found in areas like Australia, Russia, Ukraine, Netherlands and the UK. There are now established companies manufacturing alkali activated concrete materials or products (Rintala et al., 2021). Nonetheless, there is still much scope for a more widespread industrial application of the alkali activation technology. The differences in the precursor sources mean that the mix design protocols are often varied and difficult to standardise. The workability of the fresh state alkali activated cements has been recognised as a major challenge to their application (Provis & van Deventer, 2014). So far, the use of alkali activated cements despite this challenge is credited to the versatile mix designs that can be manipulated and adjusted to improve the workability, but often needing to be balanced against performance markers such as strength development and durability. This is, at least in part, because of the lack of availability of admixtures to control the workability and rheological properties of these cements.

Efforts into the use of established admixtures developed for Portland cement have generally seen less success in alkali activated cements (Najimi et al., 2020), (Tong et al., 2021). Examples of these admixtures include polycarboxylates (PCEs), naphthalene sulfonates, lignosulfonates, melamine based, vinyl copolymer, and others. These admixtures have been reported to show significant fluidising efficiency in Portland cement but lose these properties in alkali activated cements, which has been attributed to their lack of chemical stability in highly alkaline media (Palacios et al., 2009). However, contradictory accounts of the performance of these

admixtures have been published. Some successes have been shown with polycarboxylate based admixtures in improving the workability of slag activated cement, with some studies exploring the modification of the molecular structure of the PCEs to improve compatibility with alkali activated cements (Kashani et al., 2014). This is an added advantage of PCEs as there is flexibility in their molecular structure design and so they can be tailored for specific materials, improving compatibility (Houst et al., 2008). In contrast, other researchers have found that PCEs are not compatible with AAS showing no improvement in workability (Palacios & Puertas, 2005), (Palacios et al., 2008). Naphthalene sulfonates have been reported to be efficient at dispersing alkali activated slag pastes, which was attributed to their high structural stability in alkaline media (Palacios & Puertas, 2005), (Palacios et al., 2008). Similar success was found in fly ash activated pastes where Xie and Kayali (2016) found that naphthalene sulfonate was slightly better at improving the workability of low calcium fly ash activated cement compared to Portland cement. The other previously mentioned admixtures have generally not improved the workability of alkali activated pastes and were also detrimental to the compressive strength development (Puertas et al., 2003). The inconsistency in these results is likely due to the variation in the materials used and the testing conditions.

Understanding of the fundamental aspects of chemistry and materials science that control the formation of these alkali activated binder systems has been in development, and extensive research has been done in this area in the last couple of decades (Provis & Bernal, 2014), (Provis, 2018), (Shi et al., 2019). The current study offers a review on how far this technology has come and what remains poorly understood. Admixtures are an important component in achieving high performance concrete that has improved workability, high strength and good durability (Uchikawa et al., 1997). The impact that admixtures have on the alkali activation process and the properties achieved are presented.

### **2.1.1 Fresh state behaviour of alkali activated cements**

The fresh state behaviour of cement or concrete refers to the initial stages immediately after mixing, while the cement still flows and has not started hardening and gaining strength, as shown in Figure 2.1. This is a key part of concrete production as the final hardened product cannot be achieved if the mix is not workable at the outset. This stage also has a direct impact on the surface finishing, strength development and durability properties of the hardened product at a later stage (Banfill, 2011). Rapid loss of workability is not ideal in industrial applications as enough time must be allowed for a workable mix to be transported, cast, and placed (Yousuf et al., 1995). This is often achieved using admixtures which improve fluidity while maintaining a low water content. Admixtures are also useful in deterring unwanted defects such as segregation by controlling the yield stress and plastic viscosity and allowing rheological parameters to be adjusted to fit the requirements during industrial applications (Burgos-Montes et al., 2012).



Figure 2.1 Fresh state alkali activated material.

Fresh state properties of cements are often characterised by slump tests and rheological studies. The slump test introduced in the 1920s, though an empirical method of testing the consistency of concrete, is a simple and practical test that is used in research and industry (Neville, 1995). This technique was modified in 1980 to a miniature slump test to monitor the workability of neat cement pastes and the influence of admixtures (Kantro, 1980). The rheological properties of cement are dependent on the properties of the precursor material, the mix protocols followed and the surrounding environment of the cement (Hanehara & Yamada, 1999). These rheological studies are in part an indication of the colloidal interactions in the pastes as well as the early chemical reactions in the cement system (Qing-Hua & Sarkar, 1994). Other factors influencing the rheological behaviour of cement include the water/cement ratio and mixing conditions, testing conditions, and the cement grain size and shape (Papo & Piani, 2004), (Vikan et al., 2007). These variations have led to difficulties in comparing rheological data and the establishment of standard methods of testing (Fernández-Altable & Casanova, 2006).

It has been established that cement pastes exhibit non-Newtonian behaviour with viscoelastic characteristics (Roussel et al., 2012). Rheological studies measure the response of the paste (shear stress) to an externally applied force (shear rate) and from these measurements, the experimental data can be fit to rheological models. This fit has proven to be challenging for cement systems with several models being proposed (Vikan et al., 2007):

Bingham plastic:  $\tau = \tau_y + \mu_p \cdot \dot{\gamma}$  Equation 2.1

Herschel-Bulkley:  $\tau = \tau_y + K \cdot \dot{\gamma}^n$  Equation 2.2

Power law:  $\tau = K \cdot \dot{\gamma}^n$  Equation 2.3

Casson:  $\tau^{\frac{1}{2}} = \tau_y^{\frac{1}{2}} + (\mu_p \cdot \dot{\gamma})^{\frac{1}{2}}$  Equation 2.4

Sisko  $\tau = \mu_{\infty} \cdot \dot{\gamma} + K \cdot \dot{\gamma}^n$  Equation 2.5

where  $\tau_y$  is the yield stress,  $\mu_p$  is the plastic viscosity,  $\dot{\gamma}$  is the shear rate,  $K$  is the consistency, and  $n$  is the power law index. The most used of these models are Equations 2.1-2.3. The Herschel-Bulkley model is reduced to the Bingham model when  $n = 1$ , and to the power law model when the yield stress is zero, as shown in Figure 2.2. The yield stress is often the most challenging to estimate, with different values obtained when different models are used. The yield stress also depends on the experimental protocols followed such that it is important to state whether a dynamic yield stress (minimum stress required to maintain flow) or a static yield stress (minimum stress required to initiate flow) is presented (Nachbaur et al., 2001), (Roussel et al., 2012). To date, understanding the impact of admixtures on the fit of experimental data to these rheological models is lacking.

More recently, the use of oscillatory rheology to measure the interactions between the cement particles has gained popularity (Liberto et al., 2022), (Kalina et al., 2022), (Sun et al., 2022). This method works to monitor the structural build-up of the cement by evaluating the linear viscoelastic region and defining important rheological parameters such as the storage and loss moduli (Kalina et al., 2022). The approach provides new insight and accuracy on the viscoelastic parameters and details the rheological behaviour of the cement more closely than can be obtained from the classical measurements where the shear stress is monitored as a function of the shear rate of a rotational viscometer (Mbasha et al., 2015).

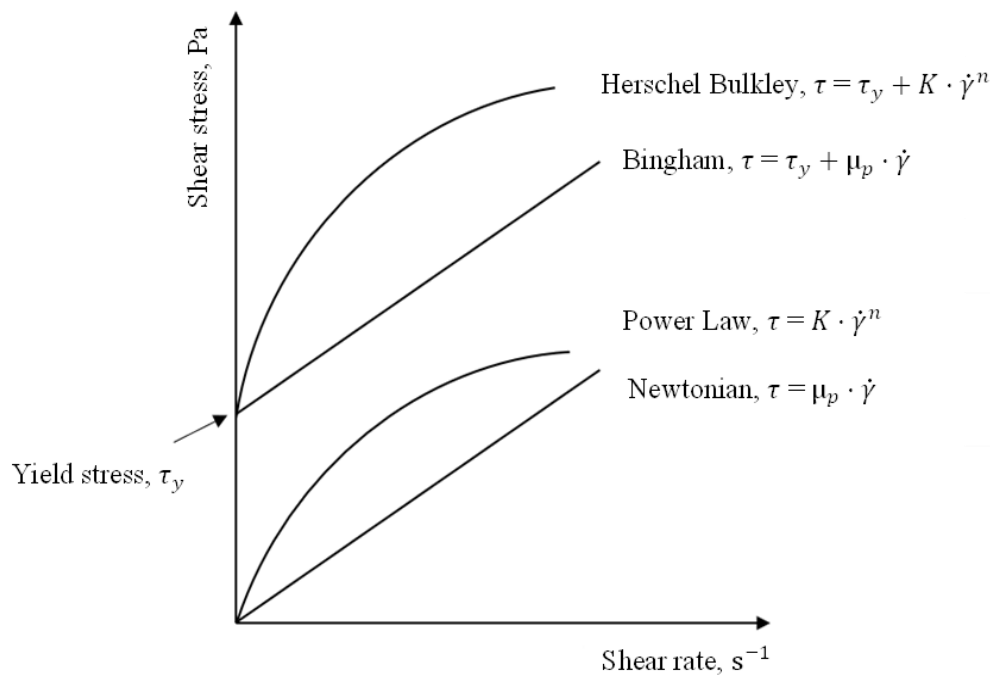


Figure 2.2 Rheological models conventionally applied to the description of the shear stress – shear rate relationship of cementitious pastes. Adapted from (Malvern Instruments Limited, 2016).

In alkali activated cements, the presence of the activator which has its inherent viscosities contributes significantly to the paste fluidity and rheology as confirmed by Puertas et al., (2014). The rheological behaviour of Portland cement pastes is that of a concentrated granular suspension, while alkali activated paste rheology is greatly controlled by the viscosity of the interstitial fluid (Banfill, 2006). For example, the sodium silicate solution is a Newtonian fluid with a viscosity 10 to 100 times higher than that of water (Vyšvařil et al., 2018). Increasing the modulus and Na<sub>2</sub>O concentration dramatically increases its viscosity as shown in Figure 2.3. An example of the effect of the activator is that sodium silicate-activated slag pastes and mortars have been shown to fit a Herschel-Bulkley model, but behave like Bingham fluids when NaOH is used as an activator (Palacios et al., 2008). When in contact with the sodium silicate activating solution, slag particles tend to disperse, and this dispersion effect is increased as the activator dosage is increased (Tan et al., 2017). It is difficult to measure the extent to which the rheological behaviour of the paste can be attributed to the particle-particle interactions as opposed to the effect of the activator, however, the focus of the current study will be on the effect of admixtures in these systems.

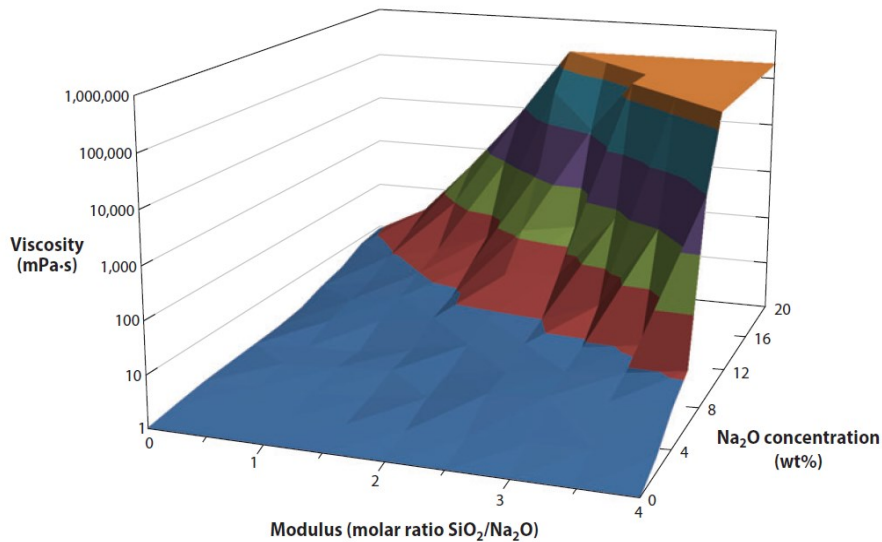


Figure 2.3 Viscosity of sodium silicate solutions as a function of modulus and  $\text{Na}_2\text{O}$  concentration. Used with permission of Annual Reviews, Inc, (Provis & Bernal, 2014), permission conveyed through Copyright Clearance Center, Inc.

Concentrated suspensions of particles in a liquid state may exhibit thixotropic behaviour as demonstrated in Figure 2.4 (Papo & Piani, 2004). Thixotropy is a phenomenon whereby materials subjected to a constant shear rate show a decrease in viscosity with time which is then recovered to the initial viscosity after the strain is removed (Fernández-Altable & Casanova, 2006). This is often characterised by a hysteresis gap between the up and downward curves of a shear stress vs shear rate curve. In AAS, this behaviour is dependent on the nature of the activator used, for example, Palacios et al., 2008 found that waterglass activated slag produced a larger hysteresis compared to when NaOH was used as a activator as shown in Figure 2.4.

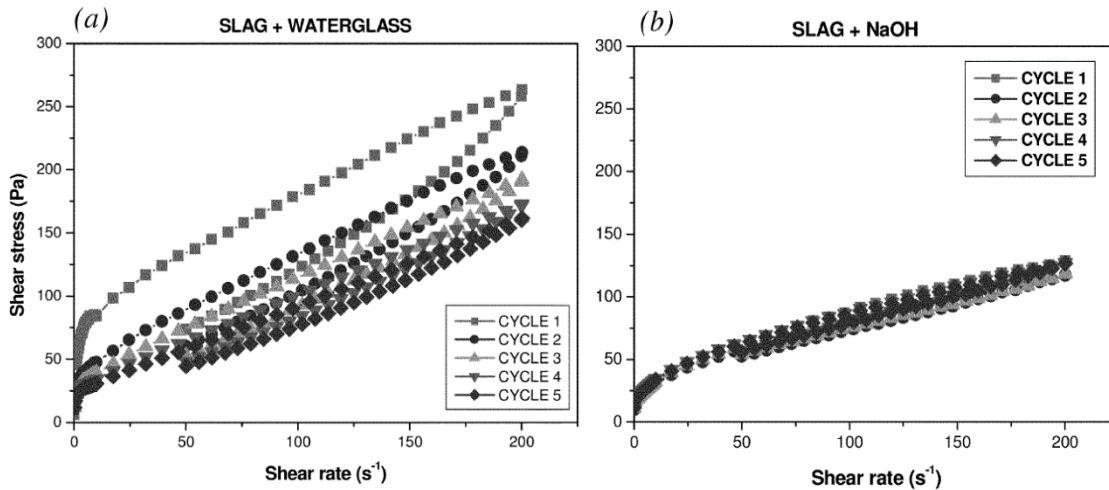


Figure 2.4 Thixotropic behaviour of alkali activated slag. Immediately after stopping mixing, the pastes underwent pre-shearing followed by cycles at 5, 10, 15, 20 and 25 minutes. Adapted from Palacios et al., 2008.

### 2.1.1.1 Effect of admixtures on the fresh state properties

The fluidity of a cement paste varies when different admixtures are added, and when the same type of admixture is added to different cements (Hanehara & Yamada, 1999). This highlights that compatibility plays an essential role on the use of admixtures. Xie and Kayali, (2016) showed that polycarboxylate and naphthalene-based admixtures were less effective in enhancing the workability of low and high calcium fly ash activated cements, than Portland cement. This was attributed to the difficulty in the negatively charged admixtures adsorbing to the anionic  $\text{Si}(\text{OH})_4$  and  $\text{Al}(\text{OH})_4^-$  surface of the low calcium fly ash particles. Conversely, Carabba et al, (2016) showed that PCE based admixtures have a high efficacy in improving the workability of activated fly ash mixtures.

Hanehara and Yamada, (1999) reported that the addition time of the admixture did not have a significant impact on the fluidity of the paste. In contrast, Uchikawa et al., (1995) demonstrated that a delayed addition where the admixture was added 30 s since start of mixing

improved the fluidity of the paste better than simultaneous addition where all the components were mixed in at the same time. A slight reduction in the plastic viscosity of waterglass fly ash activated pastes was reported by Criado et al., (2009) for a range of carboxylate, melamine and lignosulfonate based admixtures, which suggests that these chemicals served their plasticising purpose in these cements. However, this effect was short lived, and the admixtures lost their plasticising ability after 10 minutes. Lignosulfonates have also been reported to not significantly improve the workability of AAFA at both low and high dosages by Carabba et al., (2016). These unsatisfactory results obtained for the use of lignosulfonates in alkali activated materials have been attributed to the instability of these polymers in highly alkaline solutions (Criado et al., 2009), however, this theory has not been evaluated in detail to show such structural breakdown to the lignosulfonate in AAMs hindering their dispersion capacity.

Admixtures commonly used in cement systems have the ability to alter particle interactions and the overall rheological properties of the pastes, including thixotropy, structural breakdown and workability (Burgos-Montes et al., 2012). The yield stress will depend on the interparticle forces and how these are modified in the presence of an adsorbed layer of admixture (Houst et al., 2002). Polycarboxylate admixtures decrease the thixotropic values of pastes in Portland cement owing to dispersion (Fernández-Altable & Casanova, 2006). Various other admixtures have also been reported to modify this thixotropic behaviour breaking down the structure and reducing the hysteresis gap (Papo & Piani, 2004). In alkali activated cements, there is limited study on the effect of admixtures on this rheological property.

### **2.1.2 Reaction kinetic studies**

Isothermal calorimetry has long been an essential tool in the characterisation of alkali activated cement hydration kinetics, especially during the early stages of reaction (Shi & Day,

1995). This technique follows the rate of heat evolution as the reactions proceed. The dissolution of the precursor occurs immediately upon mixing, and this is associated with the first peak in the heat released curve (Fernandez-Jiménez & Puertas, 1997). This first exothermic peak is attributed to the wetting and dissolution of the precursor upon contact with the activator and it is significantly influenced by the concentration of the activator since its magnitude is enhanced by increasing the concentration (Sun & Vollpracht, 2018). This is followed by an induction period and then a high intensity acceleration and deceleration period evidenced by the second peak (Bernal et al., 2015). This second peak is associated with the nucleation, growth and precipitation of the reaction products. Finally, the last stage is at low reactivity, sometimes called decay, when the reaction approaches completion (Fernandez-Jimenez et al., 1998). These stages can be seen in Figure 2.5.

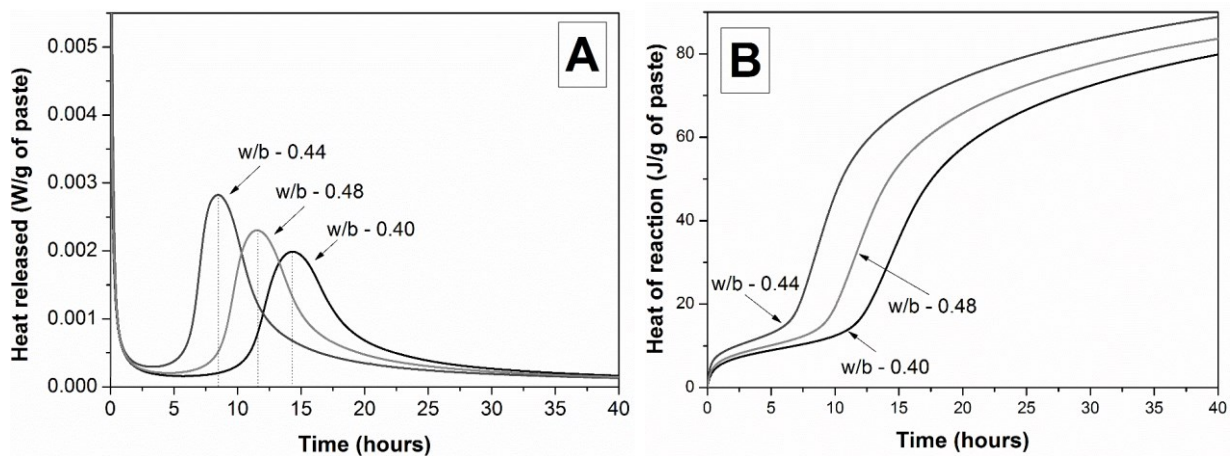


Figure 2.5 Isothermal calorimetry curves for slag metasilicate activated slag pastes, as a function of the water content. Adapted from Bernal et al., 2015.

The intensity of the peaks, duration and when they occur is largely dependent on the type and concentration of the activator used, and the water content (Bernal et al., 2015). Even though distinct peaks can be attributed to certain processes taking place during activation, the reaction

steps overlap each other and so the dissolution of the precursor, accumulation of reaction products and polycondensation occur almost simultaneously (Palomo et al., 1999).

The effect of admixtures on the reaction rate of cements depends on the type of admixture used. It has been established that lignosulfonates retard the hydration of Portland cement as shown by the thermal power against hydration time curves in Figure 2.6. This is evidenced by the appearance of the peak maxima at a later time as the concentration of the admixture is increased (Danner et al., 2015). The cumulative curve shows that the extent of reaction is not affected by the presence of the admixture at longer hydration times. A similar effect of admixtures on the heat evolution of alkali activated cements can be expected.

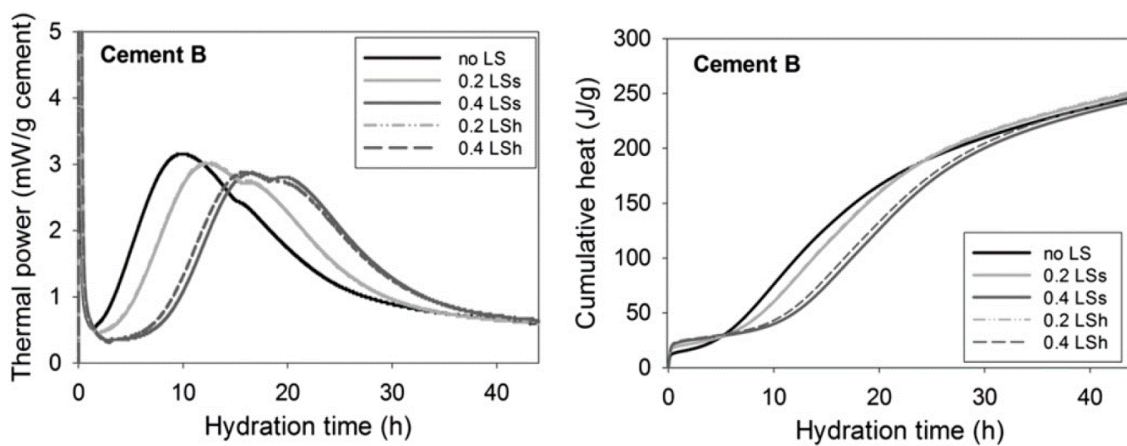


Figure 2.6 Thermal power and cumulative hydration of cements with additions of lignosulfonate admixture. Adapted with permission (Danner et al., 2015) Copyright Elsevier 2015.

In alkali activated cements, the ongoing reactions upon mixing result in the onset of setting where the cement starts to harden. As the silicate ions from the activating solution undergo a condensation reaction with the  $\text{Ca}^{2+}$  ions dissolving from the slag, they form a primary calcium silicate hydrate gel (Shi & Day, 1996). The onset of setting occurs due to the precipitation of

these hydrate phases. The rate at which this occurs depends on the starting materials and it is influenced by the water/cement ratio in the system such that decreasing the w/c decreases the setting time (Chang, 2003). It is also affected by the modulus ( $\text{SiO}_2/\text{Na}_2\text{O}$ ) of the activator such that when the modulus is increased above 3, the setting time is reduced (Qing-Hua & Sarkar, 1994). The mixing protocol has a direct impact on the fresh state behaviour of the cements. Palacios et al., (2008) found that extending the mixing time from 10 to 30 minutes resulted in an increase in setting time of up to 8 hours. It was concluded that an increased time of shearing prolonged the setting times. A concern with the use of high concentration activator is the quick setting of waterglass activated slag cements, however, for industrial applications, the cement should have a reasonable setting time to allow for transportation time and placement (Chang, 2003).

The setting mechanism of fly ash activated pastes follows a gel percolation process (Rouyer & Poulesquen, 2015). Unreacted, isolated, and weakly reacted particles are connected through the formation and deposition of reaction products to form a cementitious matrix and this connectivity is dependent on factors such as the water to binder ratio (Fernández-Jiménez et al., 2005). Low calcium fly ash based cements tend to have long setting times depending on the mix design and the reactivity of the fly ash, and so heat curing is sometimes used to accelerate the hardening of these cements (Provis, 2018).

The interaction between cement and admixtures may cause an early setting or a retardation of the paste (Hanehara & Yamada, 1999). For Portland cement, set retarding admixtures influence the early reactions of the cement (Young, 1972). Different admixtures have varying degrees of retardation on the setting times of Portland cement as shown in Figure 2.7 (Uchikawa et al., 1995). Several theories have been proposed to explain the retardation mechanism of admixtures in Portland cement such as complexation, formation of a protective layer, or poisoning of nucleation to prevent growth of reaction products (Tong et al., 2021).

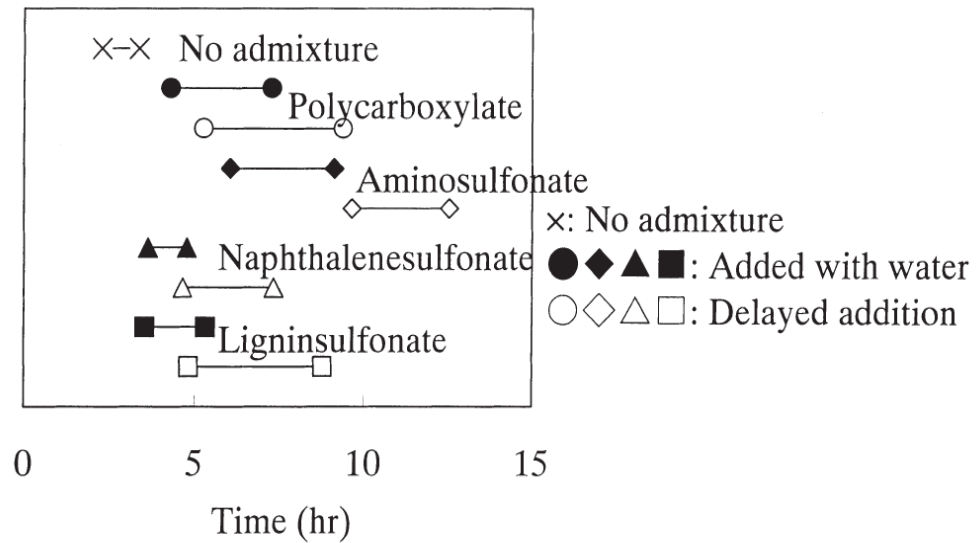


Figure 2.7 Effect of admixtures on setting time of Portland cement at  $w/c = 0.27$ . Adapted with permission (Uchikawa et al., 1995) Copyright Elsevier 1995.

Lignosulfonates have been found to form complexes with  $Ca^{2+}$  delaying setting of Portland cement (Vikan et al., 2007). It is well known that sugars facilitate the significant retardation of the setting of cements and that lignin have sugars naturally retained after sulfonation, but even so, sugar free lignosulfonates also have a strong retardation effect (Gelardi et al., 2015). Therefore, it is not only the effect of sugar that is responsible for the retardation effect of lignosulfonates. Their effect on the setting mechanism of alkali activated cements has not been explored in detail and is poorly understood (Kusbiantoro et al., 2013), (Assi et al., 2018).

### 2.1.3 Reaction and phase assemblage of activated FA and BFS cements

The properties of the precursor, activator as well as the curing conditions determine the reactions that occur during alkali activation, and the products formed (Kovalchuk et al., 2007). Figure 2.8 shows the reaction pathways of both the calcium-rich and low-calcium precursors during alkali activation. It is proposed that the initial dissolution and exchange of species in solution is common to both pathways, the difference is that for the same activator, different species are released depending on the composition of the starting material (Provis & Bernal, 2014). At this stage, the activator is the main driver and the polarising effect of  $\text{OH}^-$  at these high pH values induces the breakage of Ca-O, Mg-O and a significant amount of Si-O-Si, Al-O-Al and Si-O-Al bonds hydrolysing into the pore solution (Shi & Day, 1995).

For ground granulated slag, the weaker Ca-O and Mg-O bonds are broken first, releasing more  $\text{Ca}^{2+}$  and  $\text{Mg}^{2+}$  into the pore solution and leaving an Si/Al-enriched layer on the surface (Chang, 2003). As the pH is increased even more, calcium solubility decreases while silica and alumina solubilities increase (Provis & van Deventer, 2014). At pH values between 9 and 10.7, the solubility of the amorphous silica in the precursor increases due to the formation of silicate ions in equilibrium with the solid phase, and as the pH is increased beyond 10.7, the solid phase dissolves to form a soluble silicate (Puertas & Torres-Carrasco, 2014). As there is an uptake of  $\text{Ca}^{2+}$  ions from solution by formation of the C-A-S-H reaction product, this drives further Ca dissolution of the slag (Provis & van Deventer, 2014). The alkaline elements (cations) in the activator compensate for the negative charge brought about by the substitution of  $\text{Si}^{4+}$  by  $\text{Al}^{3+}$  in the structural network (Criado et al., 2009), (Provis & Bernal, 2014). Other researchers have suggested that slag is a latent hydraulic cement such that when initially reacted with water, an aluminosilicate shell is formed on the surface of slag grains which remains impermeable to water until the shell is broken or dissolved. They suggest that the high alkaline environment

provided by the activator breaks this shell and only then is further dissolution of the slag and product formation possible (Gebregziabiher et al., 2015). However, this hypothesis was not supported by any experimental data, and no evidence of the shell has been presented.

For low calcium precursors such as fly ash, the activator facilitates hydrolysis of the glass structure, breaking bonds and releasing ionic species such as  $\text{Al}(\text{OH})_4^-$  and  $\text{Si}(\text{OH}_3)\text{O}^-$ . Gel nucleation results in what is usually described as a N-A-S-(H) gel, but can also be presented as N,K-(C)-A-S-(H) where partial substitution of sodium and potassium by calcium is possible (Provis & Bernal, 2014). When sodium silicate is used as an activator, additional silicon is available to increase the Si/Al ratio, as a result the dissolution of aluminium becomes rate determining and therefore in these systems, aluminium plays a critical role in N-A-S-(H) formation (Mills et al., 2022). Low calcium fly ash forms this tetrahedral N-A-S-(H) gel type structure based on silicon and aluminium (Provis & Bernal, 2014).

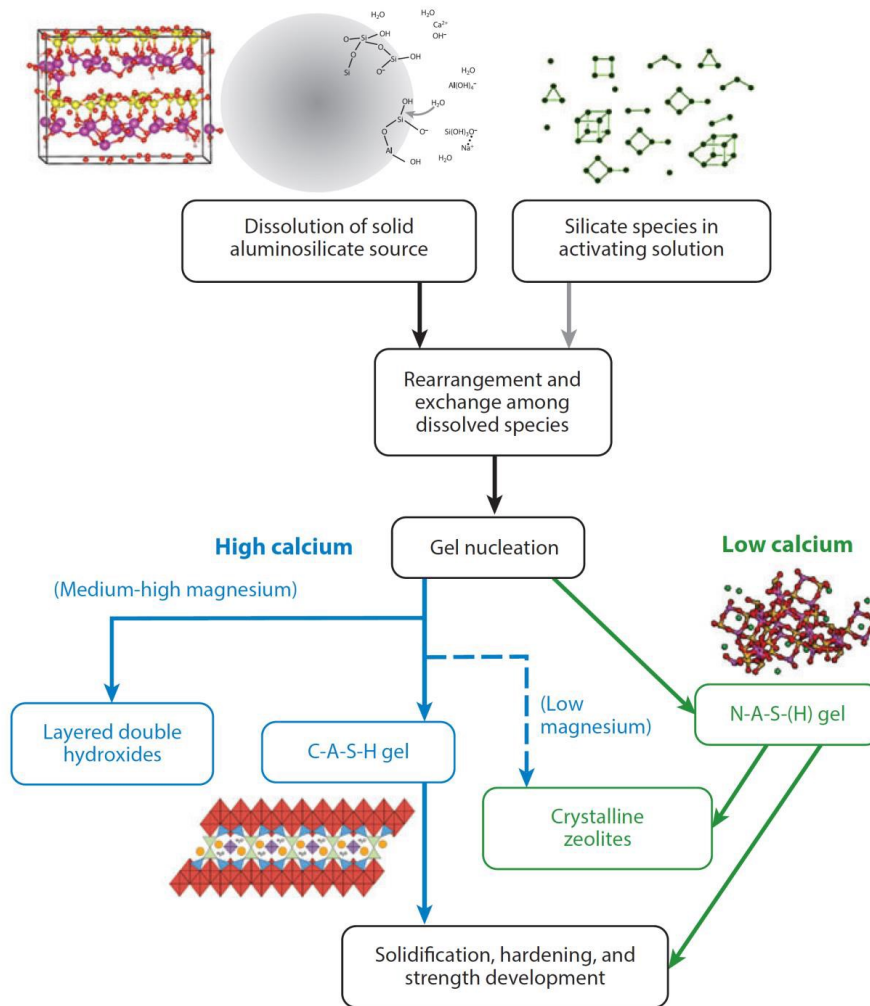


Figure 2.8 Alkali activation reaction route for low and high calcium precursors. Used with permission of Annual Reviews, Inc, (Provis & Bernal, 2014), permission conveyed through Copyright Clearance Center, Inc.

The reaction products of activation are found in the space between the slag grains, indicating a dissolution and precipitation mechanism at early ages (Wang & Scrivener, 1995). Over an extended curing time, the gels undergo solidification, hardening and strength development (Marchon et al., 2013; Provis & Bernal, 2014). Other commonly observed secondary hydration products from slag activation are AFm layered hydrous calcium aluminates (e.g monosulfate,

$C_3A \cdot CaSO_4 \cdot nH_2O$ ) including the Si-containing AFm phase stratlingite, hydrotalcite like (Mg,Al)-layered double hydroxides, and zeolites (Provis & Bernal, 2014).

#### **2.1.4 Mechanical properties development**

As previously mentioned, high mechanical performance, improved durability, as well as high resistance to aggressive environments can be achieved when alkali activated cements are properly designed (Palacios et al., 2009). The curing conditions also play an important role in the microstructural and mechanical strength development of AACs (Kovalchuk et al., 2007).

For AAS, a wide range of high strengths - from 60 MPa to 150 MPa after 7 days of curing can be achieved with the use of a waterglass activator, and without the use of additives or high temperature curing. These cements continue to gain strengths of 100-200% higher than at 28 days after 10 years of service (Wang et al., 1995). The mechanical properties of AAS are comparable to Portland cement but with some added advantages when waterglass is used as an activator (Fernández-Jiménez et al., 1999). Some of the factors influencing the mechanical strength development of alkali activated slag cements are the slag chemistry, degree of reactivity, curing temperature, and more importantly the nature and concentration of the alkaline activator (Fernández-Jiménez et al., 1999), (Winnefeld et al., 2015). As expected, the mechanical strength will increase as the curing time increases, and this is because over time the cement densifies, reducing the total porosity of the system and thereby increasing the strength (Winnefeld et al., 2015). The activators result in the highest mechanical strengths in the following order: Na silicate  $\gg$   $Na_2CO_3$   $>$  NaOH (Fernández-Jiménez et al., 1999). The waterglass activated slag tends to be more condensed, have more microporosity and lower total porosity (Puertas & Torres-Carrasco, 2014). Increasing the molarity of the activator or the modulus ( $SiO_2/Na_2O$ ) concentration of the sodium silicate solution increases the strength

(Thomas et al., 2016). The silicate species from the dissolving slag and those supplied by the sodium silicate activator react with the calcium and aluminium to form solid binder products. However, this activator has been associated with high rates of autogenous and drying shrinkage, while other activators may present shrinkages comparable to Portland cement (Puertas et al., 2011).

As a rule of thumb for Portland cement, decreasing the water to cement ratio increases the compressive strength of the hardened product (Yousuf et al., 1995). For this reason, admixtures are used to achieve highly improved workability at low water to cement ratios leading to improved compressive strength and permeability (Plank et al., 2015). Altan and Erdoğan (2012) demonstrated a similar trend in alkali activated slag cements where they measured a 150% improvement in the compressive strength of a slag mortar when the water to slag ratio mass was decreased from 0.53 to 0.38. They also reported an improvement in the rate of strength gain over time. This finding is of relevance to the current study because efficient admixtures can help achieve these low water/cement ratios by improving the workability of the AAC mixes while maintaining or improving the compressive strengths of the cements.

The mixing protocol also influences the mechanical strength as longer mixing times improve matrix cohesion and compactness of the AAS, so that up to 30 mins of mixing can lead to the enhancement of strength by up to 11% (Palacios & Puertas, 2011). The use of admixtures allows for better mixing, reducing the mixing time while achieving the same cohesion and compactness desired.

For low calcium precursors such as silicious fly ash and metakaolin, the strength development may be slow at room temperature and the final mechanical properties can often be improved by thermal curing after mixing (Provis & Bernal, 2014). Sometimes, thermal curing for extended periods is used to enhance the compressive strengths of AAFA. The

mechanical properties depend strongly on the characteristics of the continuous precipitate interconnecting the unreacted fly ash particles, where the mechanical performance is reduced if this continuity is disturbed (Fernández-Jiménez et al., 2006).

In earlier studies where sodium lignosulfonate was used as an additive in alkali activated slag mortars, Douglas and Brandstetr, (1990) demonstrated a decrease in the overall strength of the samples of about 6% with addition of sodium lignosulfonate, without any improvement on the workability. This finding was supported by Wang et al, (1994). Most researchers have reported a decrease in the compressive strength of AAS cements when lignosulfonate admixtures were added. In Portland cement mortars, the reduced mechanical strength in the presence of polycarboxylate-based admixtures was explained by a high entrainment of air (Palacios & Puertas, 2005). No significant changes in the mineralogical composition of the pastes were found when PCEs were added to Portland cement (Puertas et al., 2005). In alkali activated cements, there is still very limited research on the fate of chemical admixtures. Nonetheless, a summary of the effects of these admixtures on alkali activated cements in presented in Table 2.1.

Table 2.1 Summary of the use of admixtures in alkali activated cements.

Authors	Mix	Admixture	Positive effects	Negative effects
(Douglas & Brandstetr, 1990)	AAS – waterglass (Wg)	Sodium lignosulfonate, sulfonated naphthalene		No improvement in workability Reduced compressive strength
(Bakharev et al., 2000)	AAS	Lignosulfonate (LS), Naphthalene formaldehyde (NF)	Increase in workability	Reduced compressive and flexural strength development with LS Quick set with NF
(Puertas et al., 2003)	AAFA & AAS	vinyl (V) and polyacrylate copolymers (Z)	Gain in fluidity at early stages with Z for AAFA	V delayed hydration and reduced the compressive strength. Both did not improve fluidity of AAS
(Palacios & Puertas, 2005)	AAS - Wg AAS - NaOH	Polycarboxylate (PCE)	AAS-NaOH: N reduced l/s ratio, prolonged	AAS-Wg: none increased the slump

		Vinyl copolymers (V), melamine (M), naphthalene (N)	flowability, significantly longer setting time. PC, V, M increased fluidity in the first 10 minutes	
(Palacios et al., 2008)	AAS-NaOH	Polycarboxylate (PCE), Melamine formaldehyde (M), Naphthalene formaldehyde (NF) and Vinyl copolymer (V)	Naphthalene enhanced fluidity significantly	AAS-NaOH; quick loss of fluidity with M. No change in rheology with the other admixtures AAS-Wg: V raised the yield stress
(Criado et al., 2009)	AAFA	PCE, LS, M	All plasticised in the early stages.	LS and M ability vanished in a short period of time
(Palacios et al., 2009)	AAS-NaOH	V, N	V most effective at low pH N most effective at high pH	
(Bilim et al., 2013)	AAS-Wg	Shrinkage reducing polypropylenglycol (SHR) Set retarding admixture based on modified polymer (SSRe)	SSRe increased the flow rate Reduced shrinkage especially SHR	No impact on the setting times, reduced compressive strength at 2 days
(Nematollahi & Sanjayan, 2014)	AAFA (class F) – NaOH AAF - Wg	N, M, modified PCE	AAFA-NaOH: N improved workability the most, no negative effect on the compressive strength AAFA-Wg: PCE most effective	AAFA-Wg: 29% decrease in compressive strength
(Kashani et al., 2014)	AAS	Modified PCEs	Mild increase in workability	
(Xie & Kayali, 2016)	AAFA (class F and C)	N, PCE	PC more effective with class C N better in class F	Both SPs are less effective than Portland cement
(Garg & White, 2017)	AAS & AAMk (alkali activated metakaolin)	Nano-ZnO	Effective in hydration retardation	
(Rakngan et al., 2018)	AAFA (class C)	Sodium gluconate, Borax, Sodium naphthalene sulfonate (SNS)	Borax, SNS – no effect on slump. Sodium gluconate-improved slump, increased workable time	Sodium gluconate – decrease in compressive strength at dosages above 0.35%
(Najimi et al., 2020)	AAS	Malic acid, LS	Setting time delayed	Drastic reduction in compressive strength. LS also reduced workability

## 2.2 Lignosulfonate admixtures

### 2.2.1 Structure and composition

Lignin is the second most abundant (after cellulose) sustainable material with 70 million tonnes being produced every year. The majority of this production is used for energy recovery and regeneration by combustion in pulping processes, while only 5% is used to form chemical products (Gelardi et al., 2015). Lignin forms an amorphous, irregular three dimensional and highly branched phenolic polymer (Lu et al., 2017). It is made up of building units and interunit linkages, composed of p-hydroxyphenyl (H), guaiacyl (G), and syringyl (S) units in varying proportions, interconnected by ether and carbon-carbon bonds (Elder & Fort, 2010), (Lapierre et al., 1995). These interunit linkages are shown in Figure 2.9. Softwood lignin is comprised of G units while hardwood lignin contains a mix of G and S units (Nimz et al., 1981). The ratios of these units can directly affect the reactivity of the lignin as well as the molecular composition and properties of the lignosulfonates produced (Ruwoldt et al., 2020). The linkages found in lignin are predominately  $\beta$ -O-4 (making up 50% of the polymer) as well as  $\alpha$ -O-4, 5-5,  $\beta$ - $\beta$ , 5-O-4, and  $\beta$ -1 interunit linkages (Lapierre et al., 1995). The exact structure of lignin remains unspecified; however, a proposed structure is proposed in Figure 2.9.

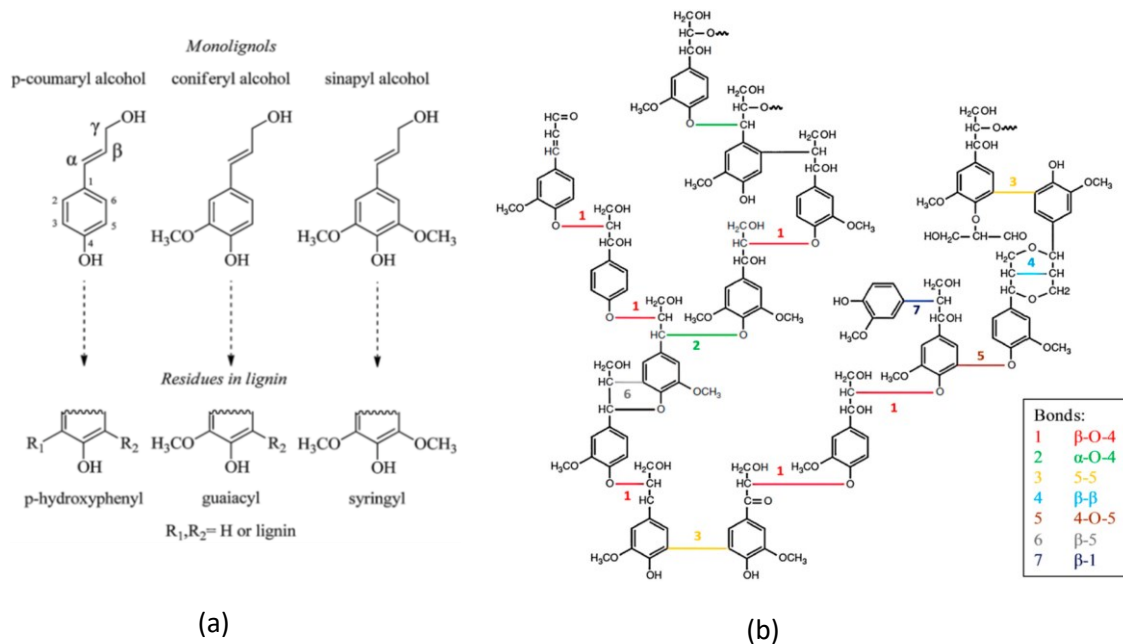


Figure 2.9 Proposed structure of the (a) interunit linkages and (b) lignin polymer. Adapted from Ruwoldt, 2020.

To obtain lignin, it must first be separated from biomass (wood), and there are several processes such as soda pulping, sulfite pulping, solvent pulping and kraft pulping used to achieve this extraction (Ruwoldt, 2020). Sulfite pulping is one of the more common extraction processes and it produces liginosulfonates as a by-product. This lignin extraction is a delignification process involving the use of sulfite ( $\text{SO}_3^{2-}$ ) or bisulfite ( $\text{HSO}_3^-$ ) salts at elevated temperatures (140-170°C) (Gelardi et al., 2015). The lignin undergoes fragmentation where its molecular weight is reduced because of the cleavage of the  $\beta$ -O-4 and  $\alpha$ -O-4 linkage units in lignin. This is followed by sulfonation, a process in which sulfonate groups are grafted onto the backbone skeleton of the polymer as shown in Figure 2.10, making the polymer water soluble (Myrvold, 2008) (Vainio et al., 2012).

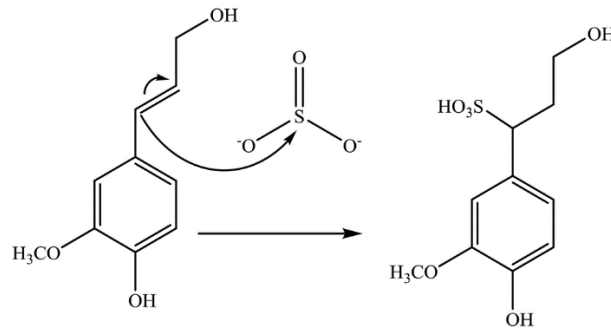


Figure 2.10 Sulfonation process of lignin to obtain liginosulfonate. Adapted from Eraghi Kazzaz et al., 2019.

It has been suggested that the sulfonation of side chains increases the resistance to biodegradation of the liginosulfonates when compared to lignin (Li et al., 2012). The insoluble cellulosic fibers are then separated by ultrafiltration to obtain “spent liquor” which consists of poorly sulfonated lignins, inorganic salts, and sugars from the acidic hydrolysis of the cellulosic fibers (Gelardi et al., 2015).

During liginosulfonate production, the original structure of lignin is preserved to a certain degree, and hence the polymer possesses amphiphilic properties (Ruwoldt, 2020). The amount of lignin present depends on the source i.e. softwood LS have a higher content of lignin (27-37%) compared to hardwood (16-29%), and have varying molecular masses and amounts of functional groups (Arel & Aydin, 2017). The amount of bonds and types of linkages retained is dependent on the route of production, for example, liginosulfonates from the sulfite process contain low amounts of the  $\beta$ -O-4 linkage (less than 10%) but high amounts of C-C bonds (Hemmilä et al., 2020). Further modifications are then carried out to achieve the desired product depending on the end use in different industries as dispersants, surfactants and adhesives, and for other uses, taking advantage of their versatile nature (Ruwoldt, 2020).

Liginosulfonate end products are highly cross-linked macromolecular polymers made up of a hydrophobic backbone containing aliphatic and aromatic groups, as well as a random

distribution of hydrophilic side chains such as carbonyl, sulfonic, and phenolic hydroxyl groups (Yan et al., 2010). A simplified structure of a lignosulfonate showing all the key components is shown in Figure 2.11. These polar functional groups make the macromolecule soluble and very chemically active, thereby enhancing their adsorptivity and dispersive ability (Qiu et al., 2010), (Li et al., 2012). Lignosulfonates have been particularly applicable in the cement industry as they can be modified for use, and are among the earliest organic materials used as admixtures in the modern cement industry dating back to the 1930s (Gelardi et al., 2015).

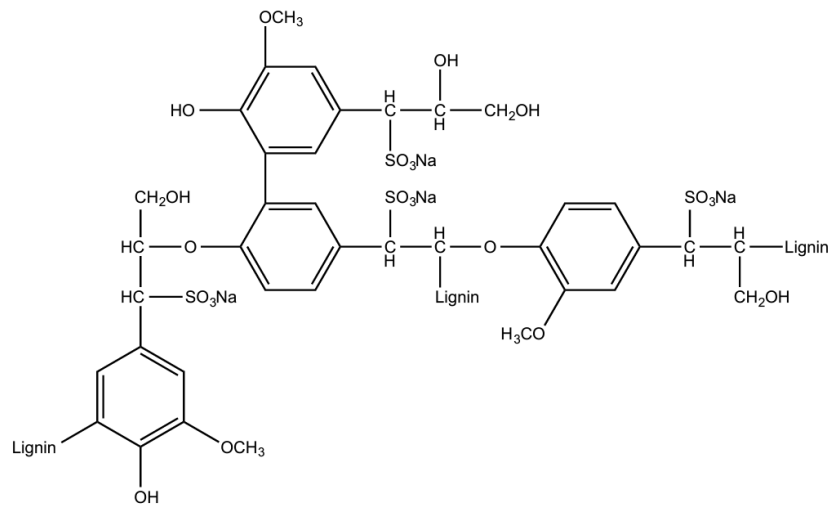


Figure 2.11 Simplified structure of a lignosulfonate. Adapted with permission (Gelardi et al., 2015) Copyright Elsevier 2015.

## 2.2.2 Chemical action of lignosulfonates in alkaline media

In alkali activated cements, the low efficiency of lignosulfonates in improving their workability has often been attributed to chemical instability in the high pH aqueous environment. Previous researchers have suggested that there is a loss of functionality of the admixture due to structural breakdown and loss of key functional groups, particularly the

sulfonate groups (Palacios & Puertas, 2005), (Criado et al., 2009). They suggest that as anionic sulfonate groups induce repulsion between cement grains upon adsorption, when lost from the polymer, this fluidising effect is also lost hence the reduced efficiency. These claims have been confirmed for naphthalene sulfonate admixtures (Palacios & Puertas, 2005) and then assumed by extension for lignosulfonates due to their similarities in having sulfonate groups on their surfaces (Criado et al., 2009). Thus far, no evidence has been brought forward to confirm this chemical instability for lignosulfonate admixtures. A detailed characterisation monitoring these changes is still lacking.

Studies have been carried out on the behaviour of lignosulfonates since the 1900s with the aim of elucidating their chemical structure and behaviour in aqueous environments (Gardon & Mason, 1955). Despite this extended period of research, there are still debates on this poorly understood topic to this day. Bolatbaev et al., (2010) correctly pointed out that the lack of data/research on the fundamental properties and behaviour of lignosulfonates hinders their purposeful selection and use. Understanding their behaviour ensures optimum usage in systems that are compatible with their structure and chemical behaviour.

A great advantage of these materials is the versatility of their polymeric structures which allows for a wide range of application in different chemical environments. The structure of lignosulfonates has recently been described as randomly branched polyelectrolyte molecules, with functional groups attached that introduce charges and induce dipoles on the chains of the polymers, making them water soluble and compatible with the polar environment of the aqueous medium (Myrvold, 2008). In this aqueous medium, these macromolecules dissolve to form concentrated finely dispersed and stable colloidal solutions (Shul'ga et al., 2010).

Lignosulfonates are flexible polyelectrolytes that will undergo chemical changes in the presence of electrolytes in solution (Gardon & Mason, 1955). It has been established and

widely accepted by previous researchers that these chemical changes involve the dissociation and ionisation of some functional groups in the presence of simple electrolytes in solution (Gardon & Mason, 1955), (Bolatbaev et al., 2010), (Qian et al., 2011). As a result of this ionisation, the polymer is left with a charge that can be measured through conductivity measurements to obtain conductivity curves. However, this technique has a limitation in that it provides the overall charge of the polymer and gives no quantitative data on the functional groups undergoing ionisation.

In previous studies, there has been no consensus on which of the factors or parameters drive the chemical changes observed when lignosulfonates are in aqueous media. Gardon and Mason, (1955) stated that the process of ionisation is driven by an equilibrium that exists between the ions attached to the polymer and those in solution, such that a low concentration of ions in solution favours more ionisation from the polymer. And so, ionisation is proportional to the concentration of the polyelectrolyte as well as the electrolytes present in solution. These researchers suggested that since this equilibrium is the main driving force for ionic dissociation, the concentration of the lignosulfonate in solution is a key parameter influencing the degree of ionisation. It was also proposed that this equilibrium is reversible and dependent on the pH of the solution. Most researchers highlight pH as one of the key factors to consider. The pH influences the degree of ionisation which in turn determines the amount of charge on the polymer. At low pH, the degree of dissociation is reduced and the polymer is weakly charged, whereas at high pH a larger fraction of the monomers is dissociated and the polymer charge saturates at its maximum value (Borukhov et al., 2000). Contrary to this, Bolatbaev et al., (2010) found that lowering the pH in fact enhances the surface activity of lignosulfonates, thereby increasing the degree of ionisation. Lignosulfonates can be classed as pH-responsive polymers because they change their surface activity, conformation and solubility when interacting with increasing pH of solutions (Kocak et al., 2017). The high pH environment

presented by the cement pore solution means that the acidic functional groups of the lignosulfonates are essentially dissociated (Perche et al., 2003).

There are other factors such as temperature which also influence the degree of dissociation, such that an increase in temperature favours more dissociation of the polymer (Bolatbaev et al., 2010). The intrinsic properties of the lignosulfonate, such as the molecular structure, also affect the degree of ionisation, with researchers seeing an increase in the degree of dissociation as the molecular weight of the polymer decreases. This is because easily dissociating groups are more predominant in low molecular weight lignosulfonates (Bolatbaev et al., 2010).

In alkaline media, the dissociation and ionisation degree of lignosulfonates can be investigated by monitoring key functional groups and how they can be affected by the chemical environment. One of the key functional groups to observe are methoxyl groups found on the side chains of the lignosulfonates. These groups are known to be labile and susceptible to chemical attack and hydrolysis. They are capable of donor-acceptor interactions where they donate electrons. They also undergo cleavage by nucleophilic substitution in highly alkaline media where the  $\text{OH}^-$  acts as a nucleophile and attacks the electron deficient carbon bonded to the oxygen as shown in Figure 2.12.

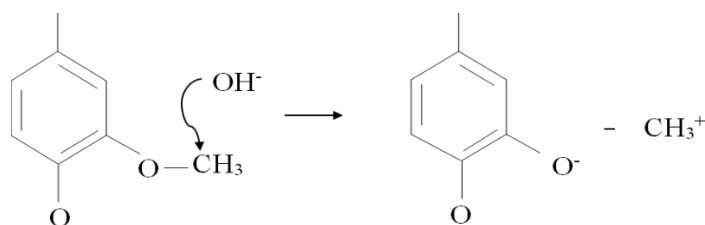


Figure 2.12 Nucleophilic substitution of the methoxyl group in highly alkaline media.

There are also phenolic hydroxyls, which are weakly acidic and hydrophilic groups that may undergo a reaction with sodium hydroxide solution in which the OH<sup>-</sup> is lost in formation of sodium phenoxide and water, as shown in Figure 2.13.

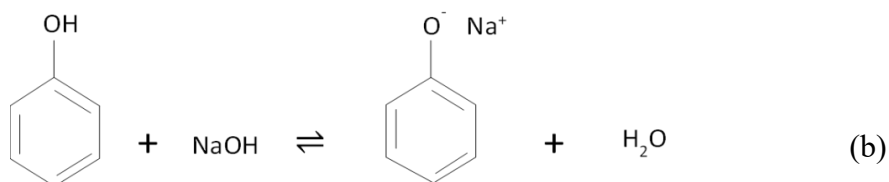
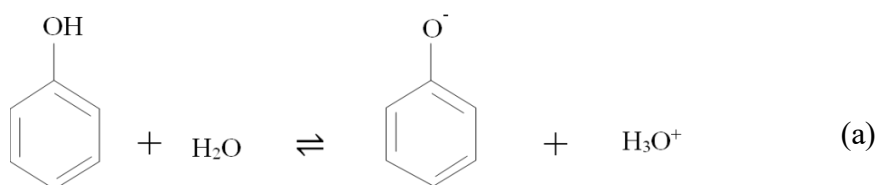
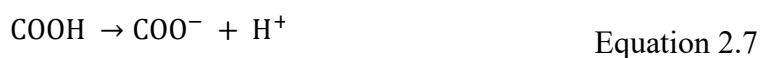


Figure 2.13 Reaction of the phenolic hydroxyls in (a) water and (b) sodium hydroxide.

The two other and perhaps more important functional groups in the context of admixture use are sulfonic and carboxyl groups. These groups are both acidic and hydrophilic and will deprotonate in solution leaving the polymer with a negative charge, Equation 2.6 and Equation 2.7. When dissolved in alkaline solution, lignin molecules present a negative charge on their surface as a result of dissociation of the hydroxyl and carboxyl groups (Ajao et al., 2018).



It is difficult to perform a quantitative analysis of each functional group in the polymer due to the complex structure and chemical composition of the lignosulfonates. However, the carboxylic group has been reported to ionise at a low pH of about 3.5, while phenolic groups ionise at a high pH of 9-11 (Deng et al., 2010), (Qian et al., 2011). Different lignosulfonates have varying amounts of these functional groups and so the extent of deprotonation also varies, which highlights differences in their charged surfaces.

### **2.2.3 Conformational effects of lignosulfonates in alkaline media**

Conformational effects of lignosulfonates have received attention in research and are still a matter of debate as different researchers propose different spatial arrangements in solution. It is of interest in the current study to investigate how the chemical environment influences these conformational effects, as they may in turn have a direct effect on the efficiency of lignosulfonate admixtures in cements.

Early studies have established that lignosulfonates present some flexibility and coiling as they interact with the aqueous solution (Gardon & Mason, 1955), (Le Bell, 1984). It was hypothesised that the shape taken by this macromolecule in solution is due to its electrical charges; it curls up when uncharged and takes a flat shape when charged (post ionisation of some functional groups) due to the electrostatic repulsion between the neighbouring groups (Gardon & Mason, 1955). This conclusion was reached based on the assumption that the LS molecules at low concentrations have a high charge, are therefore extended in solution, and have measurable high viscosities. As the concentration increases, the charge is reduced, and low viscosities are observed due to the coiling of the molecules (Gardon & Mason, 1955). However, this study relied on empirical equations to reach these conclusions without any

evidence of coiling or extension of the polymer presented. There are more powerful characterisation techniques in the present day that can be coupled with such studies to present a more complete picture of these arrangements.

Several conformations of this polymer in solution have been proposed. Goring et al., (1979) demonstrated by electron microscopy that the lignosulfonate macromolecule has a flat, disk-like conformation with a thickness between 1.5-2.1 nm, while Qiu et al., (2010) proposed a flat oblate ellipsoid conformation. It has also been shown that lignosulfonates coil into a spherical shaped molecule that is negatively charged due to the sulfonic and carboxylic groups on the surface (Myrvold, 2008). These charged groups are distributed as far apart as possible due to electrostatic repulsion (Le Bell, 1984). In contrast, Bolatbaev et al., (2010) suggested that the acidic groups of lignosulfonates may be localised in the internal structure of the polymer and there is restricted accessibility to these groups therefore they are less susceptible to chemical attack in high molecular weight lignosulfonates. The researchers went on to support their claims by highlighting the increased steric hindrances of these high molecular polymers. Vainio et al., (2012) disagreed with these claims and argued that lignosulfonates adopt a flat conformation at the interface, which is not at all affected by the molecular weight of the polymer. However, the researchers did highlight that these conformational effects can only be observed in dilute solutions. When the salt concentration is increased the electrostatic charges of the polymers are screened and unimportant, therefore there are no conformational effects (Myrvold, 2008), (Ouyang et al., 2011). However, Le Bell, (1984) stated that in highly concentrated electrolyte environments, lignosulfonates can swell and shrink. When in aqueous media, the polyelectrolyte expands and changes from a spherical shape and becomes elongated and stretched out (Myrvold, 2008). This unwinding of the molecule when charged exposes more functional groups to chemical attack hence further ionisation occurs (Bolatbaev et al.,

2010). Some of the proposed structures and shape of lignosulfonates in solution are presented in Figure 2.14.

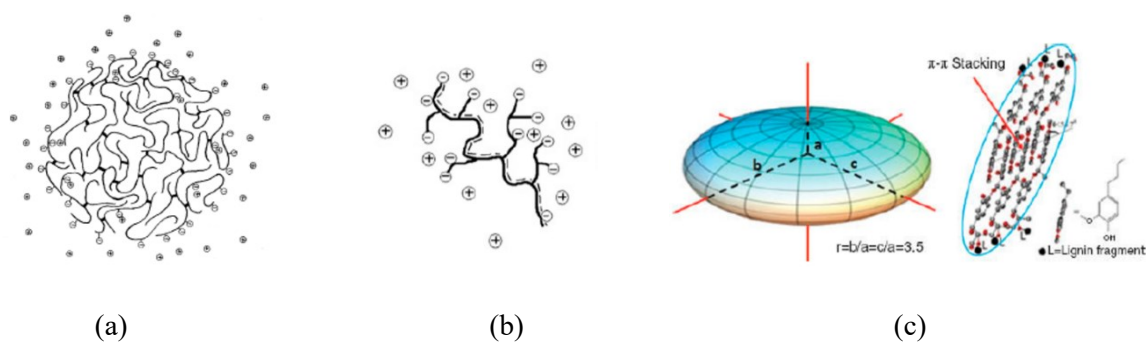


Figure 2.14 Some of the proposed conformations of lignosulfonates in solution, (a) microgel, (b) branched polyelectrolyte, (c) oblate ellipsoid model and possible  $\pi$ - $\pi$  stacking Adapted from Ruwoldt, 2020.

The behaviour of lignosulfonates in aqueous alkaline media such as conformation, self-association, and adsorption is strongly linked to the chemical composition and structure of the polymer (Ruwoldt, 2020). Deng et al., (2012) explained that when in aqueous solution, the hydrophobic aromatic groups in sodium lignosulfonates tend to come together to reduce the entropic loss and the hydrophilic functional groups extend into the aqueous solution to keep the polymer stable. As the ionic strength is increased, the repulsion between adjacent sulfonate groups within the same chain is reduced, allowing the polymer to take a more coiled arrangement in solution (Houst et al., 2008).

When the concentration of lignosulfonates is increased in solution, aggregation can occur (Vainio et al., 2012). The behaviour of lignosulfonates at interfaces is dependent on this aggregation behaviour, and as the ionic strength of the solution increases, the charge screening

reduces the spatial dimensions of the lignosulfonate molecules and aggregates (Ruwoldt et al., 2020).

It has been reported that the dense conformation of lignosulfonates results in a greater dosage required to cover the surface of cement particles (Kauppi et al., 2005), while polymers which stretch out on the surface area have a higher dispersion efficiency (Plank et al., 2015).

## **2.3 Interaction of admixtures with cement at the solid-liquid interface**

### **2.3.1 Theory and background**

Zeta potentials are of great importance in quantifying the particle interactions in colloidal systems where particles are finely dispersed in electrolyte solutions, reflecting the stability of these systems (Malvern, 2000). This technique is based on the principle that once dissolved in aqueous media, particles will carry a charge (Lowke & Gehlen, 2017). This charge may be due to the ionisation and preferential loss of ions from the surface of the particles, or adsorption of ions onto the surface (Malvern, 2000). Depending on the nature of the solvent and the pH, acidic groups may dissociate to produce a negative charge, while basic groups may dissociate to form a positively charged surface. The development of the net charge around the particle results in a redistribution of the ions around the interfacial region, so that there is a high concentration of counterions near the surface of the particle, resulting in an electrical double layer (EDL) (Lowke & Gehlen, 2017). This layer consists of a rigid and immobile layer of ions that are opposite in sign to the surface of the particle, called a Stern layer (inner layer), where ions are strongly bound, and also a diffuse layer (outer layer) made up of a cloud of hydrated ions that are less firmly associated (Park & Seo, 2011). The electric double layer is shown in Figure 2.15. The direct measurement of the potential at the surface is rendered impossible

because of the counterions that are adsorbed; the Stern layer is affected by the degree of hydration that is unknown, therefore, only the zeta potential can be measured (Flatt & Ferraris, 2002).

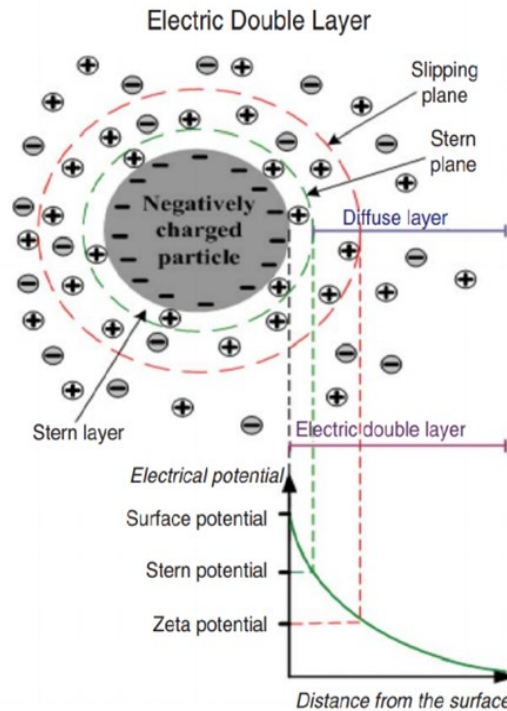


Figure 2.15 Schematic showing the formation of an electric double layer around a negatively charged particle suspended in an electrolyte solution. Reproduced with permission (Park & Seo, 2011) Copyright Elsevier 2011.

The zeta potential measurement follows the Derjaguin-Verway-Landau-Overbeek (DVLO) theory which suggests that the stability of the system is the sum of the potential energy ( $V_T$ ), with various contributors:

$$V_T = V_A + V_R + V_S \quad \text{Equation 2.8}$$

Where  $V_A$  and  $V_R$  are the attractive and repulsive forces respectively, and  $V_S$  is a contribution of the solvent which is insignificant at nanoscale separations. The  $V_A$  and  $V_R$  are

much larger in magnitude and work over a longer separation range. In a colloidal system, the particles undergo Brownian motion, and the forces acting between the particles depend upon the distance between them (Uchikawa et al., 1997). Upon approach, the particles are subjected to van der Waals attractive forces, as well as electrical double layer repulsive forces, and an energy barrier exists because of the repulsive forces and prevents approach and adhering of particles to each other as shown in Figure 2.16. At the minimum, the colloidal system is unstable, and this is indicated by a low magnitude of the zeta potential values. On approach, the electric repulsion potential dominates the van der Waals attraction potential resulting in a maximum repulsive barrier (Park & Seo, 2011). Flocculation occurs if particles collide with enough energy such that this barrier is overcome. If, however, the repulsion is high enough, the particles will disperse and resist flocculation, in which case the system is said to be stable and high magnitude zeta potential values can be measured. For the system to remain stable, the repulsive forces must always be dominant.

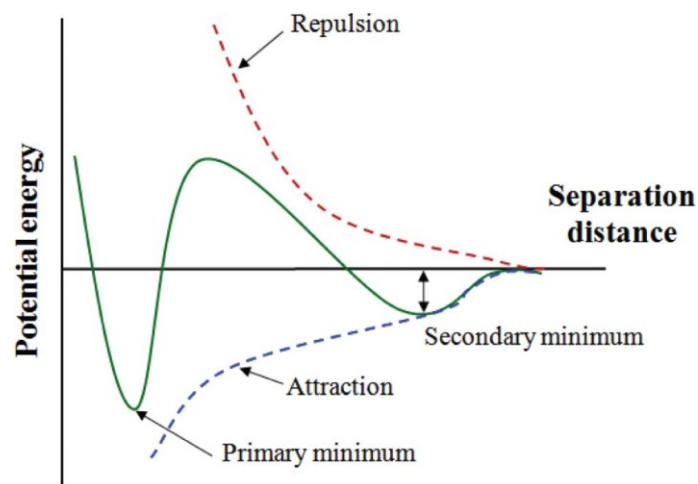


Figure 2.16 Potential energy as a function of distance between interacting particles. Reproduced with permission (Park & Seo, 2011) Copyright Elsevier 2011.

Generally, the distinction between stable and unstable systems is taken at either -30 or +30 mV, where zeta potentials outside of this range are considered stable. The point between these extremes where a zero zeta potential is measured is often referred to as the isoelectric point, and this is when the colloidal system is least stable (Malvern, 2000).

There are currently no standards available to follow for the methodology and sample preparation procedures for zeta potential measurements of cements. Due to this lack of standardisation, the procedures followed by researchers differ and often key considerations that directly impact the results are ignored. Previously, researchers have prepared pastes and then diluted them with pure water to make suspensions for zeta potential measurements (Yoshioka et al., 2002). This is not an appropriate method of preparation because an equilibrium exists between the number of species adsorbed on the particle surface and the solution. If this starting suspension is diluted, these species will desorb from the surface and establish a new equilibrium and these two systems will present different zeta potentials and therefore different stabilities (Brookhaven, 2002).

To mitigate against this, zeta potential measurements must be performed on low solid fraction suspensions because the velocity of individual particles must be measured under the influence of an electric potential (Flatt & Ferraris, 2002). This also ensures that there is less sedimentation of particles, which can be expected at high solid fractions. The particle size distribution is one of the parameters decreasing the accuracy of the technique and so the powders must also not have a wide size distribution which may result in sedimentation of larger particles and measurement of only finer particles (Flatt & Ferraris, 2002). A large range in the particle size distribution of the cement particles means that errors arise as the particles cannot be fully sampled by the electroacoustic technique (Perche et al., 2003). One may argue that the low-solids suspensions are not representative of the cement systems being studied. However, they do provide insight into what is happening on the surface of the individual cement particles.

Although zeta potential measurements have been found to produce reliable and reproducible data that can be correlated with the behaviour of more concentrated systems, there is a need for more appropriate techniques and equipment to further the study of the surface chemistry of cement in the future.

Zeta potential measurements are often coupled with adsorption measurements because it is this adsorption of admixtures that provides the surface charge. The most used method of quantification of adsorbed admixtures on cement particles is the depletion method, which relies on the principle that the amount of admixture adsorbed is the difference between the amount added and the amount in the pore solution (unadsorbed) (Perche et al., 2003). Though commonly used, the depletion method does not distinguish between the amount of admixture consumed via other mechanisms and adsorption onto the particle surface (Houst et al., 2002). There has not been a significant use of any other method in quantifying the adsorption of admixtures on cement surfaces according to recent literature. The concentration of admixtures in the pore solution is often determined via the Total Organic Carbon (TOC) or UV-visible spectroscopy techniques. The adsorption data obtained can be fitted to adsorption models to determine the best correlation to the experimental data (Wang et al., 2012). The most common models include Langmuir, Freundlich and Dubinin-Radushkevich (D-R) isotherms. The Langmuir and Freundlich models are best known, and have been used widely to describe adsorption isotherm data and explain the nature of the adsorption process (Wang et al., 2012). The Langmuir model describes homogenous surfaces and assumes an ideal monolayer formation, while the Freundlich model describes heterogenous surfaces with a multilayer formation (Li et al., 2012). The former would not in theory be applicable to cement systems where the particles have heterogenous surfaces that evolve over time due to hydration processes taking place. In practice, both adsorption models have been used to describe the adsorption of

admixtures on cement particles because their functional forms give rather similarly shaped isotherms across the concentration regions of relevance to cement systems.

There currently does not exist a standard for the methodology and sample preparation procedure that should be followed for adsorption measurements in cement. However, key considerations should be made, and such considerations include the effect of contact time. Not only are the particle surfaces evolving over time due to hydration processes, but the chemical composition of the solution is also changing immediately after mixing until liquid-solid separation. The effect that these changes have on the adsorption of the admixtures has been investigated by observing the amount adsorbed over different contact times. It can be expected that there is a rapid increase in the rate of adsorption at the beginning of the test, which then plateaus at a later stage (Wang et al., 2012). The contact time should therefore be enough to allow for adsorption such that the adsorption models can be applied, but not too long that hydration effects dominate.

### **2.3.2 Zeta potential of cements**

Zeta potential has been shown to be a characteristic property of cement materials (Nägele & Schneider, 1987). In early cement surface chemistry research, zeta potentials played an important role in providing new information on the early hydration of cement (Nägele, 1985), (Nägele, 1986), (Nägele & Schneider, 1987), (Nägele & Schneider, 1989). The measured zeta potential of cement particles is attributed to the surface charge of the particles i.e., surface constituents/composition, concentration of adsorbed species, or to a displacement of the slipping plane (Nägele, 1985). This technique allows for the surface chemistry of the particles to be monitored by changing parameters of the aqueous medium and therefore elucidating the interactions occurring and the mechanisms by which these interactions occur. The EDL

controls the properties on the surface of the particles, and the interparticle interactions which in turn affects the observable properties of the cementitious suspensions (Lowke & Gehlen, 2017). These properties include coagulation, thixotropy, structural build up, rheology, sedimentation, and adsorption of admixtures (Lowke & Gehlen, 2017).

One of the limitations of the zeta potential technique in measuring cement suspensions is that they do not have a well-defined surface, that is, the surface reacts with the aqueous medium and so the surface area and composition vary with time as the hydration process also progresses (Nägele, 1985). Therefore, both the hydration process and the chemical environment (solvent) significantly affect the electrical double layer. This is due to the continued release of ions at the interface between the unhydrated cement and hydration products, and so the electrical double layer is not at equilibrium. The hydration process of the cements makes it difficult to quantify the charge distribution on the particles. However, the zeta potential can be well defined when the system is in the induction period of hydration, and at a much later stage of hydration; at this latter stage the double layer represents the zeta potential between the bulk solution and the primary hydration products (Nägele, 1985). To reduce these effects, model powders are sometimes used for zeta potential and adsorption studies, e.g., MgO is often used to simulate Portland cement. MgO has been found to be useful to model Portland cement due to its low surface charge (representative of CaO which is mainly found on cement surfaces) and inertness at high pH. Although model powders may offer attractive advantages, they are often not as inert as required. Perche et al., (2003) found that direct measurements on cements and model powders give similar results, with the model powders reproducing the same trend as the cement systems.

In cement systems, stability is achieved by the addition of poly-anionic admixtures that adsorb onto the surface of particles and induce repulsive forces that prevent particles agglomerating. This adsorption is only possible when there is a positive charge, or when the

admixture desorbs an already adsorbed anion (Plank & Hirsch, 2007). In alkali activated cements, the addition of an alkaline activator provides a higher pH and much higher ionic strengths compared to Portland cement, which means that there are differences in the surface charges and interactions between the particles (Kashani et al., 2014). The zeta potential of precursors such as ground granulated slag depends strongly on the composition of the slag and route of production. This is because the final composition of the slag will govern which species are dissolved when in aqueous media, and it is the release of these species that then result in a charge distribution around the slag particles (Habbaba & Plank, 2012).

For fly ashes, negative zeta potentials are often obtained as can be expected for silicate materials dissolved in water (Nagele, 1986). The zeta potential of these materials is influenced by their specific surfaces depending on the type of combustion route followed to produce them i.e., fly ashes with high surface areas have higher zeta potentials than fly ashes with lower specific surfaces (Nagele, 1986).

Figure 2.17 shows the effect of pH on fly ash and blast furnace slag over a wide pH range; and the slag had a zeta potential minimum at pH 7, while a minimum at pH 8 was reached for fly ash. For both these materials, an increasing zeta potential as alkalinity increased was attributed to the enrichment of  $\text{Ca}^{2+}$  ions in the electric double layer (Nagele & Schneider, 1989). At high pH, cement suspensions have an electrostatic surface potential very close to zero (near the isoelectric point) and this is due to the production of high concentrations of  $\text{Ca}^{2+}$  and alkali cations (Perche et al., 2003), (Habbaba & Plank, 2010). The  $\text{Ca}^{2+}$  ions become potential-determining at high pH values (Viallis-Terrisse et al., 2001).

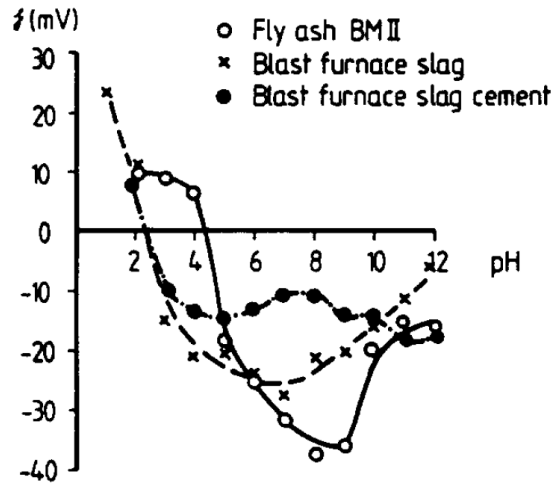


Figure 2.17 Effect of pH on measured zeta potential values of fly ash, slag and slag cement (a Portland and BFS blend). Reproduced with permission (Nagele & Schneider, 1989) Copyright Elsevier 1989.

Nagele and Schneider, (1989) established that the zeta potential of the fly ash and blast furnace slag is determined by not only the pH value of the surrounding solution but also by the electrolyte that is used to adjust the pH. The ionic concentration of the solution also influences the measured zeta potential such that an increase in ionic concentration results in a decrease in the magnitude of the zeta potentials (Perche et al., 2003). The concentration of ions in the system will affect the thickness of the electric double layer. As the ionic strength increases, the EDL becomes compressed thereby reducing the magnitude of the zeta potential and making the colloidal system less stable. It also depends on the type of ions in solution, for example, a recent study showed that the presence of divalent cations reversed the sign of the zeta potentials in a metakaolin colloidal system, but also that  $\text{Ca}^{2+}$  had more of an effect than  $\text{Mg}^{2+}$  ions (Derkani et al., 2022). The valency of the ions in solution will also affect the thickness of the EDL such that higher the valences will compress the EDL even further.

### 2.3.3 Admixture adsorption behaviour in cements

In cement research, adsorption studies are conducted to evaluate the amount of admixture adsorbed to fluidise the cement. The adsorption of the admixture polymer on the cement particles and hydrates determines the dispersion efficiency (Colombo et al., 2017). Anderson et al., (1986) concluded that the adsorption process is kinetically driven and showed that the adsorption of an admixture polymer progressed over time towards a maximum where the surface was saturated.

Adsorption isotherms present the amount of admixture adsorbed as a function of the dosage added and the shape of the adsorption isotherm curve is indicative of the adsorption mechanism taking place, whether it is a monolayer coverage or multilayer (Colombo et al., 2017). However, if other mechanisms of polymer consumption are taking place, adsorption isotherms do not take this into account and only consider how much free polymer is still in solution. Figure 2.18 shows the typical adsorption isotherms when lignosulfonates are adsorbed on a MgO model surface; almost all cement-admixture adsorption isotherms present curves of shapes similar to these. At low dosages of the admixture, a linear correlation with the adsorbed amount is observed; the adsorbed LS is directly proportional to the amount adsorbed. The second part of the curve is non-linear, the adsorbed amount increases until it plateaus and the surface is completely covered at the saturation point (Houst et al., 2008). Beyond this point, further additions of the admixture have no effect on the fluidity of the cement. This describes the monolayer adsorption mechanism in which a plateau is reached once the entire surface is covered by the admixture, and there are no available sites for adsorption. Monolayer adsorption of lignosulfonates was proposed as the main adsorption mechanism of lignosulfonates on high surface area Portland cements independent of the mode of addition (Colombo et al., 2017).

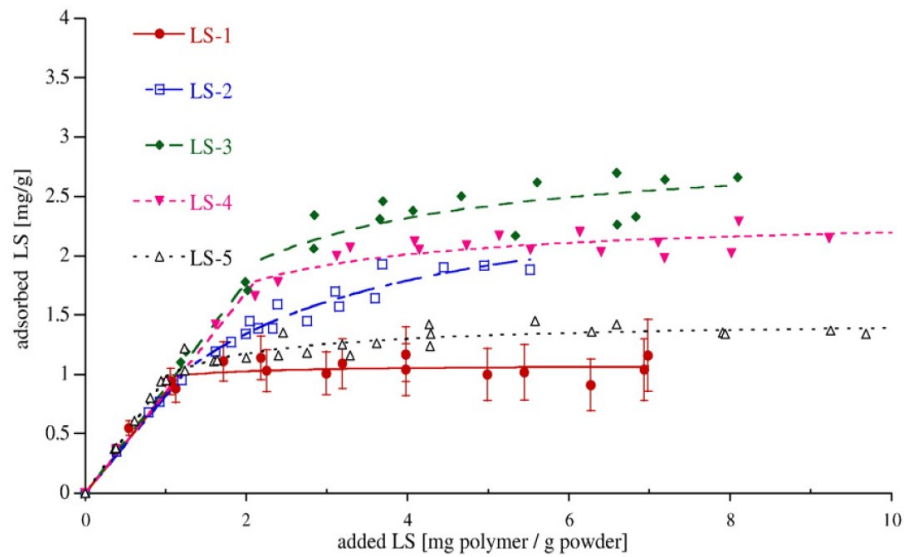


Figure 2.18 Adsorption isotherms of lignosulfonates of different compositions onto a MgO surface in NaOH solution. Reproduced with permission (Houst et al., 2008) Copyright Elsevier 2008.

The thickness of the adsorbed layer of admixtures must be considered because once adsorbed, the arrangement of the admixture affects the steric hindrances and therefore the dispersion efficiency. Earlier studies investigating the thickness of the adsorbed layer on the surface of a clinker explored the use of Auger electron spectroscopy (AES). More recent studies measure the thickness of the steric layer by Atomic Force Microscopy (AFM) (Kauppi et al., 2005). AFM provides a more detailed analysis of the topography of a surface while simultaneously probing surface forces, allowing for direct measurements of the forces between the particles as well as determination of conformational effects of polymers (Maver et al., 2013).

### 2.3.4 Admixture working mechanism

The working mechanism of chemical admixtures in cement systems involves the adsorption of the polymers onto the particle surface, changing their charge distribution and leaving the total charge on the surface of the particle negative, subsequently lowering their zeta potential (Kashani et al., 2014). As these now negatively-charged particles approach each other, there are inter-particle electrostatic repulsions and steric hindrances induced that prevent the formation of agglomerates (Colombo et al., 2017). A schematic diagram of these mechanisms is shown in Figure 2.19. These electrostatic repulsions are due to the charges on the particles while the steric forces are due to the overlapping of the adsorbed layers upon approach. The extent of steric forces induced depends on the thickness of the adsorption layer as well as the arrangement of the adsorbed polymer in solution (conformational effects) after adsorption (Houst et al., 2008), (Flatt et al., 2009). This adsorption thickness when sufficient keeps the particles separated and at these separations the van der Waals forces are too weak to cause the particles to attract (Malvern, 2000). Steric repulsive forces were first evidenced in cements by experimentation via atomic force microscopy and zeta potential studies by Uchikawa et al., (1997). In this study, researchers found a linear correlation between the forces acting between the particles and the flow of the cement, while this correlation was not found between zeta potentials and the flow of the cement, especially with addition of a polycarbonate based admixture. This suggests that another force other than the electrostatic repulsive force contributed to the dispersion of the cement particles (Uchikawa et al., 1997). For lignosulfonate admixtures, the high degrees of cross-linking and polydispersity mean that significant steric forces can be induced as the adsorbed coil can only occupy a small area on the cement particles. A proposed adsorption mechanism is presented in Figure 2.20. Kauppi et al., (2005) even suggested that steric hindrances may be greater contributors to dispersion than electrostatic

repulsions for these admixtures, therefore greatly affecting their efficiency. Steric stabilisation of high electrolyte systems by lignosulfonates was suggested by Le Bell, (1984) who considered that given the ability of lignosulfonate molecules to expand and shrink in different electrolyte concentrations, it is probable that the sulfonate groups reach out farther into the solution, dragging part of the diffuse layer with them (Le Bell, 1984). In contrast, Uchikawa et al., (1997) maintained that the dispersion of particles with addition of a naphthalene sulfonate based admixture, similar in structure to lignosulfonates, was attributed mainly to electrostatic repulsive forces.

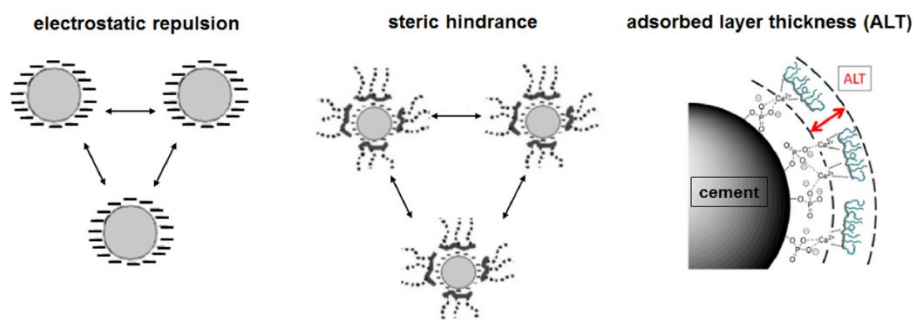


Figure 2.19 Schematic of the electrostatic and steric repulsive forces induced by the adsorption of dispersant admixtures onto cement particle surfaces. Adapted with permission (Lei et al., 2022) Copyright Elsevier 2022.

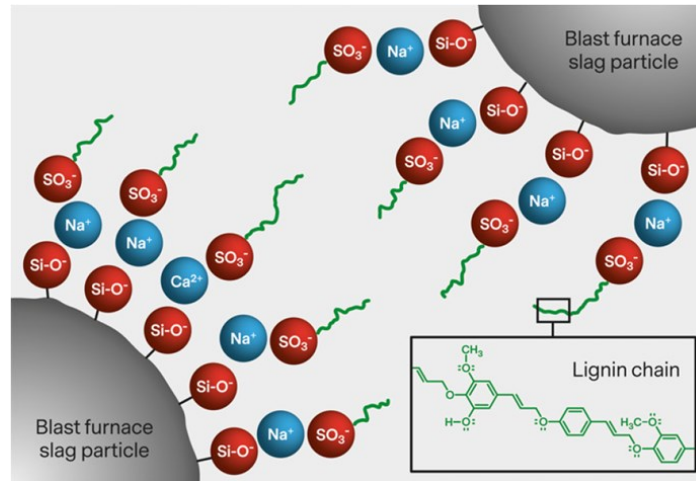


Figure 2.20 Schematic of the adsorption of lignosulfonate on slag particles (Luukkonen et al., 2019) © **copyright 2019** Reprinted by permission of Informa UK Limited, trading as Taylor & Taylor & Francis Group.

The effective adsorption of the admixture is in part dependent on the affinity of the polymer to the surface and this is influenced by the inherent molecular characteristics of the admixture (Houst et al., 2008). It has been suggested that that polymers with a large molecular weight, highly polydisperse, and with high anionic charge tend to have a higher adsorption efficiency (Puertas et al., 2005), (Flatt et al., 2009). There may also be competitive adsorption between the admixtures and the other ionic species such as hydroxyls, sulfate ions, and other polymeric admixtures in the system, which reduces their adsorption (Marchon et al., 2013). Anderson et al., (1986) reported that increasing the concentration of calcium sulfate decreased the amount of admixtures adsorbed by the cement likely due to the competition for adsorption between the sulfate ions and the anionic admixture.

The formation of ettringite during early hydration of Portland cement leads to further uptake of admixtures by this product phase due to its positive zeta potential (Plank & Hirsch, 2007). As lignosulfonates are anionic admixtures, they adsorb to the positive sites on the cement particles. In Portland cement, there is an uneven adsorption of lignosulfonate onto the four

main cement phases (Colombo et al., 2017), with much of the adsorption on aluminates and ferrite phases due to the anionic nature of the polymer (Yoshioka et al., 2002). Adsorption on the hydration products also occurs, with ettringite being the main adsorbing phase. This is because ettringite has the highest positive zeta potential of all the hydration products and therefore has the highest potential for adsorption (Plank & Hirsch, 2007). Small amounts of admixture also adsorb onto the C-S-H phases as more  $\text{Ca}^{2+}$  becomes incorporated (Johann Plank & Hirsch, 2007). As hydration proceeds, there will be loss of slump over time because of the loss of the admixture from the particle surfaces as hydration products form (Miyake et al., 1985). This loss of slump is due to the formation of the main hydration phase, C-S-H or C-A-S-H gel, as their bonds overcome the electrostatic and steric forces between the particles. The amount of the phase with the highest potential for adsorption in the cement greatly determines the uptake and therefore the dosage of the admixture. However, when added in excess, admixtures can cause problems such as substantial retardation and bleeding (Fernández-Altable & Casanova, 2006).

For low calcium systems such as silica fume, the interaction between the surface of the cement particles and polycarboxylate based admixtures follows adsorption via the hydroxyl groups on grafted side chains, which form hydrogen bonds with the silanol groups on the silica-rich surface of the particles (Hommer, 2009), (Walkley et al., 2022). It would be reasonable to assume a similar adsorption mechanism for other low calcium systems such as low calcium fly ash and metakaolin.

Adsorption of lignosulfonate on cement particles may not be the only mode of admixture consumption in cement. A previous study by Palacios et al., (2009) presented findings that Portland cement pastes adsorbed twice as much admixtures (naphthalene, melamine and vinyl copolymer admixture) as alkali activated slag pastes with similar surface areas, and that pH was not a contributing factor to this adsorption behaviour. Admixtures may undergo

intercalation in the hydration products, mainly in the AFm phases. This intercalation in the layered double hydroxide (LDH) compounds occurs when anionic polyelectrolytes replace some of their hydroxides (Colombo et al., 2017). This means that the intercalated admixture is not available for adsorption and particle dispersion, and therefore a higher dosage is required to reach the desired workability.

Another mechanism is complexation, whereby the functional groups from the admixture form complexes with the calcium ions in the pore solution, thereby inhibiting the nucleation and growth of Ca-rich species (Puertas et al., 2005). This mechanism increases the uptake of admixture, and simultaneously decreases the amount of free  $\text{Ca}^{2+}$  in the pore solution. These complexes may still adsorb on the cement particle and hydrates to form multilayers, similarly to the multilayer adsorption mechanism already discussed (Colombo et al., 2017). After monolayer adsorption is complete, the particles are left with a negative charge on which  $\text{Ca}^{2+}$  ions are electrostatically attracted and bond with them. The now positive double layer has more adsorption sites for more lignosulfonates to adsorb, thereby increasing their uptake (Colombo et al., 2017).

## **2.4 Conclusions**

In summary, there has been a lot of research and development towards the use of alkali activation as a route to yield high performing cements with a lower environment impact than the conventional cement. This has resulted in increased interest in this field from both academic research and industrial applications over the years. The use of admixtures in addressing the issues of uncontrollable workability and unpredictable rheological properties of alkali activated cements has yielded inconsistent and even contradictory results. The mechanisms by which the

interactions of alkali activated cements with admixtures bring about the properties of these cements are poorly understood and rarely discussed. A closer look at the lignosulfonates used as admixtures highlighted that the performance of these materials is highly dependent on the chemical environment around them such as pH and ionic strength. It has been elucidated that the working mechanisms of these admixtures in cements are driven by electrostatic repulsions and possibly some steric hindrances. The limited understanding of how these admixtures perform in alkali activated cements has contributed to a limited progress in the open literature.

The following chapters will endeavour to apply the knowledge on the chemical action of lignosulfonates in alkaline media to better understand how they behave in the chemical environment presented by alkali activated cements. The study challenges the hypothesis suggesting chemical instability of lignosulfonates in alkaline media, and therefore presents a detailed account of the behaviour of these admixtures in varying chemical environments. The working mechanisms of lignosulfonates as admixtures in alkali activated cements are studied to provide advances in understanding their dispersion potential in these cements.

## Chapter 3 MATERIALS AND EXPERIMENTAL METHODS

### 3.1 Materials

#### 3.1.1 Precursors

A low calcium fly ash from Baumineral GmbH, Germany and ground granulated blast furnace slag (GGBFS) supplied by ECOCEM, France were used as precursors in this study. The chemical composition of the fly ash and slag determined by X-ray Fluorescence (XRF) spectroscopy are reported in Table 3.1. The particle size distribution (PSD) obtained by laser diffraction using a Malvern Mastersizer 3000 is shown in Figure 3.1. The PSD showed  $D_v(90)$  values of 85.2 and 29.9  $\mu\text{m}$  for fly ash and GGBFS, respectively. The slag had a specific density of 2880  $\text{kg/m}^3$ , a BET surface area of 1070  $\text{cm}^2/\text{g}$  and a Blaine fineness of  $450 \pm 30 \text{ m}^2/\text{kg}$ . The fly ash had a specific density of 2360  $\text{kg/m}^3$ , a BET surface area of 1700  $\text{cm}^2/\text{g}$  and the Blaine fineness of the fly ash was not determined. The materials were characterised for the RILEM technical committee (Provis et al., 2019). The fly ash and GGBFS were used in Chapter 5 and Chapter 6.

Table 3.1 Chemical composition of the precursors determined by XRF. LOI corresponds to the loss on ignition measured in air at 1000 °C .

Materials	Chemical composition (wt.%)								
	SiO <sub>2</sub>	Al <sub>2</sub> O <sub>3</sub>	CaO	MgO	Na <sub>2</sub> O	K <sub>2</sub> O	Fe <sub>2</sub> O <sub>3</sub>	TiO <sub>2</sub>	LOI
<b>Fly ash</b>	54.5	22.7	5.8	2.5	0.9	1.8	7.3	0.9	0.4
<b>Blast furnace slag</b>	37.4	10.5	43.4	7.0	0.2	0.3	0.4	0.5	0.0

The GGBFS chemical composition gives a basicity coefficient  $K_b = (\text{CaO} + \text{MgO})/(\text{SiO}_2 + \text{Al}_2\text{O}_3)$  of 1.05, a CaO/SiO<sub>2</sub> ratio of 1.16 an Al<sub>2</sub>O<sub>3</sub>/SiO<sub>2</sub> ratio of 0.28, considered suitable for

alkali activation (Provis & van Deventer, 2014). This high Al/Si ratio indicates that there would be an expectation of a high degree of aluminium substitution for silicon in the C-(A)-S-H structure during product formation.

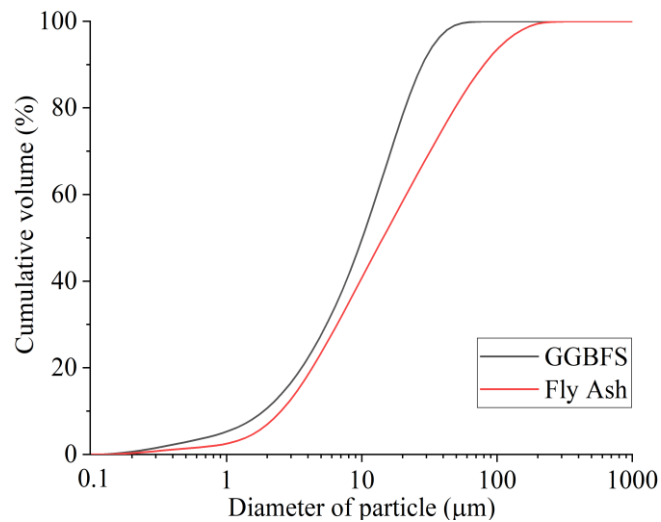


Figure 3.1 Particle size distribution of the ground granulated blast furnace slag and fly ash obtained by laser diffraction using a Malvern Mastersizer 3000.

The microstructural characteristics of the starting raw materials were evaluated by scanning electron microscopy (SEM) and X-ray diffraction (XRD). The slag has more angular particles while fly ash presented more spherical particles as shown in Figure 3.2. These properties are expected to have an impact on the rheological properties under study.

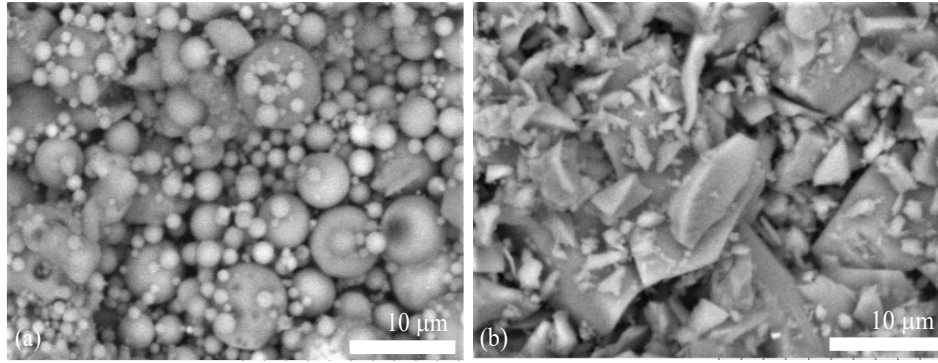


Figure 3.2 Scanning electron micrographs of (a) fly ash and (b) GGBFS.

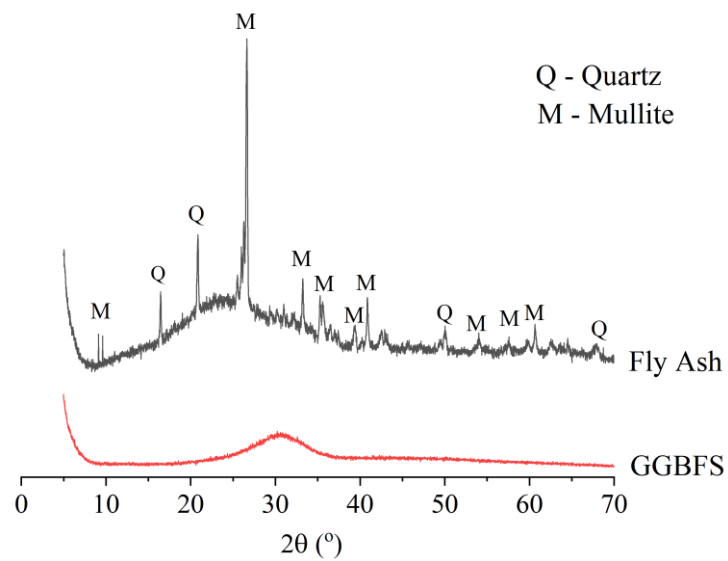


Figure 3.3 X-ray diffractograms of the starting materials fly ash and ground granulated blast furnace slag.

The X-ray diffractogram of the precursors shown in Figure 3.3 show that these materials have different crystallinities. It has already been established by previous researchers (Fernández-Jiménez & Palomo, 2003) that this crystallinity plays a key role in the reactivity of the materials during activation. The slag consists of a mainly amorphous phase which is more readily dissolved by the alkaline solution thereby increasing its reactivity (Fernández-Jiménez & Palomo, 2003). The broad peak from the slag at around 30–31° 2θ reflects the short range order of the CaO-Al<sub>2</sub>O<sub>3</sub>-MgO-SiO<sub>2</sub> glass structure (Wang & Scrivener, 1995). The fly ash has

an amorphous component as evidenced by a halo between 20-35 °2θ, with some minor crystalline phases, mainly quartz and mullite, which are considered to be inert (Fernández-Jiménez et al., 2006). This contributes in part to the lower reactivity of the fly ash compared to slag, along with differences in glass chemistry.

### **3.1.2 Activator**

The sodium silicate solution used was provided by PQ Silicates, UK and had a composition of 29.4% SiO<sub>2</sub>, 14.7% Na<sub>2</sub>O and 55.9% H<sub>2</sub>O by mass. The initial modulus (molar ratio SiO<sub>2</sub>/Na<sub>2</sub>O) was 2.06, which was reduced to 1.5 for use in experimental test work with the addition of 10 M sodium hydroxide solution. The addition of NaOH reduced the highly viscous nature of sodium silicate and also increased the pH of the activator, thereby improving the hydration capacity of the precursors (Huanhai et al., 1993). The H<sub>2</sub>O/Na<sub>2</sub>O ratio was adjusted from 13 to 11 with the addition of the NaOH solution. The sodium hydroxide solution was prepared from 98% purity NaOH pellets (Sigma Aldrich, UK) dissolved in deionised water and allowed to cool. The solutions were mixed and stirred at 84% sodium silicate and 16% sodium hydroxide by weight to achieve the required modulus and H<sub>2</sub>O/Na<sub>2</sub>O ratio. The activator was prepared 24 hours before paste mixing to allow for heat dissipation and avoid precipitation of solid hydrates if left for too long (Tan et al., 2017).

### **3.1.3 Admixtures**

Four types of lignosulfonate admixtures were used in this study; these were calcium-based lignosulfonates with varying compositions and different sources (softwood and hardwood

trees), provided by Borregaard Lignotech, Norway. A complete characterisation of the lignosulfonate admixtures is provided in Chapter 4.

### 3.1.4 Sample preparation and mixing procedure

In this study, GGBFS and fly ash were activated with the same sodium silicate activator described in section 3.1.2. The slag required a higher activator/precursor and total water/binder ratio as shown in Table 3.2 compared to fly ash, to achieve a reasonable paste workability by way of a visual assessment of the homogeneity of the paste. This is an early indication of the reduced workability of the slag compared to the fly ash, which can be attributed to the geometry of the particles and higher reactivity of the slag.

Table 3.2 Summary of the mix ratios, defined on a mass basis.

	Activator/ precursor	Water/binder
Alkali activated slag (AAS)	0.71	0.40
Alkali activated fly ash (AAFA)	0.51	0.28

The pastes were prepared by mixing the components in the above-mentioned ratios and according to the addition orders below for 5 minutes at low speeds of 100 rpm then a further 10 minutes at higher speeds of 400 rpm, in a Heidolph mixer shown in Figure 3.4. The high speed and long mixing times ensured a homogenous mixing of the pastes. Different orders of admixture addition were investigated:

- in simultaneous addition (SA) all the components were mixed at the same time,
- in delayed addition (DA) the LS was added 3 minutes after start of mixing, and

- in prior addition (PA) the admixture was initially mixed with the activator and the precursor later added.

Pastes without any admixture were prepared and used as control samples.



Figure 3.4 High speed mixing of the waterglass slag activated paste.

The efficacy of different types of lignosulfonate admixtures as a function of their dosage was determined and a wide range of dosages used to determine an optimum where the workability was improved the most and the paste had the least viscosity. The lignosulfonate powder admixture was added in dosages of 0.1, 0.3, 1.0 and 3.0 wt.% of the precursor. No pre-treatment of these powders was carried out i.e., they were used as received.

### **3.2 Analytical Techniques**

Techniques used in the analysis of the properties of the alkali activated cement discussed in Chapter 5 are introduced, as well as the theoretical background of the nuclear magnetic resonance spectroscopy and x-ray photoelectron spectroscopy techniques. Other techniques can be found in the relevant chapters.

### 3.2.1 Workability (minislump)

The workability of the pastes was investigated using mini slump tests. There currently does not exist a standard procedure for slump/spread measurements of cement pastes; this study follows the procedure outlined by (Tan et al., 2017). This is a simple and easy technique that can be used to investigate the plasticising effect of the lignosulfonate admixtures in alkali activated cement pastes. The technique works on the principle that the paste will flow under gravity, but the shear stress will keep decreasing until it is the same as the yield stress of the paste at which point it will stop flowing (Tan et al., 2017).

A mini slump test was carried out 20 minutes after stopping mixing (outlined in section 3.1.4) using a downscaled Abrams cone geometry of 19 mm top diameter, 38 mm bottom diameter and 57 mm height shown in Figure 3.5.

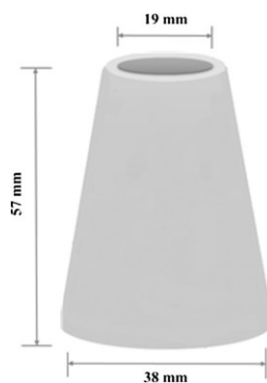


Figure 3.5 Downscaled Abrams cone.

The extended period of testing after mixing gives a good indication of slump loss of the pastes with and without lignosulfonates added. The cone was placed on a flat, level surface that had been cleaned with isopropanol to ensure there are no restrictions to the flow of the paste. The cone was filled with paste and tapped several times to remove air bubbles, and then lifted upwards very slowly to minimise inertial effects. The paste was allowed to flow until it stopped,

two perpendicular diameters were measured using vernier callipers, and the average was taken as the slump diameter. The data are presented as relative slump calculated as shown:

$$\Gamma_p = \left(\frac{d}{d_o}\right)^2 - 1 \quad \text{Equation 3.1}$$

Where,  $\Gamma_p$  is the relative slump,  $d$  is the average of 3 averaged measured diameters of the spread, and  $d_o$  is the cone bottom diameter (Nematollahi & Sanjayan, 2014).

One of the limitations of this technique is human error, it is crucial to follow the appropriate testing procedure for each sample to avoid unreliable and scattered test results. There is also an influence of the environment if the tests are carried out in ambient air and at room temperature which may result in scattered results. To reduce the effect of these limitations on the results, for the same mix, three measurements were taken and fresh replicate pastes of the same formulation to calculate an average and obtain more reliable data. These slump results show the flow extent compared to the sample without any admixture addition. The results can be related to one rheological parameter of the pastes, the yield stress, which is why they are not sufficient to completely characterise the fresh state behaviour of the pastes. The interpretation of the slump test results is limited because it is a single point test. It is therefore even more limited for comparing non-Newtonian fluids with different viscosities and shear rates (Fernández-Altable & Casanova, 2006).

### **3.2.2 Rheology**

Rheological studies were conducted to characterise the fresh state properties of the pastes further. For these studies, factors affecting rheology such as the nature of the activator, mixing

protocol, temperature and testing time were kept constant to reliably determine the effect of the admixtures on these pastes (Han & Ferron, 2015). The effect of the admixture on the internal structure of the paste can be investigated. The rheological tests initially involve increasingly exerting shear on the paste, until the yield point is reached when the network collapses and the system begins to flow due to particle deflocculation (Qing-Hua & Sarkar, 1994).

The rheological behaviour of each sample was assessed using a four-blade rotational ViscoTester VT550, starting 15 minutes after mixing was stopped. The viscotester was used to measure and record the shear rate ( $\dot{\gamma}$ ) and shear stress ( $\tau$ ) over time. The ASTM C1749, 2017 standard for the measurement of the rheological properties of hydraulic cementitious paste using a rotational rheometer, was followed in this study. The test was set up to increase the shear rate from 0 to 20 s<sup>-1</sup> for 20 s, held at 20 s<sup>-1</sup> for 5 seconds, followed by a downward ramp from 20 - 0 s<sup>-1</sup> for another 20 s. This is illustrated in Figure 3.6. These low shear rates were used to avoid inertial effects, and preliminary tests showed a hysteresis at high shear rates due to the high viscosities of the AAS pastes.

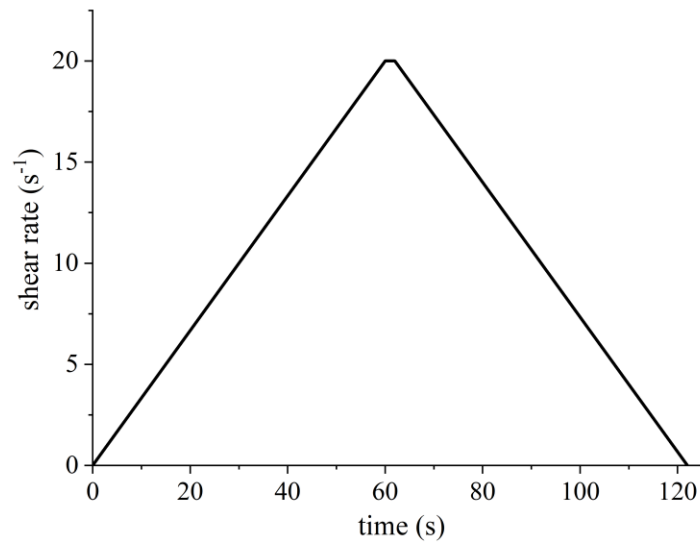


Figure 3.6 The upward and downward ramp of the rheology test.

The downward ramp was used for result interpretation as the system is at equilibrium and more reliable results can be observed. The following assumptions were made in following this technique; the paste is homogenous, the slip at the wall is negligible, and the flow is laminar (Feys, 2012). Particle migration where the paste moved outward away from the blade was observed at very high shear rates; this error may result in incorrect interpretation of thixotropic behaviour. Therefore, to avoid the effects of particle segregation and migration, low shear rates ( $<20 \text{ s}^{-1}$ ) are used for interpretation of the rheological behaviour of these pastes. Lower shear rates are followed for these pastes to avoid paste being ejected from the rotor or the formation of a plug around the rotor leaving a thin layer between the plug and the container wall, which may happen at high shear rates (Palomo et al., 2005).

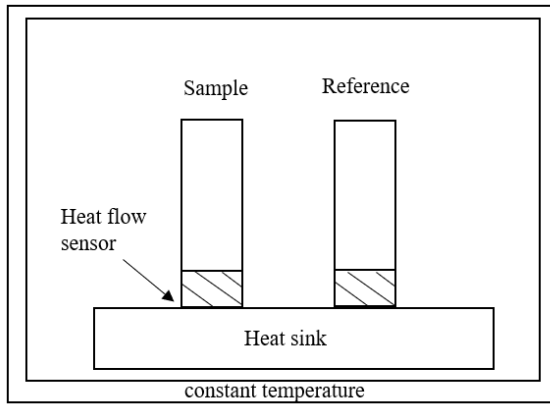
The experimental data were fitted using the Herschel-Bulkley model to describe the rheological behaviour of the pastes after mixing. This is a generalization of the Bingham and power law models. The experimental data was fit into this model and the rheological parameters determined. The estimation of the static yield stress ( $\tau_y$ ) relies on the measurements

at the lowest flow rates where uncertainty of the measurement is highest, which is a limitation of this model fitting procedure. This limitation is discussed in section 2.1.1.

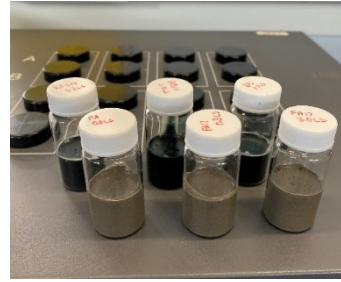
### **3.2.3 Isothermal Calorimetry**

The exothermic nature of the cement reactions allows for monitoring of the heat produced under constant temperature which is related to the rate of reaction during the activation of the precursors with an alkaline solution. This technique is ideal for quantifying the effect of the lignosulfonate admixtures on the hydration process of these cements. Key information on the stages of hydration and the effect that cement-admixture interactions have on the chemistry of these processes can be obtained. This technique also provides insight into the setting characteristics, early strength development as well as compatibilities between the admixtures and the cement pastes.

The isothermal calorimeter shown in Figure 3.7 measures the heat released from of a sample which is linked to a reference by a heat sink. The reference is a substance with similar thermal properties to the sample but has no heat production. A temperature gradient exists between the sample and the heat sink, as heat is produced by the sample and a voltage output is produced across the heat flow sensor. The measured signal is the difference between the sample-signal and reference-signal. The voltage produced is proportional to the rate of heat and the total heat produced by the sample. The heat evolution from isothermal calorimetry correlates to the continuous cement hydration of the pastes over time. The effect of the admixture will then be reflected by the changes on the hydration curves obtained. The shape of the rate of heat flow vs time curve shows the hydration process of the cement while the integrated heat flow vs time curve shows the extent of cement hydration.



(a)



(b)

Figure 3.7 Schematic of the isothermal calorimetry setup (a), examples of the alkali activated fly ash and alkali activated slag pastes after testing (b).

The isothermal calorimeter used in this study was a TA Instruments TAM Air calorimeter maintained at 20 °C. The sample preparation procedure followed for this study is as outlined in the ASTM C1679, 2017 standard. The mix design components are as outlined in section 3.1.4; however, the mixing time was reduced to 3 minutes which is the maximum time allowable. Immediately after mixing, 20 g of paste was transferred to a glass ampoule, and water at the same mass as in the sample was used as the reference sample and introduced to the calorimeter. The total loading time after the end of mixing was less than 2 minutes. All results were normalized by the total mass of the paste loaded. For a relative comparison of the hydration kinetics of the samples, the dosage of the different types of lignosulfonates was varied as follows; 0, 0.3 and 3 wt.% relative to the mass of the precursor.

Isothermal calorimetry is a highly sensitive (registering heat flows to a precision of  $\pm 4 \mu\text{W}$ ) and useful technique in quantifying the effect of the admixture on the hydration process of these cements to yield highly reproducible results. One of the notable limitations of this technique is the initial loss of heat to the surrounding during mixing as the samples are mixed

outside the calorimeter because the reaction between the precursor and activator is immediate. However, in-situ mixing of these samples was not possible due to the high viscosity of the pastes. Regardless, comparisons can be drawn between the control sample without any admixture and the samples with increasing doses of lignosulfonates.

### 3.2.4 Compressive strength testing

The mechanical properties of the alkali activated pastes were investigated by compressive strength testing with the set ups shown in Figure 3.8 and Figure 3.9. This is an important and common test used in research to determine the adequacy of the mix design and curing conditions, as well as key insights into the hydration process of the products. It is used commonly in industry to examine if the products meet the design requirements and to perform quality control checks. In this study, compressive strength testing is used to determine the mechanical strength development of the pastes using the optimised mix designs and evaluate how lignosulfonates affect this development. This provides insight into the chemical or physical changes to the hardened alkali activated cement matrix brought about by the addition of lignosulfonate admixtures.



Figure 3.8 The 300 kN Shimadzu at start of sample testing and untested and crushed samples.



Figure 3.9 3000 kN cube crusher and the test setup.

The mixing procedure is as outlined in section 3.1.4, the pastes were then cast into 50 mm cubes according to the ASTM C109/109M-16a, 2016 standard test method, sealed, and stored in plastic bags. A 100% relative humidity environment was provided using a damp tissue material to avoid drying and microcracking of the cubes. The samples were then demoulded after 1 day and cured for a total of 7 and 28 days in a 20 °C environment chamber. The 300 kN Shimadzu machine shown in Figure 3.8 was used to measure the maximum load applied before failure for the 7 days cured samples and the 3000 kN cube crusher shown in Figure 3.9 was used for the higher strength alkali activated slag 28 days cured samples. To ensure a uniform load distribution, the upper and lower plates were held in central position and the cubes were placed in the centre of the stage with the smooth sides facing the plates. When applying the load, the upper plate of the 300 kN Shimadzu approached the sample at a rate of 100 mm/min until it touched the smooth surface of the sample at 50 N, followed by a gradual

loading rate of 1200 N/s, which was applied until the force reached half the maximum load and stopped.

For each sample, the maximum load was taken as the average of 3 cubes and used to calculate the compressive strength as shown:

$$f_m = \frac{P}{A} \quad \text{Equation 3.2}$$

Where:

$f_m$  = compressive strength in [MPa]

$P$  = maximum load of the test machine in [N]

$A$  = cross sectional area of the cube in [mm<sup>2</sup>]

### 3.2.5 Vicat setting time

The setting time is presented as an initial setting time and final setting time. The initial setting time is the point at which the hardening of the cement starts, and the final setting time is when the cement has fully hardened and lost its plasticity. The hydration retardation or acceleration of the pastes due to the addition of lignosulfonates can be investigated by this method.

This study followed the ASTM C191, 2019 standard test method using the Vicat apparatus to determine the initial and final setting times. This test method is based on monitoring the depth of needle penetration into the paste. The apparatus is set up such that there are periodic penetrations of the 1 mm thickness needle into the paste. Before initial setting, the needle can penetrate the full depth of the paste, but upon initial setting this full penetration is inhibited, and the final setting of the paste is achieved when the needle can no longer penetrate the paste.

The initial setting time is the time elapsed between the initial contact of precursor and activator and the point at which the needle stopped penetrating the full depth of the paste. The final setting time is the total time elapsed between the initial contact of the precursor and activator and the point at which the needle penetrates a constant depth. These points are illustrated in Figure 3.10.

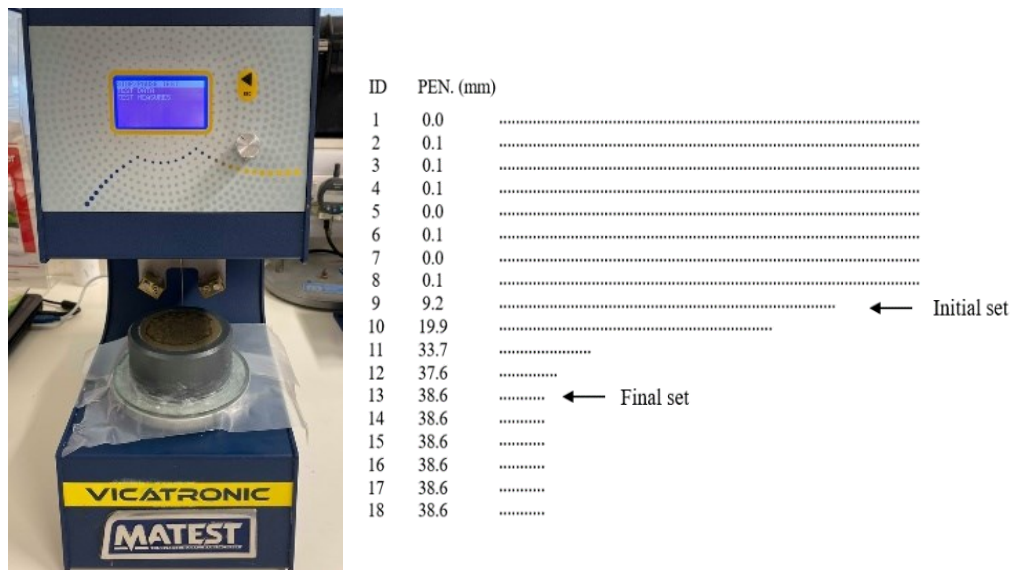


Figure 3.10 Vicat instrument and the experiment sheet showing the penetration depths over time.

The sample preparation procedure is as outlined in section 3.1.4. The Vicat apparatus was kept in a temperature-controlled environment, at 20 °C and 98% humidity. There may be variations in setting times with mixes of the same mix designs, and so the setting times were taken as averages of three measurements of pastes prepared at different times with the same formulations.

### **3.2.6 Scanning electron microscopy**

The hardened cement paste was cut and mounted on epoxy resin. This was followed by grinding and polishing to a 0.25  $\mu\text{m}$  finish using a diamond suspension. Before analysis the polished surface was carbon coated. Analysis was conducted on a low vacuum Hitachi analytical benchtop SEM TM3030 with an integrated Bruker Quantax 70 EDX detector, at an accelerating voltage of 15 kV.

### **3.2.7 Thermogravimetric Analysis**

The hardened cement paste was cut, ground, and sieved through a 63  $\mu\text{m}$  aperture sieve ahead of analysis. The equipment used was a Perkin Elmer TGA 4000 coupled with a Hiden Analytical Mass Spectrometer (HPR-20 GIC EGA). 40 mg of the samples were monitored at a heating rate of 10  $^{\circ}\text{C}/\text{min}$  from 30 – 1000  $^{\circ}\text{C}$  using alumina crucibles and nitrogen gas as the purge gas flowing at a rate of 40 ml/min.

### **3.2.8 Fourier Transform Infrared spectroscopy (FTIR)**

FTIR is an absorption spectroscopy technique that measures the amount of infrared radiation (IR) a sample absorbs at each wavelength. The principle behind this is based on the vibrations of the atoms of a molecule, where the molecules absorb IR at frequencies that are characteristic of their structure. A beam of IR passes through a sample and when the frequency of the IR is the same as the vibrational frequencies of the bonds (resonant frequencies), absorption occurs. The infrared radiation absorbed by the molecule is converted to energy of molecular vibration, and this energy is also accompanied by rotational energy changes. Therefore vibrational-

rotational bands at certain frequencies can be monitored. These vibrational-rotational changes are dependent on the mass of the atoms, the force constants of the bonds and the geometry of the atoms (Silverstein et al., 2005).

The FTIR spectra are presented as plots of absorbance or transmittance intensities vs wavenumber (number of wavelengths per centimetre). Functional groups can then be identified with the use of reference peaks from literature. Stronger bonds and lighter atoms vibrate faster and can be expected to be seen at high wavenumbers on the spectrum. Examples of such bonds are at wavenumbers 4000 - 1500  $\text{cm}^{-1}$  and include functional groups such as -OH, C=O, N-H and  $\text{CH}_3$  where there are H single, double and triple bonds. Below 1500  $\text{cm}^{-1}$  is the fingerprint region where bands are generally due to the intramolecular interactions and are highly specific to the material under investigation (Silverstein et al., 2005).

To measure the FTIR spectra, a pellet was prepared by measuring 0.2 g of solid KBr (which is transparent to IR) with 0.2 mg of the sample and grinding for 3 minutes to get a homogenous mixture. This mixture was then transferred to a mould and flattened. A pressure pump was used to make the pellet by applying 1 tonne of force for 1 minute followed by 10 tonnes for another minute. The pressure was released gently to ensure that the pellet did not have any cracks due to a sudden change in pressure. The pellet was then placed on the FTIR for measurement of 32 scans for the range of 4000 – 400  $\text{cm}^{-1}$ . A blank KBr pellet was used to measure the background before sample measurement. The measurements were taken in transmission resolution. Isopropanol was used to clean everything between scans to avoid contamination.

### 3.2.9 Nuclear Magnetic Resonance (NMR)

NMR was used to further ascertain the chemical structure of the lignosulfonates before and after chemical treatment. NMR works on the principle that atomic nuclei are electrically charged when a magnetic field is applied. This interaction with the magnetic field results in a nuclear spin, which is an intrinsic property of each nucleus. This spin presents as an alignment of magnetic moment parallel or antiparallel to the magnetic field. This is then pulsed with radiofrequency to produce a movement of spin and elevates the nuclei to a higher spin state. When the pulse is removed, the relaxation back to the equilibrium is recorded and is referred to as a free induction decay. This is then converted by Fourier transform to generate a spectrum of amplitude against frequency (recorded as a chemical shift relative to a known standard). Nuclei in different chemical environments can experience different magnetic field due to the shielding effects of neighbouring nuclei and will therefore differ in resonance frequency and therefore different chemical shifts (Silverstein et al., 2005).

Solid state NMR was more appropriate in this study as a solvent is not required which may otherwise interact further with the sample after treatment, this meant samples could be studied in their native state. Solid state NMR is known to have a relatively low resolving power compared to NMR in solutions, however, this can be improved by magnetic angle spinning and a cross polarisation technique which has a higher sensitivity than carbon NMR. This  $^{13}\text{C}$  cross polarisation magnetic angle spinning ( $^{13}\text{C}$  CPMAS NMR) approach was used in this study. Magnetic angle spinning (at  $54.74^\circ$  relative to the static magnetic field) minimises the line broadening of the spectrum. Cross polarisation allows for magnetisation to be transferred from one abundant nucleus e.g., protons to another e.g.,  $^{13}\text{C}$  nuclei (Leary & Newman, 1992). The proton nucleus is first excited, and its energy is then transferred to the carbon atom using a long low power pulse. The parameters used in this study are presented in section 4.3.2. The NMR

data was collected at the University of Sheffield chemistry department and performed by Dr Khalid Doudin.

### **3.2.10 X-ray photoelectron spectroscopy (XPS)**

XPS allows for high precision analysis of the surface chemistry of a sample. This is a well-established technique for polymer characterisation with a large chemical database. With this technique, the elemental composition, chemical and electronic states of the elements that exists in the materials can be identified.

XPS relies upon the photoelectric effect. Photons with known energy are directed at a surface, interact with and transfer photon energy to a core electron. The core electron is then ejected from the surface of the sample and is referred to as a photoelectron as illustrated in Figure 3.11 (Wren et al., 2011). The kinetic energy is measured by the XPS spectrometer, and the binding energy is determined as the difference between the photon energy, the kinetic energy, and the spectrometer work function ( $\Phi$ ). The binding energy is the energy required to remove an electron. Information about the electronic structure of molecules can then be obtained because the binding energy is characteristic of the chemical environment of the parent atom. The XPS spectra are identified by the core shell from which the electrons are emitted (1s, 2s, 2p, 3s, 3p, 3d etc) (Wren et al., 2011).

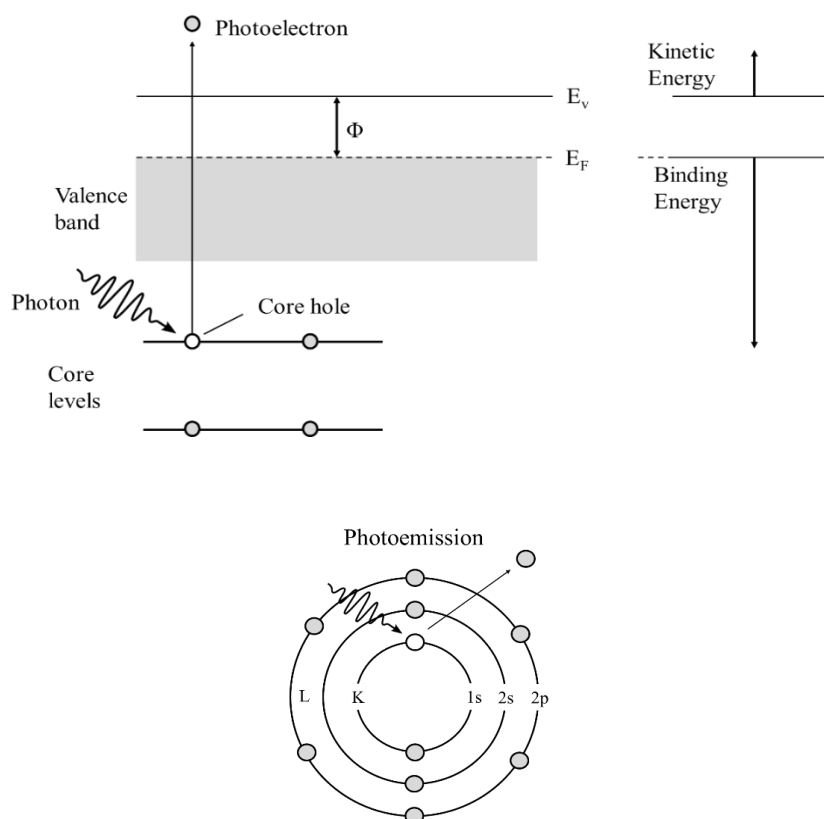


Figure 3.11 Schematic of the photoemission and Auger process adapted from Wren et al., 2011.

The conducting property of the lignosulfonates make these ideal for XPS analysis as an absolute energy scale can be established. There is no charge build up or need for charge compensation due to electrons being removed, as the material is conducting. The peak intensities give information on how much of a material is on the sample while the peak positions indicate the elemental and chemical composition. The parameters followed for this measurement are presented in detail in section 4.3.2. The XPS data was collected at the Harwell XPS – EPSRC National facility for XPS and the measurements were performed by Dr. Mark Issacs, University College London.

### 3.3 Experimental plan outline

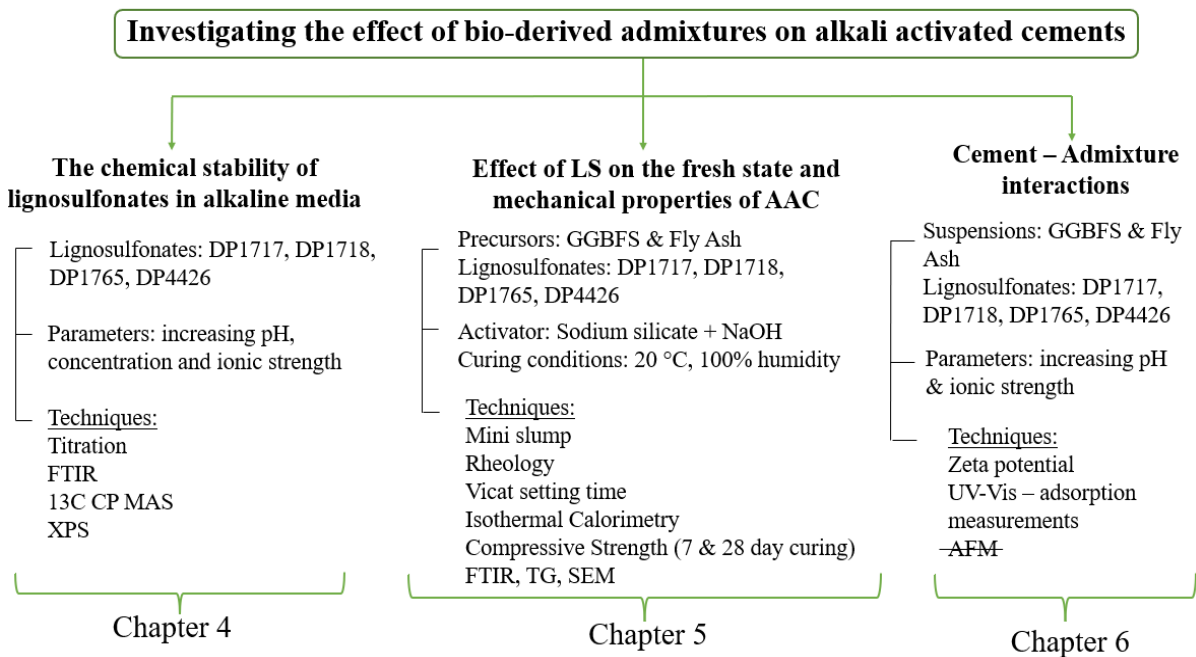


Figure 3.12 An experimental plan to achieve the main objectives of the study.

A summary of the experimental plan is outlined in Figure 3.12. The initial plan included wet cell Atomic Force Microscopy studies to better understand the adsorption behaviour of admixtures on alkali activated cements. This technique allows direct measurements of the interactive forces between the particles as a function of the distance from the surface when in aqueous solution. Steric forces can be investigated as well as conformation of the polymer once adsorbed on the surface. Unfortunately, due to the Covid-19 pandemic which resulted in limited to no access to laboratories for an extended period, it was not possible to carry out this study.

## **Chapter 4 CHEMICAL ACTION OF LIGNOSULFONATE ADMIXTURES IN ALKALINE MEDIA**

### **4.1 Introduction**

This chapter explores the fundamental behaviour of lignosulfonates in different chemical environments to establish if there are any chemical and structural changes to these polymers in these conditions. With this approach, we aim to better understand the effect that highly alkaline environments like those presented in cements have on the structure of these macromolecules. Alkali activated cementitious materials present highly alkaline environments with different ionic species; the behaviour of the polymers in such conditions becomes an important aspect to study and to establish if there is a correlation with their dispersion efficiency. Investigating the behaviour of lignosulfonates in alkali activated cement matrices presents a great challenge as the complexity is increased by the high concentration of electrolytes from the activator, ionic species from the precursor, and overall, very high ionic strengths. In trying to appreciate these complexities, an investigation into the chemical action/stability of lignosulfonates in dilute to concentrated solutions simulating the activator is a good starting point when trying to understand forthcoming interactions with the cementitious materials.

Insight into the behaviour of these polymers may be a step closer to explaining issues of incompatibility with the different cement precursors and activators used in these systems, where the chemical behaviour of the polymer may be suited for one chemical environment and not the other. The results obtained in this chapter may be correlated with the dispersion efficiency of the lignosulfonates in cement pastes to be discussed in Chapter 5. The data presented here also have relevance to other areas of research where lignosulfonate polymers are used. The increased knowledge and understanding of their behaviour may drive towards

the optimum use of these materials in different environments and may also highlight areas where there can be structural improvements to improve their efficiency. The differences in the molecular composition and structure of lignosulfonates has a direct effect on their physicochemical properties and therefore their applications (Madad et al., 2011). High and low molecular weight (Mw) lignosulfonates are investigated to ascertain whether molecular weight is a determining factor when the polymer is under chemical attack. High sugar and low sugar lignosulfonates are also investigated to determine the resistance of these molecules to chemical attack when the sugar content is reduced, as may be the case for some of the admixtures.

In previous studies, the procedures followed for chemical treatment and characterisation of superplasticisers to ascertain their stability are questionable. This is because in some studies there was no attempt to remove the solvent used for treatment, or this was not sufficiently done. It has been established that these polymers are pH-responsive, and therefore any adjustments enacted post-treatment that change their pH compared to the control may affect their behaviour and therefore the results obtained. One of the early studies investigating the degradation of admixtures in high alkaline solution carried out by Yilmaz et al., (1993) came to the conclusion that chemical treatment degraded sulfonated melamine formaldehyde while sulfonated naphthalene formaldehyde remained unaltered. In this study, upon treatment with KOH solution, the samples were neutralised with HCl, and the solvent evaporated off. In contrast, Palacios and Puertas (2005) did not outline any further steps post chemical treatment, that is, after mixing the admixtures with the alkaline solvent and before characterisation; conclusions were drawn that chemical admixtures are unstable in highly alkaline media. The presence of the solvent in these samples during characterisation was not considered and may have altered the results obtained. This study is referenced in much of the discussion about the instability of these polymers in cement systems. The two studies discussed above both investigated the

melamine-based and naphthalene-based superplasticisers in alkaline solutions but came to contrasting conclusions. And so, the methodology followed in this chapter was crucial.

## 4.2 Materials

Four types of lignosulfonate admixtures are studied in this chapter; these are calcium-based lignosulfonates with varying compositions and different sources (softwood and hardwood trees), provided by Borregaard Lignotech, Norway. The lignosulfonate powders as they were received are shown in Figure 4.1 and their chemical compositions are provided in Table 4.1. The characterisation of these samples was done by Vibeke Spernes in the “Lignosulfonate for future concrete project” in collaboration with the University of Sheffield and Borregaard.

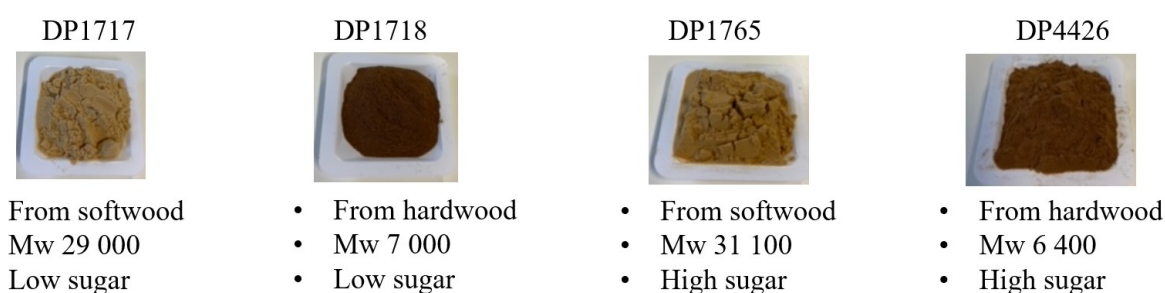


Figure 4.1 Lignosulfonate powders as received.

Table 4.1 Composition of the lignosulfonate powders as received.

		Full sugar, Ca-based from hardwood, <b>DP4426</b>	Low sugar, Ca-based from hardwood, <b>DP1718</b>	Full sugar, Ca-based from softwood, <b>DP1765</b>	Low sugar, Ca-based from softwood, <b>DP1717</b>
DM, %		97.9	98.9	98.2	98.1
MWD	Mw	6400	7000	31100	29000
	Mn	500	600	2200	2100
Total sugar, % on DM		11.5	<0.2	21.6	8.3
Total S, % on DM		6.1	7.3	5.5	6.5

Inorganic S, % on DM	1.1	1.9	1.8	1.9
Organic S, % on DM	5.0	5.4	3.7	4.6
SO <sub>4</sub> , % on DM	0.9	3.5	0.8	0.9
SO <sub>3</sub> , % on DM	0.2	<0.1	2.9	2.7
COOH, % on DM	10.4	15.1	5.9	7.1
Phenolic -OH, % on DM	1.5	1.6	1.4	1.4
Methoxyl, % on DM	13.4	14	8	9.9
Ca, % on DM	4.0	3.0	3.8	4.6
Na, % on DM	0.11	0.56	0.9	0.9
Al, mg/kg on DM	56	22	13	16
Cr, mg/kg on DM	0.5	0.7	0.4	0.5
Cu, mg/kg on DM	1.8	1.4	40	49
Fe, mg/kg on DM	75	74	42	54
Mg, mg/kg on DM	0.13	0.25	565	715
Mn, mg/kg on DM	62	64	201	239
Zn, mg/kg on DM	3.1	4.9	20	25
Ash, % on DM	10.5	11.7	10.7	12.3
Insoluble, w/w-%	1.1	3.0	0.02	0.55

DM: Dry matter

MWD: Molecular weight distribution

Mw: Weight average molecular weight

Mn: Number average molecular weight

The sodium hydroxide solutions were prepared by dissolution of the appropriate amount of NaOH pellets (Fisher Scientific UK) in deionised water.

### 4.3 Analytical techniques and procedures

Lignosulfonates present complex chemical structures, and a range of complimentary techniques are used in this chapter to provide a complete characterisation of these polymers to identify the structural differences between the untreated and chemically treated samples. Some

of the techniques used are presented in Chapter 3, and those specific to the current chapter are presented below.

### 4.3.1 Titration

The chemical behaviour and stability of the lignosulfonates as received were initially investigated through acid-base titrations. This simple technique allows qualitative and quantitative analysis of the polymer in increasingly alkaline and acidic environments. Interpretation of the forward and backward titration curves gives insight into the chemical and physical behaviour of the different types of lignosulfonates in these low and high pH environments.

In the relatively dilute solutions used here, the pH is defined by the negative logarithm of the hydronium ion concentration in the solution, as shown:

$$pH = -\log[H_3O^+] \quad \text{Equation 4.1}$$

The pH measurements were taken using the SevenExcellence pH meter supplied by METTLER TOLEDO. This instrument works by using electrode sensors. One sensor with a glass membrane is sensitive to the hydronium ions in solution, detecting the reaction between itself and the sample and then producing a signal. A second sensor which is referred to as the reference sensor is not responsive to the hydronium ions and will therefore produce the same, constant potential against the pH sensor potential which is measured (Mettler Toledo, 2007). The pH meter used in this study used a combination of the reference and pH electrode called a

combined pH electrode. The difference between the potential of these two sensors is used to determine the pH value of the solution, using Equation 4.2.

$$E = E_o + 2.3RT / nF * \log[H_3O^+] \quad \text{Equation 4.2}$$

Where:

E = measured potential

E<sub>o</sub> = constant (V)

R = gas constant (J·K<sup>-1</sup>·mol<sup>-1</sup>)

T = temperature in kelvin

n = ionic charge

F = Faraday constant (C·mol<sup>-1</sup>)

These measurements have an accuracy of ±0.05 pH units (Mettler Toledo, 2007).

The pH meter was initially calibrated before the start of every set of measurements with buffer/standard solutions of pH 4.01, 7.00, and 9.21. A magnetic stirrer was used throughout the pH measurements to ensure that the sample remains homogeneous and the potential measured is representative of the whole sample and not just the local environment of the electrode. There was also enough sample to ensure complete immersion of the electrode. When preparing the solutions, 0.4 g of lignosulfonate powder was mixed in 40 ml of deionised water, and complete dissolution of the lignosulfonate powder was ensured through mechanical agitation. The initial pH of the suspension was noted. These solutions were then titrated with a strong base of 0.1 M NaOH solution where small increments were added, and the pH was measured after each addition to produce a forward titration curve. NaOH was added until this curve plateaued, and further addition of the alkaline solution did not change the pH of the

solution, at which point titration was stopped. The back titration of the same solution was performed with a strong acid, 0.1 M HCl solution. This produced a curve that eventually plateaued and further additions of HCl did not change the pH of the solution, at which point titration was stopped. The back titration was carried out immediately after stopping forward titration and at a later age; after 3 days (samples were kept in an airtight and sealed bottle and under 20 °C during this period). The latter was carried out to determine if there was a time dependence on the chemical/physical action of these polymers in alkaline media.

The limitations of the sampling procedure followed in this study:

- There was no temperature control of the environment. The pH value of a sample is temperature-dependent, and the pH electrode gives a temperature-dependent measurement. The SevenExcellence pH meter is designed to record the temperature dependence using a temperature sensor and then compensates for it. This compensation is possible because a linear relationship exists between the temperature and the potential measured, and therefore the behaviour is fully predictable and compensated for by the inbuilt buffer temperature correction of the pH meter (Mettler Toledo, 2007).
- The experiment was done under ambient air conditions. It is important to consider the dissolution of atmospheric carbon dioxide into the solution while taking measurements as this may affect the results obtained. This would be expected to be more significant at high pH values, however, the experiment was not done for extended periods of time for a significant ingress of CO<sub>2</sub> to occur and the solutions were also kept in airtight and sealed containers.

### 4.3.2 Chemical treatment and characterisation

For a more detailed study of the chemical stability of lignosulfonates, the admixture samples described in Table 4.1 were subjected to different chemical environments; deionised water at neutral pH and increasing concentrations of NaOH solutions at 0.05, 0.1, 0.5, 5, and 10 M. The chemical treatment and washing procedures are shown in Figure 4.2. The treatment was achieved by manually mixing 2 g of LS powder with 2 ml of the solution attaining a homogenous mix. It is worth noting that it was observed that the dissolution of LS became increasingly limited as the concentration of the solution was increased. The mix was then dried under vacuum for 3 days in a desiccator. Sodium chloride salt and silica gel were placed inside the desiccator to absorb the evaporated water and accelerate the drying process.

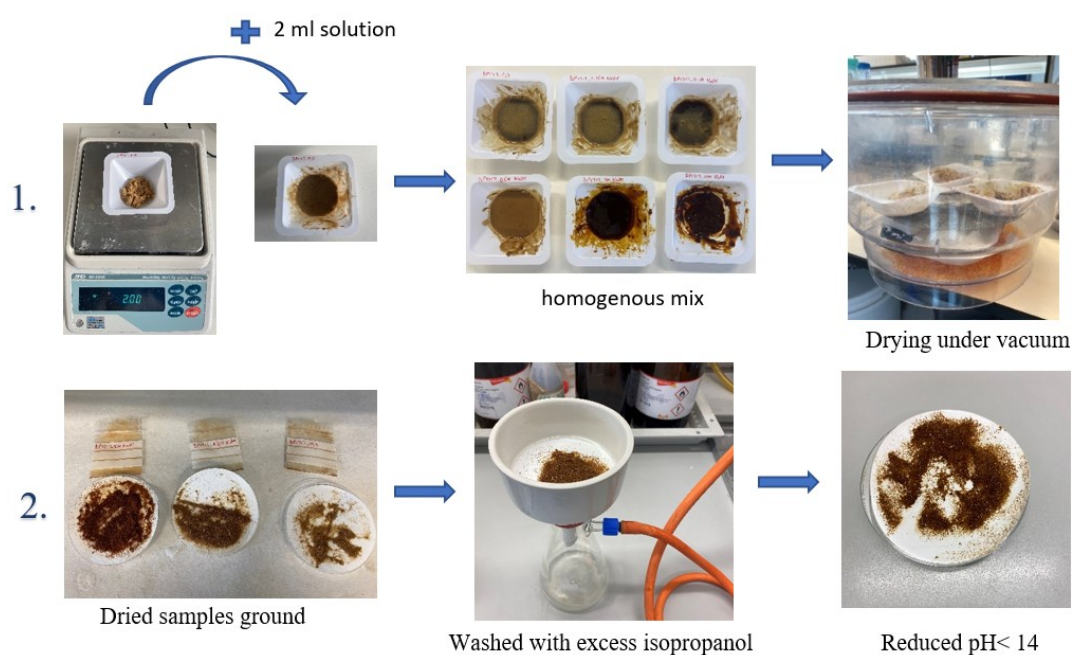


Figure 4.2 Procedure followed for the chemical treatment and washing process of the lignosulfonates.

Lignosulfonates are insoluble in organic solvents, and so upon drying, the now solid samples were ground and washed with excess isopropanol under vacuum filtration to remove the excess NaOH and reduce the pH of the sample to below pH 14, and then left to evaporate the isopropanol. It was apparent that washing with isopropanol was not sufficient as the pH was still high (especially for the high NaOH concentration samples) compared to the reference sample. As previously discussed in section 2.2, lignosulfonates are pH sensitive and so the varying pH values after only washing with isopropanol were not ideal for characterisation. This meant that the solution used for treatment was still present and so the excess  $\text{Na}^+$  and  $\text{OH}^-$  species on the sample had to be removed before characterisation. This was achieved by the ion exchange process using an Amberlite IRC120 H, hydrogen form resin supplied by Supelco, Sigma-Aldrich. The resin was initially activated and excess  $\text{H}^+$  ions on the resin were also removed by rinsing the resin with deionised water. A batch process was followed for this ion exchange step where 0.5 g of the now dried LS powder was first dissolved in 2 ml of deionised water and then mixed with the appropriate amount of resin. The measured amounts of the resin used were based on its ion exchange capacity. This step facilitated the removal of  $\text{Na}^+$  ions from the sample exchanged with  $\text{H}^+$  from the resin; the excess  $\text{OH}^-$  reacted with the  $\text{H}^+$  to reduce the pH even further. The ion exchange process is shown in Figure 4.3, following Equation 4.3 and Equation 4.4.

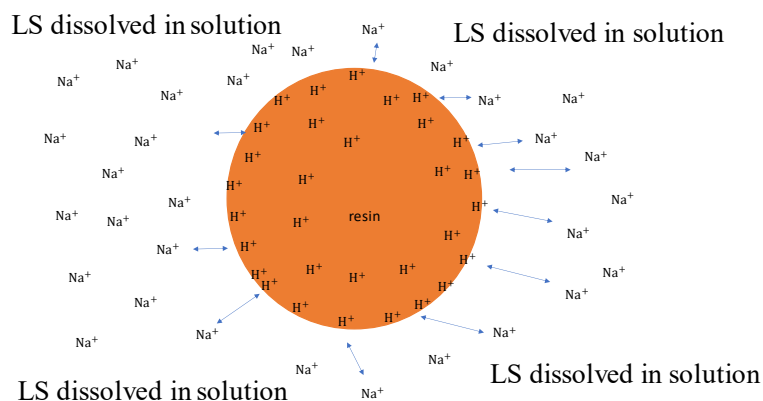
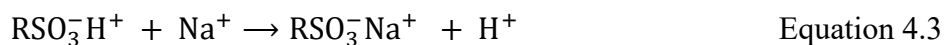


Figure 4.3 Schematic of the ion exchange process between the resin and the solution with lignosulfonate dissolved.



The final stage of the sample preparation process involved the separation of LS solution from the resin by vacuum filtration. The final product obtained was a concentrated suspension that was kept in a desiccator under a vacuum for the removal of excess liquid to obtain a solid sample. Sodium chloride salt and silica gel were placed inside the desiccator to absorb the evaporated water and accelerate the drying process. This rigorous washing and ion exchange step was essential to the characterisation of the lignosulfonate post-treatment that is not obscured by the presence of the treatment solution.

The compositional and structural changes of the lignosulfonates were determined by Fourier Transform Infrared (FTIR) spectroscopy using a PerkinElmer 100 FTIR spectrometer, operating with a resolution of 2 cm<sup>-1</sup> and recording 32 scans per sample. The sample preparation procedure is as outlined in section 3.2.8.

The samples were further analysed with solid state cross-polarisation magic-angle spinning  $^{13}\text{C}$  CPMAS NMR using a Bruker AVANCE III 400 spectrometer. For acquisition of the spectra, a spinning rate of 10 kHz MAS, with a 4s relaxation delay and 2 ms contact time were used. The spectrum was derived from 2000 scans with the chemical shift given as  $\delta$  in ppm from the external reference compound dimethyl sulfoxide (DMSO). All data were processed using Bruker TopSpin 4.1.3 software. This technique allowed for a non-destructive characterisation of the lignosulfonates; the key functional groups and bonding can be identified without destroying the native nature of the polymer.

Further analysis was done by X-ray photoelectron spectroscopy (XPS) to identify the elements present on the surface of the lignosulfonates before and after chemical treatment. This technique also gives information on what these detected elements are bonded to, and therefore any bond breaking or bond formation that occurs due to chemical treatment can be monitored.

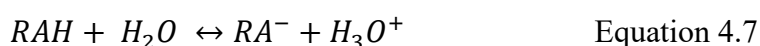
The XPS data was acquired using a Kratos Axis SUPRA using monochromated Al  $K\alpha$  (1486.69 eV) X-rays at 15 mA emission and 12 kV HT (180 W), and a rectangular analysis area of 700 x 300  $\mu\text{m}$ . High resolution spectra were obtained using a pass energy of 20 eV, step size of 0.1 eV and sweep time of 60s, resulting in a line width of 0.696 eV for Au  $4f_{7/2}$ . Survey spectra were obtained using a pass energy of 160 eV. Charge neutralisation was achieved using an electron flood gun with filament current = 0.4 A, charge balance = 2 V, filament bias = 4.2 V. Successful neutralisation was adjudged by analysing the C 1s region wherein a sharp peak with no lower BE structure was obtained. Spectra have been charge corrected to the main line of the carbon 1s spectrum (adventitious carbon) set to 284.8 eV. All data was recorded at a base pressure below  $9 \times 10^{-9}$  Torr and a room temperature of 294 K. Data was analysed using CasaXPS v2.3.25PR1.0. Peak fitting of the high resolution spectra was done with a Shirley background prior to component analysis.

## 4.4 Results & Discussion

### 4.4.1 Titration

The functionality of the lignosulfonate polymer is dictated by its chemical composition and molecular structure, which in turn affect its behaviour in aqueous media. The amphiphilic nature of the lignosulfonate is important in allowing the functionality of this polymer (Deng et al., 2010). In aqueous media, the polymer undergoes dissociation of the ionic groups which results in a charge on its surface bringing about the electrostatic ability that is key to the performance of the lignosulfonate as an admixture (Gardon & Mason, 1955). This is discussed in section 2.2.2. The titration data presents a starting point to observe this behaviour.

Lignosulfonates can be classified as weakly acidic polyelectrolytes which can dissociate in solution in the reactions as shown in Equation 4.5 and Equation 4.7 (Nyman et al., 1986).



Where  $R$  represents the organic part of the polymer and  $AH$  the attached functional group (Nyman, Rose and Ralston, 1986). In an aqueous solution, the weakly acidic polymers exist as conjugate acid-base pairs and only partially dissociate in solution. The degree of dissociation is a function of the amount of charge on the polyelectrolyte chain which is dependent on the solution. At low pH, the polymer is weakly charged, whereas at high pH a larger fraction of monomers are dissociated and the polymer charge saturates to its maximal value (Borukhov et al., 2000).

Figure 4.4 shows the forward and back titration of the DP1717 (high molecular weight and low sugar content) sample, which had a slightly acidic starting pH of 5.01 when dissolved in water. This is attributed to the dissociation of the polymer. When NaOH is added in small increments an increase in pH can be observed. NaOH is a strong base that is completely dissociated into  $\text{Na}^+$  and  $\text{OH}^-$ , and so the  $\text{OH}^-$  ions react with the  $\text{H}_3\text{O}^+$ . This consumption results in an increase in pH as it is a function of the concentration of  $\text{H}_3\text{O}^+$  ions as shown in Equation 4.1. However, at these small NaOH volumes, the pH remains acidic as the solution still contains predominately  $\text{H}_3\text{O}^+$  ions. There is a slight step increase in pH at 0.5 ml of added NaOH, followed by a rapid increase in the pH as more NaOH is added. The solution reaches the equivalence point, at which point all the  $\text{H}_3\text{O}^+$  ions from the partial dissociation of the lignosulfonate polymer are neutralised and equal to the  $\text{OH}^-$  ions.

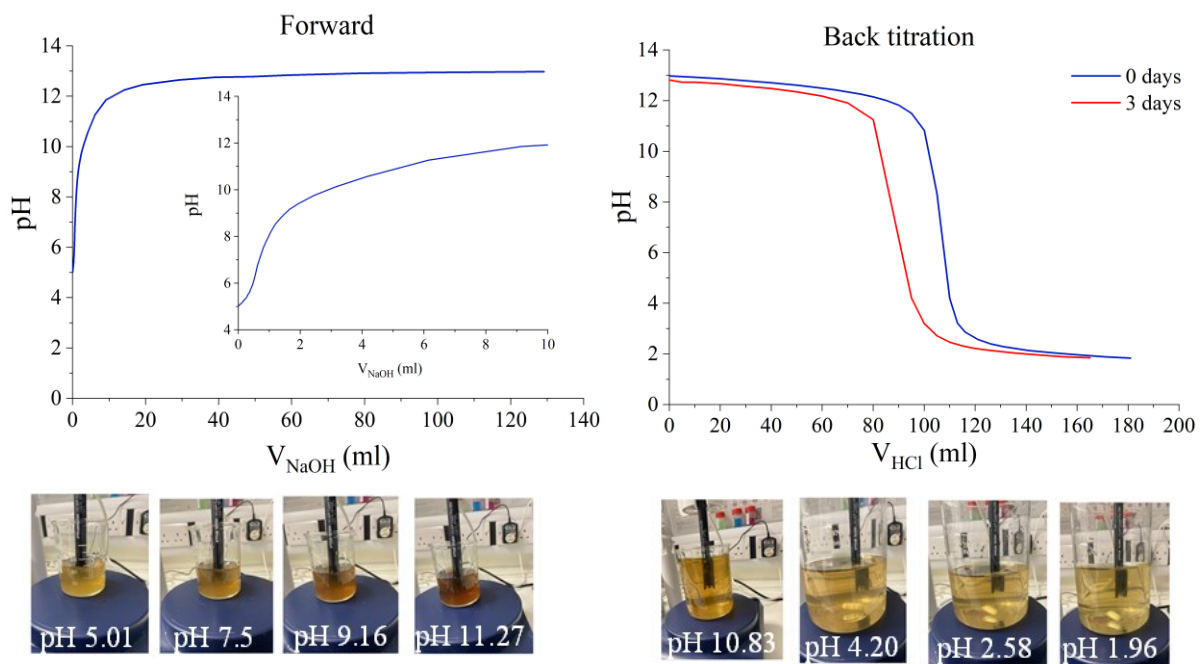


Figure 4.4 The forward and backward titration curves of the DP1717 (high Mw, low sugar) sample.

The curve then follows a steep increase past the equivalence point and begins to slow down after 1.5 ml of NaOH and finally plateaus at high volumes of NaOH. Beyond the point of neutralisation, the pH increases as there is excess of OH<sup>-</sup> until the system reaches a point where further addition of NaOH does not notably change the pH due to the logarithmic nature of the pH scale.

The back titration curves obtained from additions of 0.1 M HCl are characteristic of strong base–strong acid curves (Deng et al., 2010). This is because, at the end of the forward reaction, the solution has NaOH in excess. The key observation in these plots is found in the comparison between 0 and 3 days back titration. It can be noted that less HCl was required to neutralise the solution after 3 days compared to immediate back titration at 0 days. The solutions were kept in tightly sealed containers to prevent the ingress of CO<sub>2</sub> from the atmosphere and therefore, it can be postulated that this observation is due to the presence of free H<sub>3</sub>O<sup>+</sup> ions in solution due to deprotonation from the polymer and further hydrolysis of the bonds.

Figure 4.5 shows the results for the lignosulfonate (DP1718) with a lower molecular weight in contrast to the DP1717 discussed above, but a similar low sugar content. This sample also had a low starting pH of around 5.08 when dissolved in water which would suggest that in water the deprotonation of the polymer is not dependent on the molecular weight. This is not consistent with the composition data presented on Table 4.1, which shows that the DP1717 sample has more acidic groups that can be deprotonated in solution. However, this deprotonation is dependent on the pH, and at near neutral pH the acidic sites are only slightly contributing to the pH for both lignosulfonates. The forward titration curve shows a steep increase in pH from the onset of a titration at small additions of NaOH. However, at volumes between 2 and 12 ml of added NaOH, there appears a slight decrease in the rate of change of the pH as a function of NaOH addition, and then an increase beyond this point. This trend is indicating a buffering effect by the lignosulfonate as more NaOH is added. This may be due to

a large number of carboxylic groups originally in the sample that release more  $\text{H}_3\text{O}^+$  into the solution to react with the added  $\text{OH}^-$  and result in a reduced rate of increase in pH. Beyond this point, there is an increase in pH until it plateaus as discussed above for DP1717.

The back titration curve in Figure 4.5 is indicative of a reaction between a strong acid and a strong base as the excess NaOH in the solution reacts with the HCl being added. After 3 days, less acid is required to neutralise the solution which indicates that further dissociation/deprotonation of the lignosulfonate occurred over time, similar to the high molecular weight DP1717 sample previously discussed.

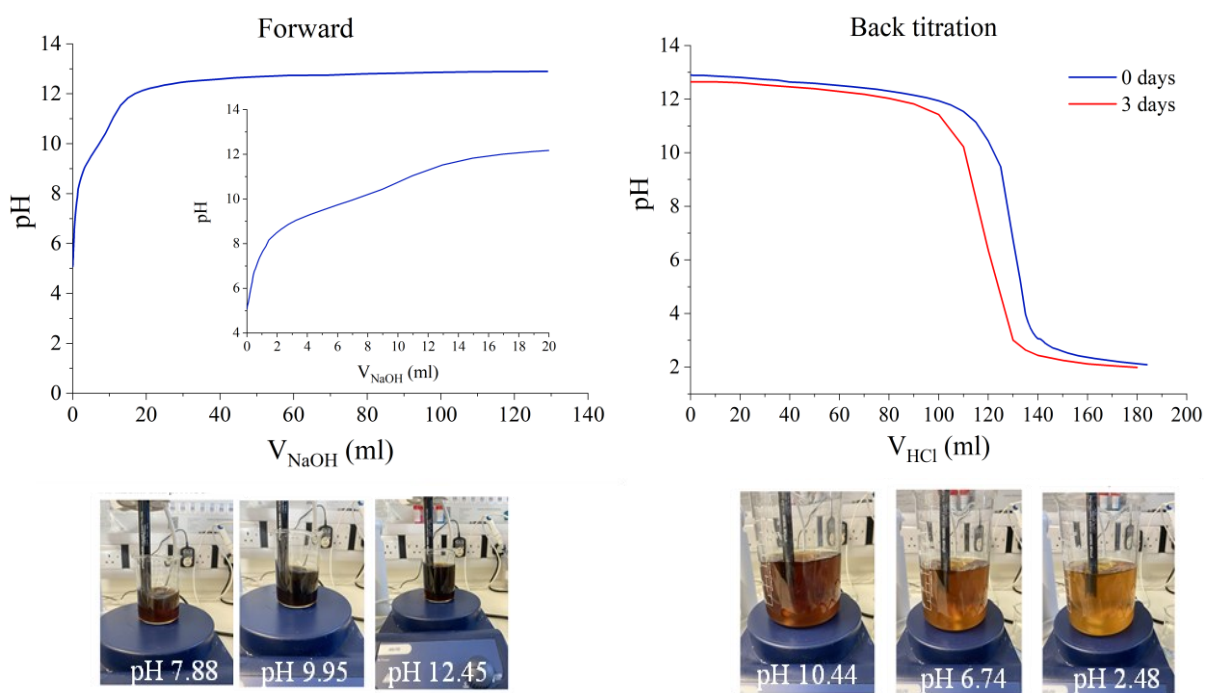


Figure 4.5 The forward and backward titration curves of the DP1718 (low Mw, low sugar) sample.

Figure 4.6 shows the titration curves for the DP1765 lignosulfonate sample with high molecular weight (similar to DP1717) but with high sugar content. In this sample, we can observe the effect of sugar on the dissociation of the polymer. The sample when dissolved in

deionised water had a starting pH of 5.02. The forward titration curve shows a steep increase at small additions of NaOH and a buffer region as was observed with the DP1718 sample, followed by an increase in pH which then gradually plateaus off.

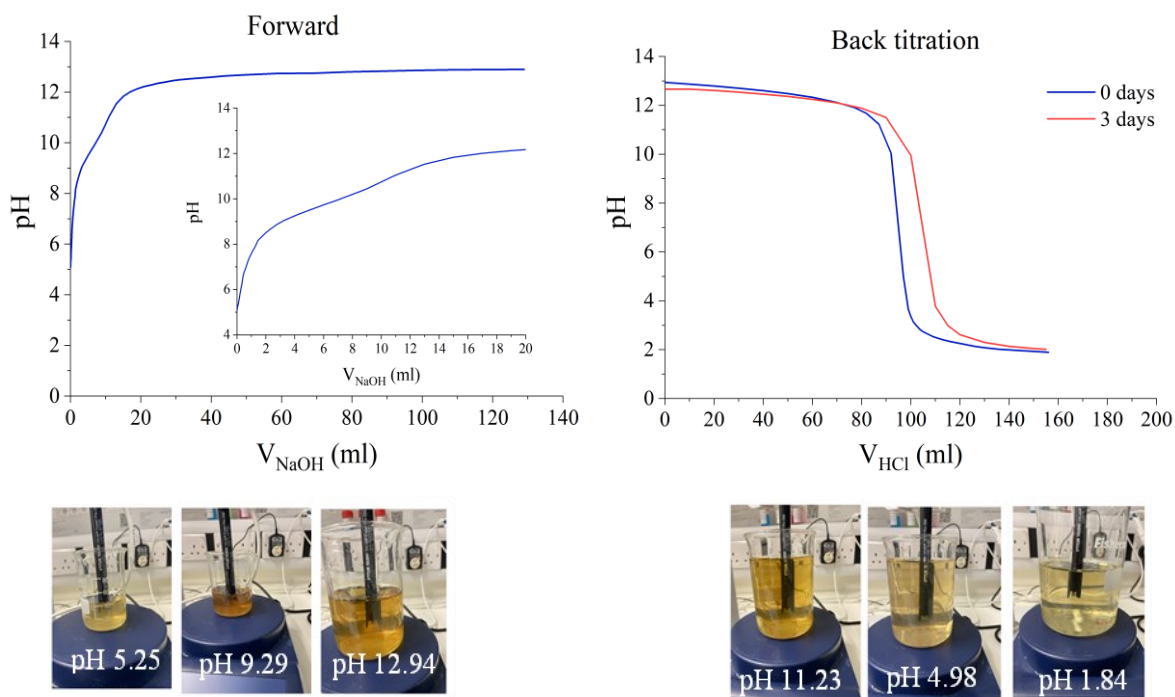


Figure 4.6 The forward and backwards titration curves of DP1765 (high Mw, high sugar) sample.

At the onset of the forward titration, the DP1765 sample with high molecular weight and high sugar content also showed a step in the pH at low volumes of NaOH, similar to the DP1717 high Mw and low sugar sample. More interesting is the back titration which shows a greater amount of acid required for back titration after 3 days compared to zero days. This is likely due to the presence of sugar in the sample. Sugar is a polyprotic acid with multiple OH groups which can be deprotonated during the initial NaOH titration. So, as HCl is added it reacts with the excess NaOH in solution as well as protonating the deprotonated OH groups of the sugar molecules. Some of the sugars likely to be present in these LS are xylose, arabinose, mannose,

glucose, galactose and uronic acid (GreenAgroChem, 2022). These sugars range in pKa values around 12 (Shapley, 2022), and these high pKa values encourage the protonation process.

Figure 4.7 shows the low molecular weight (similar to DP1718) but high sugar content lignosulfonate DP4426 undergoing titration. Unlike the previous three samples discussed, this lignosulfonate had a slightly alkaline starting pH of 7.44. This LS being slightly alkaline may be due to the generation of hydroxide ions when dissolved in water with these ions dissociating from the sugar (pKa ~12) in the polymer. This was not observed in the high Mw and high sugar DP1765 sample, which indicates that dissociation of the low Mw sample was at a greater extent than the high Mw sample. This may be due to the arrangement of the polymer (conformational effects) in solution where the low Mw sample present more readily available groups for dissociation while the high Mw LS is less accessible (Bolatbaev et al., 2010). The dissociation of these polymers has previously been directly linked to the position and number of other charged groups (Borukhov et al., 2000). An initially rapid increase in pH is observed upon small additions of NaOH, which then gradually increases to a plateau. Similar to DP1765, the 3-days aged solution required more acid to neutralise compared to the immediate back titration sample.

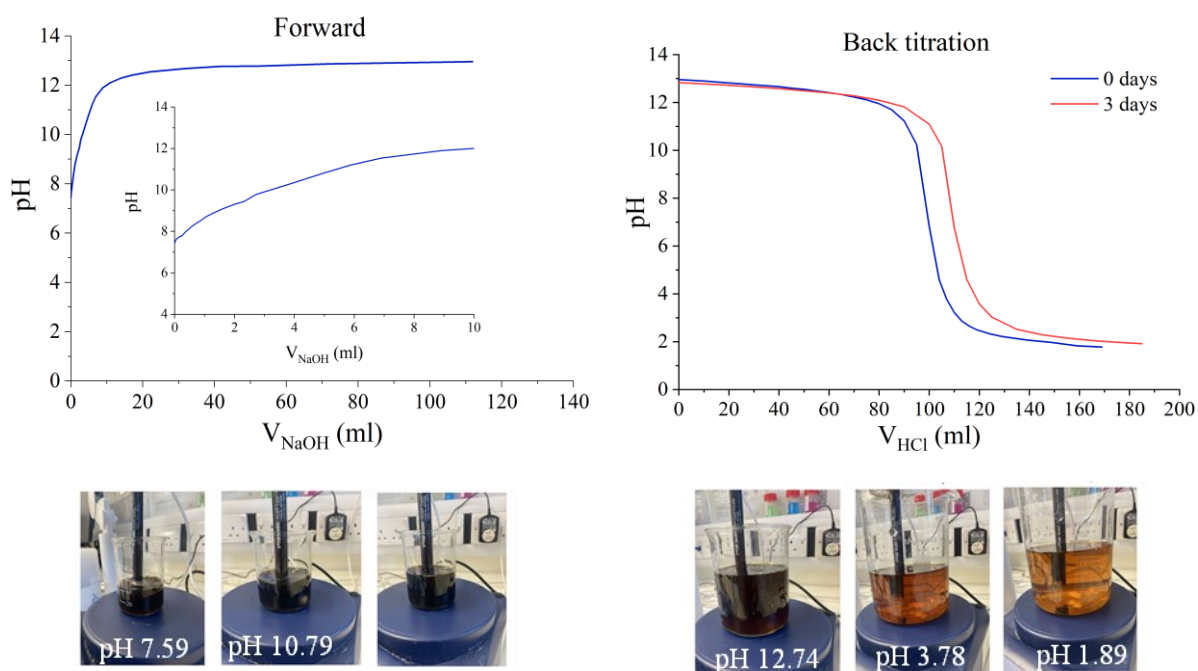


Figure 4.7 The forward and backward titration curves of the DP4426 (low Mw, high sugar) sample.

Another interesting observation that can be seen across all samples as shown in Figure 4.5-4.7, was colour changes. The characterisation and analysis of the colour of lignin is often overlooked even though irregularities in the colour of products can play a role in limiting its use in certain applications (Ajao et al., 2018). The solutions became darker as more NaOH was added and lighter when back titration with HCl was carried out. This observation may be due to either chemical or physical changes to the liginosulfonate and appears to be reversible depending on the acidity and alkalinity of the solution. Lignin as a natural compound is almost colourless, and the reason for the colouration of liginosulfonates is not well understood. The colouration process has been reported to occur by a demethylation reaction due to a nucleophilic attack by  $\text{OH}^-$  followed by auto-oxidation to yield the coloured o-quinoid structures as shown in Figure 4.8 (Dilling & Sarjeant, 1984).

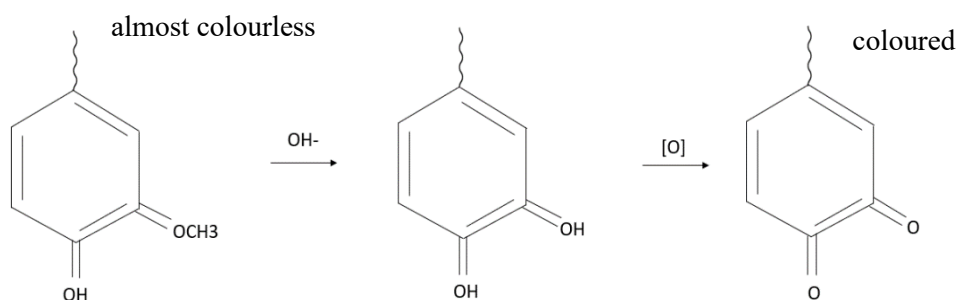


Figure 4.8 Colour change of lignosulfonates in NaOH solution (Dilling & Sarjeant, 1984).

In summary, the pH of the solution can influence the chemical behaviour of the lignosulfonates as well as physical changes. The data set shows that the shape of the titration curves and therefore behaviour of the lignosulfonate in solution is dependent on its molecular structure and sugar content. When dissolved in water, the molecular weight is not a determining factor of the starting pH and therefore does not significantly affect the rate of dissociation of the polymers in water; this was observed in the low sugar samples (DP1717 and DP1718) having similar starting pH values regardless of their molecular weight. These samples however, presented different trends during forward titration which suggests that they undergo different routes of dissociation and at different rates due to differences in their Mw. The effect of sugar can be observed in the back titration of the samples, with low sugar samples requiring less HCl while the high sugar samples require more acid. In high pH solutions, the dissociation of lignosulfonates is kinetics-dependent, such that the lignosulfonates require time to rearrange in solution allowing for more groups to undergo ionisation.

#### 4.4.2 Fourier Transform Infrared Spectroscopy (FTIR)

Figure 4.9 shows the FTIR spectra of the four untreated, as received lignosulfonate samples. These spectra are characteristic of typical lignosulfonate samples with strong bands at high

wavenumbers above  $3000\text{ cm}^{-1}$  indicative of the presence of hydroxyl group in phenolic and aliphatic structures (OH stretching vibration) (Yan et al., 2018). The peaks between  $3000$  and  $2750\text{ cm}^{-1}$  are due to the C-H stretching in methyl, methylene groups found in the side chains of the polymer, and methoxyl groups attached to the benzene ring (Boeriu et al., 2004), (Lu et al., 2017). The fingerprint region is perhaps more complicated for peak assignment due to the overlapping of peaks of functional groups in this broad and interlinked polymer due to various vibrational contributions (Yan et al., 2018). Regardless, some peak assignments can be made. The bands at  $1715\text{ cm}^{-1}$  corresponds to the unconjugated C=O band, and  $1670\text{ cm}^{-1}$  can be attributed to the carboxyl/carbonyl group (Boeriu et al., 2004). The region  $1600 - 1500\text{ cm}^{-1}$  corresponds to the benzene ring stretching vibrations (Yan et al., 2018). The strong vibrations from  $1216-1200$  can be associated with the C-C, C-O, and C=O stretching (Stark et al., 2016). In this region, the band at  $1215\text{ cm}^{-1}$  and  $1266\text{ cm}^{-1}$  are associated with the C-O of the syringol rings and guaiacyl rings, respectively (Yan et al., 2018). There is also a strong vibration at  $1040\text{ cm}^{-1}$  which can be attributed to the C-O, C-C, and C-OH bending in polysaccharides found in most lignosulfonates (Boeriu et al., 2004). The dominance of these polysaccharides is to be expected in lignosulfonates. The S-O stretching of the sulfonic groups can be found at low wavenumbers of  $650-525\text{ cm}^{-1}$  (Rodríguez-Lucena et al., 2009). A summary of the peak assignments is presented in Table 4.2.

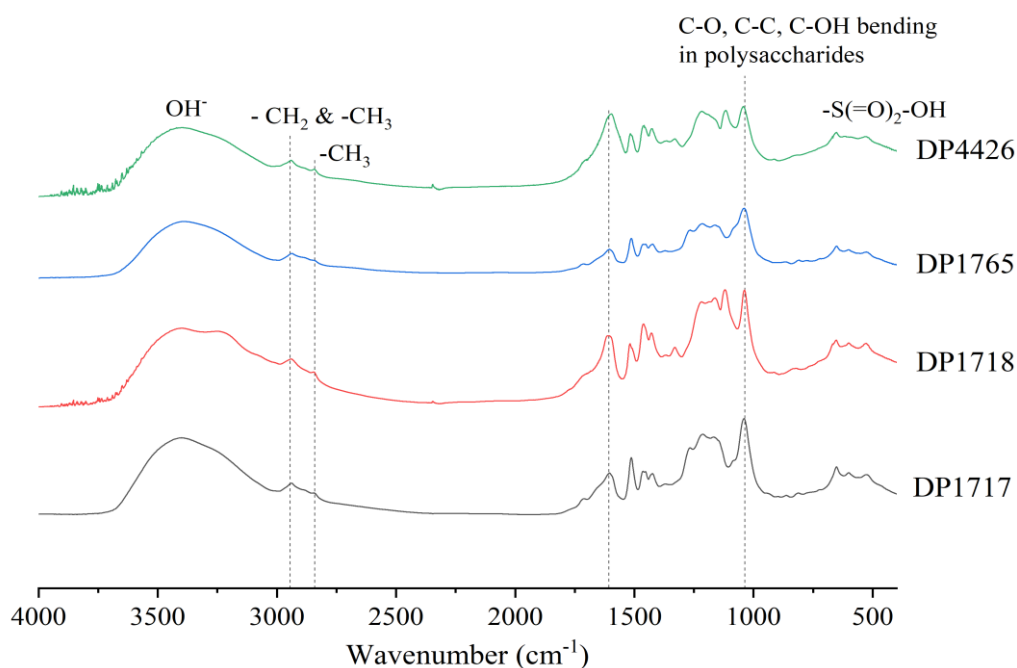


Figure 4.9 The FTIR spectra of the lignosulfonates as received; DP1717 (high Mw, low sugar), DP1718 (low Mw, low sugar), DP1765 (high Mw, high sugar) and DP4426 (low Mw, high sugar).

Table 4.2 The FTIR peak assignments of the lignosulfonates as received (Boeriu et al., 2004), (Rodríguez-Lucena et al., 2009), (Yan et al., 2018).

Bands (cm <sup>-1</sup> )	Assignment
3600 - 3300	Hydroxyl group in phenolic and carboxylic acids
2938	C-H stretching (methyl and methylene group)
2844	C-H stretching (methoxyl group)
1715, 1670	Unconjugated carbonyl-carboxyl stretching
1702	C=O stretching
1605, 1513	Symmetric (1605) and asymmetric (1513) aryl ring stretching
1463, 1454	C-H deformation combined with aromatic ring vibrations
1424	C-C (aromatic skeleton) with C-H in-plane deformation
1371	C-O syringyl
1266, 1215, 1167	C-C, C-O, C=O stretching. Aryl ring breathing (1266)
1158	Stretching vibration of C-H bonds on the benzene ring

1040	Aromatic C-H deformation with C-O, C-C stretching and COH bending in polysaccharides
651, 601, 525	S-O stretching (sulfonic groups)

The different lignosulfonates present the same key peaks in their spectra but at varying intensities. For the DP1718 sample, however, and perhaps more interestingly is the appearance of a doublet of the OH<sup>-</sup> band at 3250 cm<sup>-1</sup> which is due to the Fermi resonance, a common phenomenon in infrared spectroscopy of organic molecules (Silverstein et al., 2005). This feature is more prominent in the DP1718 and has been reported by other researchers (Lima et al., 2013), (Rodríguez-Lucena et al., 2009), however, no theory has been put forward to explain the occurrence of this doublet for certain lignosulfonates.

Figure 4.10 shows the DP1717 spectra obtained after chemical treatment and solvent removal; a sample of the LS as received is included as the control. A sample was mixed with water and then only washed with isopropanol, while one sample also dissolved in water was washed with isopropanol but also ion exchanged, to investigate the effect of the ion exchange step on the samples. The comparison between these samples highlights if there was any impact on the structure and therefore the results due to the procedure followed post-treatment. This is because the ion exchange resin which has excess H<sup>+</sup> ions reduce the pH to acidic levels while there is no Na<sup>+</sup> and OH<sup>-</sup> ions to remove. This confirms the highly pH responsive nature of the lignosulfonates. The sample dissolved in water and ion exchanged to low pH values shows that a new peak appears at 1740 cm<sup>-1</sup>, and this peak is consistent across all the samples that were treated with varying concentrations of NaOH. Because this peak was not found in the water sample that was not ion exchanged, it cannot be attributed to the chemical treatment and is therefore due to the ion exchange step in the procedure. This artefact is acknowledged but will not be considered in detail in further analysis. The effect of ion exchange resin was further

confirmed by using an amount calculated as a ratio of the concentrations of the NaOH treatment solutions, for example, the maximum amount of resin was used at 10 M while 1/100 of the resin was used for the 0.01 M sample . The results from these repeat samples are presented in Figure 4.11.

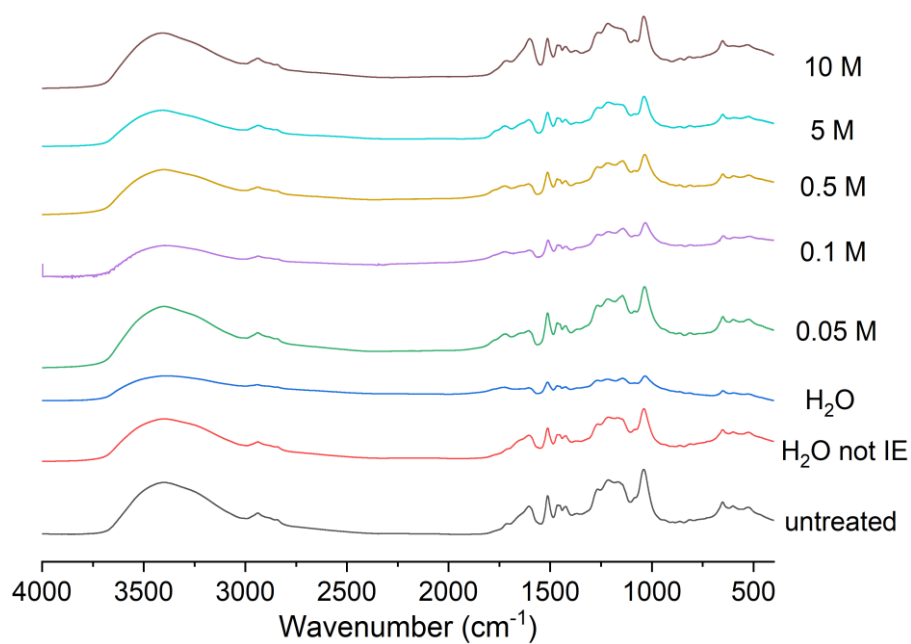


Figure 4.10 The FTIR spectra of the DP1717 sample before and after treatment with increasing concentrations of NaOH. The same amount of resin was used to ion exchange (IE) all samples.

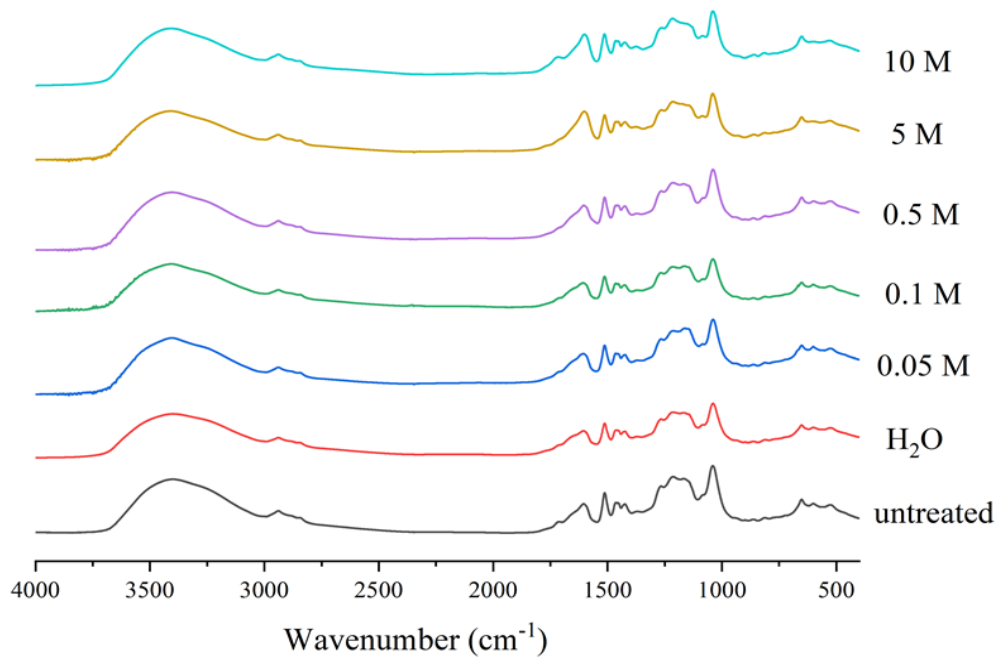


Figure 4.11 The FTIR spectra of the DP1717 sample before and after treatment with increasing concentrations of NaOH. The amount of resin used was varied according to the NaOH concentration.

As shown in Figure 4.11, it can be observed that there are insignificant changes observed in the spectra of the lignosulfonates. There was no loss of peaks as the samples were treated with increasing concentrations of NaOH solution. This indicates that the structure of the polymer and particularly its functional groups remained relatively unchanged by NaOH chemical treatment regardless of the concentration of the solution. The sulfonate groups found at the low wavenumber end of the spectra, that have been reported as most crucial to the performance of the lignosulfonate as an admixture remain unchanged by the chemical treatment. The C-H stretching bands corresponding to the side chains of the polymer also remain unaltered with increasing concentrations of NaOH during treatment.

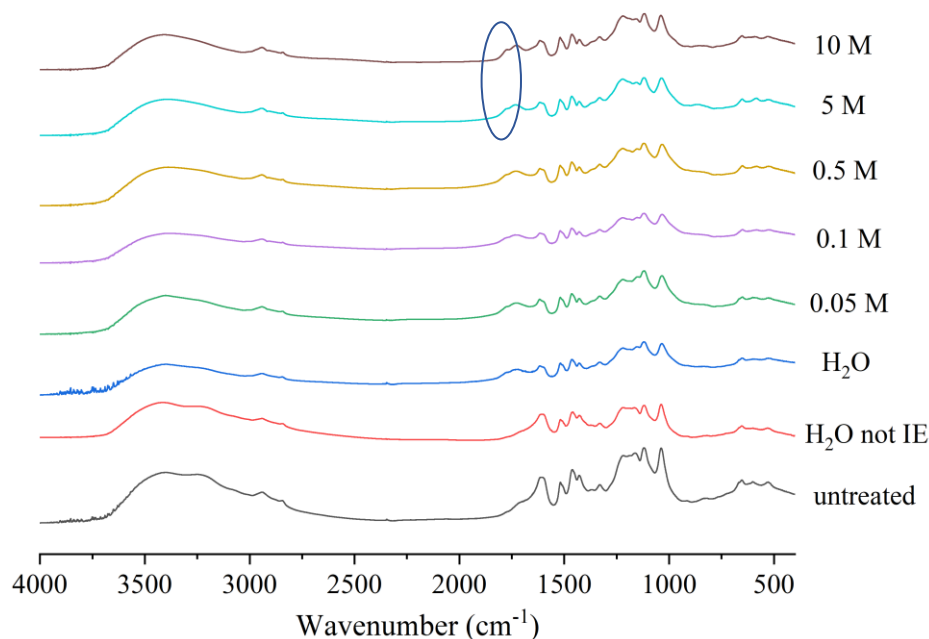


Figure 4.12 The FTIR spectra of the DP1718 sample before and after treatment with increasing concentrations of NaOH.

Like DP1717, the DP1718 sample showed no significant changes in the FTIR data as shown in Figure 4.12. The only clear change is that the doublet of the  $\text{OH}^-$  is lost upon chemical treatment. The  $\text{H}_2\text{O}$  sample that was not ion exchanged still had this doublet peak, and so it appears that this may have been due to the ion exchange step in the sample preparation. The other functional groups previously identified remain unchanged post-treatment. The samples treated with the highest NaOH concentrations present a new peak appearing at around  $1765\text{ cm}^{-1}$  marked with a circle in Figure 4.12. This can be attributed to formation of new  $\text{C}=\text{O}$  bonds. As both DP1717 and DP1718 samples remained mostly unchanged, it can be postulated that the molecular weight of the lignosulfonate samples does not greatly affect their resilience/stability in these extreme alkaline conditions.

Figure 4.13 and Figure 4.14 present the FTIR spectra of the LS samples with an increased amount of sugar. No significant changes were observed similarly to the other samples. This

indicates that the presence of sugar in these samples did not significantly affect their resilience to chemical attack.

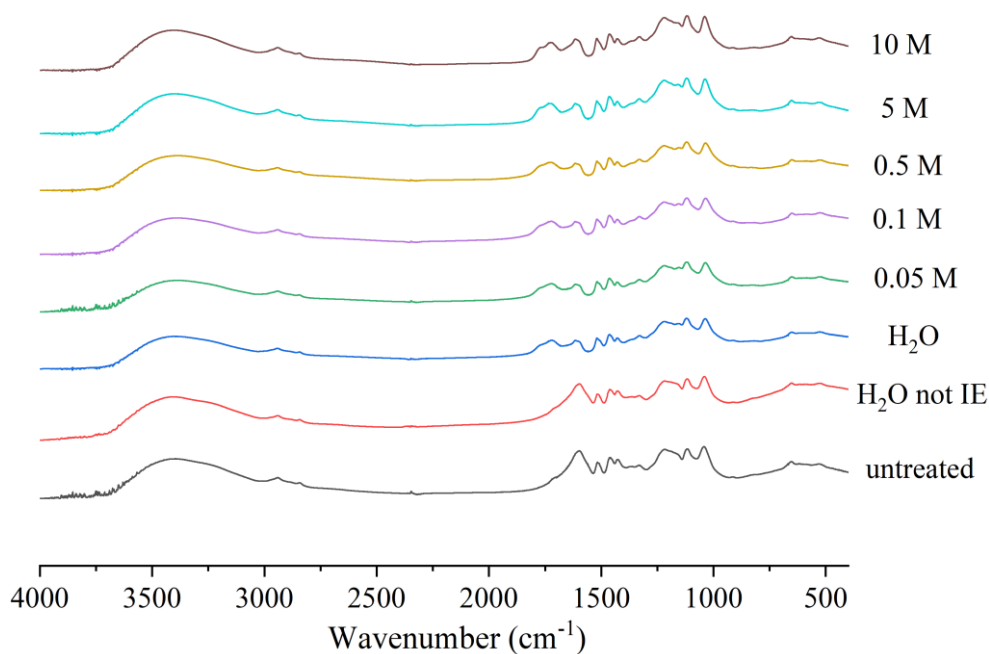


Figure 4.13 The FTIR spectra of the DP4426 sample before and after treatment with increasing concentrations of NaOH.

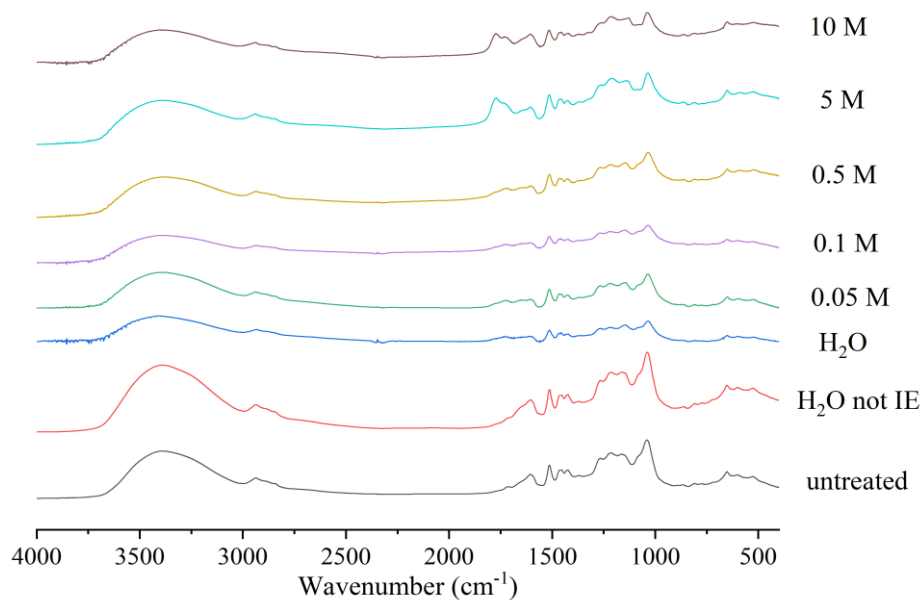


Figure 4.14 The FTIR spectra of the DP1765 sample before and after treatment with increasing concentrations of NaOH.

The FTIR data sets across the four lignosulfonate samples indicate the high alkaline durability of these samples. The results suggest that there was no loss of functional groups at increasing pH. Therefore, it can be postulated that the changes observed in the titration results previously discussed were only deprotonation/protonation reactions that were reversibly occurring in the aqueous media.

#### 4.4.3 $^{13}\text{C}$ Nuclear Magnetic Resonance spectrometry (NMR)

Figure 4.15 shows a simplified structure of the lignosulfonate. The  $^{13}\text{C}$  CPMAS NMR spectra of the untreated and as received DP1717 and DP1718 lignosulfonates are presented in Figure 4.16. The recorded signals were assigned by comparison with the literature (Lutnaes et al., 2008). The lignosulfonates are expected to present slightly different spectra as it has previously been found that even lignins of the same plant species may have differences in the ratios of their building units guaiacyl (G), syringyl (S) and p-hydroxyphenyl (H) (Nimz et al., 1981). The analysis of these control samples shows peaks in the range 110 to 160 ppm characteristic of most aromatic lignin (Evstigneyev et al., 2018). The characteristic methoxyl peak can be found at 55 ppm. At around 25 ppm, a peak associated with  $\text{CH}_3$  or  $\text{CH}_2$  group in saturated aliphatic chains (Hemmilä et al., 2020) can be found more pronounced in DP1718 than in DP1717. The peaks at around 70 ppm are associated with  $\text{C}_\gamma$  in either  $\beta$ - $\beta$  or the  $\beta$ -O-4 structure.

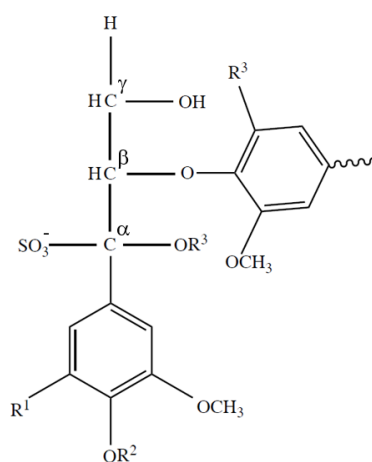


Figure 4.15 Typical structural unit of a lignosulfonate polymer, where the R can be any of: H, alkyl or aryl groups. R<sup>1</sup> can also be unsubstituted. Various linkage units can be represented by varying the substitutions. Adapted from (Gierer, 1986) and (Danner et al., 2015).

The shoulder to the C<sub>Ar</sub>C peak as labelled in Figure 4.16 can be attributed to the C-S=O<sub>3</sub> sulfonate groups. The C<sub>Ar</sub>O are found in the phenolic and methoxyl groups linked to the benzene ring. The range between 200 – 160 ppm is associated with the C=O structures; the DP1717 structure indicates low amounts while DP1718 shows higher amounts of this group which can be attributed to the Ar-CHO or R-O-CO-CH<sub>3</sub> groups (Hemmilä et al., 2020).

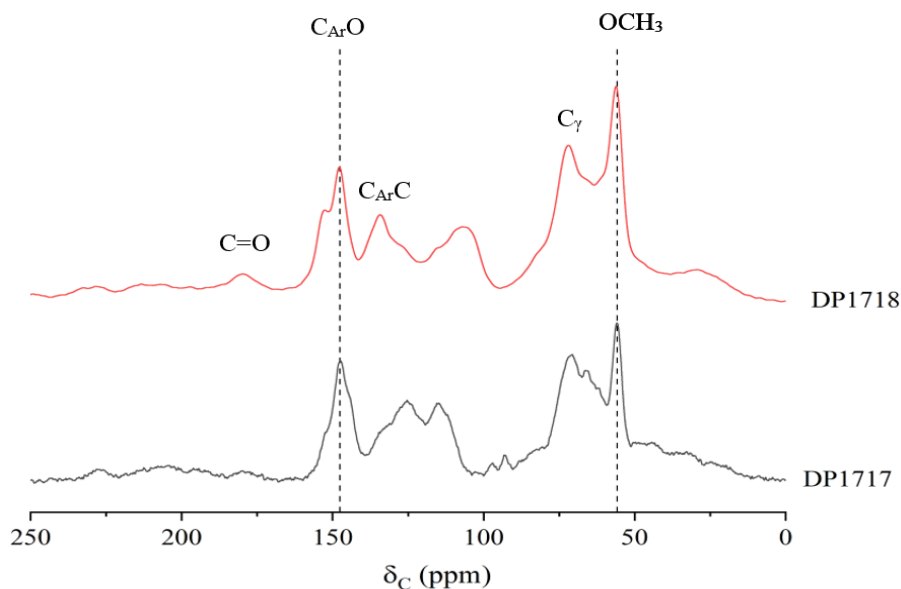


Figure 4.16  $^{13}\text{C}$  CP MAS NMR spectra of the control samples, DP1717 and DP1718 before chemical treatment. DP1717- high Mw, low sugar, DP1718 – low Mw, low sugar.

The NMR data provide more insight into any changes along the  $\text{C}_3$  chain and the attached methoxyl groups on the liginosulfonate. Figure 4.17 and Figure 4.18 show changes to some of the bonds after chemical treatment of the samples. The untreated sample compared to the increasing pH of the solution used in treatment up to pH 13 (0.1 M NaOH) are identical. There are no new peaks or any loss of peaks due to the treatment of the liginosulfonate. As the concentration of the solution is increased, there appears a slight shift of the spectrum to lower chemical shifts. This effect is more significant in the sample treated with the 10 M NaOH solution. Figure 4.17 shows that the DP1717 control sample left untreated, and the samples treated with low concentrations of NaOH up to 0.5 M do not show a peak for  $\text{C}=\text{O}$  at around 180 ppm, indicating a low amount of  $\text{C}=\text{O}$  structures in the DP1717 after treatment. For the 5 M and 10 M samples, this peak is present which suggests that there is a reaction/change when the liginosulfonate is treated with the high concentration NaOH resulting in the formation of a new  $\text{C}=\text{O}$  bond. For both the DP1717 and DP1718 samples, the  $\text{C}_\gamma$  bond is most affected by

chemical treatment. This may be due to the cleavage of the polymer along the backbone which would then facilitate the formation of the new C=O bond.

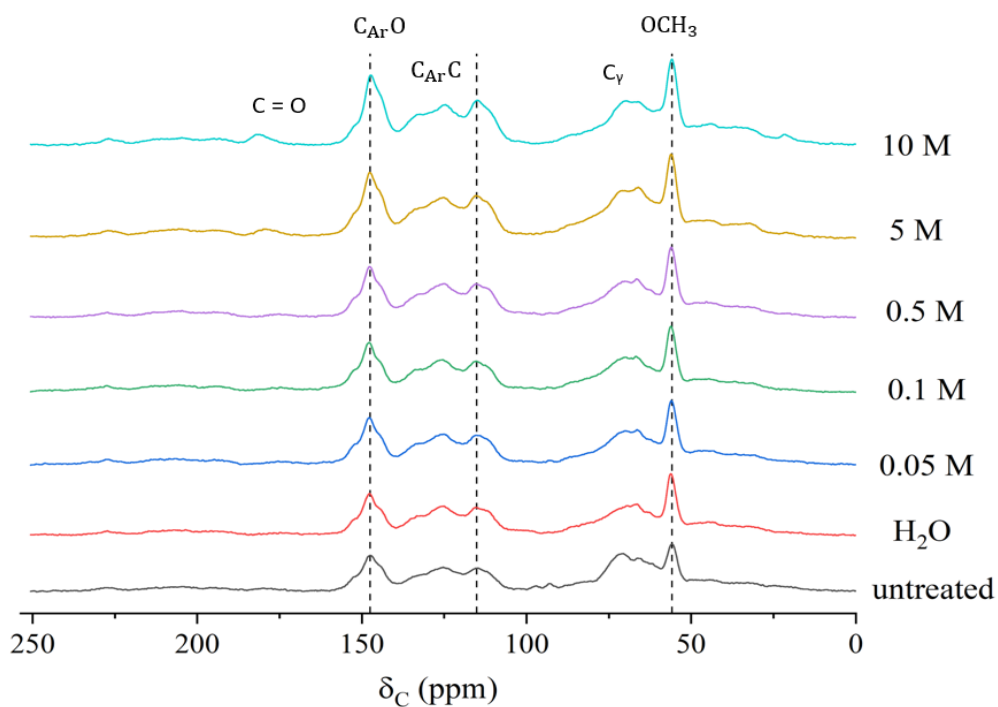


Figure 4.17 The NMR spectra of the DP1717 sample before and after treatment with increasing concentrations of NaOH.

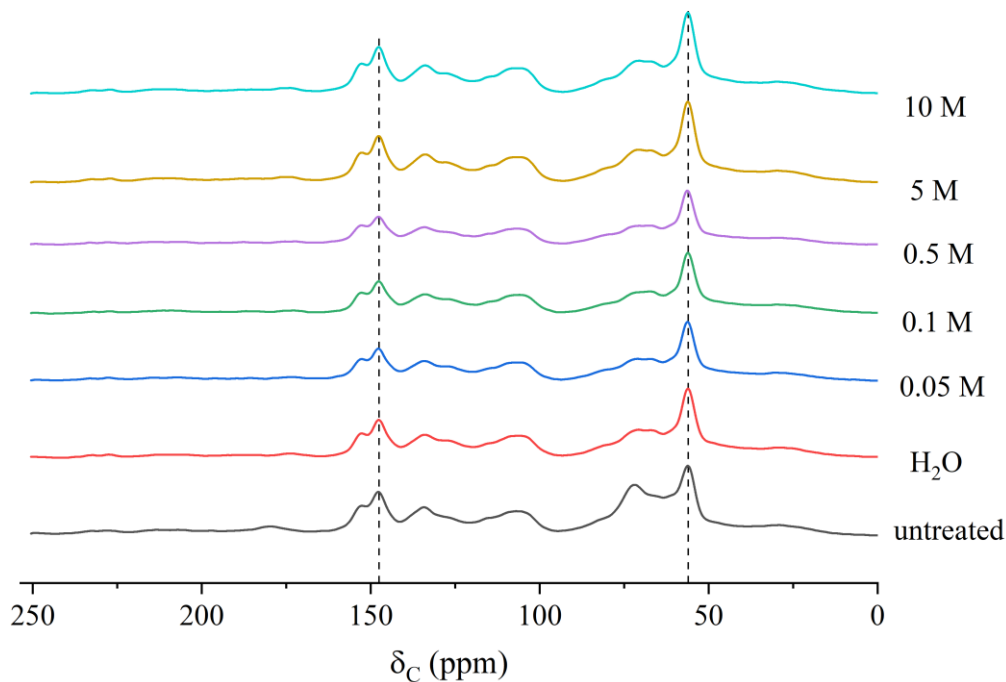


Figure 4.18 The NMR spectra of the DP1718 sample before and after treatment with increasing concentrations of NaOH.

#### 4.4.4 X-ray photoelectron spectroscopy (XPS)

XPS data presented gives further insight into changes to the surface chemistry of the lignosulfonates before and after chemical treatment with increasing NaOH concentrations. The wide angle scans of the samples are presented, and the deconvolution of the experimental data was carried out on the C 1s and S 2p spectra using a Shirley background and Gaussian/Lorentzian line shape (GL(30)). Peak fitting was constrained to an equal full width at half maximum (FWHM). The binding energy scale was referenced to C 1s set at 284.8 eV. The positions of the peaks and the atomic concentrations are also presented.

Figure 4.19 shows the XPS spectra of the DP1717 taken at 3 different points confirming the homogeneity of the sample and that the data is representative of the entire sample. The peaks identified are representative of lignosulfonates showing the presence of carbon, oxygen linkages, calcium, and sulfur.

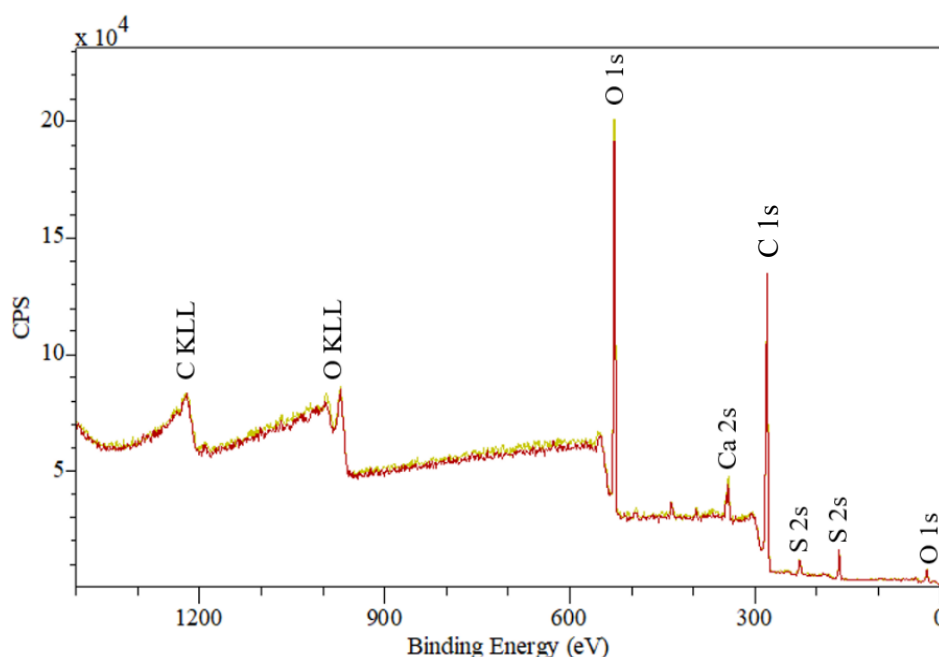


Figure 4.19 Wide angle scan of the DP1717 control sample, with 3 spectra overlaid.

Figure 4.20 shows the wide angle scans of the control lignosulfonate and the samples treated with increasing concentrations of NaOH. The peak found at 1072 eV appears when the NaOH concentration is increased above 0.1 M and is most significant in the 10 M sample. This peak corresponds to the Na 1s component, and another peak appears at these high concentrations at 507.7 eV which corresponds to Na KLL, as highlighted in Figure 4.20. These new peaks at high NaOH concentration are an indication that even though a vigorous washing and ion exchange procedure was followed, the high sensitivity of the XPS technique shows that the  $\text{Na}^+$  could not be completely removed from the sample before characterisation. Nonetheless, there are no other significant changes to the treated samples, indicating a high chemical stability of the DP1717 lignosulfonate. Table 4.3 presents a summary of the chemical composition of the control and the 10 M sample. The calculated values are averages of the analysis of 3 areas on the surface of the sample to ensure that they are representative of the entire sample. There is evidence of a reduction of the Ca 2p component by 1.13 atom % found at 347 eV for the

treated samples compared to the control as shown in Table 4.3. This may indicate that the cation is only weakly bound to the backbone of the lignosulfonate and then lost during chemical treatment.

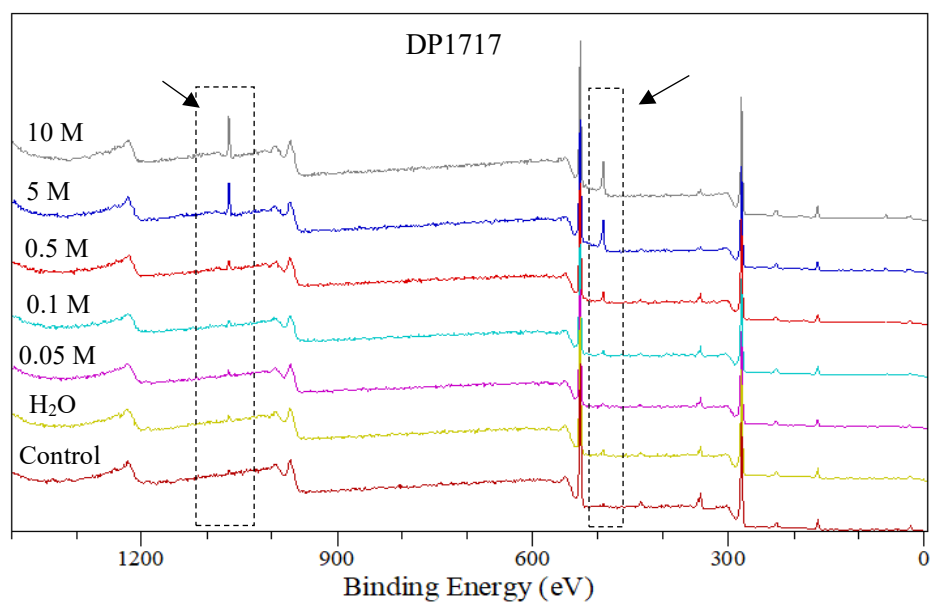


Figure 4.20 Wide angle scan of the DP1717 sample before and after treatment with increasing concentrations of sodium hydroxide solution.

Table 4.3 Composition of the control and 10 M NaOH treated LS samples.

Sample	Region	Binding Energy (eV)	Area no.	Atomic Concentration %	Average Atomic Concentration %	Standard Error
DP1717 control	C 1s	285.07	1	70.17	69.93	0.32
			2	70.32		
			3	69.3		
	O 1s	532.07	1	25.92	25.91	0.22
			2	25.52		
			3	26.28		
	S 2p	168.07	1	2.26	2.55	0.15
			2	2.74		
			3	2.65		
Ca 2p	347.07	1	1.64	1.61	0.10	
		2	1.42			
		3	1.76			
DP1717_10M	C 1s	285.07	1	69.18	68.70	0.57
			2	69.34		
			3	67.57		
	O 1s	532.07	1	26.59	26.96	0.46
			2	26.42		
			3	27.87		
	S 2p	168.07	1	3.83	3.87	0.02
			2	3.89		
			3	3.89		
Ca 2p	347.07	1	0.4	0.48	0.10	
		2	0.36			
		3	0.68			

The high resolution spectra in Figure 4.21 shows that increasing the NaOH concentration did not significantly affect the C 1s component of the lignosulfonate. This indicates that the ionic strength and the pH of the treatment solution did not greatly alter the backbone of the carbon chain. The S 2p on the other hand is more affected by these chemical conditions, showing a shift of the main peak to higher binding energies when the concentration of NaOH was increased. A shift to higher binding energies signifies a change to a higher oxidation state.

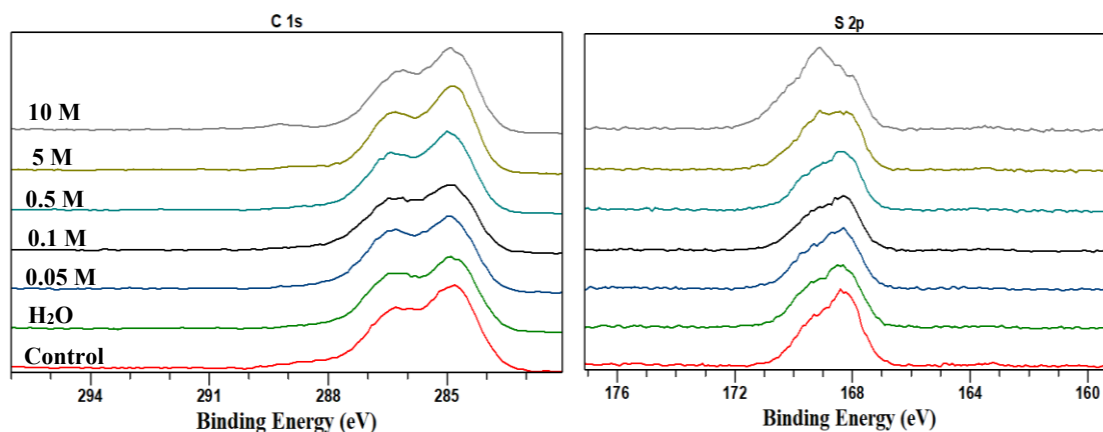


Figure 4.21 C 1s and S 2p XPS data for the lignosulfonate DP1717 after treatment with increasing concentrations of NaOH.

The deconvoluted peaks of the C 1s and S 2p spectra are presented in Figure 4.22. For the control sample, the dominant component at position 284.8 eV was attributed to the carbon atom bound to only other carbon and hydrogen atoms. The component at 286.2 eV corresponds to the C-O bond found in the interunit linkages of the lignosulfonate. The components at 286.9 eV and 288.5 eV correspond to the ether and to the doubly bonded oxygen in the carboxylic functional groups, respectively. The DP1717 sample treated with 10 M NaOH was also peak fitted to ascertain changes brought about by chemical treatment when compared to the untreated sample. This sample presents a similar distribution of peaks, with the key difference being the shift of the O=C-O component to higher binding energies. Comparable atomic concentrations are found between the two samples showing marginal and negligible differences due to chemical treatment.

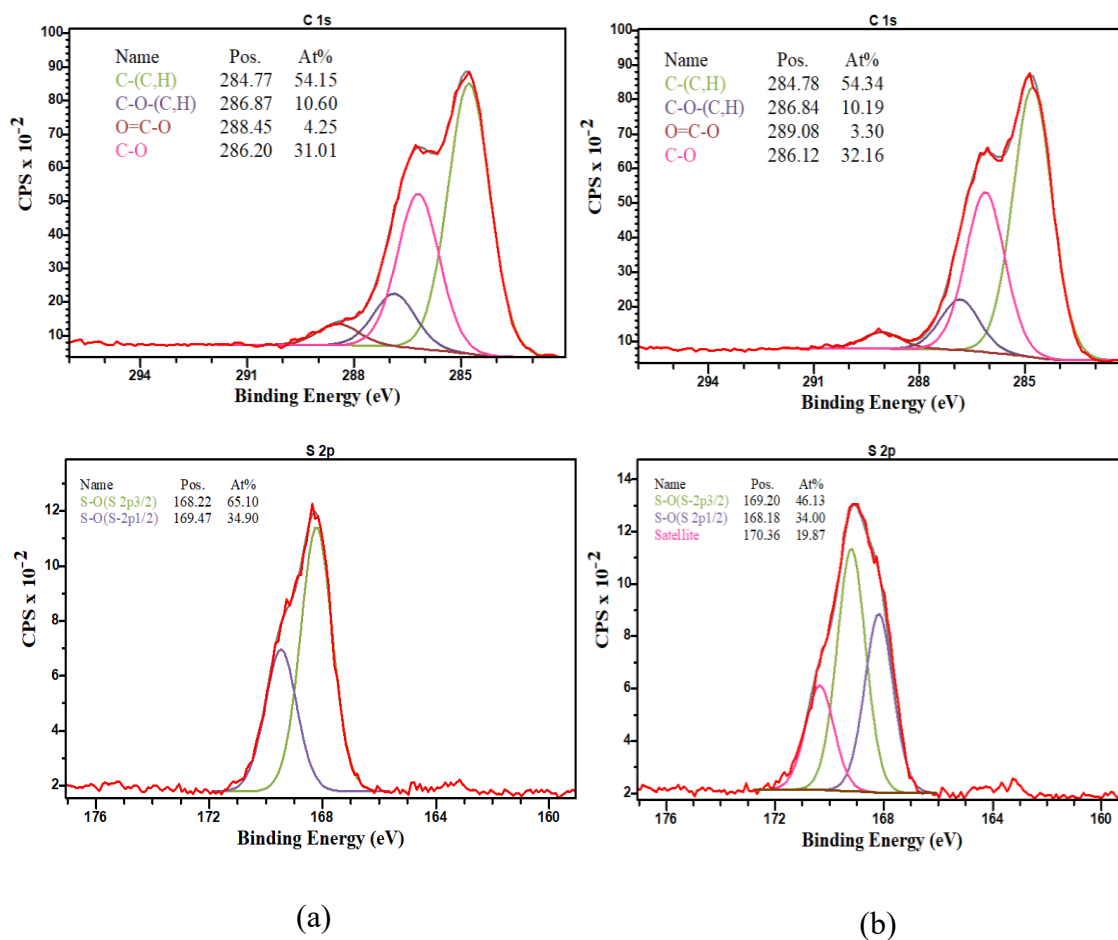


Figure 4.22 Deconvoluted C 1s and S 2p spectra of the DP1717 sample, (a) control and (b) 10 M NaOH treated sample.

The S 2p spectra of the control sample shows spin orbit splitting at ~168, 169 eV, owing to the oxygen containing sulfur groups  $-C-SO_x-C$  ( $x=2,3,4$ ) such as sulfone, sulfonate, sulfate groups (Liu et al., 2022). These peaks are due to the sulfate groups found along the side chains of the lignosulfonate polymer. The  $SO_4^{2-}$  is usually found at higher binding energies than the  $SO_3^{2-}$ . The S 2p spectra after chemical treatment with 10 M NaOH showed the presence of multicomponent peaks with multiple spin splitting orbitals. These present more significant changes to the atomic concentrations compared to the C 1s, with the  $SO_3^{2-}$  showing a significant decrease.

The wide scans of the DP1718 LS sample shown in Figure 4.23 present similar spectra to the control sample when treated with water and 0.1 M NaOH. For the 10 M sample, sharp new peaks at 1072 eV and 507.7 eV corresponding to Na 1s and Na KLL respectively, are found. These peaks are due to the contamination of the sample during chemical treatment, with this sample being more significantly affected than the previously discussed DP1717 sample. The S 2p peak found at 164 eV for the control, H<sub>2</sub>O and 0.1 M also appears to be lost in the 10 M sample. This may be due to some loss of the sulfonate group along the side chains of the lignosulfonate due to chemical treatment.

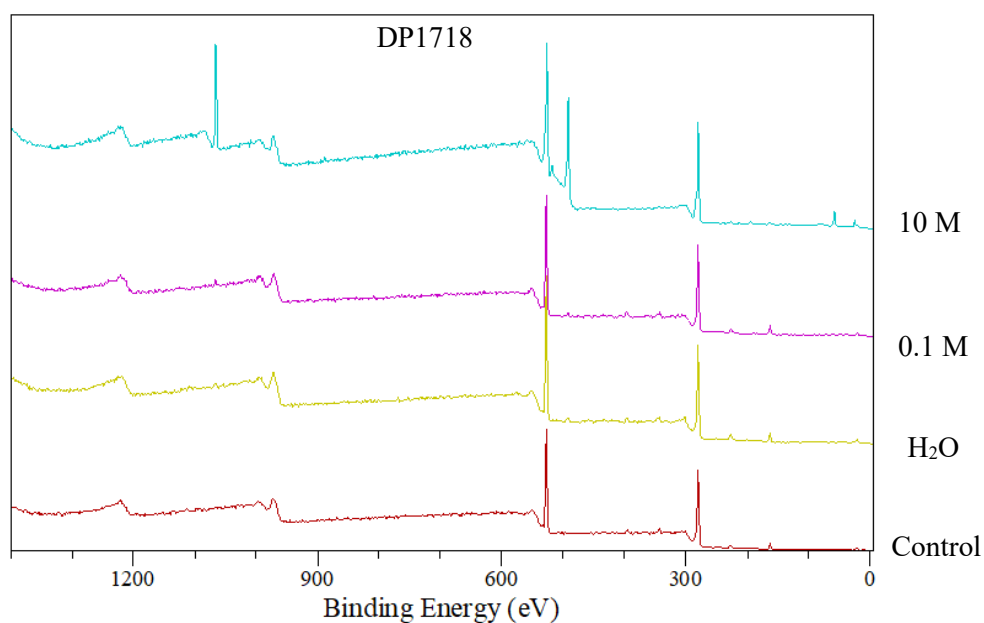


Figure 4.23 Wide angle XPS scans of the DP1718 sample before and after treatment with increasing concentrations of NaOH solution.

The high resolution C 1s spectra in Figure 4.24 shows that the most significant change is found when the highest concentration of NaOH was used for treatment while lower concentrations showed insignificant changes after treatment. The same observation can be made for the S 2p spectra, where the 10 M NaOH solution caused the most significant alteration

to this component. It should be noted that this apparent loss of sulfonate groups may also be linked to the high amounts of unremoved Na from the sample.

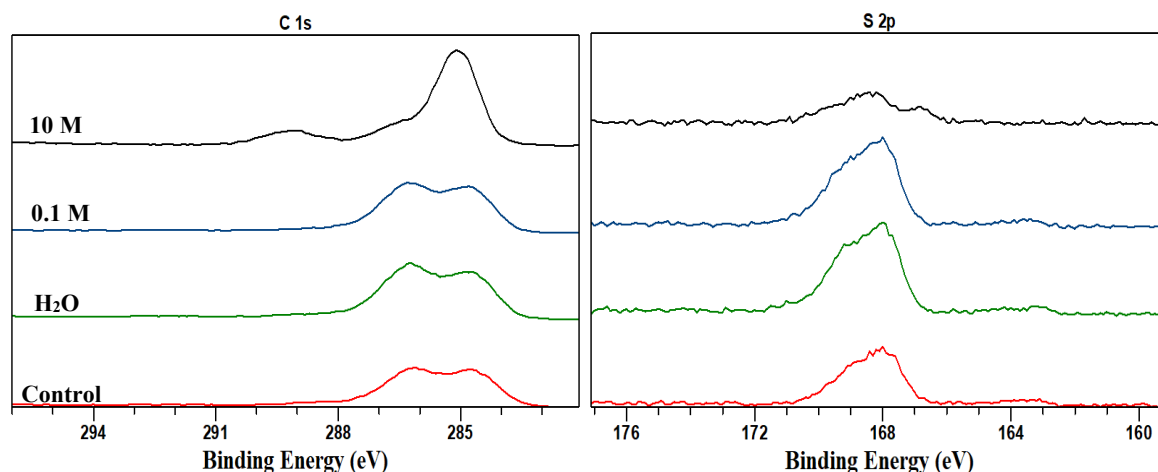


Figure 4.24 C 1s and S 2p spectra of the DP1718 sample before and after treatment with increasing concentrations of NaOH solution.

The DP1718 control and 10 M treated samples were then deconvoluted and presented in Figure 4.25 to take a closer look at the components most affected by chemical treatment. The most significant change observed is a loss of the C-O bond after treatment. This may have been due to the cleavage of the lignosulfonate linkage units ( $\alpha$ -O-4 and  $\beta$ -O-4) or the methoxyl group on the side chains of the lignosulfonate. It has already been established that methoxyl groups are labile and susceptible to chemical attack. This cleavage occurs due to the high concentration of the OH<sup>-</sup> ions and occurs by nucleophilic substitution as shown in section 2.2.2. The S 2p spectra also present slight changes due to chemical treatment. There is an increase in the S-O-(S 2p 3/2) at the expense of the S-O-(S 2p 1/2) component.

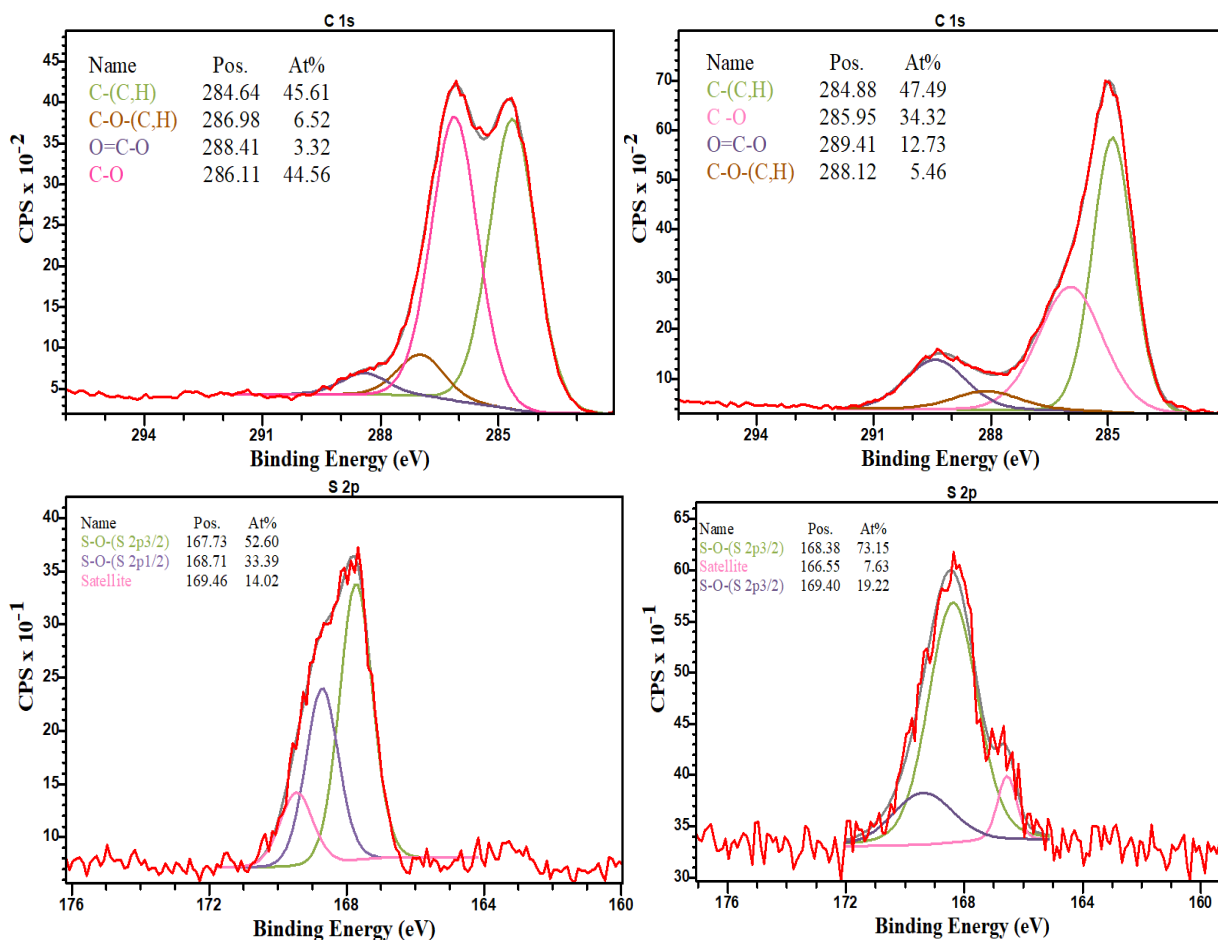


Figure 4.25 Deconvoluted C 1s and S 2p spectra of the DP1718 LS sample.

The low Mw, high sugar DP4426 sample presented in Figure 4.26 shows similar new peaks to the previous samples showing the presence of sodium on the surface of the sample. The peak at 347 eV assigned to Ca 2s is not present in the 0.1 and 10 M samples, suggesting loss during chemical treatment. There are no other significant changes brought about by the chemical treatment of the sample.

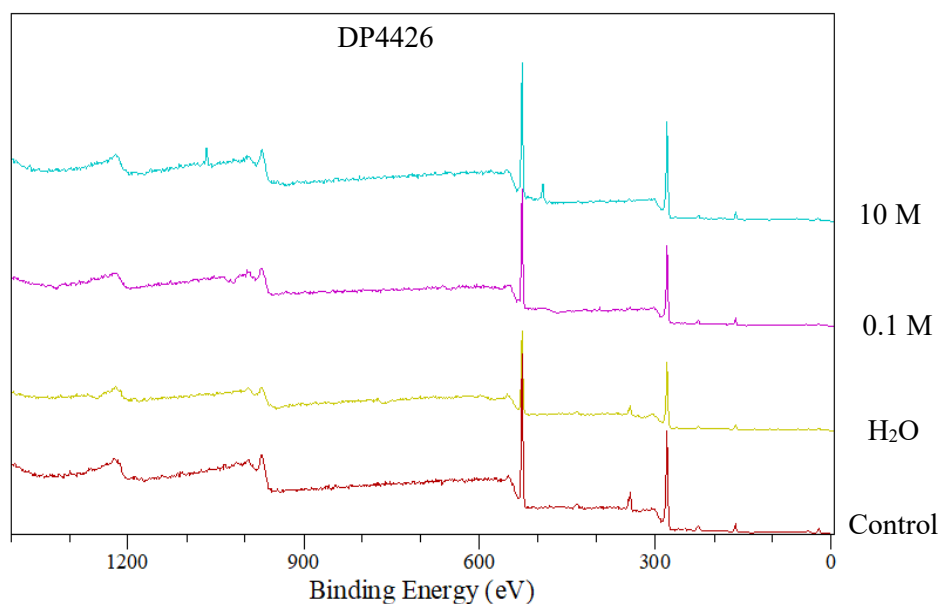


Figure 4.26 Wide angle scan of the DP4426 before and after treatment with increasing concentrations of NaOH solution.

Figure 4.27 shows a similar peak for the C 1s component, which are more defined showing a clear doublet for the 10 M treated sample. This does not suggest any breakage in the carbon chain of this sample. The S 2p component shows an insignificant decrease in the intensity of the peaks as the concentration of NaOH is increased during treatment.

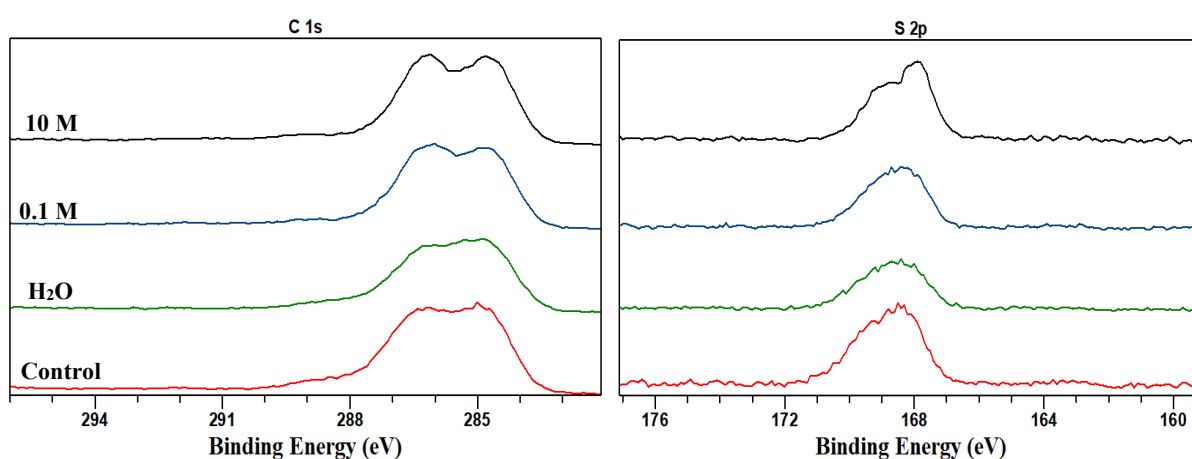


Figure 4.27 C 1s and S 2p spectra of the DP4426 before and after treatment with increasing concentrations of NaOH solution.

In Figure 4.28, the deconvoluted C 1s spectra shows a significant decrease in the C-O-(C,H) bond, and the O=C-O bond. There also appears to be an increase in the C-O bonds of the sample after chemical treatment. The S 2p spectra shows a doublet of the S-O peaks, an unidentified peak was assigned during the deconvolution of the S 2p component.

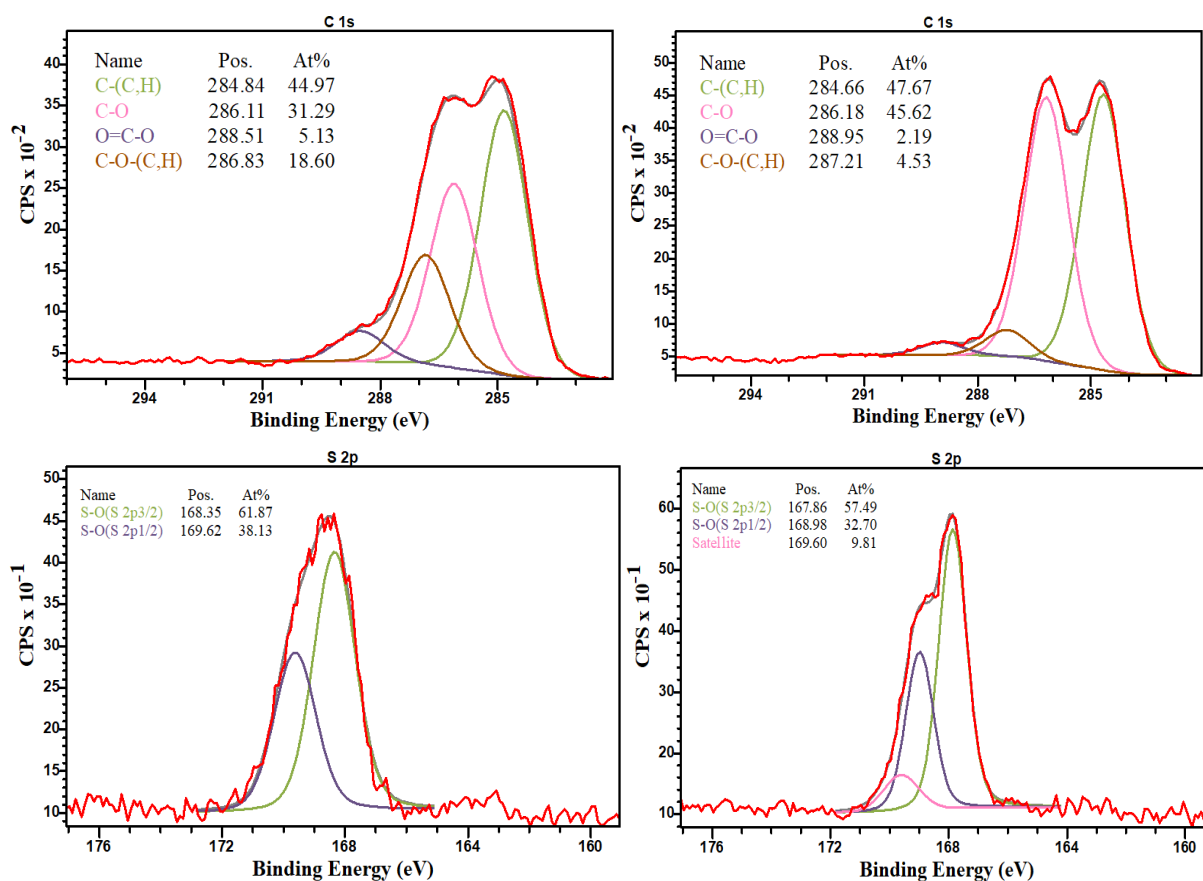


Figure 4.28 Deconvoluted C 1s and S 2p spectra for the control (left) and 10 M treated (right) samples.

The high Mw, high sugar sample DP1765 sample in Figure 4.29 also presents an unchanged XPS spectra except for the presence of Na which remains post treatment, washing and ion exchange. There are no other significant changes to the sample due to chemical treatment.

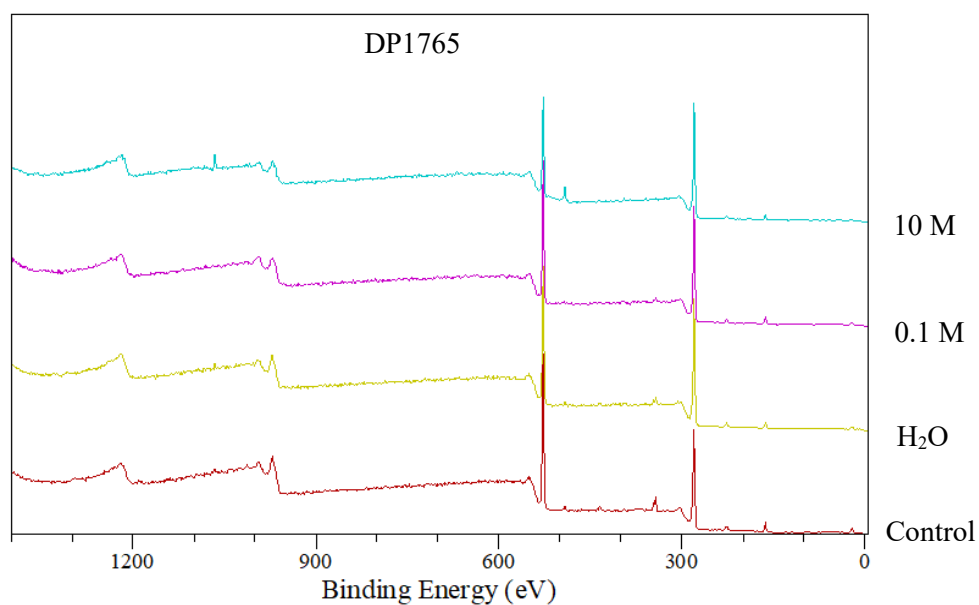


Figure 4.29 Wide angle XPS scans of the DP1765 sample before and after treatment with increasing NaOH concentration.

When increasing NaOH concentration, the highest concentration of 10 M NaOH had the most significant impact on the C 1s component as shown in Figure 4.30. The lower concentration 0.1 M NaOH and H<sub>2</sub>O spectra are similar to the control sample. This indicates that the carbon chain of the lignosulfonate is unaffected by these conditions. The S 2p spectra showed a decrease in the intensity of the peak with increasing NaOH concentration.

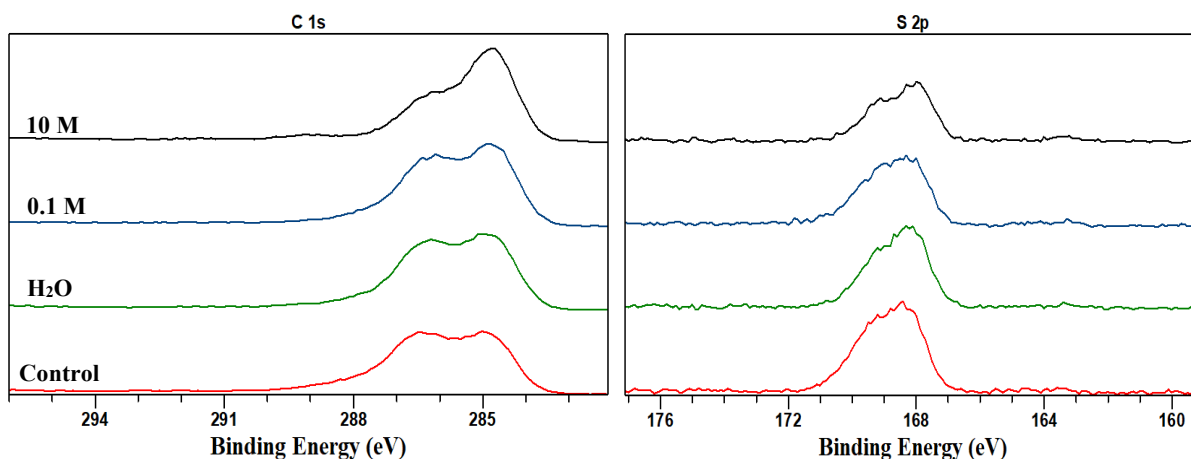


Figure 4.30 C 1s and S 2p spectra of DP1765 before and after treatment with increasing concentrations of NaOH solution.

The deconvoluted spectra in Figure 4.31 shows a significant decrease in the atomic concentrations of the C-O and the C-O-(C,H) bonds due to chemical treatment. This may indicate some structural instability, such that at high NaOH concentrations, there is breaking of the ether bonds of the lignosulfonates. These changes are accompanied by an increase in the C-(C,H) bonds of the aliphatic chains along the backbone of the polymer.

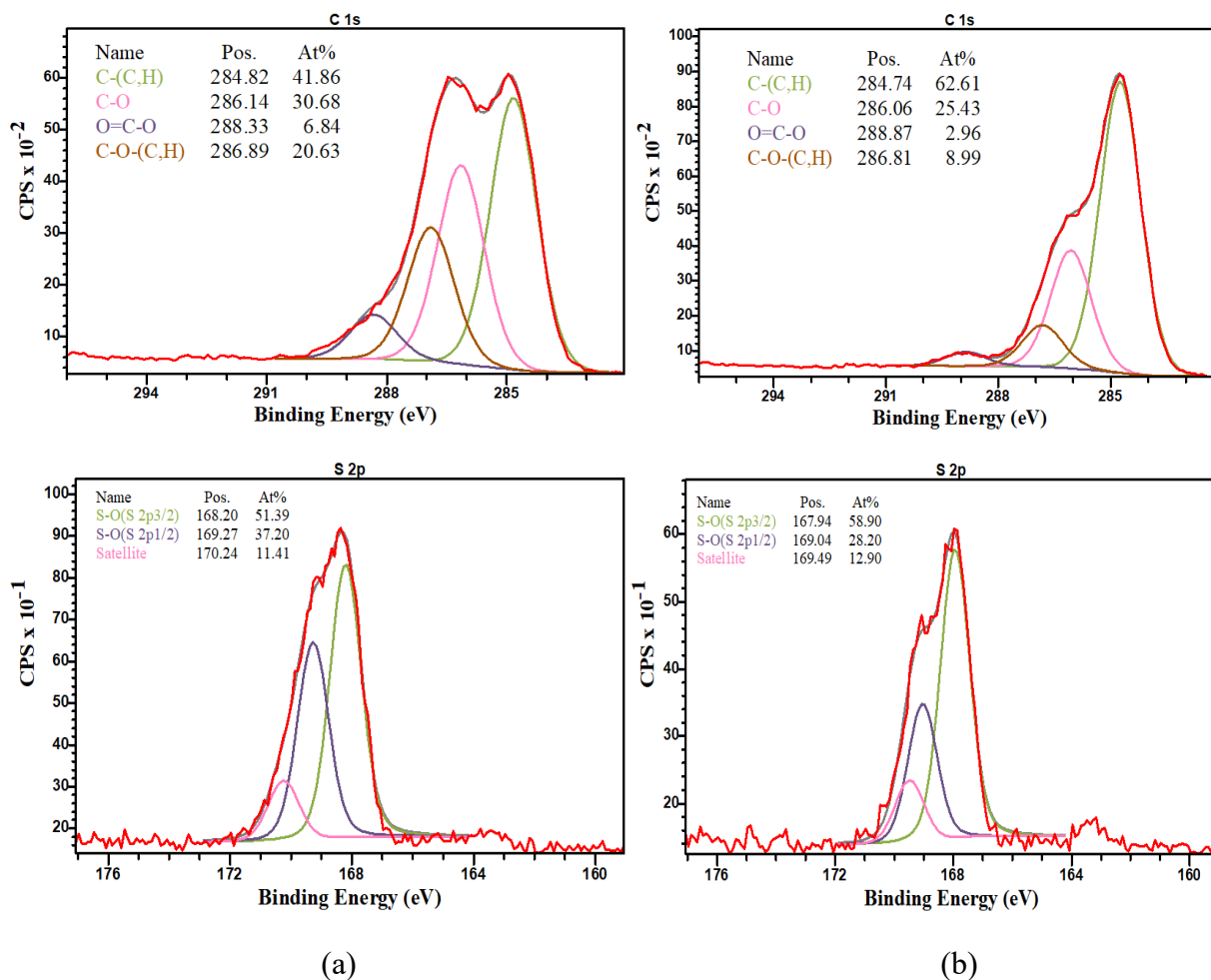


Figure 4.31 Deconvoluted C 1s and S 2p spectra of DP1765 for the control (a) and the 10 M treated (b) sample.

## 4.5 Conclusions

This chapter presented a detailed characterisation of lignosulfonates investigating the effect of chemical treatment on their structure. Titration curves reflect the potential change of the solution when lignosulfonates are suspended in deionised water. The results from these studies show that some reversible dissociation/deprotonation of the polymers occurs resulting in a change in the potential charge of the solution accompanied by a colour change. The shape of the titration curves was dependent on the molecular weight and sugar content and driven by

dissociation of the functional groups found on the surface of the lignosulfonates. There was also indication of some rearrangement of the polymers in alkaline solution.

There were no significant changes to the functional groups of the polymers in increasing pH and ionic concentration environment as observed by FTIR. No loss of functional groups was observed in both low and high Mw, and high and low sugar samples. The only change observed was the formation of a new C=O peak which was confirmed by  $^{13}\text{C}$  CPMAS NMR. This indicates that the  $\text{C}_\gamma$  along the backbone of the polymer was most affected by chemical treatment. These findings suggest that though the functional groups are unaffected, there may be some breaking of the polymer along the backbone, while its functionality is retained. The XPS data shows that the lignosulfonates are not completely immune to chemical treatment. The lignosulfonates most unaffected by the chemical treatment were the DP1717 and DP4426 which were derived from softwood while the DP1718 and DP1765 suffered some loss of the C-O bonds attributed to nucleophilic attack by the  $\text{OH}^-$  in solution.

The stability of the lignosulfonates being studied has been found to be greater than previously reported. It can therefore be concluded that the insufficient plasticising effect of the lignosulfonates in alkali activated cements which present high pH and ionic strength may not only be explained by the chemical stability of the lignosulfonates, regardless of their molecular weight and sugar content. Therefore, it can be hypothesised that other factors such as low solubility of the lignosulfonates in these environments and incompatibility with the precursor particles may be playing a more significant role on their efficiency.

# **Chapter 5 THE EFFECT OF LS ADMIXTURES ON THE FRESH STATE BEHAVIOUR AND MECHANICAL PROPERTIES OF ALKALI ACTIVATED CEMENTS**

## **5.1 Introduction**

One of the main challenges hindering the wider uptake and application of alkali activated materials is difficulties in controlling their viscosities and high yield stresses. For good workability of a cohesive concrete, low yield stresses and reasonable viscosities preventing segregation are desirable (Yousuf et al., 1995). Additives are commonly used to improve the fresh state properties of cementitious materials, and such readily available admixtures used in Portland cements are often explored as potential solutions for alkali activated cements. However, there are clear and significant differences in these systems: in starting materials, reaction mechanisms, chemical environment, and hydration products (Criado et al., 2009). Therefore, differences in the performance of these admixtures in alkali activated materials is to be expected. There remains a lack of understanding of the performance of these admixtures in AAMs, as well as contradictory results on their effect on the fresh state and mechanical performance of alkali activated cements, as previously discussed in section 2.1 of this study.

This chapter presents a complete characterisation of the properties of fresh paste: mini slump tests, rheological studies, hydration kinetics studies, setting time and mechanical strength development. This is applied to analyse two types of alkali activated cements: ground granulated blast furnace slag and low calcium fly ash, activated with sodium silicate solution. These tests are carried out on optimised mix designs, and 1<sup>st</sup> generation lignosulfonates added to investigate how they alter these properties. The study provides insight into the interactions between the admixture and the cement system, to drive towards a better understanding of the

influence of lignosulfonates on the behaviour of these cements. The effect of increasing the admixture dosage on the fresh state behaviour and mechanical properties of alkali activated fly ash and alkali activated slag is investigated, and the optimum dosage for improved workability is determined. For the first time, this study evaluates the performance of lignosulfonates with different compositions in alkali activated pastes. The dispersion efficiencies of four types of lignosulfonates with different molecular structures and compositions (low vs high Mw and high sugar vs low sugar content) are presented. This range of lignosulfonates is added to low and high calcium alkali activated cements to highlight any compatibilities - or lack thereof - between the admixtures and the cement systems.

## **5.2 Materials**

The materials used in this chapter are discussed in Chapter 3.

## **5.3 Analytical techniques and procedures**

The techniques used for characterisation and the procedures followed for sample preparation are discussed in Chapter 3.

## 5.4 Effect of lignosulfonates on the properties of alkali activated blast furnace slag

### 5.4.1 Workability

The workability of the pastes was determined from slump data and presented as relative slump as shown in Figure 5.1-5.3. The mix design for these pastes is presented in section 3.1.4. The mini slump measurements were taken 20 minutes after mixing which is a reasonable time for the pastes to remain workable; in most cases AAS pastes have poor slump retention requiring pastes to be remade rather than recycled for replicate tests (Tan *et al.*, 2017). Figure 5.1 shows that additions of low sugar, high Mw (DP1717) and low sugar, low Mw (DP1718) lignosulfonates at increasing dosages brought a slight improvement in the workability of the pastes, with a maximum slump increase observed at an admixture dose of around 0.3 wt.% by mass of the slag. Any further increase in the dosage of the admixtures resulted in a decrease in the workability of the pastes. From these results, it can be postulated that 0.3 wt.% was the optimum dosage of the lignosulfonates in these mix designs, and above this optimum, there may be saturation of the admixture and the dispersion efficiency is lost. This is because as the amount of lignosulfonates is increased, more is adsorbed on the slag surface until a maximum adsorption capacity is reached, and any excess unadsorbed LS remains dissolved, or suspended undissolved, in the pore solution (Habbaba & Plank, 2010). Due to the highly concentrated nature of the activating solution in these mix designs, the solubility of the powdered LS is reduced (Lei & Chan, 2020), and so it can be hypothesised that some of the excess lignosulfonate in fact remains undissolved in the pore solution. Lignosulfonates have been reported to be completely soluble in water due to the sulfonate groups grafted onto their backbone as discussed in section 2.2.1, however, as the concentration of the alkaline solution

is increased, the solubility of LS is severely diminished. The high concentration alkaline solutions used in these mix designs have reduced free water molecules that are needed to dissolve the lignosulfonate, as well as uniformly lubricate and hydrate the slag particles. The dissolution of LS was not investigated further in this study, however, this problem has been reported for other admixtures such as PCEs because of the high ion concentration of the activator (Lei et al., 2022). Another possible explanation is that at high dosages of LS, there may be attractive intermolecular interactions between the unadsorbed polymers in the pore solution resulting in agglomeration of the polymers instead of working to induce dispersion (Bessaies-Bey et al., 2022). At high LS dosages these interactions are stronger and there is a greater loss in workability as can be observed in Figure 5.1. Nonetheless, it should be noted that the fact that there is still some plasticising effect observed in these extreme conditions is a promising result for these admixtures.

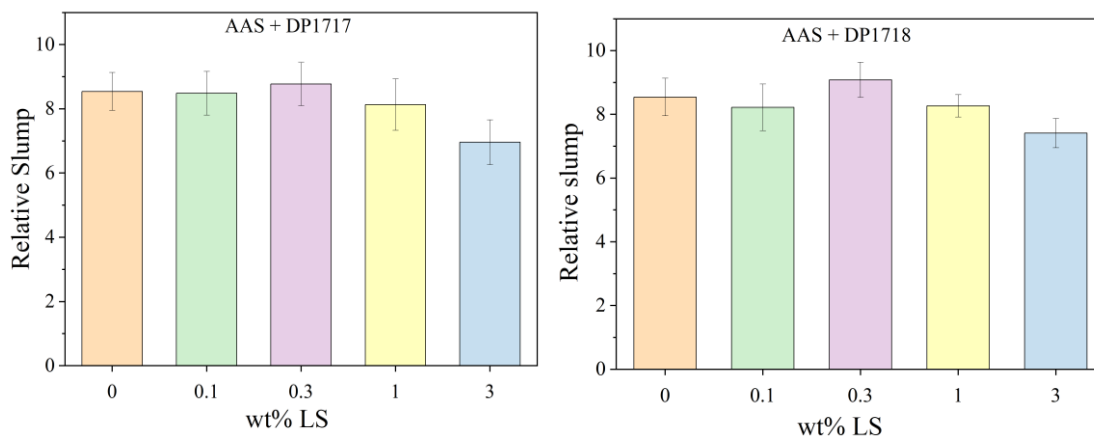


Figure 5.1 The relative slumps of AAS pastes with additions of DP1717 (low sugar, high Mw) and DP1718 (low sugar, low Mw) lignosulfonates. Error bars represent the standard error of the mean.

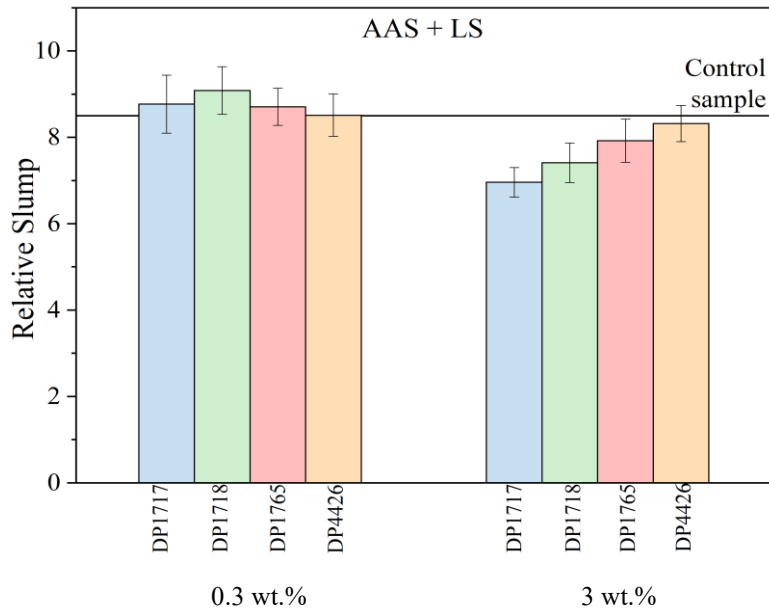


Figure 5.2 Relative slumps of AAS paste with 0.3 and 3 wt.% additions of four types of lignosulfonates; DP1717 - high Mw, low sugar, DP1718 - low Mw, low sugar, DP1765 - high Mw, high sugar, DP4426 – low Mw, high sugar. Error bars represent the standard error of the mean.

A comparison can be drawn between the dispersion efficiency of the lignosulfonates and their structural compositions. Figure 5.2 presents the relative slumps of the pastes at the optimum dosage of 0.3 wt.% and at 3 wt.% (i.e., considered excess addition) of the different types of LS. The DP1718 (low sugar, low Mw) sample performed the best out of all lignosulfonates at the optimum dosage. This may be due to the affinity of this polymer to the slag particles and the more effective adsorption surface coverage achieved at these low molecular weights. The low sugar lignosulfonates performed better than the high sugar samples at the optimum dosage but had a greater loss of slump when exceeding this at 3 wt.% dosage. This indicates that the low sugar LSs plasticise the slag pastes better and are therefore more compatible with the AAS mix designs studied than are high sugar lignosulfonates. The high

Mw samples DP1717 and DP1765 performed comparably at the optimum dosage, regardless of the amount of sugar. The effect of sugars on the dispersion of alkali activated cements must be studied in greater detail, as there is limited research in this area.

The order of admixture addition (procedure outlined in section 3.1.4) of LS into the AAS system was also investigated at the optimum dosage of 0.3 wt.% as presented in Figure 5.3. In simultaneous addition (SA) all the components were mixed at the same time, in delayed addition the LS was added 3 minutes after start of mixing and in prior addition the admixture was initially mixed with the activator and the precursor later added. Regardless of the order of addition, the DP1718 showed some dispersion efficiency when compared to the control sample without any lignosulfonate. The greatest dispersion was achieved immediately after mixing, but this improvement was not retained past 30 minutes as a loss in workability compared to the control is observed at this time point for both the simultaneous and delayed additions. The delayed and simultaneous additions methods were better than prior addition during the early stages, while the sample with prior addition remained workable for longer.

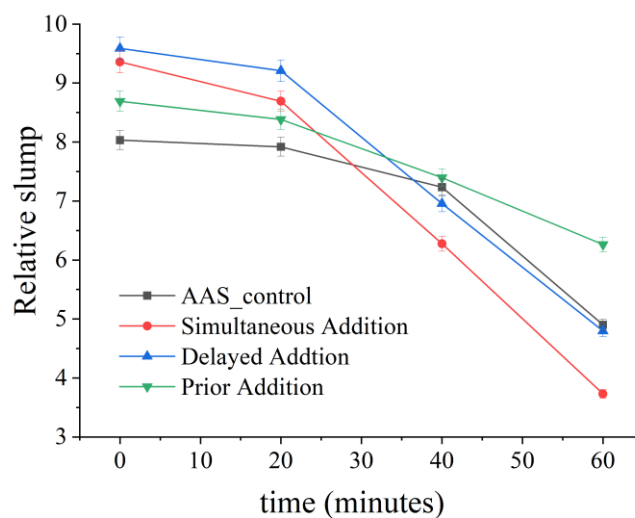


Figure 5.3 The relative slumps of the AAS pastes when different orders of addition of LS (DP1718) were followed. Error bars represent the standard error of the mean.

As well as an indication of colloidal interactions, workability of the paste can also be correlated to the setting and the rate of hydration of a cementitious binder, as rapid hydration may result in workability loss. Over an extended period of time, loss in workability is to be expected due to the hydration reaction of the cement, strengthening of the forces and bridging between the cement grains (Jiang et al., 1996).

### **5.4.2 Rheology**

The rheological behaviour of the pastes was evaluated with and without the addition of lignosulfonate admixtures. The measurements were taken at different time points after mixing, and at the same time as the mini slump tests discussed previously. The aim of this part of the study was to provide a more detailed, quantitative analysis of the fresh state behaviour of the pastes, with perhaps a more precise characterisation method than the mini slump results.

Firstly, the rheological behaviour of the control pastes without any LS was evaluated. Figure 5.4 shows the upward and downward ramp profiles of the shear stress as a function of the shear rate, which demonstrates that immediately after mixing (at 0 minutes), the curve has the lowest slope (i.e., least plastic viscosity, see discussion in section 2.1.1) that increases over time. This increase in viscosity over time is to be expected as the paste loses workability and tends towards rigidity as the initial hydration reaction processes take place. It can also be noted that the upward and downward curves are very similar, indicating that flow is reversible at these time points, which indicates that the bonds/interactions created between the cement grains at these shear rates are reversible at early age. It has previously been reported that AAS pastes tend to show thixotropic behaviour (Qing-Hua & Sarkar, 1994) (Criado et al., 2009). However, in these control samples, thixotropy was not observed. At 20 minutes after mixing was stopped, even though the viscosity increases, the pastes retained high fluidity.

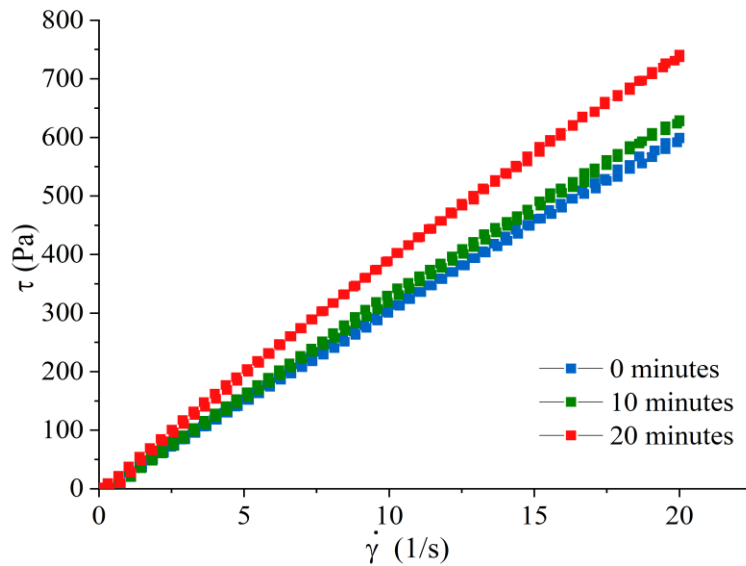


Figure 5.4 The shear stress vs shear rate curves of the AAS control paste without any LS over time after stopping mixing.

Figure 5.5 shows the shear stress vs shear rate curves of the AAS pastes at dosages of 0.3 and 3.0 wt.% of the low sugar, high molecular weight lignosulfonate at 20 minutes since stopping mixing. The control sample without any LS at these shear rates shows an almost linear profile that is similar for both the upward and downward ramp, and a close to zero yield stress, indicative of Newtonian behaviour. At a dosage of 0.3 wt.% LS, which was found to be the optimum in the previously discussed mini slump test studies, a similar curve to the control is observed, but generating the same shear rate at slightly reduced shear stresses for both the upward and downward ramps. This indicates that the addition of LS is causing some plasticising of the paste and reducing its viscosity. Increasing the LS dosage to 3.0 wt.% alters the rheological behaviour of the paste such that the upward and downward curves both have a higher slope compared to the control and 0.3 wt.% sample. The downward curve is observed at lower shear stresses than the upward because of the structure breakdown during the test. A key feature of this curve is the appearance of a hysteresis loop, which is a gap between the upward and downward curve. This feature indicates that due to the presence of excess LS

admixture, the paste is more viscous and displays non-Newtonian behaviour with pronounced thixotropy. The paste is characterised by a decreasing viscosity that plateaued off at high shear rates above  $12 \text{ s}^{-1}$  which indicates a shear thinning behaviour for both the upward and downward ramp.

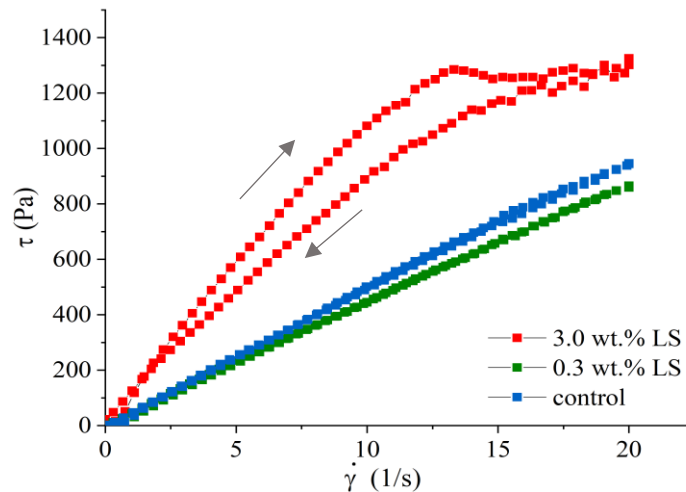


Figure 5.5 Rheometric flow curve of the AAS paste with additions of LS at selected levels.

For the 3.0 wt.% LS sample, more energy was required to break the structure that formed within the paste, and even then, the shearing the paste was subjected to was not sufficient to destroy the structure. The hysteresis is an indication of the number and strength of the bonds between the particles, whatever their nature (Fernández-Altable & Casanova, 2006). As this is only found when excess LS is added, it can be concluded that these interactions involve the excess admixture in the pore solution, although more insight is still needed into the factors that cause them.

There has not been a specific rheological model formulated for alkali activated cements, however, the currently existing models for pastes that include Portland cement have been observed to give a reasonable description of these materials (see section 2.1.1). The experimental data from the rheological measurements presented here were fitted into the

Herschel-Bulkley model, represented by the solid lines in Figure 5.6. This model is given by Equation 5.1 and has been reported to be typical of sodium-silicate activated cements (Palacios et al., 2008).

$$\tau = \tau_0 + k\dot{\gamma}^n \quad \text{Equation 5.1}$$

where  $\tau$  is the shear stress applied to the paste,  $\tau_0$  is the yield stress,  $k$  represents the consistency constant,  $\dot{\gamma}$  is the shear rate and  $n$  is the flow index (Banfill, 2006).

Figure 5.6 shows the Herschel-Bulkley model fit to the downward ramp of the shear stress vs shear rate curves. As can be observed, there does not exist a monotonic relationship between the dosage and the measured viscosities with several dosages giving higher viscosity than the control. The plastic viscosity of the pastes is represented by the gradient of the shear stress vs shear rate curves, and is related to the number and size of the flocs in the paste (Puertas et al., 2018). From these curves, it can be demonstrated that AAS pastes undergo shear thinning where the viscosity decreases under shear strain. The flow index  $n$  is a measure of the degree to which the paste is shear thinning or shear thickening, and all these pastes presented  $n < 1$  as shown in Table 5.1, indicating shear thinning. This shear thinning behaviour of sodium silicate activated slags has also been reported by other researchers (Kashani et al., 2014). When compared to the control sample, the 0.3 wt.% LS sample previously identified as the optimum dosage had the lowest shear stresses and least plastic viscosity. As the dosage of the lignosulfonate is increased, the plastic viscosity is also increased, indicating that there are much stronger interactions between the unadsorbed lignosulfonates and the flocs that are forming. The 3 wt.% LS curve had the highest viscosity and indicates a structure which is incompletely broken down during the test cycle. Conversely, the straight line of the control sample tends more towards Newtonian behaviour (Palacios et al., 2008). The shear stress values were highest

at the greatest dosage of the admixture indicating a much higher degree of flocculation. The highest dosage of LS resulted in a clear decrease in the workability of the paste. Due to the increased viscosity of the paste, some defects such as void formation as the blade is rotating caused by particle migration were observed, and a less reliable model fit was attempted.

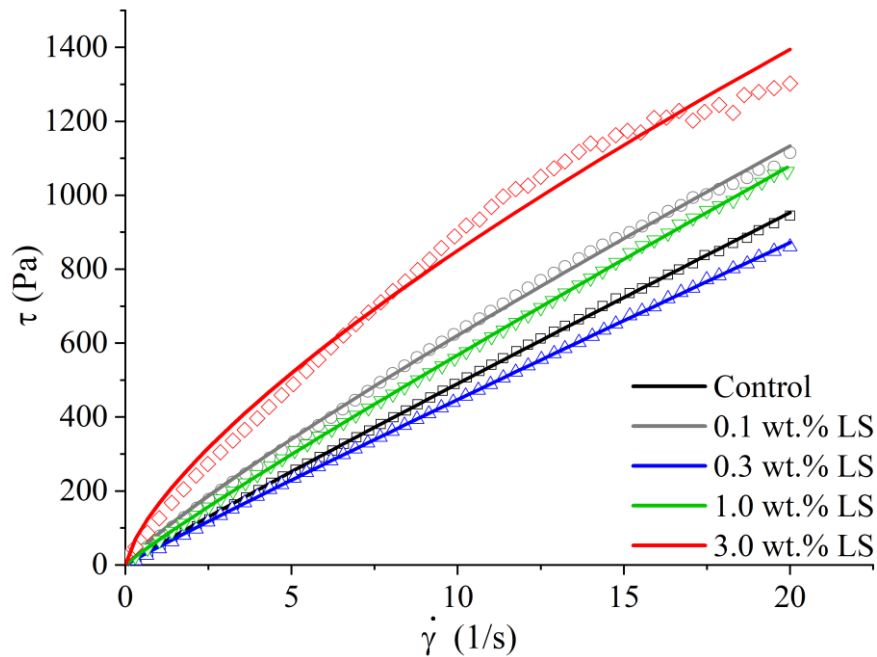


Figure 5.6 The shear stress vs shear rate curves of the AAS pastes with increasing dosages of DP1717 LS. Experimental data are the markers, and the solid lines are the model fit.

Table 5.1 The Herschel-Bulkley model parameters fitted to the curves in Figure 5.6.

wt.% LS	$\tau_0$	$k$	$n$
0	-	53.85	0.959
0.1	-	84.14	0.868
0.3	-	48.67	0.963
1	-	67.18	0.927
3	-	164.42	0.714
3 (0 – 10 s <sup>-1</sup> only)	16.5	110.74	0.899
3 (10 – 20 s <sup>-1</sup> only)	-	316.29	0.476

The yield stress relates to the strength and number of inter-floc interactions between the particles (Puertas et al., 2018). When extrapolating the Herschel-Bulkley fit to zero shear rate for determination of the yield stress, very small values of yield stresses are obtained, and therefore the exact values may not be reliable due to the limited sensitivity of the testing equipment. However, it should be noted that the low yield stresses obtained in these pastes are considered desirable in practical applications as it is an indication that the paste could approach a self-levelling/self-compacting nature, which is very important in a lot of cement applications (Feys et al., 2009). It can be assumed that the activation of the slag and formation of reaction products is not fast enough in these systems to cause significant changes to their yield stresses during the time points under study as shown in Figure 5.4. This is an added advantage of these binders, as the energy required to work concrete mix is reduced, and rapid yield stress increases during early age reaction of premixed concretes are prevented (Kashani et al., 2014). These low yield stresses in sodium silicate activated pastes are due to silicate anions, which adsorb on the particle surfaces, increasing the magnitude of repulsive double layer electric forces, and hence reducing the yield stress (Kashani et al., 2014).

Figure 5.7 presents the downward ramp of the shear stress vs shear rate curves when different types of lignosulfonates were added at an optimum dosage of 0.3 wt.%. The pastes had similar rheological behaviours, with the DP1718, DP1717 and DP1765 samples having a slightly reduced viscosity compared to the control while the DP4426 low Mw, high sugar sample performed the worst giving the highest viscosities than the other LSs. This data highlights that compatibility is an important aspect when using bio derived admixtures in alkali activated cements.

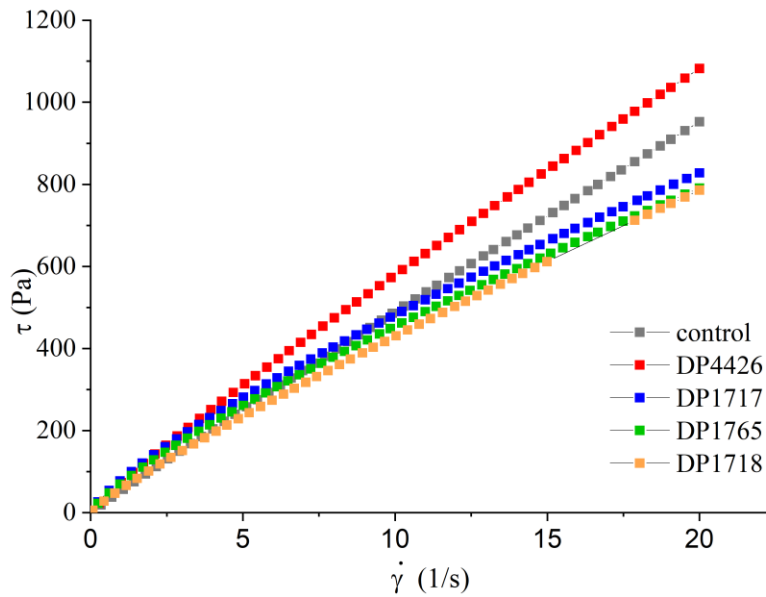


Figure 5.7 Rheological data from additions of different types of LSs at 20 minutes since stop of mixing. DP1718 – low Mw, low sugar, DP1717 – high Mw, low sugar, DP1765 – high Mw, high sugar, DP4426 – low Mw, high sugar.

This study also investigated the order of addition of the lignosulfonate and its effect on the rheology of the paste over time as shown in Figure 5.8. The hysteresis was a prominent feature in both delayed and simultaneous additions at longer times after mixing. This indicates that in the presence of LS, the pastes tend towards thixotropic behaviour over time. Papo and Piani, (2004) found that the addition of admixtures modified the pattern of the hysteresis curve such that the curves positioned at lower shear stresses with a much reduced hysteresis gap, denoting that the structure breaks down. However, it should be noted that these tests were carried out immediately after mixing and not at longer times (20 minutes after stopping mixing) as is done in the present study. The results presented in Figure 5.8-5.9 suggest that over time, the lignosulfonates have some associative thickening effects brought about by the intermolecular interactions between the unadsorbed polymers in solution (Bessaies-Bey et al., 2022).

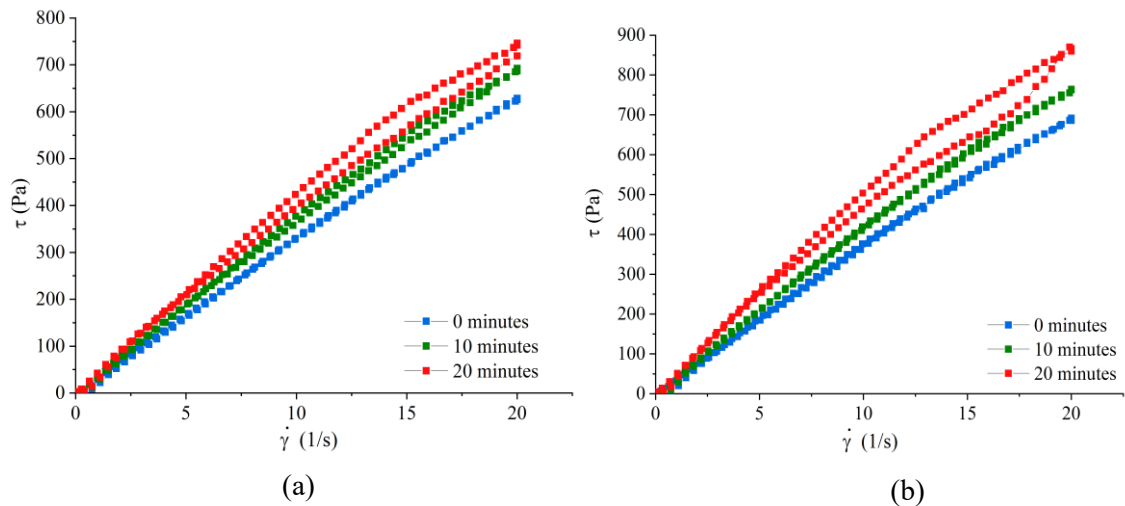


Figure 5.8 Rheological data when different modes of DP1718 LS addition were followed at a dosage of 0.3 wt.%; (a) DA and (b) SA as a function of time after the end of AAS paste mixing.

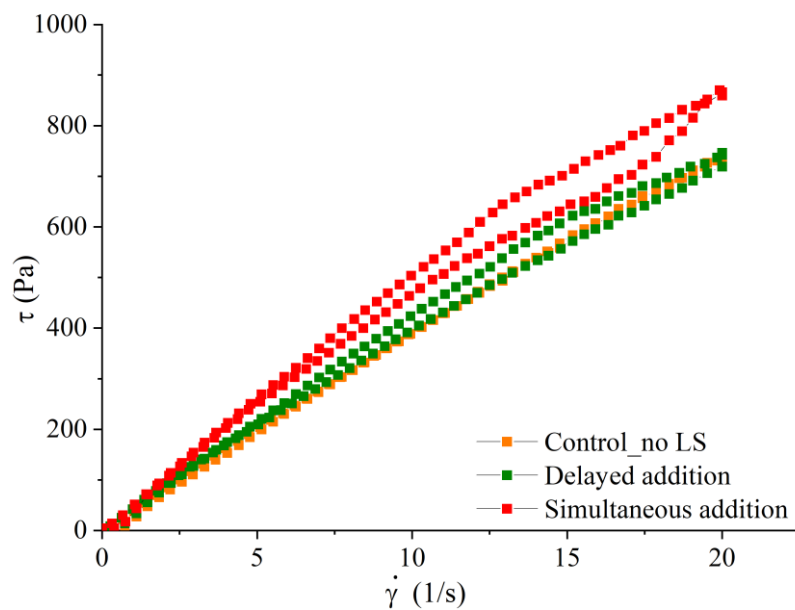


Figure 5.9 Rheological data for the AAS + DP1718 sample without LS, DA and SA, tested 20 minutes after stopping mixing.

Figure 5.9 shows that even at longer times since stopping mixing, the control sample still did not show any thixotropic behaviour. The simultaneous addition method resulted in a larger hysteresis and a higher plastic viscosity compared to the delayed addition of LS, but the

measured yield stresses remained low in all tests. This may be because the lignosulfonate polymers start to interact as soon as mixing has started, while it is observed to a lesser extent with delayed addition as the paste has already begun mixing under shear. The different rheological behaviour indicate that these methods of addition resulted in different interactions between the LS and the alkali activating system. This is investigated further by electrostatic interactions in Chapter 6 which provides more insight into the interactions occurring in these conditions.

### **5.4.3 Setting time**

The initial and final setting times of the AAS pastes with and without LS as determined by Vicat penetration tests are presented in the Figure 5.10-5.12. It is well documented that activated slag cements are prone to uncontrollable and quick setting due to the formation of initial calcium silicate hydrate (C-S-H), particularly at high activator doses. The control samples without LS attained initial and final setting times of 1 h 20 mins and 1 h 40 mins, respectively, which are reasonable for these mix designs. The low sugar, low Mw DP1718 and low sugar, high Mw DP1717 appear to increase both the initial and final setting times of the alkali activated slag pastes as the dosage of these admixtures is increased. This indicates that the presence of LS delays the setting mechanism of these AAS pastes, without the presence of high levels of sugars. The high Mw sample delayed the setting mechanism to a greater extent than the low Mw sample, with final setting times of over 2h30mins at dosages  $\geq 0.3$  wt.%, as shown in Figure 5.10. These results demonstrate that lignosulfonates can be used to control/delay the setting of AAS pastes.

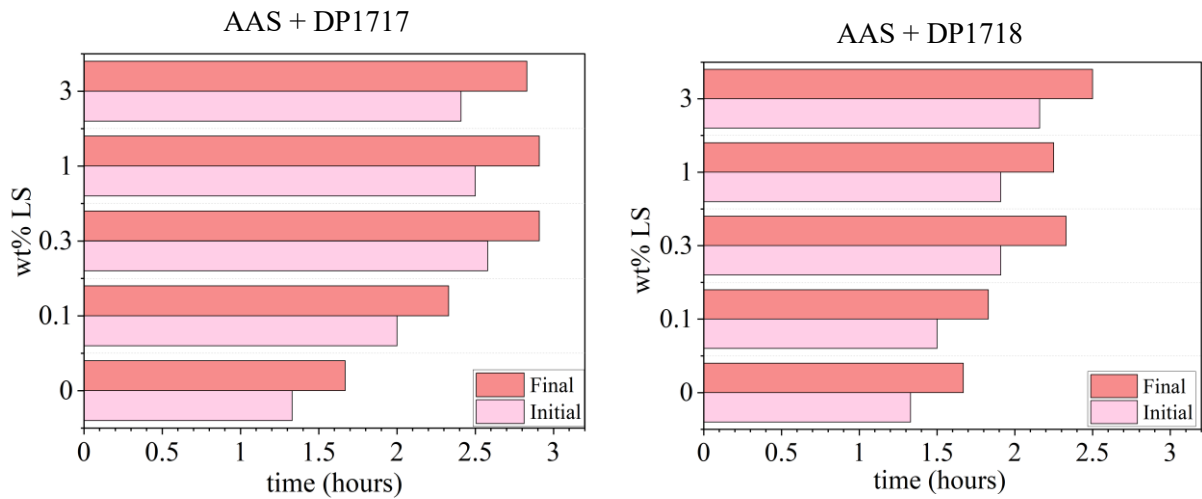


Figure 5.10 The initial and final setting times of the AAS pastes with increasing dosages of the low sugar, high Mw DP1717 and low sugar, low Mw DP1718.

Figure 5.11 shows that the high sugar lignosulfonates appear not to affect the setting of the pastes significantly, showing only a slight increase in the initial and final setting times. It has long been established that sugar has a retardation effect on Portland cement (Bishop & Barron, 2006), but, in these AAS pastes, the presence of sugar in the LS did not significantly delay the setting of the pastes. In fact, the high sugar LS resulted in faster setting pastes compared to the low sugar samples. This observation warrants a closer look at the effect of sugar on the properties of alkali activated cements.

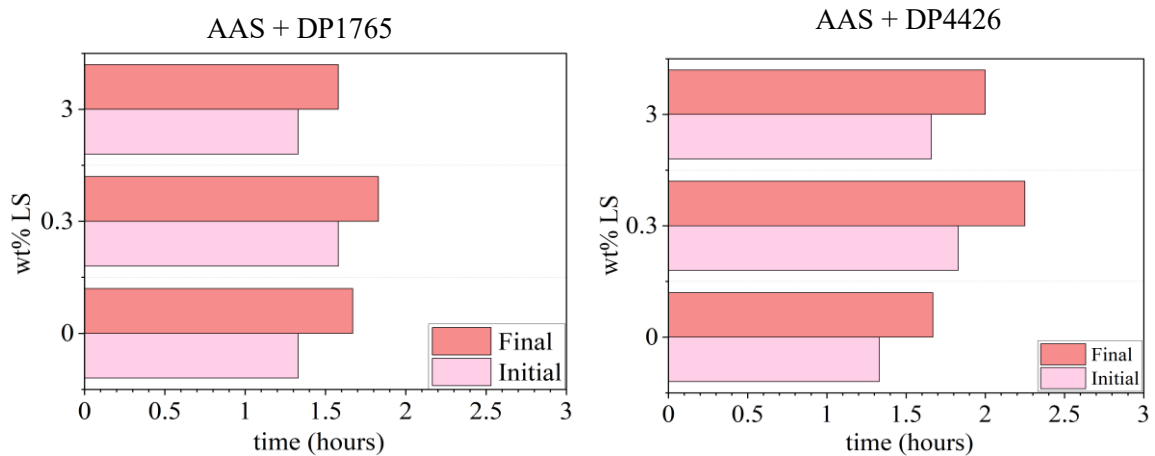


Figure 5.11 The initial and final setting times of the AAS pastes with increasing dosages of the high Mw, high sugar DP1765 and low Mw, high sugar DP4426.

A possible retardation mechanism bringing about these changes in the setting of AAS pastes is the formation of complexes between the calcium ions in solution and the sulfonate groups on the lignosulfonate, during the early stages of hydration. This bonding nature of the organic LS molecule was reported in Portland cement systems (Uchikawa et al., 1992). This means that the calcium ions are consumed from the pore solution, and therefore fewer are available to form the C-A-S-H product and the onset of setting from its precipitation is delayed (Vikan et al., 2007). This means that the setting of the paste is delayed further as more lignosulfonates are added to the system.

#### **5.4.4 Compressive strength**

After 7 and 28 days of curing, the AAS pastes without any admixture had developed high mechanical strengths of 89 and 120 MPa respectively, as shown in Figure 5.12. The compressive strength increased with an increase in curing time as is expected. This is because over time the skeleton of the pastes is densified and strengthened as more hydration products are formed, resulting in increased compressive strengths (Fernández-Jiménez et al., 1999). These high mechanical strengths can be attributed in part to the high shear and prolonged mixing of the pastes improving the cohesion and compactness of the pastes (Palacios & Puertas, 2011), (Kashani et al., 2014). The sodium silicate activator at a modulus of 1.5 and high alkalinity is the main reason for these high compressive strength performances. The effect of lignosulfonates is apparent; as LS were added there was a decrease in the compressive strengths

of the pastes, regardless of the time of curing. There was a decrease in the compressive strength with the most decrease at the highest dosage of 3.0 wt.%, for both 7 and 28 days of curing.

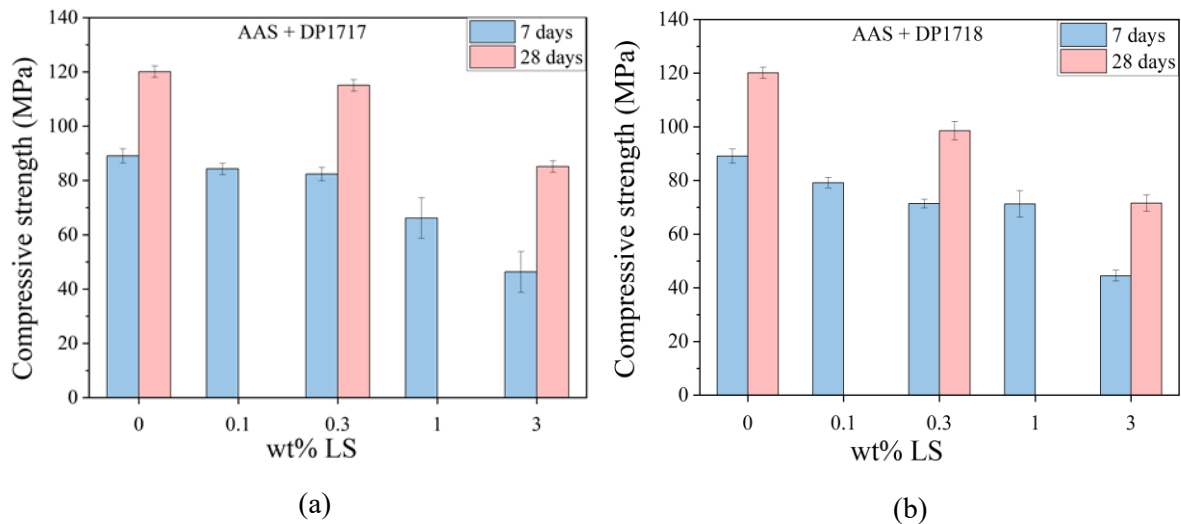


Figure 5.12 The compressive strengths of the AAS pastes after 7 and 28 days of curing at 20 °C with increasing additions of lignosulfonates. (a) DP1717 – high Mw, low sugar and (b) DP1718 – low Mw, low sugar. Error bars represent the standard error of the mean.

The lignosulfonate sample with low Mw and low sugar (DP1718) suffered a slightly greater decrease in compressive strength at 7 days compared to the high Mw and low sugar (DP1717) sample. This change was even greater at 28 days of curing for DP1718 compared to DP1717. These results are an indication of the effects of these different lignosulfonates on the compactness and densification of the cement matrix; this is discussed further in section 5.4.6 to explore the fate of lignosulfonates as the pastes are hydrating over time.

Further comparison can be drawn between the low and high sugar lignosulfonates on the effect of compressive strength development of the slag pastes at 0.3 and 3 wt.% dosages. As shown in Figure 5.13, there was a reduced strength for all LS-containing samples at both dosages after 7 days of curing. This decrease was even more significant at high dosages of 3

wt.% LS. The DP1717 sample least affected the compressive strength at 0.3 wt.% while the paste sample with DP1765 had the greatest decrease in strength. At high dosages, it appears the effect from the four lignosulfonates is similar.

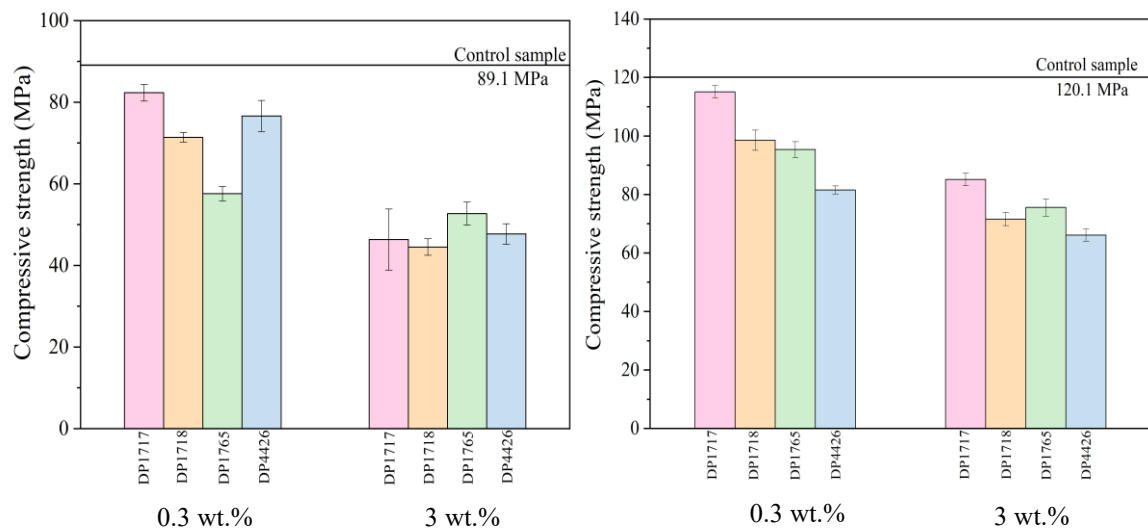


Figure 5.13 Compressive strengths of the AAS hardened pastes with additions of four types of lignosulfonates, measured at 7 days of curing. DP1717 – high Mw, low sugar, DP1718 – low Mw, low sugar, DP1765 – high Mw, high sugar, DP4426 – low Mw, high sugar. Error bars represent the standard error of the mean.

In Portland cement pastes, sodium lignosulfonate has been reported to inhibit the hydration process by reducing the formation of  $\text{Ca(OH)}_2$  and lowering the degree of polymerisation of the silicate anions (Yousuf et al., 1995). A lowering of the degree of polymerisation in these AACs may be the reason for the loss in mechanical strength, however, this needs to be investigated as  $\text{Ca(OH)}_2$  is not an issue in AAS. It is also possible that the addition of the polymer resulted in entrainment of an excessive amount of air (Łażniewska-Piekarczyk, 2014) which would result in the decrease in the compressive strengths of the pastes, however, this was not investigated in this study. The decrease in compressive strength across all samples,

dosages and curing times may be linked to the poor dissolution of lignosulfonates in highly alkaline media. At excess addition levels of lignosulfonates, these powders remain undissolved in the pore solution. This reduces the interconnectivity of the paste, and as the pastes set and hardened, the LS are embedded into the cement matrix and may adversely affect the structural integrity of the system.

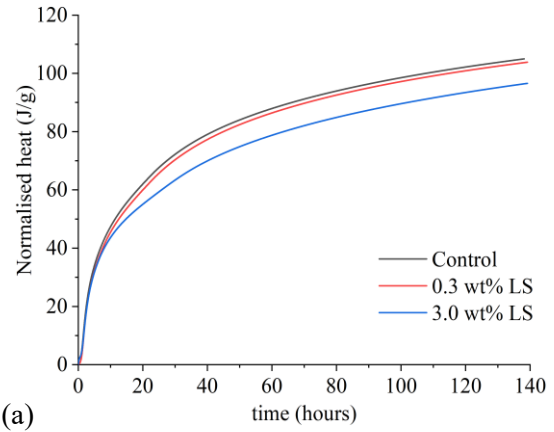
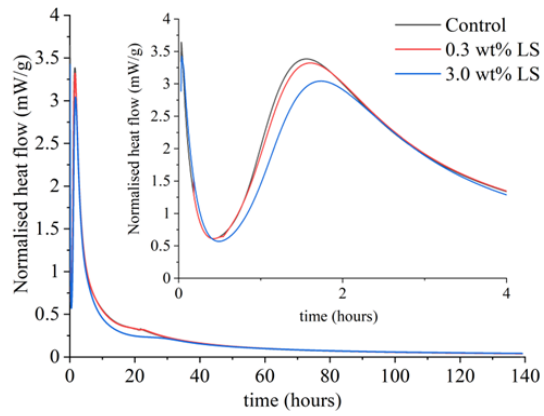


Figure 5.14 The cubes of the AAS pastes after 7 days of curing. (a) control, (b) LS added at 0.3 wt.% and (c) LS added at 3 wt.%.

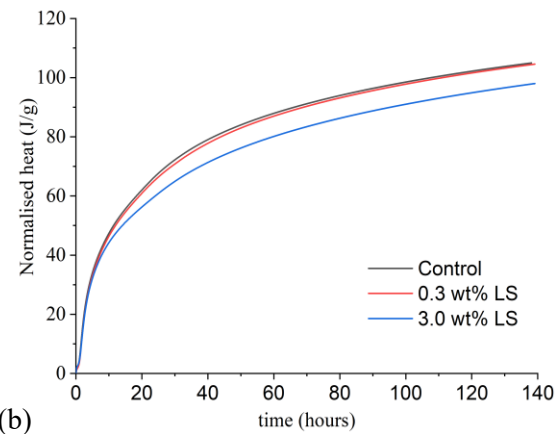
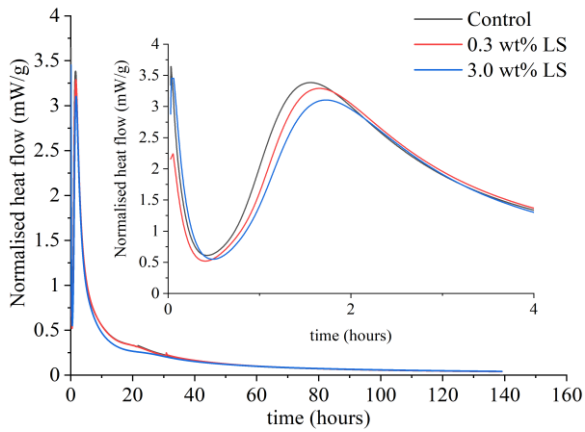
The cube moulds before compressive strength testing were stored in an unsealed mould with a damp tissue to ensure 100% humidity (at least at the beginning of curing). From the images shown in Figure 5.14, when lignosulfonates are added to the pastes, there is evidence for increased evaporation of water from the exposed surface of the cubes. This loss of water is followed by cracking on the surface with some cubes having more cracking propagating further into the cube. This effect was more significant in samples with the highest dosage of LS and cured for longer periods of time. To reduce the contribution of this loss of water to compressive strength development, it must be ensured that the moulds are completely sealed, the damp tissues re-wetted or the cubes water cured.

### **5.4.5 Isothermal Calorimetry**

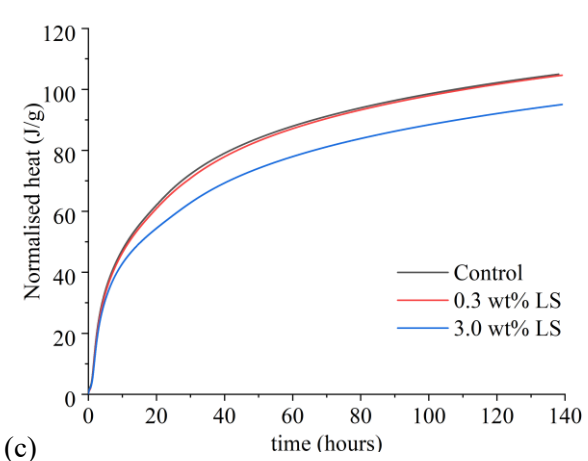
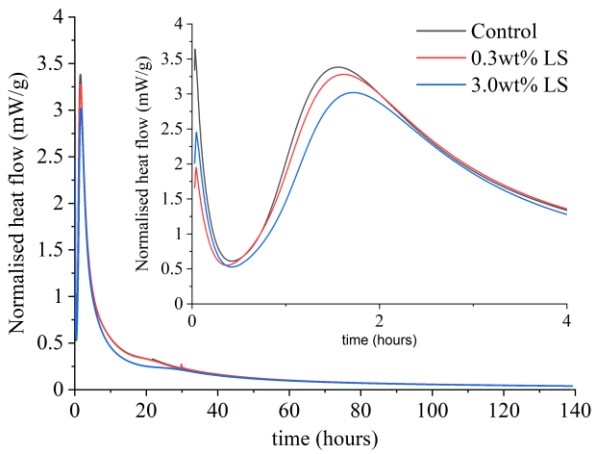
The hydration characteristics of alkali activated cementitious materials have been widely investigated through calorimetry studies due to the exothermic nature of the alkali activation process (Shi & Day, 1995), (Criado et al., 2018), (Sun & Vollpracht, 2018). The isothermal calorimetry study shows the associated chemical changes, both in the solid phases as well as the pore solution during the early activation of the pastes. The influence of the admixture on the kinetics and hydration of waterglass-activated slag pastes is thus able to be investigated.



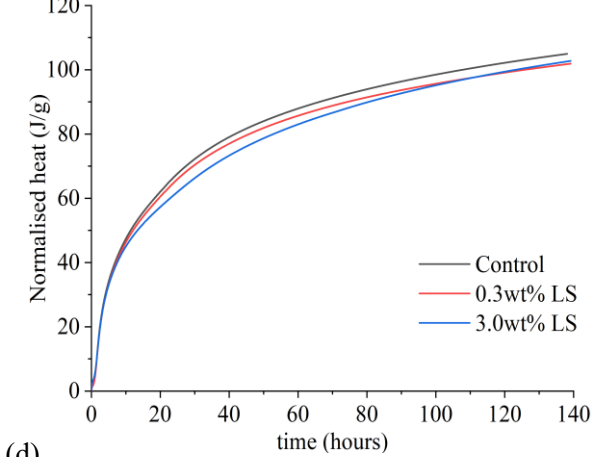
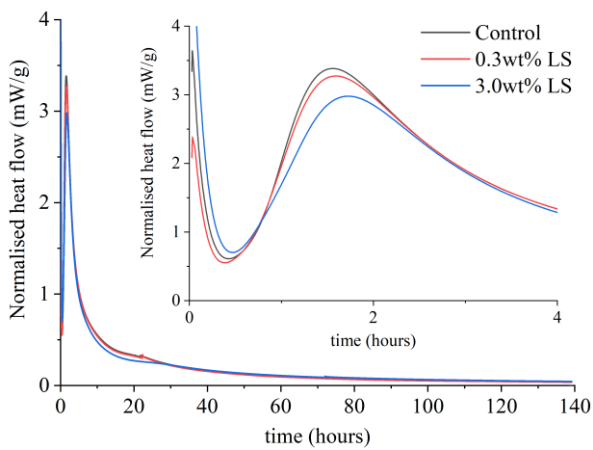
(a)



(b)



(c)



(d)

Figure 5.15 The heat evolution for AAS pastes with the four types of lignosulfonates: (a) DP1718, (b) DP1717, (c) DP4426 and (d) DP1765.

The heat evolution of AAS pastes with and without additions of different types of lignosulfonates is presented in Figure 5.15. For all the rate of heat evolution curves, there is a single sharp peak in the early hours of hydration, and no other recorded peaks. Due to fast reaction of the pastes upon mixing, the initial peak that corresponds to the wetting and dissolution of the particles cannot be observed (Shi & Day, 1995). The single peak observed in Figure 5.15 for all paste samples is the accelerated hydration peak that corresponds to C-A-S-H phase formation. With the addition of 0.3 and 3.0 wt.% LS, the hydration peaks were lower than for the control samples, regardless of the type of lignosulfonate added. As this peak is an indication of product phase formation, it can be deduced that LS has a slight effect on this process which is more pronounced when excess LS is added. The cumulative heat release curves show only a slight decrease in the total heat at dosages of 0.3 wt.%, and a more significant decrease at high dosages of 3.0 wt.% LS. These curves are an indication of the extent of reaction; the presence of the LS admixtures evidently reduced the extent of the hydration reactions. This correlates to the decreased strength of the pastes at increased LS dosages as previously discussed.

#### **5.4.6 The fate of lignosulfonates in alkali activated slag pastes**

Characterisation of the pastes at 7 and 28 days of curing was conducted for a more detailed look into the effect of lignosulfonates on the product formation during alkali activation. The fate of lignosulfonates after curing of AAS pastes was investigated.

Figure 5.16 presents the FTIR spectra highlighting the key product formation features of the AAS pastes. The band at  $460\text{ cm}^{-1}$  is attributed to the Si-O-Si bond vibrations while the lower intensity peak at  $669\text{ cm}^{-1}$  is due to the stretching vibrations generated by the Al-O bonds in the  $\text{AlO}_4$  groups (Puertas & Torres-Carrasco, 2014). The peak at  $1655\text{ cm}^{-1}$  is a result of the bending vibrations due to the OH groups in the water (Puertas & Torres-Carrasco, 2014). Paste carbonation or weathering is confirmed by the presence of peaks at  $1420\text{ cm}^{-1}$  and a shoulder in the region between  $875$  and  $780\text{ cm}^{-1}$  attributed to  $\text{CO}_3^{2-}$ . The bands in the pastes showed similar positions but more pronounced widths and intensities for longer cured samples at 28 days compared to 7 days. The addition of lignosulfonates had an insignificant effect on these bands, which indicates that these admixtures did not have a direct effect on the hydration product formation. The 0.3 wt.% at both 7 and 28 days of curing have a more pronounced peak at  $980\text{ cm}^{-1}$  attributed to the asymmetric stretch in the Si-O-(Si-Al) bonds compared to the control and the 3.0 wt.% samples. This peak signifies the formation of the most important hydration product, the C-A-S-H gel. This pronounced peak may be due to the improved workability and mixing at this LS dosage, which allows for better dissolution and bond formation in the paste. However, this does not correlate with the strength development of the pastes previously discussed. This suggests that other factors such as physical contributions of the LS as well as the curing conditions had a significant impact on the mechanical strength development of the pastes. Due to a reduced humidity, the presence of LS contributed to a rapid water loss as discussed in section 5.4.4, which may be a key factor in the decline in the compressive strengths of the pastes. The hydration products are unaffected by this loss of water because it is the unbound water in the pore structure that is lost, the bound water involved in the hydration process ensures product formation.

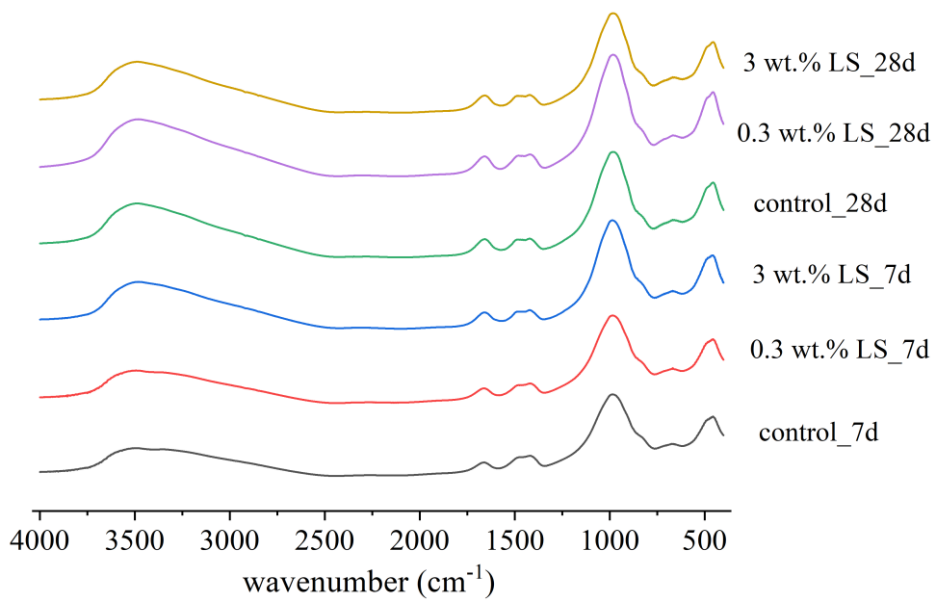


Figure 5.16 The FTIR spectra of the AAS pastes with and without DP1718 LS additions after 7 and 28 days of curing at 20 °C.

A thermogravimetric analysis of the pastes was conducted after 7 and 28 days of curing and presented in Figure 5.17. The progressive mass loss observed below 200 °C is associated with the decomposition of the main reaction product, the C-A-S-H gel. At temperatures of about 350 °C the decomposition of the hydrotalcite is observed and at 700 -800 °C, the decomposition of calcium carbonate (Rashad et al., 2012).

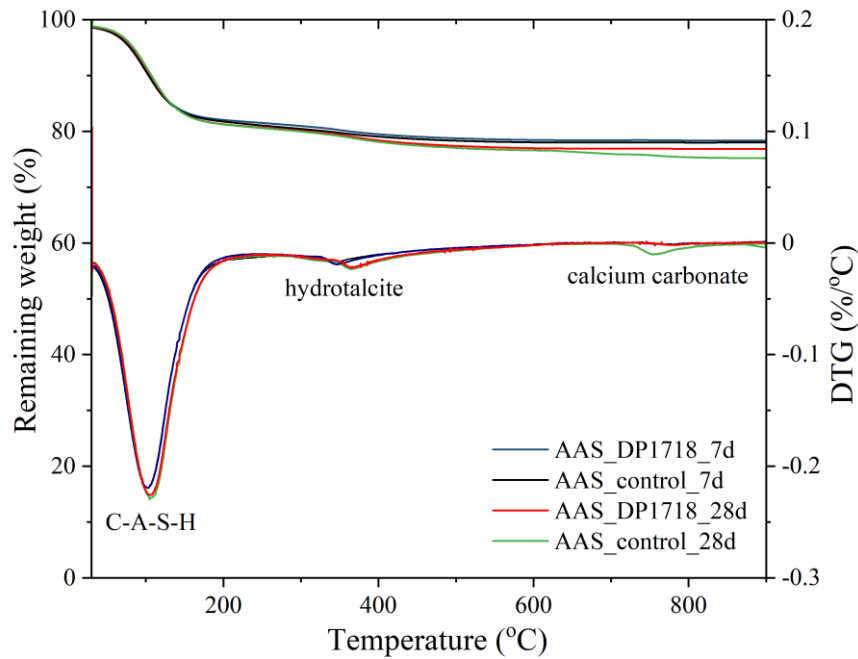


Figure 5.17 Thermogravimetric analysis of the AAS pastes after 7 and 28 days of curing at 20 °C, with and without addition of DP1718 LS at 0.3 wt.% dosage.

The increased calcium carbonate found on the control sample at 28 days of curing is due to carbonation effects. This is likely due to the environmental curing conditions of the pastes such that a change in parameters such as a reduction in the relative humidity increased the carbonation effects (Kovalchuk et al., 2007).

Scanning electron microscopy (SEM) was used to investigate any compositional and microstructural changes taking place during activation of slag due to the presence of lignosulfonate admixtures. Figure 5.18 shows an image of the slag control sample, which shows a dense cement matrix with some large angular particles which are lighter in contrast embedded in the paste; these are unreacted slag particles. The SEM image of the LS is also presented, which shows that the admixture is made up of mainly spherical particles with varying sizes. The paste sample with addition of LS shows the presence of undissolved lignosulfonates embedded in the cement matrix, with their spherical shape retained. These may

be contributing to the reduced structural integrity of the pastes during compressive strength testing. The cracks observed in the higher magnification images are typical of AAS images and these are due to the sample grinding and polishing process that utilised isopropanol, drying up the surface in the process and leading to cracks. This were enhanced further by the high vacuum effect of the SEM required during imaging. These microcracks, especially at early ages of curing have been attributed to tension from drying shrinkage effects brought about by sample preparation (Brough & Atkinson, 2002).

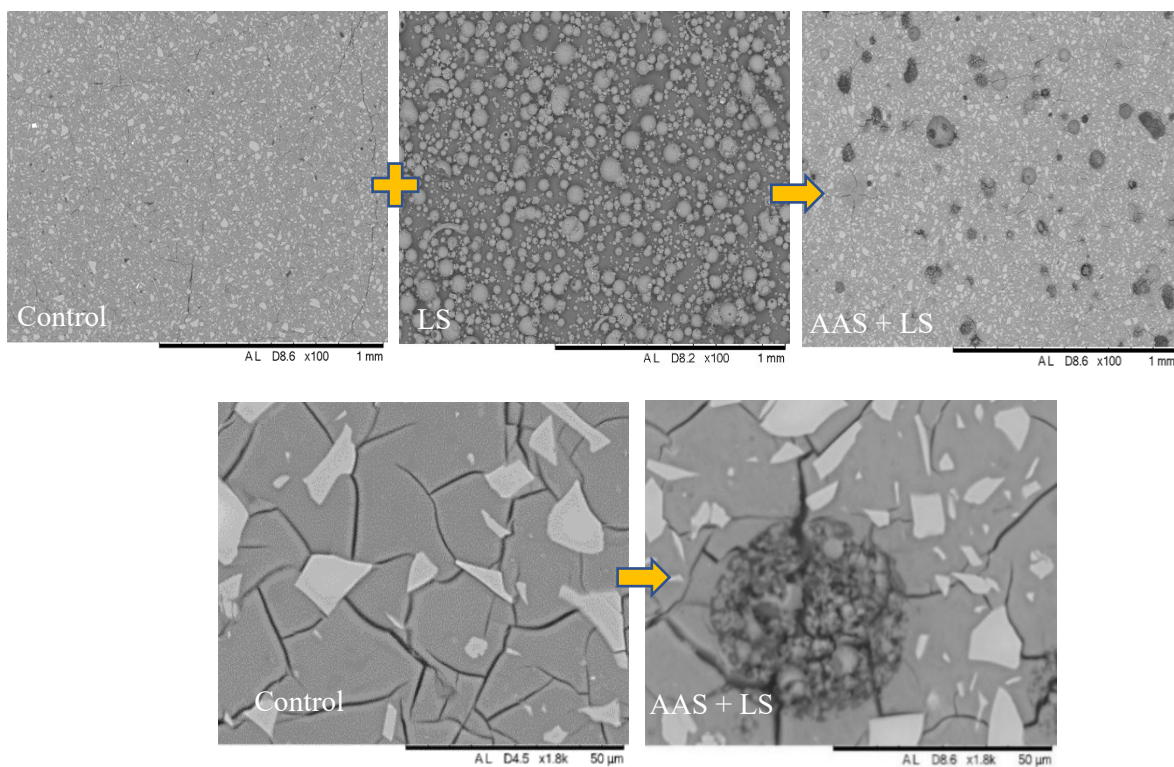


Figure 5.18 The scanning electron micrographs of the AAS pastes with and without 3 wt.% addition of LS after 7 days of curing. Top row: low magnification; bottom row: higher magnification.

## 5.5 Effect of lignosulfonates on the properties of alkali activated fly ash

### 5.5.1 Workability

The workability of the waterglass-activated fly ash pastes (denoted AAFA) is presented as relative slumps in Figure 5.19-5.21. The mix design for these pastes is presented in section 3.1.4. Unlike AAS pastes which tend to have challenging workability, fly ash inclusion has been reported to improve the workability of blended pastes, and this is attributed to their spherical geometry which improves the rheological properties of the pastes. Without any addition of lignosulfonates, the AAFA paste at a water/binder ratio of 0.28 was very workable, had high fluidity and mixed well, even at short mixing times. This fluidity was retained over extended periods of time (~ 1 hour) after stopping mixing.

Figure 5.19 shows that the low sugar, high Mw lignosulfonate (DP1717) admixture had a negative effect on the workability of the low calcium alkali activated fly ash pastes (AAFA) at all dosages. As more DP1717 was added, there was no additional dispersion of the paste, but instead the relative slump gradually declines. This loss in workability may be due to the incompatible surface chemistry of the fly ash particle, being dominated by silicate ions instead of  $\text{Ca}^{2+}$ , such that the negatively charged LS cannot be adsorbed (Wang et al., 2021). This means that dispersion of the particles is not induced hence no improvement in workability can be observed. The unburnt carbon in the fly ash (LOI of 0.6%) also has the ability to absorb some the admixtures such that there is less available to induce dispersion of the paste (Hill et al., 1997). On the other hand, the low sugar, low Mw lignosulfonate (DP1718) showed a slight improvement in the workability when this admixture was added. The highest improvement in slump was observed at 0.1 wt.% followed by 0.3 wt.%, while higher dosages did not improve the workability of the paste. This suggests that there is some dispersion induced by this LS as

some compatibility exists between the fly ash particles and LS. However, no conclusion can be drawn at this stage because the changes observed are only marginal.

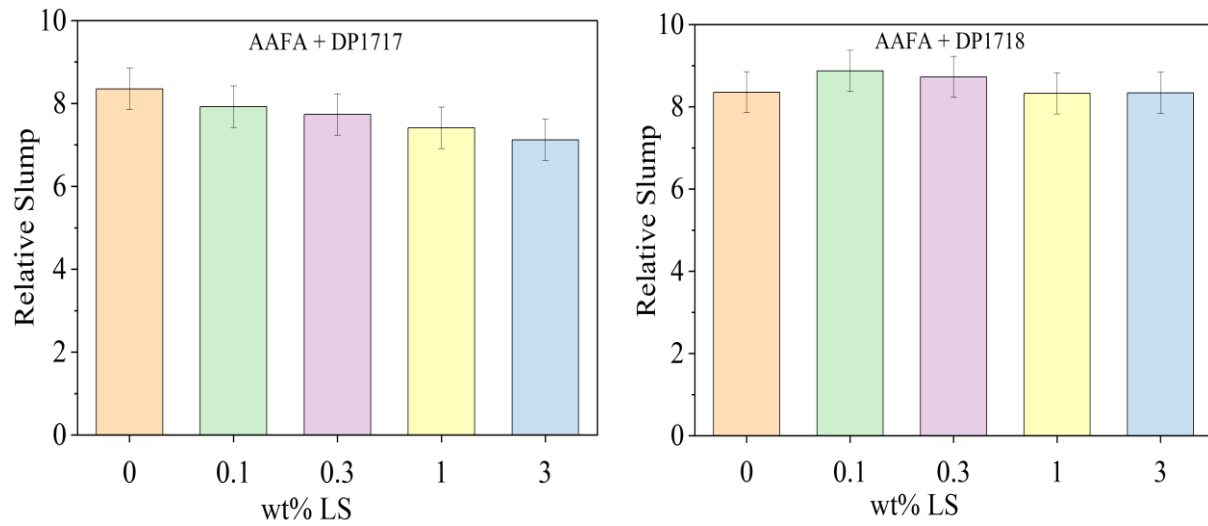


Figure 5.19 The relative slumps of AAFA pastes with increasing additions of DP1717 (low sugar, high Mw) and DP1718 (low sugar, low Mw) lignosulfonates. Error bars represent the standard error of the mean.

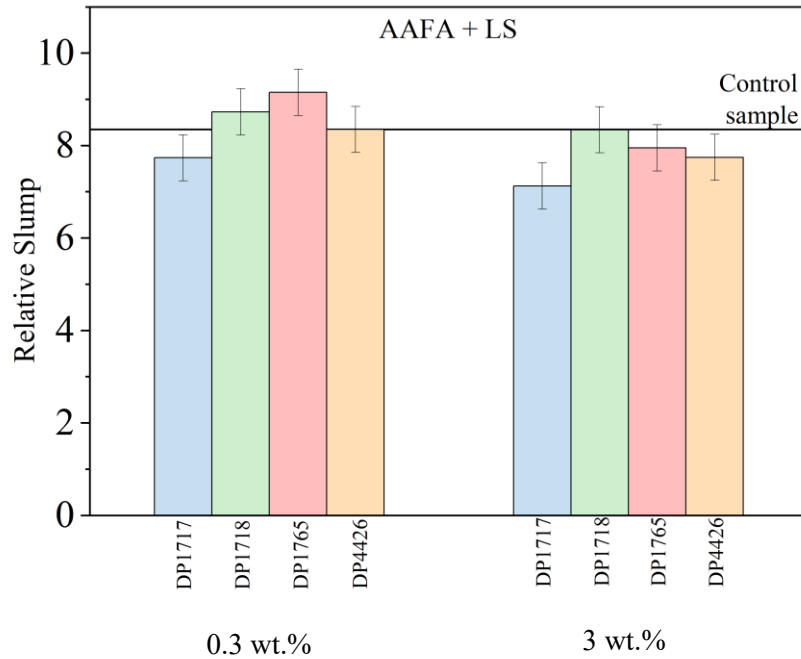


Figure 5.20 Relative slumps of AAFA with 0.3 and 3 wt.% additions of four types of lignosulfonates; DP1717- high Mw, low sugar, DP1718 - low Mw, low sugar, DP1765 - high Mw, high sugar, DP4426 - low Mw, high sugar. Error bars represent the standard error of the mean.

The lignosulfonates with high sugar content were also added to the mix to ascertain their efficiency in improving the workability of the AAFA pastes as shown in Figure 5.20. The high sugar, high Mw sample gave the highest improvement in the slump of the pastes when compared to the control sample. The low sugar, low Mw sample also improved the workability while the high sugar, low Mw LS (DP4426) showed no change. The low sugar, high Mw LS (DP1717) performed the worst out of the four types of lignosulfonates, with a decrease in the relative slump of the pastes. These results do not show conclusively which properties of the lignosulfonates are more compatible with the fly ash activated system. However, they do show that one type of lignosulfonate can improve the workability of fly ash while another can be detrimental, which highlights the compatibility issues between the precursor material and admixtures.

## 5.5.2 Rheology

The rheological behaviour of the pastes as fly ash was activated with waterglass, with and without lignosulfonate admixtures, was evaluated. The control AAFA pastes without lignosulfonate are presented as a function of time since stopping mixing, in Figure 5.21, which shows the curves produced during the upward and downward ramp. It can be observed that the paste had the least viscosity (slope) immediately after mixing (0 minutes), which then increases over time due to the onset of reaction processes and particle interactions. It is to be expected that the paste loses some fluidity over time due to these processes. There are only slight differences between the upward and downward ramps regardless of the time of measurement, with a barely noticeable hysteresis at higher shear rates that does not change over time. These pastes showed highly fluid behaviour even when measured 20 minutes after stopping mixing, as characterised by the low shear stresses recorded.

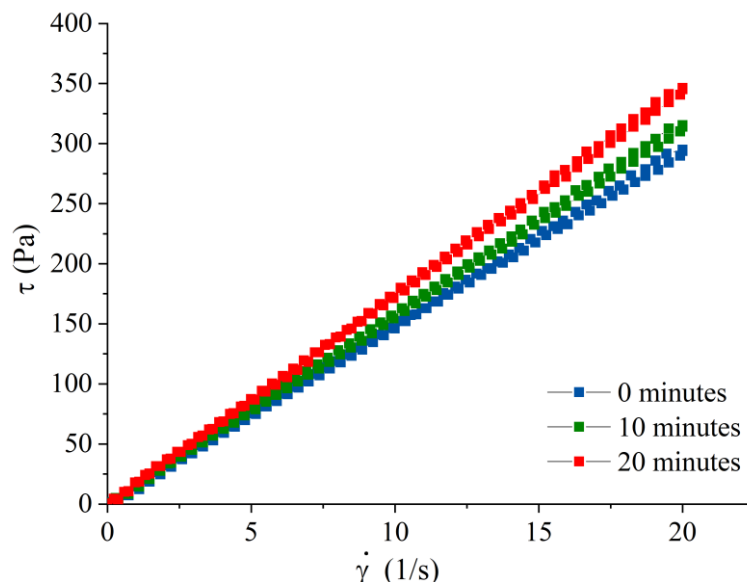


Figure 5.21 The shear stress vs shear rate curves of the AAFA control paste as a function of time after stopping mixing.

Figure 5.22 shows the rheological behaviour of the pastes upon addition of a low sugar, high Mw (DP1717) lignosulfonate. The control and the sample with 0.3 wt.% LS added present similar shear stress vs shear rate curves, which indicates that there was not much plasticising of the paste by the lignosulfonate admixture. In fact, the viscosity is slightly higher in the 0.3 wt.% LS sample than the control, which correlates to the mini slump results previously discussed. The 3 wt.% LS sample on the other hand had a markedly different rheological behaviour, reaching high shear stresses when imposing the same shear rate as the other samples. The viscosity for this sample was thus significantly increased at the high dosage of LS, and the presence of a hysteresis loop can be observed. This indicates that the excess LS present adversely altered the interactions of the particles in the paste and reduced its fluidity.

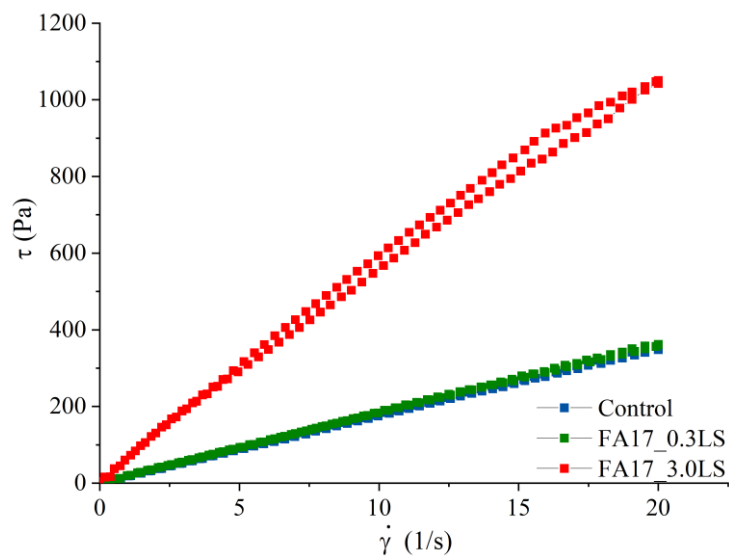


Figure 5.22 Rheometric flow curve of the AAFA paste with 0.3 and 3.0 wt.% additions of LS.

Figure 5.23 shows that the hysteresis loop mentioned previously occurs at 20 minutes since stopping mixing and not before. This confirms the development of thixotropic nature in the paste at these high dosages and increased timeframes. This highlights that due to the presence

of this high dose of LS, the pastes may lose fluidity quicker over time than without admixture addition.

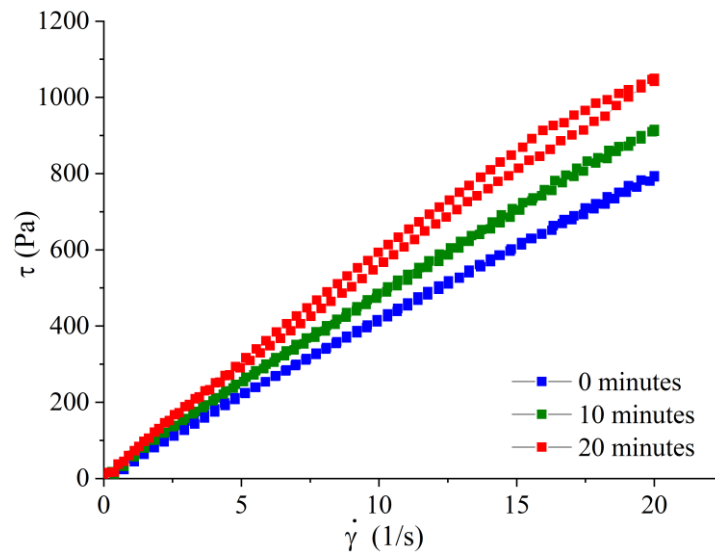


Figure 5.23 The shear stress vs shear rate curves of the pastes with the highest LS dosage (3 wt.% of DP1717) since stopping mixing.

The experimental data was fitted using the Herschel-Bulkley model, as represented by the solid lines in Figure 5.24. The control paste and the low LS dosages (0.1 and 0.3 wt.% LS DP1717) had negligible yield stresses and  $n$  very close to 1.0, indicating that they tend towards Newtonian behaviour as shown in Table 5.2. When LS was added in excess, the rheological data showed a Herschel-Bulkley behaviour with increased yield stresses. At this dosage, the viscosity is once again increased. This rheological data set confirms that the low sugar, high Mw LS was not compatible with the AAFA system, as it reduced the fluidity of the paste instead of plasticising it.

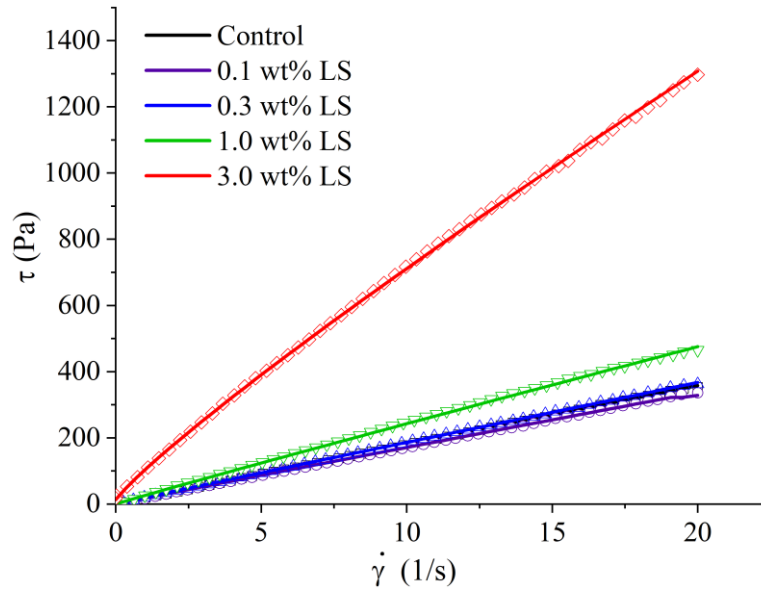


Figure 5.24 The shear stress vs shear rate curves of the pastes with increasing dosage of the DP1717 LS. Experimental data are the markers, solid lines are the model fit.

Table 5.2 The Herschel-Bulkley model parameters fitted to the curves shown in Figure 5.25.

wt.% LS	$\tau_0$	$k$	$n$
0	0	18.03	0.997
0.1	0	17.28	0.993
0.3	0.004	19.33	0.982
1	0	27.77	0.948
3	10.09	93.63	0.876

At the same dosage, different types of lignosulfonates (low Mw vs high Mw, low sugar vs high sugar) were added to the pastes to investigate their compatibility with the AAFA cement system. Figure 5.26 presents the model fit of the downward ramp curves when a dosage of 0.3 wt.% of each LS was added. The curves retained a linear form, and the admixture that resulted in the least viscosity was the high sugar, low Mw (DP4426) sample. In general, the high sugar

samples performed better than the low sugar samples, which suggests some plasticising effect due to the presence of the sugar in the LS.

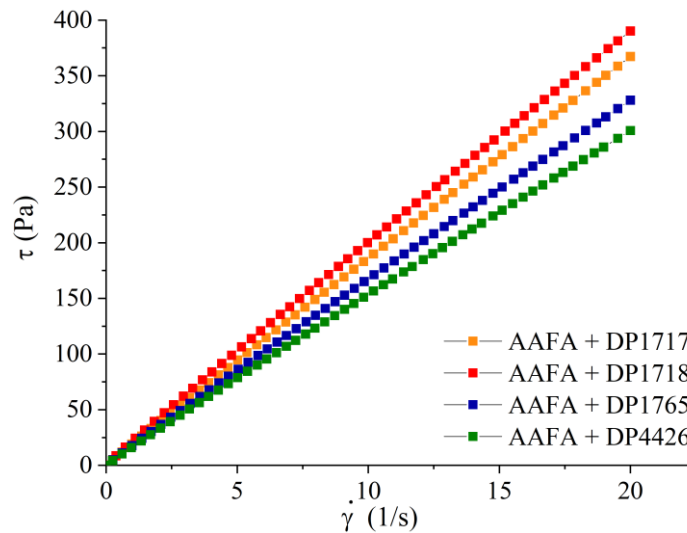


Figure 5.26 Effect of different types of lignosulfonates on the rheology of the AAFA pastes. DP1717 - low sugar, high Mw, DP1718 - low sugar, low Mw, DP1765 - high sugar, high Mw, DP4426 - high sugar, low Mw.

### 5.5.3 Setting time

Long setting times are characteristic of low-calcium alkali-activated fly ash activated pastes, as their low reactivity means that they harden slowly at ambient temperatures (Kovalchuk et al., 2007). The mix designs presented long setting times with an initial setting time of 7 h 20 mins and a final setting time of 9 h 40 mins for the control samples without any admixture. Addition of lignosulfonates increased the setting times of the pastes, and some difficulties in determining these times were faced, because the paste was sticky and adhered to the needle. As the needle penetrated, the paste was pushed outwards and so the 40 mm initial depth could

not be maintained as shown in Figure 5.27. As a result, the data presented are estimated where necessary, as averages from 3 measurements of the same mix.



Figure 5.27 AAFA paste during setting time testing.

The low sugar, high Mw DP1717 sample delayed the setting of these pastes as shown in Figure 5.28. Even low dosages of 0.1 wt.% LS significantly increased the initial and final setting times, which increased further as the dosage of the LS was increased. Setting times of over 20 hours are recorded for the highest dosage of 3 wt.%. However, the low sugar, low Mw LS (DP1718) showed the opposite behaviour in that, when the dosage of the LS was increased, the setting of the paste was accelerated. The highest dosage of 3 wt.% DP1718 resulted in reduced setting times of 5 hours for initial setting and 6 h 40 minutes for final setting. This indicates that the molecular weight of the LS had a significant impact on the setting mechanisms of the AAFA pastes.

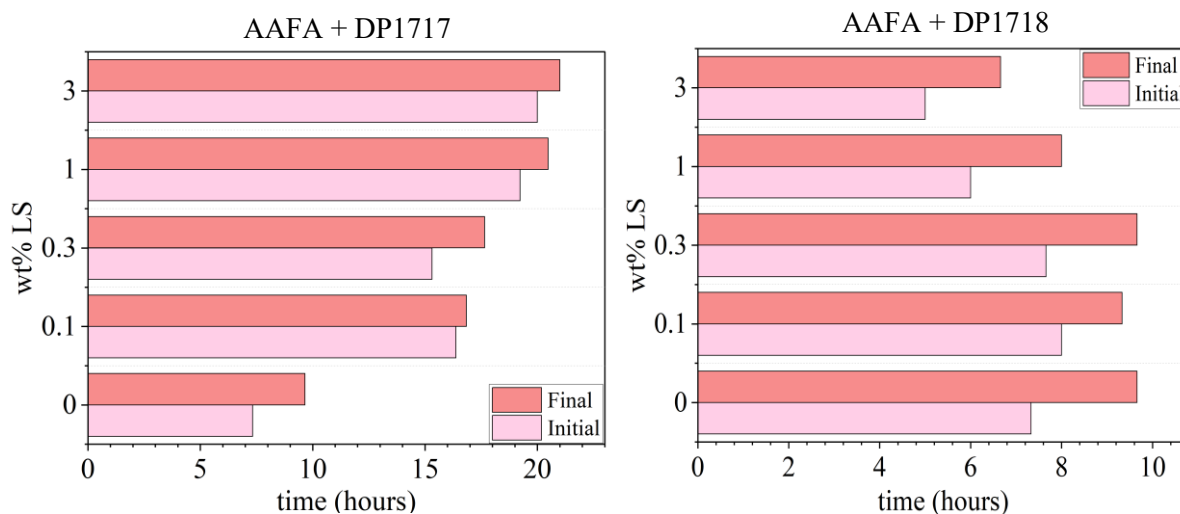


Figure 5.28 The initial and final setting times of the AAFA activated pastes with increasing dosages of the low sugar samples DP1717 (high Mw) and DP1718 (low Mw).

The high sugar samples DP1765 and DP4426 samples resulted in a delayed setting of the pastes as shown in Figure 5.29. The low Mw DP4426 sample increased the setting time more than DP1765, as the dosage of the lignosulfonate was increased. This may indicate that sugar is a more important determining parameter than Mw.

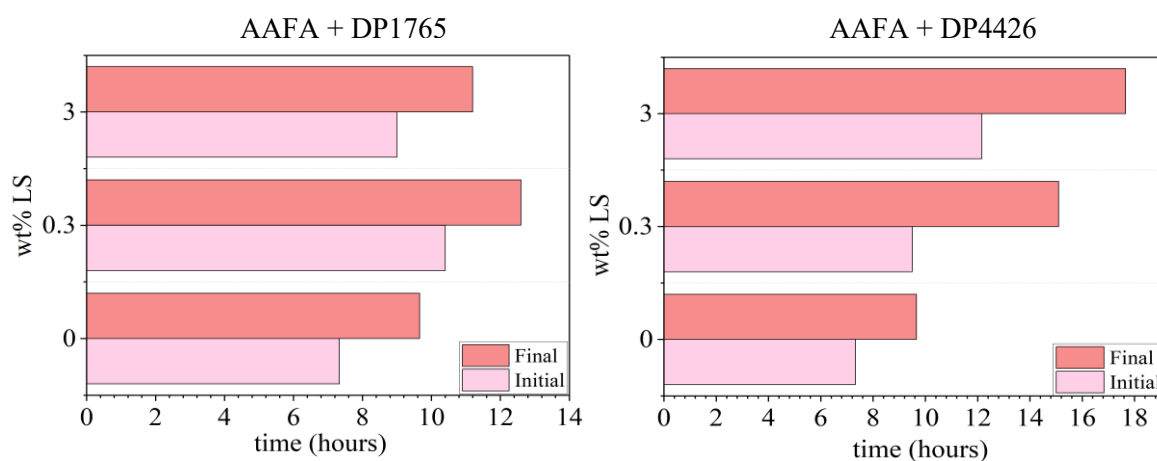


Figure 5.29 The initial and final setting times of AAFA pastes for the high sugar sample DP1765 (high Mw) and DP4426 (low Mw).

Some researchers have reported that a lignosulfonate admixture takes up  $\text{Ca}^{2+}$  from the mixing water, and with the inherently low concentration of  $\text{Ca}^{2+}$  provided by fly ash, the overall concentration of these cations is lowered (Hanehara & Yamada, 1999). It has been suggested that the admixture adsorbs on the surface of the cement particles, forming a protective film that slows down the reaction. This results in the increased setting times of the fly ash activated cements. The data in this study suggest that this effect is enhanced by the presence of sugar in these cement systems.

The extended setting times are a concern for industrial application of AAFA when lignosulfonates are added. To benefit from the use of lignosulfonates in improving the fresh state properties of the pastes, increasing their curing temperature would improve their setting time.

#### **5.5.4 Compressive strength**

After 7 and 28 days of curing at 20 °C, AAFA pastes without any addition of LS had developed mechanical strengths of 11 and 54 MPa respectively. Figure 5.30 shows that during compressive strength testing, the propagation of cracks as the material fails is different. The higher strength cubes failed to a conical shape while the low strength cubes underwent complete failure across the sample.

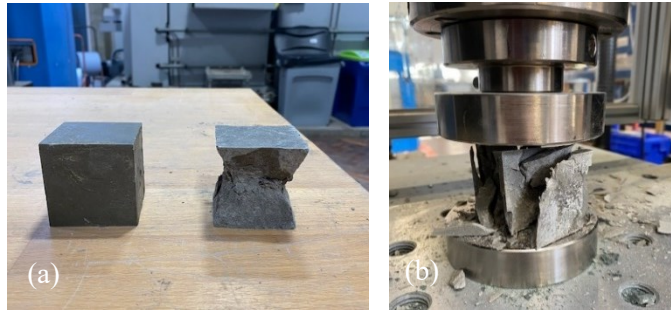


Figure 5.30 The 50 mm paste cubes cured for 28 days before and after compressive testing strength testing, (a) AAFA\_control, (b) AAFA + 3.0 wt.% LS.

The effect of lignosulfonates on the compressive strengths at 7 days of curing are marginal as shown in Figure 5.31. There appears to be a slight increase in the compressive strengths of these pastes as more LS is added. These results indicate that there is no interference of the product phase formation with LS at these early ages. This slight increase in compressive strength may be an indication of the formation of different reaction products or a more compact cementitious product than is formed without the additive. The DP1718 sample shows more fluctuation with this increase in compressive strength. At later ages, 28 days of curing, this effect is lost as a gradual decrease in compressive strength is observed with addition of more lignosulfonate. This may be due to the decrease in alkalinity over time or the consumption of  $\text{Na}^+$  ions in solution due to the interaction with LS, resulting in a decrease in the further formation of the aluminosilicate gel. The gel product from activation of AAFA is amorphous with minor crystalline phases (Kovalchuk et al., 2007) and there may be formation of new crystalline phases due to the interaction of the polymer with the paste. A good correlation between the total porosity of the AAFA pastes and their compressive strength has already been established by previous researchers (Kovalchuk et al., 2007), (Puertas & Torres-Carrasco, 2014). At early ages, the addition of LS may have contributed to a more densified product with fewer pores and an improved compressive strength. At later stages, the presence of LS had an

adverse effect likely due to the disintegration of the undissolved LS particles over time. This is discussed in more detail in section 5.5.6.

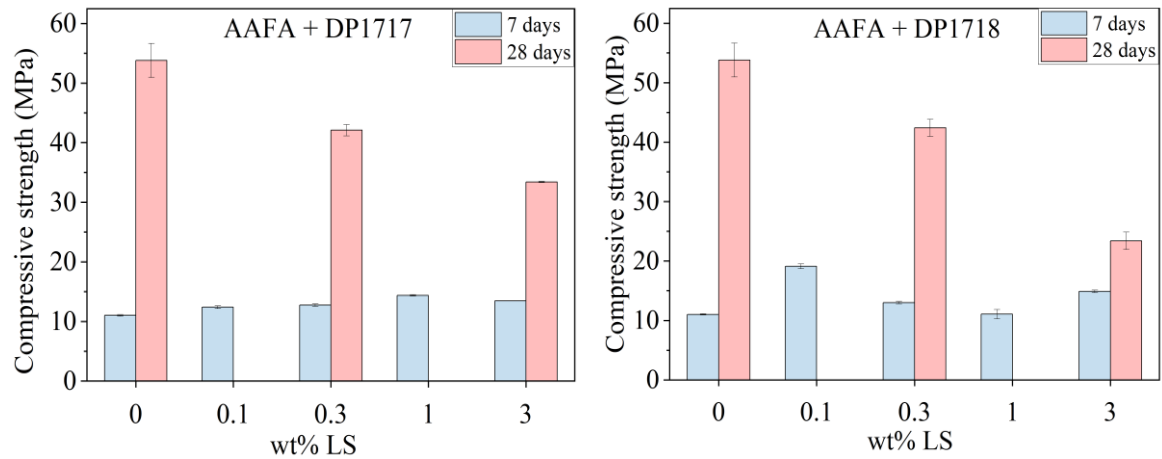


Figure 5.31 The compressive strength of AAFA hardened pastes after 7 and 28 days of curing at 20 °C. Error bars represent the standard error of the mean.

The effect of sugars accompanying the lignosulfonates on the compressive strengths of the AAFA pastes was also investigated and is presented in Figure 5.32. The low sugar LS samples showed improved paste compressive strengths after 7 days of curing, while the high sugar samples showed a reduction in paste strength development. This improvement is observed even at high dosages of 3 wt.% LS. This indicates that the lignosulfonates did not compromise the strength development of the pastes. It would be expected that an improvement of compressive strength may be attributed to the improved workability brought about by the admixture because a better mixed paste contributes to a more densified cement matrix. However, in this case the greatest improvement in workability was observed with the DP1765 sample, which does not present the greatest compressive strength improvement. The DP1717 sample performed the worst in the workability studies but gives an improved compressive strength. This lack of correlation suggests that the lignosulfonates contribute to the strength development in another

way than expected. At early curing ages, the sugar content in the lignosulfonates may have interfered with the hydration product formation or the densification of the AAFA cement matrix. At later ages (28 days curing), there was a reduction in the compressive strengths of the pastes regardless of the type of lignosulfonate added.

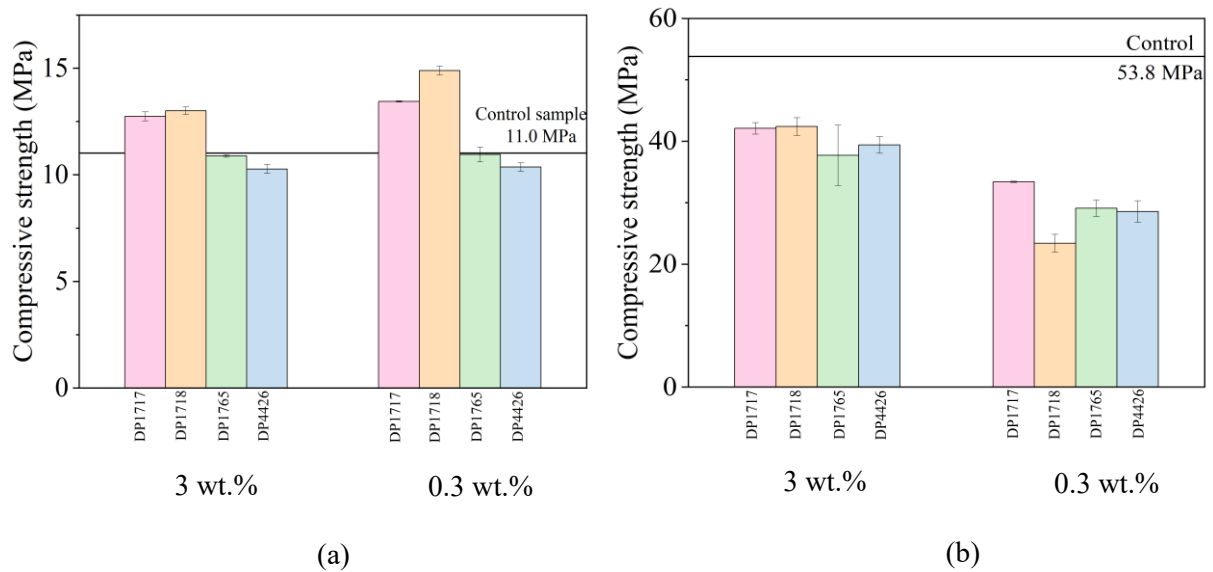


Figure 5.32 The compressive strength of AAFA pastes at (a) 7 days and (b) 28 days of curing at 20 °C. Error bars represent the standard error of the mean.

Unlike the AAS pastes, the AAFA pastes were not susceptible to drying and cracking due to loss of water. This is likely because water does not form an important part of the fly ash reaction processes. In fact, during N-A-S-(H) formation, the gel is hardly hydrating, and so the cubes were unaffected even at long curing times. The effect of self-desiccation which is the lowering of internal relative humidity is the key difference between C-A-S-H in AAS pastes and N-A-S-H in AAFA pastes, as the latter does not self-desiccate (Češnovar et al., 2021).

### 5.5.5 Isothermal Calorimetry

The influence of the different lignosulfonates on the hydration kinetics of the AAFA paste was investigated. This influence is dependent on the dosage and type of lignosulfonate added. At a dosage of 0.3 wt.% LS, the hydration kinetics are similar to the control sample, indicating that the reaction was not significantly impacted at these dosages, particularly the rate of heat evolution. Most of the lignosulfonates resulted in a higher peak heat flow at 3 wt.% LS addition compared to the control and 0.3 wt.% LS sample.

At longer times, the rate of heat evolution curves cannot be distinguished between the three dosages. The high Mw, low sugar DP1717 sample was the only one that showed a lower peak than the control sample. The cumulative heat released curves are indicative of the extent of reaction showed almost identical curves for the control and 0.3 wt.% LS sample, regardless of the type of lignosulfonate added. This suggests that these admixtures do not alter the extent of the reaction and/or extent of product formation during fly ash activation, particularly at the early stages. However, when the dosage is increased to 3 wt.%, the extent of reaction is reduced as can be seen in Figure 5.33.

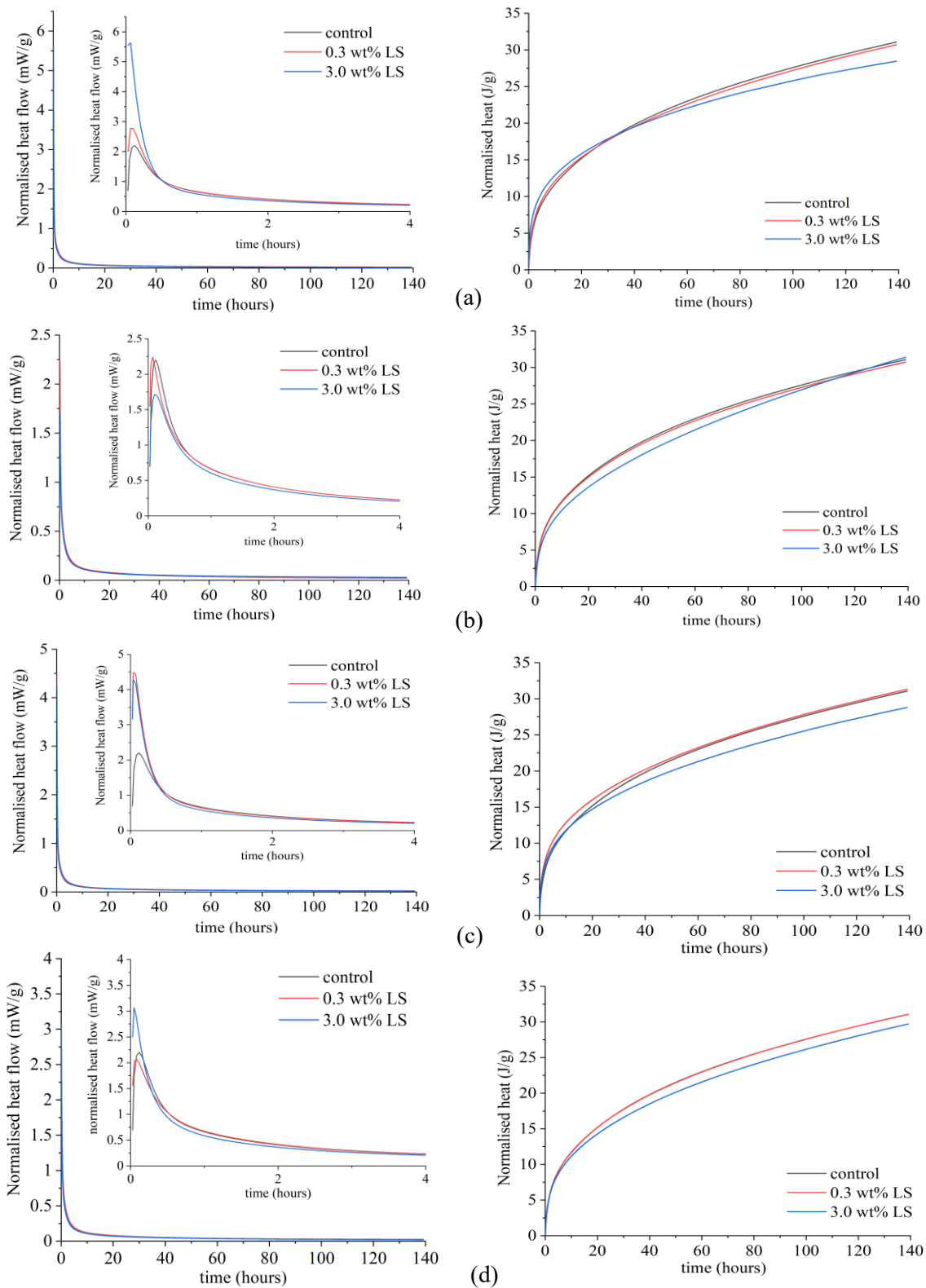


Figure 5.33 The heat evolution of AAFA pastes with addition of the four types of lignosulfonates, (a) DP1717, (b) DP4426, (c) DP1718, and (d) DP1765.

### 5.5.6 The fate of lignosulfonates in alkali activated fly ash pastes

Figure 5.34 presents the FTIR spectra of the AAFA pastes after 7 days of curing. The band at  $440\text{ cm}^{-1}$  relates to the octahedral  $\text{AlO}_6$  in aluminate or aluminosilicate phases from the unreacted mullite in the fly ash. The most significant peak is observed in the region between  $850 - 1250\text{ cm}^{-1}$ , this peak is often found in at  $1060\text{ cm}^{-1}$  in the unreacted fly ash due to the T-O band (tetrahedral Si or Al) (Kovalchuk et al., 2007). Upon activation and formation of the reaction products, the peak moves to lower frequencies at  $1000\text{ cm}^{-1}$  (Palomo et al., 1999) as can be observed in Figure 5.34. A small peak is observed across all samples at  $1660\text{ cm}^{-1}$  which can be attributed to the bending vibrations of the H-OH as chemically bound water (Puertas & Torres-Carrasco, 2014). A broad peak is observed in the OH region at  $3500\text{ cm}^{-1}$  indicating the presence of a small amount of water bound in the hydrates. The lack of intensity of this peak shows that hydration is not the main reaction process for this system.

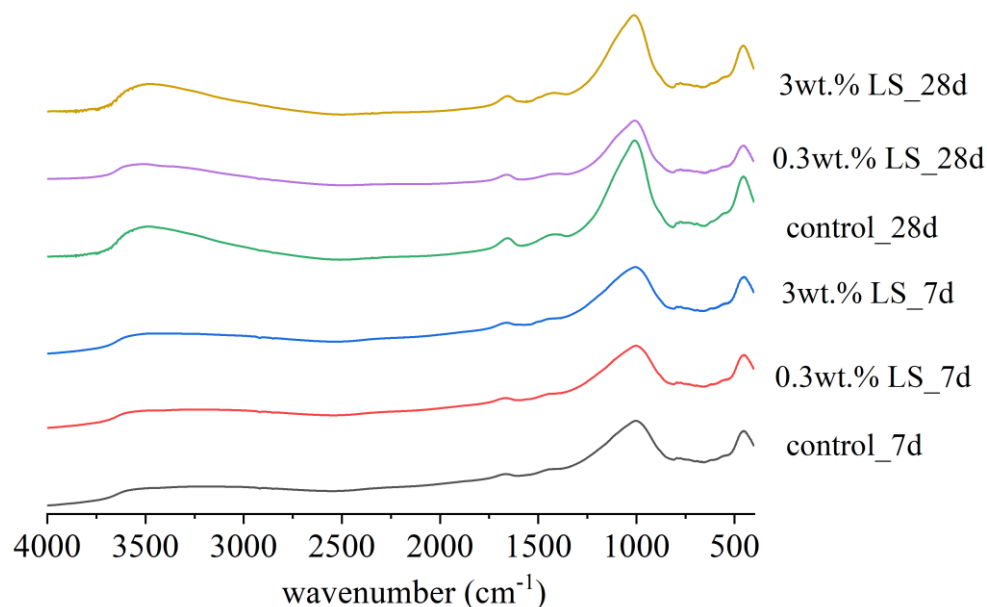


Figure 5.34 FTIR spectra of the AAFA paste after 7 and 28 days of curing with increasing additions of DP1717 LS.

It can be observed that the addition of lignosulfonate did not alter the spectra of the AAFA paste after 7 days of curing. This close similarity in spectra may be an indication that the admixture does not interfere with the activation process of the pastes.

Further investigation with thermogravimetric, analysis is presented in

Figure 5.35. The main peak found below 200 °C is associated with the reaction products from activation of the fly ash. After 7 days of curing and increasing dosage of LS, the most significant change is the appearance of a peak on the 3 wt.% LS sample at temperatures of about 700 °C. This peak is associated with the decomposition of calcium carbonate. At later ages of curing (28 days), a similar observation can be made with the 3 wt.% LS sample. This suggests that high dosages of lignosulfonate leave the paste more vulnerable to carbonation, regardless of the curing age. This carbonation process indicates that the durability of the cement is adversely affected when high dosages of LS are added.

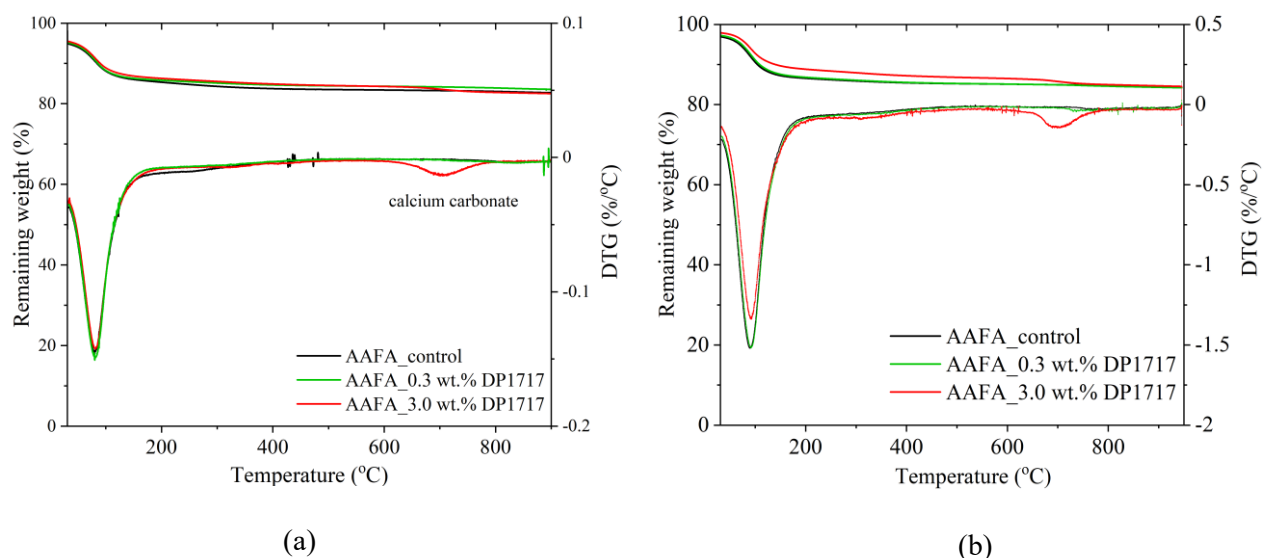


Figure 5.35 The thermogravimetric analysis of the AAFA paste after (a) 7 days and (b) 28 days of curing at 20 °C, with and without DP1717 LS addition.

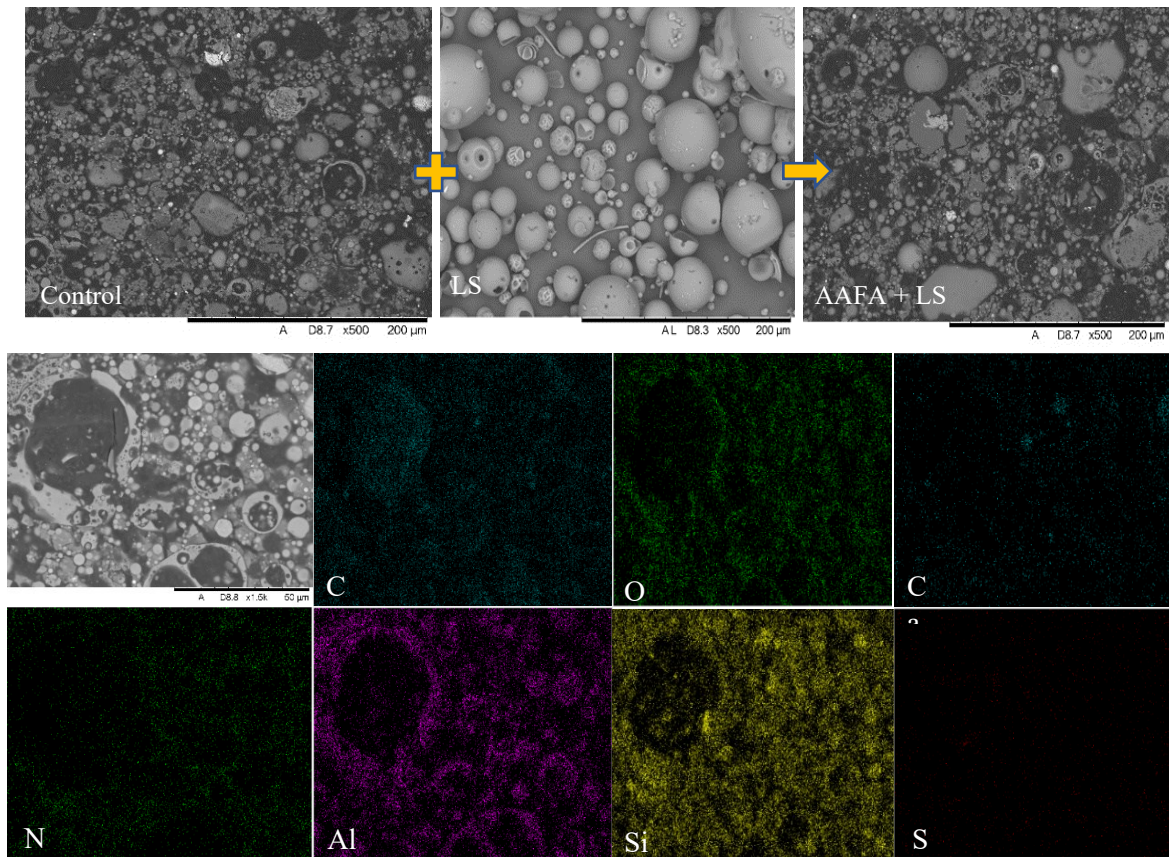


Figure 5.36 The scanning electron micrographs of the AAFA pastes with and without 3 wt.% additions of LS after 7 days of curing, and elemental maps corresponding to the higher-resolution image shown.

The SEM images in Figure 5.36 show that the addition of the LS did not significantly affect the microstructure of the pastes. The control sample shows some spherical unreacted particles typical of fly ash. The matrix is not dense and is characterised by high amounts of porosity and unreacted material. This is due to the low reactivity of the low calcium fly ash. The lignosulfonate is not present in the reacted final product indicating complete dissolution, unlike in the AAS system previously discussed. The lack of cracks in the AAFA images compared to the AAS explains why there was no loss of compressive strength in these pastes at 7 days of curing, as they were less affected by drying shrinkage.

## 5.6 Conclusions

The chapter aimed to attain a better understanding of the effect bio derived admixtures have on the alkali activation process, formation of reaction products and the performance of these pastes. Some success in improving the workability of the pastes was found at certain dosages for both AAFA and AAS cements. The optimum dosage appears to be at around 0.3 wt.% of LS. High dosage above 0.3 wt.% LS reduced the fluidity of the pastes. The sugar content of the LS did not contribute to an improved fluidity of the pastes. The efficiency of the LS can be improved by following a delayed mode of addition. The rheological behaviour of the pastes was significantly changed when high dosages of LS were added, showing a decreased viscosity and a thixotropic behaviour that has not been reported before. This was observed in both the AAS and AAFA pastes. These data confirmed that the interactions of the particles in the presence of LS are dependent on the type and dosage of the admixture.

The setting time was delayed by the addition of LS for both the AAS and AAFA systems. This delay was more significant with low sugar samples compared to the high sugar samples for the AAS pastes. The AAFA pastes were significantly delayed with setting times of over 20 hours. The addition of LS resulted in a reduction in the compressive strength of AAS pastes at both 7 and 28 days of curing. This reduction was more significant at high dosages of LS. The effect of LS on some properties such as loss of compressive strength would have to be mitigated to benefit from the improved workability. The AAFA pastes on the other, did not suffer this reduction at 7 days of curing, while a reduction was observed at longer curing times. The calorimetry data showed that LS reduced the rate of reaction and the extent of reaction, more significantly at dosages of 3 wt.% for both low and high calcium systems.

Further characterisation of the hardened pastes through FTIR, TG and SEM showed that the product formation was not directly affected by the presence of LS in the system. These

techniques confirmed that there were no other reaction products as a result of LS addition. This is an indication that the changes to the paste properties may be more physical than chemical. Physical hinderances may be due to solubility issues, admixture-precursor and precursor-precursor interactions. Investigating the effect of different types of LS highlighted the compatibility between the admixtures and the cement system, and therefore careful consideration should be taken when choosing the type of admixture to use. The interactions discussed are investigated in more detail in the next chapter of this study.

# Chapter 6 ALKALI ACTIVATED CEMENT - LIGNOSULFONATE ADMIXTURE INTERACTIONS

## 6.1 Introduction

The working mechanisms of admixtures in cement systems have been well established for Portland cement. These mechanisms are understood to be mainly through electrostatic interactions and in some cases, additional steric hindrances from the admixtures adsorbed onto the cement particles (Palacios et al., 2009). These interactions then alter the observable fresh state properties of the cement systems. Extensive studies have been conducted on 3<sup>rd</sup> generation polycarboxylate ether (PCE) superplasticisers investigating their molecular structure and interactions with the cement; this focus has led to new molecular structures being proposed for improved efficiency. On the other hand, there is much that is not understood about the interactions of the 1<sup>st</sup> generation admixtures with cement, and more specifically alkali activated cements. Despite this limited literature, the widely accepted working mechanisms of these admixtures in alkali activated cements mirrors that in Portland cement. They adsorb to the surface of the particles, lowering the zeta potential and inducing steric and electrostatic repulsion, thereby increasing the fluidity of the pastes and improving workability (Łączniewska-Piekarczyk, 2014), (Carabba et al., 2016). This is discussed in more detail in section 2.3.

This chapter investigates the fundamental surface chemistry of the slag and fly ash precursor particles and their interactions lignosulfonate admixtures in different chemical environments. This is important to investigate as the charge on the surface of the polymer changes according to the chemical environment it is interacting with, and consequently altering the electrostatic interactions between the admixtures and the cement particles. This is crucial for the efficiency of this polymer as an admixture. The effect that surrounding ions and admixture polymers have

on the electrical double layer of slag particles in a colloidal system is explored. It is important to establish which of these ions are charge determining and how they affect the overall surface charge and therefore the electrostatic interactions. The main aim of this chapter is to drive towards a better understanding of the working mechanism of the lignosulfonates being studied, and their interactions with the precursors through zeta potential and adsorption studies.

The surface chemistry of the particles can be examined by altering the characteristics of the aqueous medium such as pH, ionic strength, and type of lignosulfonate. The efficiency of lignosulfonates as dispersants is also determined by their molecular weight and charge density. These parameters are in turn influenced by their composition, in particular the number of anionic groups (Le Bell, 1984). The adsorption mechanisms may also be influenced by the molecular composition and structure of the lignosulfonates. It has been suggested that lignosulfonates with higher molecular weight have hydrophobic interactions as their main driving force, while at lower Mw, LS adsorption is driven by hydrogen bonding and the attractive power of the anionic groups (Madad et al., 2011), (Yang et al., 2015). The effect of four different types of lignosulfonates (high and low Mw, high and low sugar content) on ground granulated blast furnace slag and fly ash was investigated to determine the correlation between these properties and the electrostatic changes induced.

In previous research, the zeta potential and adsorption measurements have been extensively studied as a function of the dosage of various admixtures (Palacios et al., 2009), (Habbaba & Plank, 2010). The results from these studies have largely been congruent. The consensus is that the superplasticisers will adsorb and reach saturation at which point no further adsorption takes place, and this gives the typical Langmuir isotherm characterised by an initial increase and plateau (Yoshioka et al., 2002), (Perche et al., 2003). It has been established that the ionic composition of the pore solution greatly governs the interactions between the cement particles (Houst et al., 2002). The current study is more focused on the effect of increasing the pH (via

OH<sup>-</sup> ion concentration) on the zeta potential and adsorption measurements, and so the LS dosage is kept constant while the aqueous environment is altered. This approach allows for a more detailed account of what is happening on the surface of the particles as the system reaches a more alkaline environment, simulating the highly alkaline conditions found in alkali activated cement systems.

## 6.2 Materials

The precursor materials studied in this chapter have been presented in Chapter 3. A complete characterisation of the lignosulfonate admixtures has also been presented in section 4.2.

## 6.3 Analytical techniques and procedures

### 6.3.1 Zeta potential measurements

This technique follows the charge distribution of a colloidal system created when finely sieved particles are dispersed in solutions, as discussed in section 2.3.1. Zeta potential measurements are based on electrophoretic mobility. An electric field is applied, resulting in the movement of particles in the liquid medium towards the oppositely charged electrode (Anderson et al., 1986). The velocity of the particles is measured, and the mobility ( $\mu_E$ ) is calculated from:

$$\mu_E = \frac{V}{E} \quad \text{Equation 6.1}$$

Where,  $V$  is the velocity of the particle and  $E$  is the electric field strength.

The zeta potential is then calculated using a chosen model from the two most common models, the Hückel and Smoluchowski equations (Brookhaven, 2002). In this study, the equipment calculated the zeta potentials of the suspensions from electrophoretic mobilities according to the Smoluchowski approximation shown in Equation 6.2:

$$\mu_E = \frac{E\zeta}{\eta} \quad \text{Equation 6.2}$$

where  $\eta$  is the viscosity of the liquid, and  $\zeta$  is the zeta potential.

The instrument used was the Brookhaven ZetaPALS with an SR-0153 electrode. The ZetaPALS is capable of measurements of very low mobilities and is ideal for the high ionic strength and viscous media being studied (Brookhaven, 2002). To avoid particles adhering to each other and forming aggregates that may sediment under gravity, the slag powder was first sieved through a 20  $\mu\text{m}$  aperture sieve. When investigating the effect of pH, 50 ml solutions batches were produced at pH 7, 11, 12, 13, and 14, using a 1 M NaOH solution to adjust pH. The finely sieved slag particles were then added to the solution at 0.33 wt.% and mechanically mixed. Low solid fractions are required because the ZetaPALS measures the charge around the individual particles and so in a dilute dispersion, the equipment can fully sample the particles, greatly improving the error margins. Sedimentation under gravity can also be minimised at these low solid fractions. The superplasticiser was then added at 0.3 wt.% of the slag, which was the optimum dosage obtained during workability tests as determined in Chapter 5. The dispersion was then left on a roller bed for 1 hour to allow for adsorption.

The ZetaPALS zeta potential analyser was turned on several hours before the measurements were taken, to allow the laser to stabilise. 3 ml of the dispersion was pipetted into a clean 4 ml disposable cuvette ensuring no contamination, and the electrode was fully immersed in the

dispersion. The cell was then tapped a few times to remove any air pockets that the laser may interpret as particles and interfere with the measurements. For each sample, mean values were taken from 30 runs at 5 cycles per measurement. Under this increasing pH environment, a control sample without any LS was measured as well as with addition of different types of lignosulfonates (low and high Mw, low and high sugar content).

For the dispersions with silicate solution added, a set amount of silica was added (at the same weight fraction as the pastes, 0.6 wt.%), and then pH adjusted with NaOH as required. Silica  $[\text{Si}(\text{OH})_4]$  is a polyprotic weak acid which has a buffering effect on the solution, particularly at high pH, and so NaOH was added until the required pH was reached.

### **6.3.2 Adsorption measurements**

Adsorption measurements were used to determine the amount of admixture adsorbed on the precursor particles using Ultraviolet-Visible spectroscopy (UV-Vis); the setup is shown in Figure 6.1. When molecules absorb light, they gain energy and cause excitation of electrons; longer wavelengths of light are absorbed by the more easily excitable electrons. UV-Vis measures this transition from the ground state to the excited state, which is then processed into a spectrum. The amount of energy absorbed is inversely proportional to its wavelength and the amount of UV or light absorbed is dependent on the sample composition and concentration. This technique allows for qualitative and quantitative determination of the amount of a particular functional group in a sample (Hofmann, 2010).

The instrument used in this study was the Ocean Optics USB2000+ spectrometer, with a DT-MINI-2-GS light source which combines the output of deuterium and halogen sources in a single optical path from 215 to 2000 nm. The deuterium source emits in the UV range (100 –

400 nm) while the halogen emits in the visible range (400 – 700 nm). A 1 cm path length glass-clear polystyrene cuvette was used. The SpectraSuite software was used for data processing.

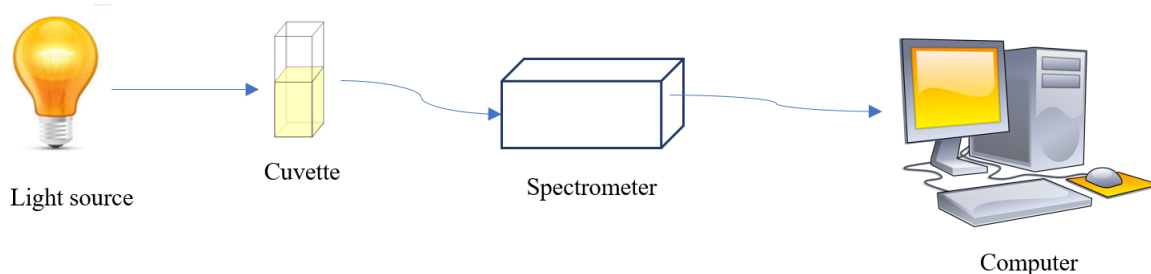


Figure 6.1 A schematic of the Ocean Optics UV-Vis setup.

Absorbance measurements determine how much light a sample absorbs for each wavelength of interest, and produce a spectrum based on the equation:

$$A_{\lambda} = -\log_{10} \left( \frac{S_{\lambda} - D_{\lambda}}{R_{\lambda} - D_{\lambda}} \right) \quad \text{Equation 6.3}$$

Where  $A_{\lambda}$  is absorbance,  $S_{\lambda}$  is the sample intensity,  $D_{\lambda}$  is the dark intensity and  $R_{\lambda}$  is the reference intensity.

Absorption isotherms were obtained from the concentration measurement of the dispersions following the depletion method. These measurements utilised Beer's law, which states that the absorbance is proportional to the concentration of the substance interacting with the light as shown in Equation 6.4.

$$A_{\lambda} = \epsilon_{\lambda} c l \quad \text{Equation 6.4}$$

Where  $\varepsilon_\lambda$  is the extinction coefficient,  $c$  is the concentration of the absorbing species and  $l$  is the optical path length of the absorption (Ocean Optics, 2009). The extinction coefficient and path length are fixed such that  $A_\lambda \cong c$ . The depletion method assumes that the lignosulfonates interact with the particles only by adsorption and no intercalation of the admixture occurs as previous literature suggests (see section 2.3.4), and therefore this is a reasonable assumption to make for these systems.

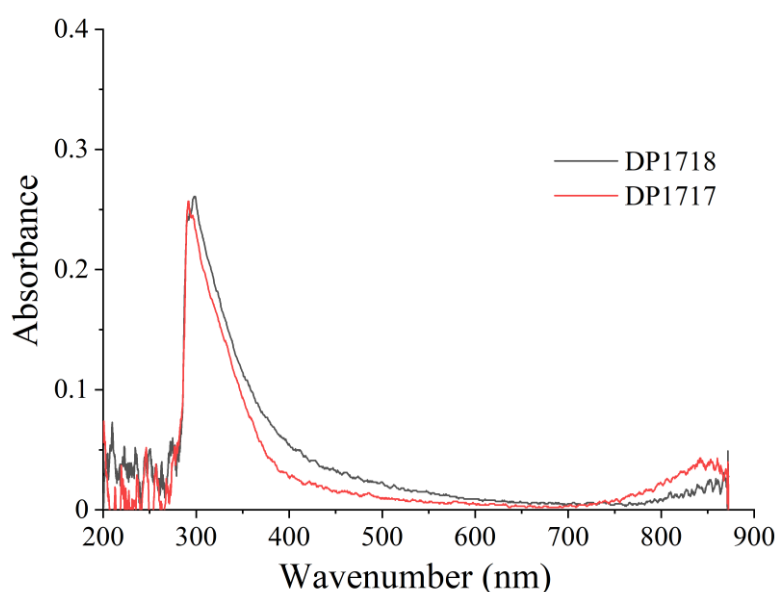


Figure 6.2 UV-Vis spectra of DP1718 and DP1717 dissolved in water.

To determine the concentration of the lignosulfonate in the liquid phase, a calibration procedure followed the preparation of a predetermined series of concentrations: 0.0015, 0.005, 0.01 and 0.02 g of lignosulfonates in 50 ml of HPLC water. Preliminary tests suggested the use of an integration range from 280-350 nm corresponding to the maximum amount of lignosulfonate as shown in Figure 6.2. In previous studies (Deng et al., 2010), (Li et al., 2012), (Li et al., 2013), it was customary to select a single point around 280 nm as a basis for concentration measurements for lignosulfonates; but in this study a range was used to achieve

a more robust concentration measurement with a less fluctuating final measurement value. A linear calibration curve as shown in Figure 6.3 was then obtained from calculating the absorbance of these concentrations. The parameters used were an integration time of 8 milliseconds, averaging over 5 scans with a boxcar width of 5. A 1<sup>st</sup> order regression of the calibration for each sample achieved R<sup>2</sup> values greater than 0.99 for all samples as shown in Figure 6.3.

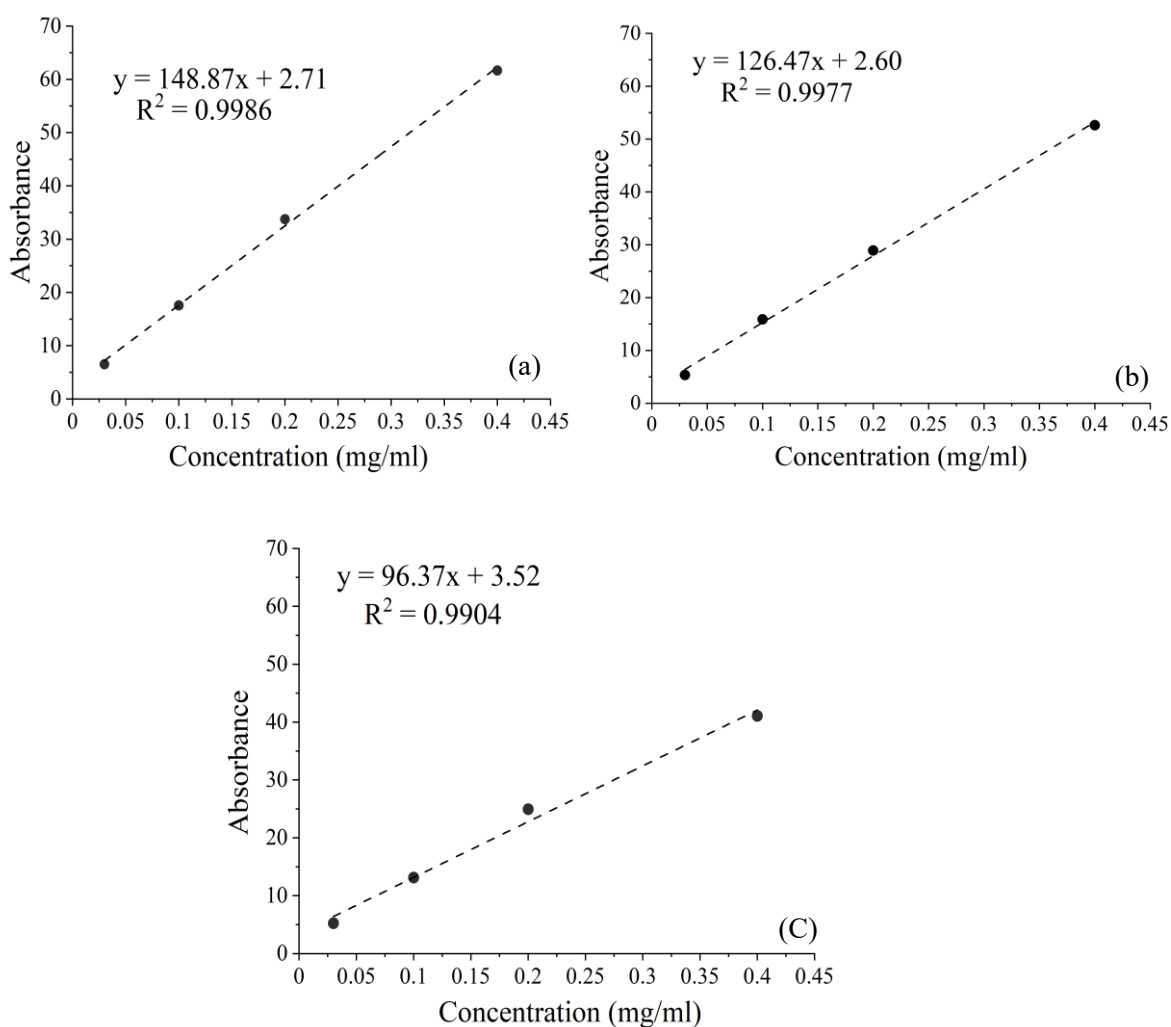


Figure 6.3 Calibration curves for (a) DP1718, (b) DP1717 and (c) DP1765.

The sample preparation for adsorption measurements was as follows:

- The solutions, in 50 ml batches were set to pH values of 7 (just HPLC water), 11, 12, 12 and 14 using a 1 M NaOH solution (this was prepared by dissolving NaOH pellets in HPLC water).
- 10 g of ground granulated blast furnace slag was added and mixed to get a homogenous suspension.
- 0.03 g of lignosulfonate powder was measured, added to the suspension, and stirred.
- The suspension was kept in sealed containers and left on a roller bed for 45 minutes to allow for admixture adsorption.
- The suspension was then filtered under vacuum through a 2.7  $\mu\text{m}$  filter paper. There may be loss of admixture during the filtration process, though this is expected to be minimal.
- The filtrate was dried and FTIR analysis conducted to ascertain the reactivity of the particles in solution and any interactions between the LS and precursor.
- 1 ml of the supernatant was diluted 10-fold in HPLC water for the pH 7 sample. 1 M HCl was also used to adjust the pH of the higher pH samples, to a pH range of 7.2 - 7.9. This neutralisation was necessary to ensure that the changing extinction coefficient under varying pH environments was not affecting the spectrum of the UV-Vis which would in turn affect the calculation of the concentration (Deng et al., 2010).
- Two control samples were also prepared: one without any slag and one without any lignosulfonate.

## 6.4 Results & Discussion

### 6.4.1 Zeta potential ( $\zeta$ ) a function of pH

The pH of the solution influences the surface charge of the cement particles as well as the dissociation of functional groups on the lignosulfonates. Figure 6.4 shows the zeta potential of the slag dispersions measured with increasing pH ( $\text{OH}^-$  concentration) in solution, from water (pH 7) to pH 14 (1M NaOH). It was necessary to first study the surface chemistry of the slag in water without any pH adjustment or addition of admixtures, from which a high negative charge indicated by a zeta potential of -26.64 mV was obtained. This is comparable to findings from other researchers who measured zeta potential values of slag of -35 mV in water (Elakneswaran et al., 2009). This is because when the slag is dissolved in water, the pH of the suspension is raised to above pH 10, at which point the silanol groups on the surface of the particles become wetted/hydrated and partially dissociate to  $[\text{SiO}^-]$  therefore inducing a net negative charge (Elakneswaran et al., 2009), (Kashani et al., 2014). This pH value is dependent on the slag material used, its route of production and final composition, meaning that other researchers such as Kashani et al., (2014) found the pH range for their slag to be between pH 11.3 and 11.7 at 3 wt.% in suspension. Nonetheless, the same deprotonation process explains the highly negative zeta potential, comparable to other studies.

Nagele and Schneider, 1989 established that the system used to adjust the pH has a direct effect on the zeta potential. This is confirmed in this study because as NaOH is added the zeta potential becomes less positive due to the shielding effect of the  $\text{Na}^+$  ions in solution. These cations are adsorbed and provide positively charged sites in a double layer structure, hence reducing the magnitude of the zeta potential and making the colloidal dispersion less stable. As even more NaOH is added and high pH values are reached, the change in zeta potential is

reduced because the effect of slag dissolution is enhanced. The OH<sup>-</sup> ions in solution induces a polarising effect, breaking down the Ca-O and Mg-O bonds and releasing more Ca<sup>2+</sup> and Mg<sup>2+</sup> into the solution (Chang, 2003). These cations are then attracted back onto the negative surface of the slag particles, forming a positive Stern layer, and reducing the magnitude of the zeta potential even more. This is enhanced by the contraction of the electric double layer due to the increased concentration of ions in solution. In some studies, it has been found that at these high pH values, Ca<sup>2+</sup> is the charge determining ion (Habbaba & Plank, 2012) and the result in this study suggest this may be the case.

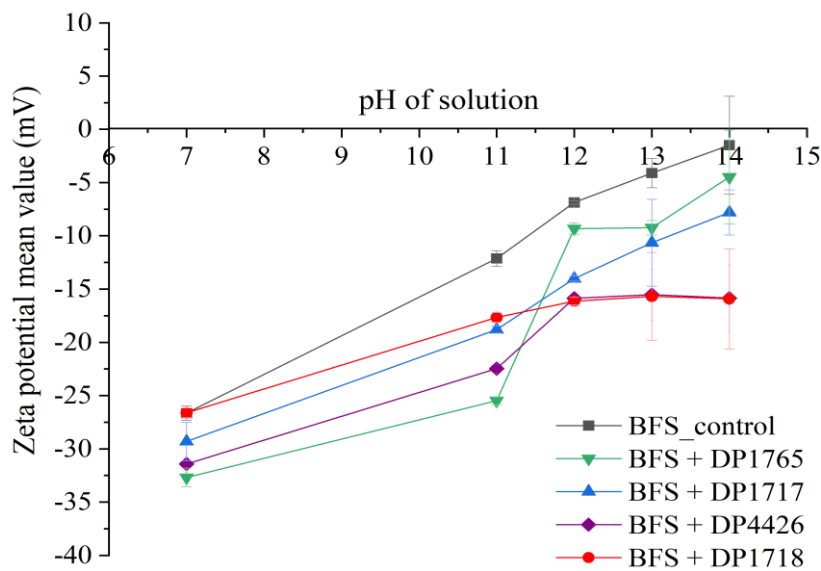


Figure 6.4 Zeta potential profile of slag in dispersions of increasing pH adjusted by NaOH with different types of LS: DP1718 (low Mw, low sugar), DP1717 (high Mw, low sugar), DP1765 (high Mw, high sugar), DP4426 (low Mw, high sugar).

The control sample without any lignosulfonate has zeta potential values very close to the isoelectric point (zero zeta potential) at high pH. However, even with this enrichment of Ca<sup>2+</sup>

ions on the electric double layer, the isoelectric point was not found in all systems, and the zeta potential is still slightly negative for the control sample at high pH. This is because the positive ions must accumulate on the double layer in order to induce a charge reversal, however this is not the case in this system because the double layer is not in equilibrium due to the slow chemical reactions (Nagele & Schneider, 1989).

The effect that the four types of lignosulfonates added at a constant dosage (0.3 wt.% of the slag) have on the zeta potential of the system is also presented in Figure 6.4. The results show that at different pH values, the LS have a varying degree of impact on the zeta potential depending on their molecular weight and sugar content. However, this impact is insignificant at low pH values, and this is because the surface of the slag has a net negative charge as previously discussed, and the LS has anionic groups on its surface. Repulsive forces arise due to the like negative charges on the slag and LS surface resulting in limited adsorption of the admixture. At these low pH values, the LS with high sugar content appear to affect the zeta potential of the system slightly more significantly compared to their low sugar counterparts. This may be because the low pH favours the preferential adsorption of these LSs onto the double layer despite the repulsive forces. It is also relevant to note that the high sugar lignosulfonate samples were found to have a higher pH in water (particularly DP4426 that was slightly alkaline) as investigated in section 4.4.1, indicating the release of  $\text{OH}^-$  ions into solution leaving the polymer with a slightly positive charge. This leads to some attraction, though limited and adsorption on the negatively charged slag surface.

As NaOH is added, the LS can partially adsorb on the now available positive sites provided by the  $\text{Na}^+$  ions. This is indicated by a more negative zeta potential than the control, which is established for all types of lignosulfonates. The DP1717 and DP1765 samples do not show a plateau at high pH unlike the DP1718 and DP4426 counterparts as shown in Figure 6.4. This suggests that at these high pH values, the effect of the molecular weight of the polymers can

be observed; low Mw lignosulfonates have more negative zeta potentials than the high molecular weights, suggesting they are more preferentially adsorbed. It has been reported previously that low molecular weight LS are considered to act as dispersants while high molecular weight LS may exhibit some flocculation properties (Le Bell, 1984). This was confirmed in Chapter 5 of this study, where the low Mw DP1718 LS sample was the most efficient in improving the workability and rheological properties of the pastes.

When the fly ash studied here was dispersed in water, a negative zeta potential of -14.29 mV was obtained as shown in Figure 6.5. The magnitude of this zeta potential ranges depending on the composition of the fly ash, with other researchers obtaining values of -23 mV (Wang et al., 2021). The negative zeta potential of the fly ash in water is due to the dissociation of the Si-OH and Al-OH groups from the surface of the particles (Wang et al., 2021). The shielding effect of the Na<sup>+</sup> ions is observed as more NaOH is added. Some researchers have reported a more negative polarity of the electrical double layer as more NaOH is added, due to the further dissociation of these groups (Malek & Roy, 1985), (Gunasekara et al., 2015). However, this is not the case in this study as an increase in pH reduced the magnitude of the zeta potential. At high pH values above 12, a charge reversal to positive zeta potentials is established. This is because of the accumulation of the Na<sup>+</sup> ions that become charge determining in these conditions. The Na<sup>+</sup> ion is readily adsorbed on the electrical double layer thus changing the potential to positive values (Nagele, 1986).

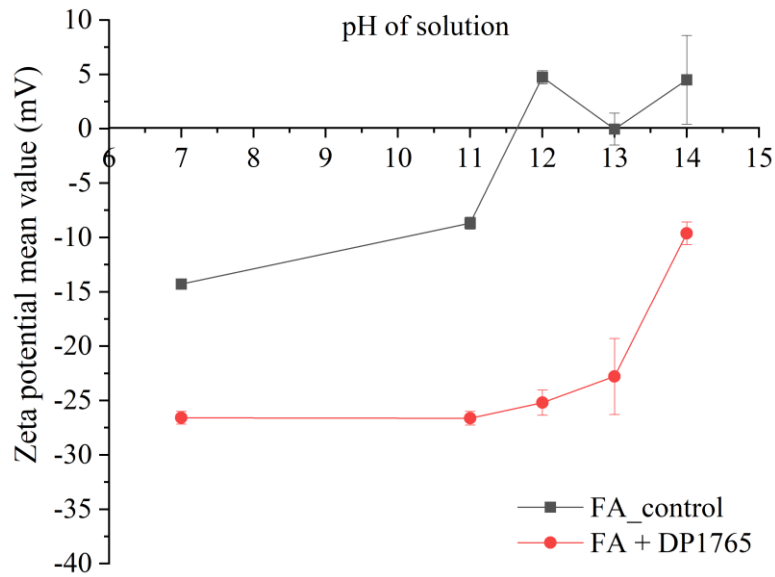


Figure 6.5 Zeta potential of fly ash in increasing pH adjusted by NaOH and with addition of the DP1765 (high Mw, high sugar) sample.

The DP1765 sample was found to improve the workability of the AAFA pastes the most (see discussion in section 5.5.1) and was chosen for further analysis of the electrostatic interactions. When LS was added, more negative zeta potentials than the control are achieved which indicates some plasticising effect taking place. These more negative values suggest a more stable system than the control without any admixture added. However, there is a sharp increase in the zeta potential at high pH values, indicating the potential of a sudden loss in plasticising effect by the lignosulfonate.

#### 6.4.2 Zeta potential ( $\zeta$ ) as a function of order of addition

Figure 6.6 shows the zeta potential measurements of the slag dispersions when the same type of lignosulfonate is added at different times during the mixing stage. The DP1718 performed the best out of the LS in slag activated pastes as demonstrated in section 5.4.1 and

was selected for this investigation. The delayed addition (DA) procedure was: the pH was set with NaOH, then slag added followed by lignosulfonate at a dosage of 0.3 wt.%. For the prior addition mode (PA), the lignosulfonate was added and mixed for 3 minutes before the slag, while for the simultaneous addition (SA), the LS and slag were added at the same time into the solution of set pH. The control suspension without any LS is also included as a reference in this data set.

All the orders of addition showed more negative zeta potentials than the control, although small, and this indicates some plasticising effect of the LSs, which has a direct effect on the workability and rheological properties of the pastes (discussed in section 5.4.1). At low pH, simultaneous addition performed slightly better than the delayed addition, while the prior addition produced the most negative zeta potential. However, as the pH is increased above 11, the delayed addition mode resulted in a more negative zeta potential than the other methods. This suggests that the efficiency of the order of addition is dependent on the pH of the suspension such that at high pH values, the delayed addition method performed the best. The workability tests concur with these results as discussed in section 5.4.1.

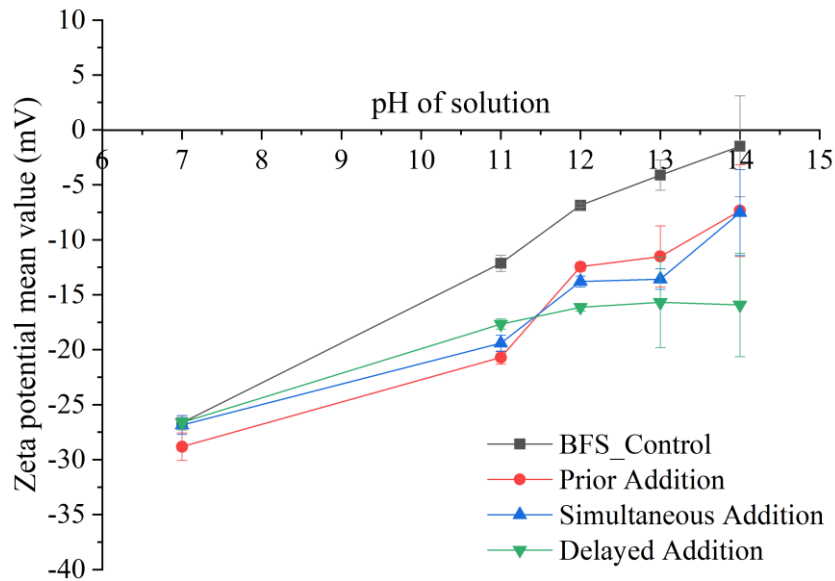


Figure 6.6 Zeta potential profiles of slag dispersions with DP1718 LS added at different stages.

From these data, the delayed addition of the lignosulfonate is encouraged over the other orders of addition. The PA and SA orders of addition may not have performed as well due to the partial loss of plasticising ability when the pH of the solution was increased. Previously this has been associated with the chemical instability of the lignosulfonates as they interact with the activating solution (Criado et al., 2009). This may also be due to poor solubility of the lignosulfonates in the high pH, high electrolyte environment of the activating solution. It has also been suggested that some competitive adsorption between the LS and the anions in solution occurs, hindering the adsorption of the admixtures on the surface of the slag particles (Hanehara & Yamada, 1999). This is more likely to occur when the PA and SA orders of addition are followed. For delayed addition, the adsorption of the LS onto the slag surface was facilitated by the availability of the positive sites due to increased slag dissolution which provides positive sites for adsorption. This means that immediate absorption could occur, and a greater degree of plasticity is achieved compared to the other orders of addition.

### 6.4.3 Effect of silicate ions on $\zeta$

Figure 6.7 shows the zeta potential as a function of increasing pH with a constant addition of sodium silicate solution with a modulus of 1.5 (at 0.6 wt.% of the slag). At low pH values, the addition of silicate results in a more negative zeta potential of the system. This is because of the plasticising effect of the silicate ions when adsorbed or precipitated onto the slag particles (Kashani, Provis, Qiao, et al., 2014). The silicate anions adsorb on the slag surface in the positive sites provided by the cationic  $\text{Na}^+$  ions. Due to their anionic nature, there are greater repulsive forces between the particles resulting in greater negative zeta potential values and therefore a more stable system compared to the one with only NaOH added (Kashani et al., 2014). However, at pH values above 12, the system becomes less negative and therefore less stable. This is because of the effect of slag dissolution at these high pH values. This process reduces the fluidising effect of the silicate ions due to the presence of the divalent  $\text{Ca}^{2+}$  ions, at which point the repulsive forces brought about by the silicate ions are diminished. These results show that the system is most stable at pH values of around 12, and any further increase destabilises the colloidal dispersion. The system tends towards the isoelectric point but does not reach it.

The addition of lignosulfonate into this system has an insignificant impact on the measured zeta potentials. This is because there are limited to no positive sites for the anionic LS to adsorb onto. At high pH, it is expected that the positive sites provided by the cationic ions on the surface would be available to LS adsorption, however, this is still not the case, possibly due to competitive adsorption between the silicate ions and the LS as they have like negative charges. A similar observation was made for the fly ash suspension with the DP1765 sample not altering the zeta potential of the system as shown in Figure 6.8. This finding suggests that at high pH values, lignosulfonates are less effective in waterglass than in NaOH activated systems.

Competitive adsorption between LS and NaOH was shown by Ren, (2016). In the presence of silicate ions, this effect is exacerbated as shown by the results in this study. It can be concluded that, ions with the same charge as is presented by the activator and the admixture, can reduce adsorption due to this competitive adsorption. This may be the reason why the dispersion efficiencies observed in the pastes as discussed in Chapter 5 are less than what would be expected.

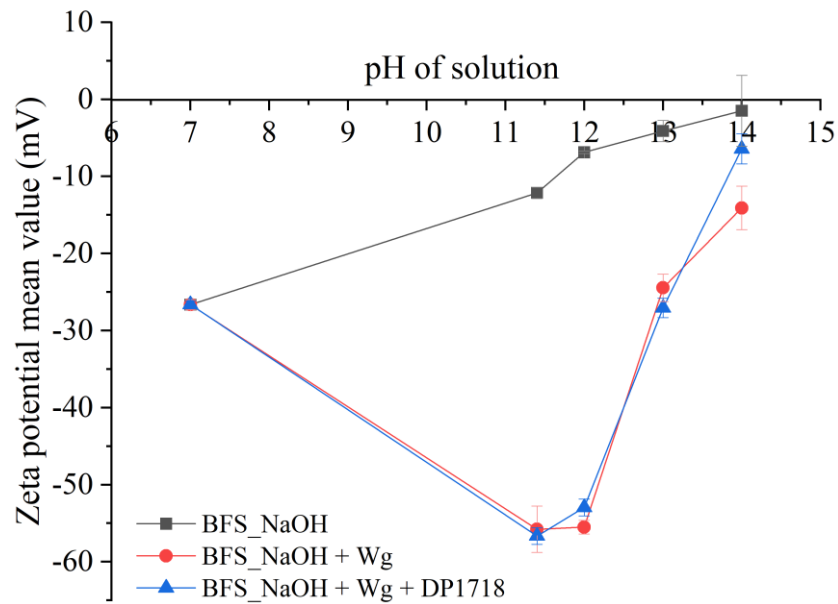


Figure 6.7 Zeta potentials of slag, pH adjusted with NaOH, a constant amount of silicate (0.6 wt.% of the slag) and DP1718 LS added.

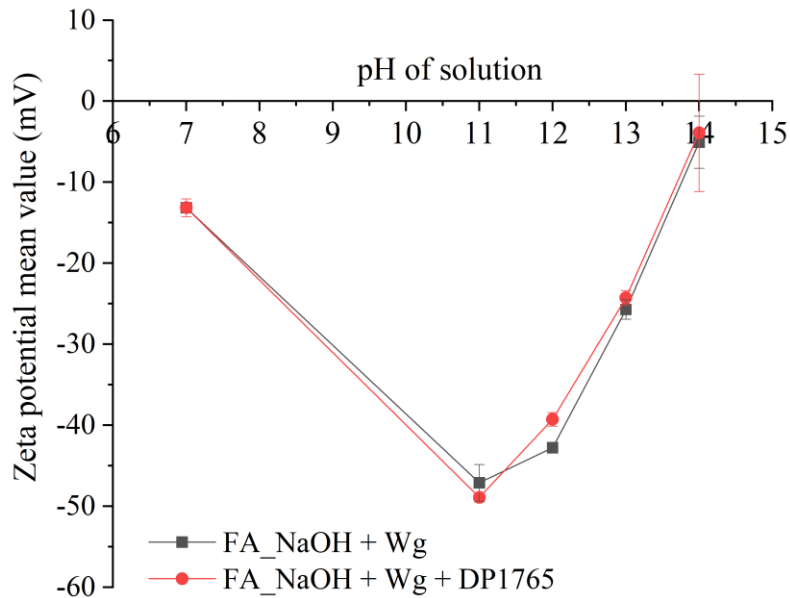


Figure 6.8 Zeta potentials of fly ash, pH adjusted with NaOH, a constant amount of silicate (0.6 wt.% of the slag) and DP1765 added.

Competitive adsorption between the anionic ions, the silicate from the solution and the LS added, was further investigated by changing their order of addition into the system as presented in Figure 6.9. It can be observed that there are no significant differences in the zeta potential measurements of suspensions regardless of whether the silicate was loaded first, or the lignosulfonate. There were no differences observed both at high and low pH values. This may be because the silicate ions are the main dispersing species/charge determining species regardless of the order of LS addition. When the lignosulfonate was added first, adsorption is expected when pH is increased as discussed in the previous sections. However, upon addition of silicate ions, there may be desorption of admixture back into solution and so their adsorption effect is minimised. This suggests that there may be a reversibility of the lignosulfonate adsorption from the surface of the slag particles. This area remains poorly understood in alkali activated cements.

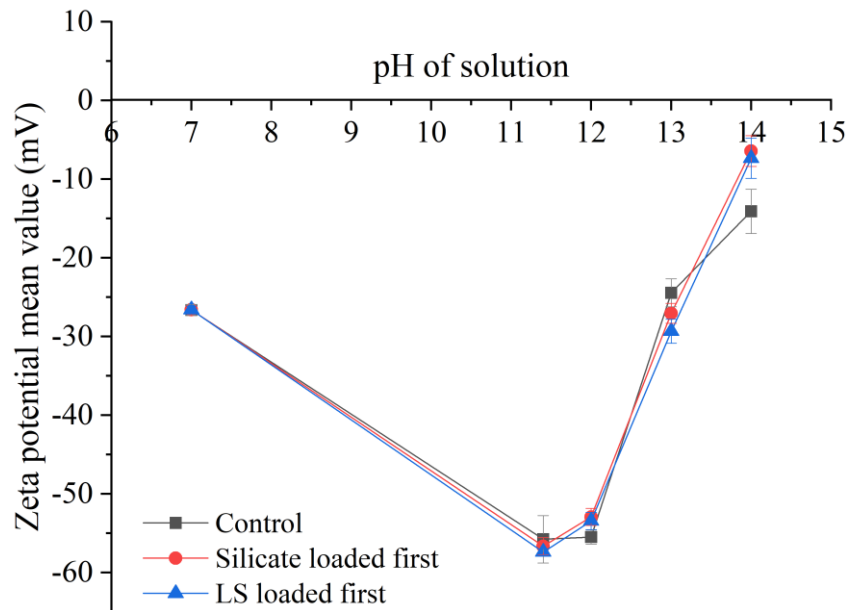


Figure 6.9 Zeta potential of slag in NaOH + Waterglass without any LS (control), and then with the silicate loaded first, and another with the LS (DP1718) loaded before the silicate.

#### 6.4.4 Zeta potential ( $\zeta$ ) as a function of ionic strength

It has previously been reported that an increase in ion concentration compresses the diffuse layer (Nagele, 1986) decreases the magnitude of the zeta potential. The effect of ionic strength on the  $\zeta$  of slag suspensions was investigated by increasing the concentration of sodium chloride at a constant pH of 13 and 0.3 wt.% LS dosage as shown in Figure 6.10. The control sample shows the slag suspension without any LS and at this high pH, the addition of NaCl reversed the zeta potential from slightly negative to positive. This indicates a change in polarity of the electrical double layer. This reversal in charge is because there is extra  $\text{Na}^+$  ions, and they become potential determining. It is evident that the chloride ion did not play a significant role on the zeta potential of the slag particles because the zeta potential did not become more negative as the chloride concentration was increased. Nägele and Schneider, 1987 also reported that  $\text{Cl}^-$  was not a potential determining ion in their studies. (Elakneswaran et al., 2009) reported

that when ground granulated blast furnace slag was dissolved in water (~pH 9.8 recorded) and the sodium chloride concentration increased, the zeta potential became slightly more negative at lower NaCl concentrations but then increased and became less negative at higher NaCl concentrations (~38 mV). This suggests that the reported behaviour in Figure 6.10, where there is charge reversal is due to the high pH environment of the suspension and indeed  $\text{Na}^+$  ions are potential determining at these conditions. The isoelectric point (zero zeta potential) was observed at low concentrations below 0.05 M of NaCl. This is the point at which the system is least stable. The increase in zeta potential even at low salt concentration indicates that the alkali ions are the counter-ions found in the diffuse double layer (Nägele & Schneider, 1987).

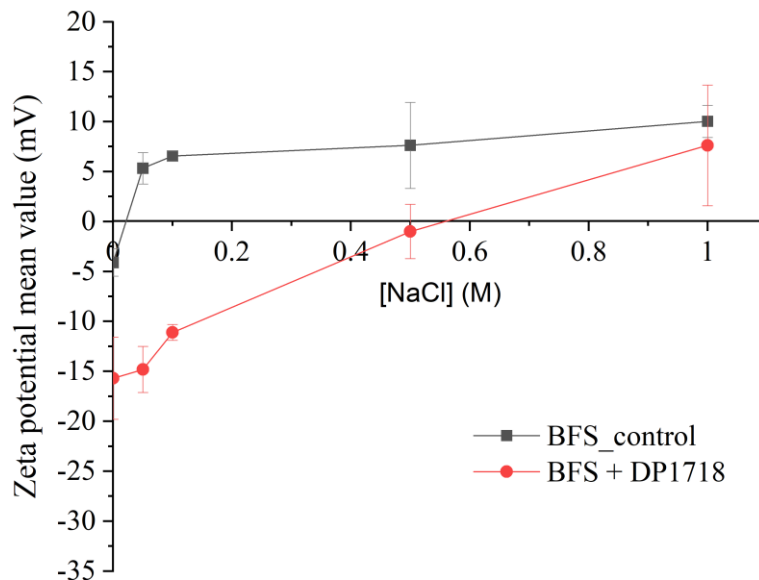


Figure 6.10 Zeta potential as a function of ionic strength adjusted with NaCl, and with addition of LS.

For the same suspensions with addition of lignosulfonate, the admixture adsorbs to the already altered electrical double layer. A charge reversal is still observed, however, higher concentrations of NaCl were required to reach the isoelectric point compared to the control. This is because the adsorption of the lignosulfonate restricts the immediate charge reversal that

is observed in the control suspension. As the NaCl concentration is increased, this effect is overcome and the charge becomes positive due to the Na<sup>+</sup> ions becoming potential determining once again.

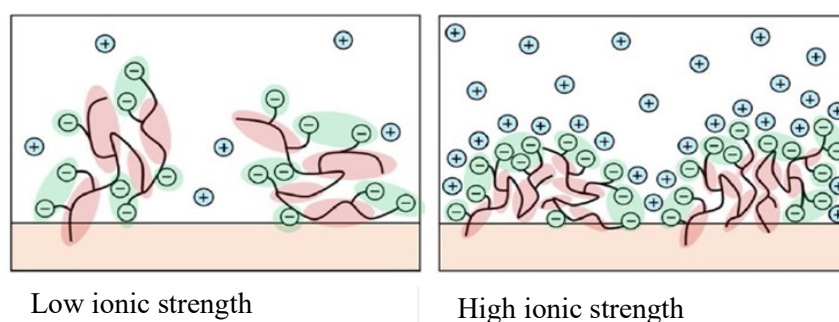


Figure 6.11 Schematic showing the effect of ionic strength on LS in solution. Adapted from (Ruwoldt et al., 2020).

It is also worth considering the effect of the high ionic strengths not just on the dispersion, but also on the lignosulfonates themselves. An increase in ionic strength with NaCl has been reported to reduce the adsorption capacity of lignosulfonates due to decreased electrostatic repulsion between the hydrophilic head groups of the polymer (Li et al., 2012). It has been documented that at high ionic strengths, the high salt concentration invokes precipitation or enhanced aggregation. The ionised group on the lignosulfonate can reach charge neutrality at high salinity as demonstrated in Figure 6.11 (Ruwoldt et al., 2020). The adsorption capacity of the lignosulfonates is therefore reduced in these conditions. To investigate this further, a lignosulfonate powder was dissolved in HPLC water at 1 wt.%. The lignosulfonate was added first to prevent irreversible agglomeration and then the NaCl salt added to achieve the desired salt concentrations. The data obtained is presented in Figure 6.12.

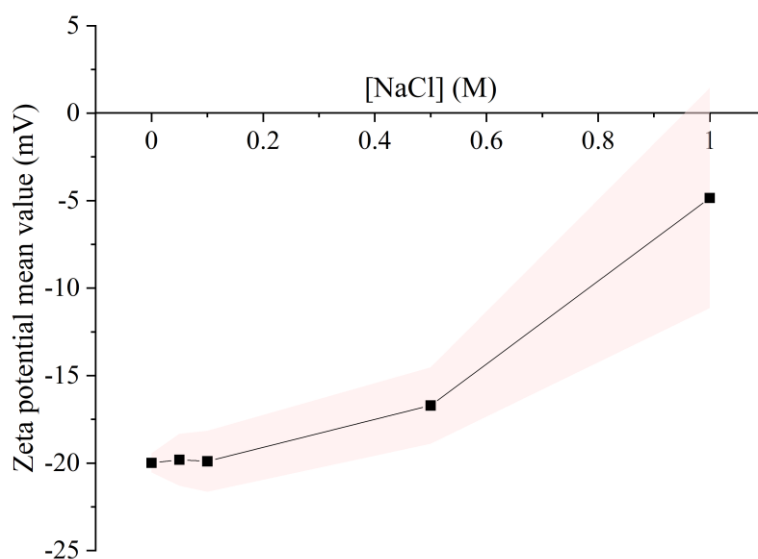


Figure 6.12 Zeta potentials of LS (DP1718) as a function of increasing ionic strengths. The pink band represents the error margins.

The initial zeta potential of the lignosulfonate (at low NaCl concentrations) is highly negative as can be expected, and this is because the acidic functional groups from the polymer are dissociated, bringing about a net negative charge. The zeta potential of the lignosulfonate is decreased as the concentration of NaCl is increased. This is due to the screening of charge which is insignificant at low NaCl concentrations and prominent at increased concentrations. Nyman et al., (1986) proposed that there is coagulation/aggregation of lignosulfonates with addition of NaCl due to the steric stabilisation of these polymers. And so, charge screening is taken as the main point of discussion in these dispersions, which would explain why the dispersion effect of lignosulfonates is significantly reduced or lost at high ionic concentrations.

### 6.4.5 Adsorption studies

The adsorption measurements presented assume that the lignosulfonates are evenly distributed on the surface of the slag particles. This is a fair assumption to make as the lignosulfonate molecules are fairly flexible and the anionic groups are evenly distributed as the charged groups would be expected to distribute themselves as far away from each other as possible (Le Bell, 1984).

The adsorption results presented in this section are calculated from the concentration measurements per gram of the slag. Figure 6.13 correlates with the zeta potential studies showing that the adsorption process of the DP1718 lignosulfonate on the slag surface is pH dependent. There is an increase in the uptake of admixture as the pH is increased and at high pH values above 12, the rate of adsorption is decreased and plateaus off. This uptake is encouraged by the  $\text{Ca}^{2+}$  ions on the surface of the slag after dissolution. As slag dissolution continues, the maximum number of adsorption sites is reached at which point no further adsorption of LS occurs and the rate of adsorption plateaus off. It has also been suggested that due to the chemical instability of the LS, there is reduced adsorption due to loss of sulfonic groups on their surface in these conditions. The chemical instability of lignosulfonates is evaluated in Chapter 4 of this study.

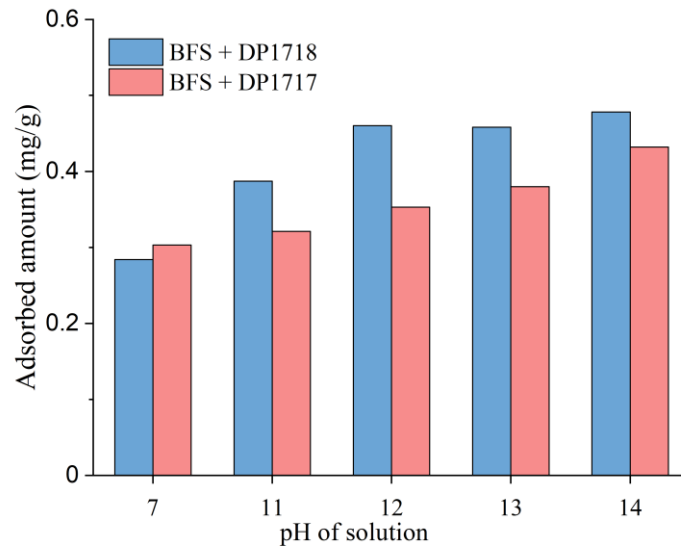


Figure 6.13 The adsorbed amount of LS DP1717 and DP1718 onto slag in an increasing pH environment (adjusted with NaOH solution).

In comparison with the high Mw and low sugar DP1717, the total amount of adsorbed lignosulfonate is less than the DP1718 across the pH range. At pH 7, where water is used as the solvent, a slightly higher amount of DP1717 was adsorbed compared to the DP1718. The amount of DP1717 adsorbed increases almost linearly with the increase in pH, which suggests that these parameters are directly proportional. This correlation can also be observed in the zeta potential results of the same sample as discussed in section 6.4.1. Upon addition of NaOH, the DP1718 sample has a higher affinity for the slag surface than does the DP1717 sample. This suggests that the molecular weight of the lignosulfonates plays a role in the adsorption capacity of these polymers on the slag particles.

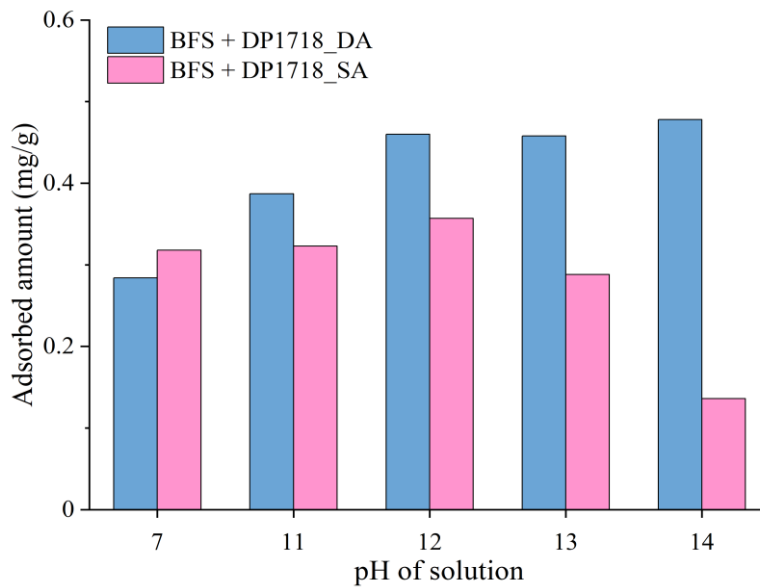


Figure 6.14 The adsorbed amounts of DP1718 when simultaneously added (SA) and addition is delayed (DA) in increasing pH environment.

Only the simultaneous and delayed additions are presented in Figure 6.14 because it can be assumed based on zeta potential results (Figure 6.6) that the simultaneous and prior addition will present similar behaviour. Simultaneous addition of lignosulfonate shows a slight increase in the amount adsorbed with an increase in pH up to pH 12, beyond which point a decrease in the amount adsorbed is observed. At pH 14, the least amount of LS is adsorbed. This may be due to the increased dissolution of the slag grains such that when simultaneously added, the LS does not have enough contact time to adsorb onto the surface efficiently. This is not the case for the delayed addition, and this is because at these high pH values, the slag surface presents some positive sites onto which the anionic lignosulfonates can adsorb.

When sodium silicate is added, this presents a different chemical environment to the previous discussion as the silicates are anionic. This means that the silicate ions and the lignosulfonates have to adsorb onto the same positive sites on the slag, which may lead to some competitive adsorption. In Figure 6.15, the sample at pH 7 shows the adsorbed amount of

lignosulfonate on the slag surface without the chemical environment being altered by NaOH or waterglass addition. As NaOH and waterglass are added and the pH is altered, the amount of LS adsorbed is reduced, regardless of the order of LS and silicate addition. There is a slight difference in the order of these additions, with the adsorbed amount of LS being more when the silicate is loaded first. This amount remains the same and then drops to the lowest at pH 14. When LS is loaded first, there is slightly more adsorbed at pH 14 than when silicate is loaded first.

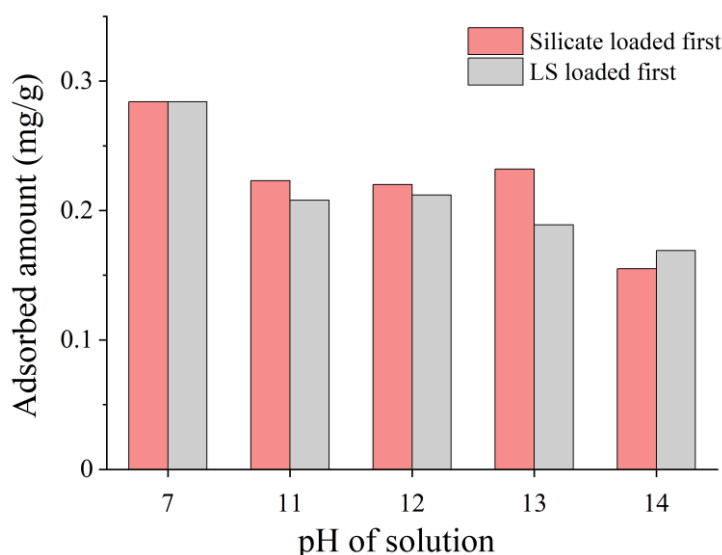


Figure 6.15 The amount of DP1718 adsorbed when there is competitive adsorption of anionic silicates and LS admixture. The sample at pH 7 serves as a control, where the BFS was only dissolved in water without addition of NaOH solution nor silicate.

The solid filtrate after adsorption was analysed with FTIR to observe any changes in the functional groups that would highlight interactions with the lignosulfonate, across the pH ranges under study. The spectra are presented in Figure 6.16. The control samples where slag was added to water and pH 14 solution showed similar spectra, with changes observed at around  $1500\text{ cm}^{-1}$ . These are associated with the asymmetric mode stretching of the O-C-O

bonds of the  $\text{CO}_3^{2-}$  group (Ismail et al., 2014). As these observations are consistent between the control samples and the samples with LS added, it can be assumed that they are due to atmospheric carbonation of the water in the samples. The bands between  $1200 - 950 \text{ cm}^{-1}$  are associated with the Si-O tetrahedron, the shoulder at  $870 \text{ cm}^{-1}$  is attributed to the asymmetric stretching of  $\text{AlO}_4$  present in the glass phases of the slag. The Al-O octahedron is found at wavenumbers of  $500 \text{ cm}^{-1}$ . It is expected that when activated, the band between  $3200$  and  $3600 \text{ cm}^{-1}$  would increase indicating formation of hydration reaction products (Ismail et al., 2014). However, this is not observed in these powders, suggesting that the time allowed for adsorption equilibrium did not result in alkali activation playing a significant role in the surface chemistry of the slag particles.

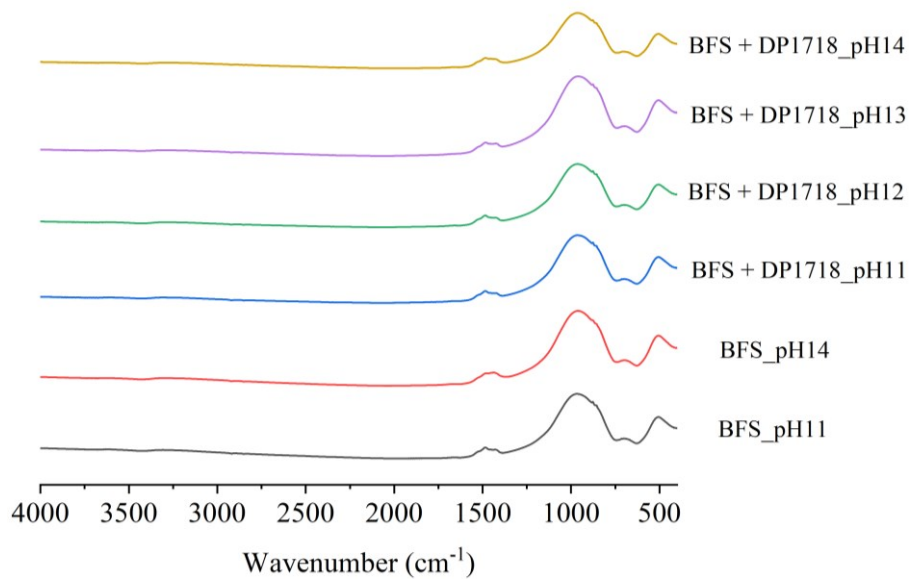


Figure 6.16 FTIR spectra of the slag solid filtrates after LS adsorption in NaOH, as a function of increasing pH.

## 6.5 Conclusions

Previously, colloidal theories have been applied to the complex systems of cement suspensions with success (Houst et al., 2002). These same theories were employed in this study and correlations can be drawn between the colloidal systems investigated in this chapter and the properties of the cement discussed in Chapter 5. The zeta potentials of the dispersed systems were highly affected by the ionic species, pH and presence of lignosulfonate admixtures. From the above discussed results of the zeta potential and the adsorption measurements, a model for the working mechanism of lignosulfonates in slag systems may be proposed in Figure 6.17. This model summarises the changes on the slag surface particles as the chemical environment is altered and the interactions with the lignosulfonate that result due to these changes. The effect of increasing pH on the zeta potential and adsorption measurements is apparent and is governed by the change in the electrical double layer on the surface of the precursor particles. There was a change from a more negative to a less negative polarity of the double layer as the pH was increased. The increase in ionic strength of the solution compressed the electric double layer and resulted in a charge reversal to positive zeta potentials. These studies also showed the change in the electrostatic interactions of the particles as the anionic lignosulfonate admixtures were added. The electric double layer at the interface between the particles moves in an electrical field and the surrounding liquid (Wang et al., 2012). The adsorption measurements were found to be complementary to the zeta potential measurements and the fresh state properties discussed in Chapter 5 which suggests that electrostatic repulsions are the main mechanism by which these bio-derived additives work in these cement systems.

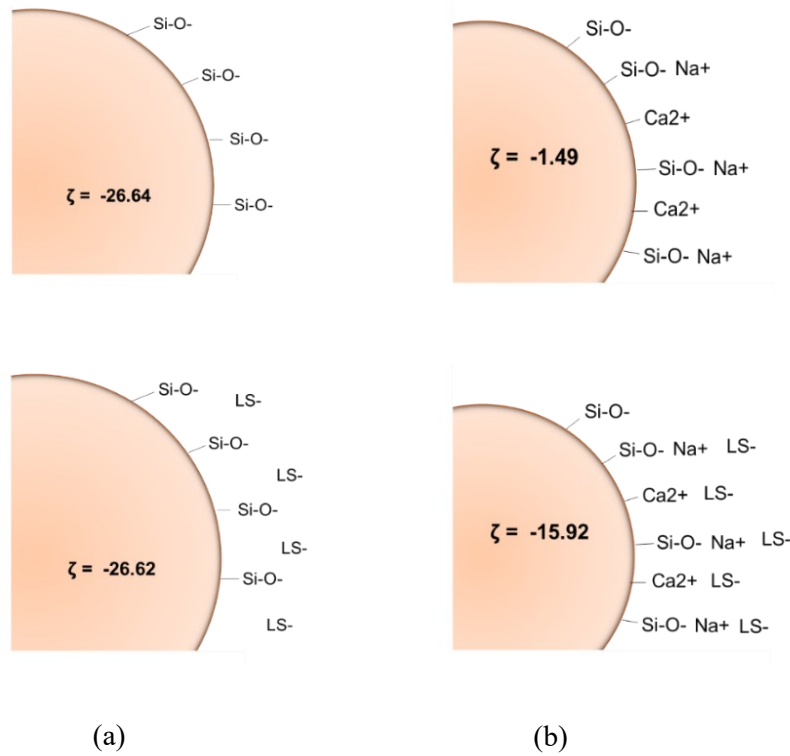


Figure 6.17 Illustration of the working mechanism of LS added when slag is dissolved in (a) water and (b) pH 14 NaOH solution.

The low Mw and low sugar lignosulfonate sample was the most efficient in improving the stability of the slag dispersion system. This suggests that the low molecular weight allows for a better adsorption capacity of the LS on the surface of the slag. This improved adsorption capacity may be because of the arrangement of the lignosulfonate in the pore solution, which allows space for adsorption of more LSs, and hence plays a role in its dispersion efficiency. Therefore, the conformational effects of these lignosulfonates in high pH and high ionic strength environments should also be taken into consideration when discussing their working mechanisms in solutions (Perche et al., 2003). This finding also suggests that with lignosulfonates, steric repulsion does not play a significant role in the dispersion efficiency of these admixtures in alkali activated pastes. If this were the case, we would expect to see much

lower zeta potentials closer to the control sample with addition of LS while still observing some dispersion of the pastes. Previous research has linked steric contributions to particle dispersion to the adsorbed layer thickness which is in turn linked to the molecular weight (Palacios et al., 2009). If the steric effects were significant, the higher molecular weight samples would have performed better than the low molecular weight LS samples. However, further research is needed in this area. Knowledge of the surface chemistry and working mechanisms is required for the design of more tailored admixtures for the efficient dispersion of alkali activated cements.

## **Chapter 7 CONCLUSIONS AND FUTURE WORK**

### **7.1 Conclusions**

The study explored the potential of bio-derived lignosulfonates as additives in alkali activated cements, further driving towards a sustainable built environment. The findings discussed in the preceding chapters have demonstrated that lignosulfonate admixtures can offer some plasticising benefits to alkali activated cements if an LS compatible with the cement system is used. This compatibility suggests that these admixtures can be tailored towards the surface chemistry of the precursors and the behaviour of the LS in the activating solution. These admixtures could offer improved sustainability via enhancing the fresh state properties of alkali activated cements.

#### **7.1.1 The chemical stability of LS in alkaline media**

A detailed characterisation of the lignosulfonates was presented, and it was discovered that lignosulfonates have a higher level of chemical stability in alkaline media than previously documented.

The titration studies demonstrate that the polymers undergo some degree of dissociation/deprotonation in alkaline environments, changing their potential charge. The composition, molecular weight, and sugar content of the lignosulfonates all had an impact on this outcome. The FTIR measurements, which indicated no appreciable alterations or loss of functional groups of the polymer in increasing pH and ionic strengths, were the first to reveal the higher chemical stability of the LS. The only change worth noting was the formation of a C=O peak which was confirmed by  $^{13}\text{C}$  CPMAS NMR. The  $^{13}\text{C}$  CPMAS NMR spectra further

demonstrated that the C $\gamma$  along the backbone of the polymer was most affected by the chemical treatment. These findings suggest that, although the functional groups are unaffected, there may be some breaking of the polymer along the backbone. The XPS measurements then revealed additional characterization of the samples surfaces, indicating that the LS may not be entirely resistant to chemical treatment. The LS derived from softwood, DP1717 and DP4426, were the least affected, while DP1718 and DP1765 from hardwood suffered some C-O bond loss attributed to nucleophilic attack by the OH<sup>-</sup> in solution. Nonetheless, the polymers are still considered chemically stable in this case as their functionality which is strongly linked to sulfonate groups is retained.

The lignosulfonates under study have been shown to be more stable than previously reported. Thus, it can be concluded that chemical instability cannot account for the insufficient plasticising effect of lignosulfonates often reported in alkali activated cements. Therefore, it might be assumed that other factors such as limited solubility of LS in these high pH, high ionic strength conditions and incompatibility with the precursor have a greater impact on their dispersion efficiency.

### **7.1.2 Effect of LS on the performance of alkali activated cements**

For both AAFA and AAS cements, some success in enhancing the workability of the pastes was discovered at specific dosages. The optimum LS dosage was found to be at around 0.3 wt.% of the precursor. The fluidity of the pastes was diminished by high dosages above 0.3 wt.% LS. The sugar content did not enhance the fluidity of the pastes, as is often reported in Portland cement. The rheological behaviour of the pastes significantly changed with addition of LS, demonstrating a decreased viscosity at the optimum dosage, no changes in yield stress values, as well as a previously unreported thixotropic behaviour. This was observed in the

AAFA pastes as well as the AAS pastes. These results also demonstrated that the type and dosage of the admixture affect the interactions of the particles. By using a delayed form of addition, the performance of LS in dispersing the pastes can be more effective.

For both the AAS and AAFA systems, the addition of LS prolonged the setting period. In contrast to the high sugar samples, this delay was more pronounced with the low sugar LS in AAS pastes. The setting timeframes for the AAFA pastes were above 20 hours, which was a substantial delay. At both 7 and 28 days of curing, the addition of LS caused a reduction in the compressive strength of AAS pastes. At higher doses of LS, this decline was more significant. On the other hand, AAFA pastes did not see this reduction after 7 days of curing, while a decline was seen after extended curing times. The calorimetry results demonstrated that LS slightly reduced the rate of reaction and the degree of reaction for both low and high calcium systems more significantly at doses of 3 wt.%.

The presence of LS in the cement did not have a direct impact on the product formation, according to further characterisation of the hardened pastes using FTIR, TG, and SEM techniques. These methods verified that there were no additional or different reaction products formed because of the LS addition. The importance of compatibility between the admixtures and the cement system was revealed through the investigation of the effects of various types of LS on alkali activated cements in this study. It is suggested that the key considerations should be taken into account when selecting the type of admixture to employ.

### **7.1.3 Interaction of lignosulfonates with slag and fly ash**

Studies of more dilute suspensions of slag and fly ash in neutral and alkaline environments revealed that the zeta potentials of the dispersions were greatly affected by the ionic species,

pH and presence of lignosulfonate admixtures. An increase in pH altered the electrical double layer and affected the adsorption of LS on the surface of the precursor particles. This was evidenced by a change from a more negative to a less negative zeta potential as the pH was increased. The electric double layer was compressed by the increase in ionic strength in solution, which caused a charge reversal to positive zeta potentials. These investigations also demonstrated that the addition of the anionic lignosulfonate admixtures altered the electrostatic interactions of the particles. The samples with LS had more negative zeta potentials than the control indicating that some dispersion of the particles is occurring, confirming the improved workability results as noted above.

The stability of the slag suspensions was improved most effectively by the low Mw and low sugar lignosulfonate sample. This shows that the LS has a stronger ability to adsorb on the surface of the slag due to its low molecular weight. The enhanced adsorption capacity of the DP1718 LS sample may be due to the arrangement of the lignosulfonate in the pore solution, which provides room for the adsorption of more LSs and hence contributes to its dispersion effectiveness. Therefore, when analysing the working mechanisms of these lignosulfonates in solutions, it is equally important to take into account their conformational effects at high pH and high ionic strength.

The adsorption data were found to be complementary to the zeta potential measurements, indicating that electrostatic repulsions are the primary mechanism by which these bio-derived additives function in these cement systems. This result implies that steric repulsions may play a role but are not significantly affecting the dispersion of lignosulfonates.

## 7.2 Future work

The work presented in this study has provided an overview of the performance of lignosulfonate admixtures in alkali activated cements. Discussions regarding the chemical stability of LS in highly alkaline media have highlighted that these admixtures are not limited by this phenomenon, and that some plasticising effect can be achieved.

For the optimum usage of lignosulfonates as admixtures in alkali activated cements, there are still some questions that need to be investigated:

- The adsorption layer thickness and conformational effects at the interface, though difficult to quantify, can provide more insight into the working mechanisms of the lignosulfonates. These conformational effects of the lignosulfonates in solution was not investigated in this study but can be a key discussion point. Once adsorbed, the distribution of the lignosulfonates on the surface can be studied, providing insight on the adsorption isotherms and models that these materials follow. These studies can be correlated to the adsorption studies to correlate the adsorption thickness on the particle surface with the amount of admixture adsorbed. This has often been achieved by Atomic Force Microscopy, however, the main challenge with this technique is producing the suitable substrates and AFM probes that would mimic the cement system more closely. This is one of the main challenges to be addressed in the future. The other limitations of the technique are that it is limited by the roughness and porosity of the surface, and therefore requires a smooth, unreactive surface. The current study aimed to achieve this objective, but due to Covid19 lockdown and laboratory shutdowns this was not possible.

- In investigating the chemical action of LS in alkaline media, further investigations are required to validate the observed changes, and identify and quantify the dissociated species from the polymer as the pH is varied. This can be achieved by coupling conductivity measurements with more advanced techniques. The charge density of the polymer linked directly to the amount of dissociable functional groups in the polymer determined at different pH environments can give further insight into the behaviour of lignosulfonates in these chemical environments. In studying the effect of chemical treatment, quantifying the change in the functional groups alongside analysis of the molecular weight would give more insight into any breakage of the polymer along the backbone as is hypothesised in this study.
- The effect of LS on the other properties of hardened pastes such as drying shrinkage and porosity can be investigated further. The addition of LS may have contributed to a change in the pore structure of the cement matrix, and this can be investigated through pore size distribution measurements with mercury intrusion porosimetry (MIP). There is very limited published research on the effect of admixtures on the porosity of AAMs which is also essential for durability studies.

## References

- Ajao, O., Jeaidi, J., Benali, M., Restrepo, A. M., El Mehdi, N., & Boumghar, Y. (2018). Quantification and variability analysis of lignin optical properties for colour-dependent industrial applications. *Molecules*, *23*(2), 377.
- Altan, E., & Erdoğan, S. T. (2012). Alkali activation of a slag at ambient and elevated temperatures. *Cement and Concrete Composites*, *34*(2), 131–139.
- Anderson, P., Kumar, A., Roy, D., & Wolfe-Confer, D. (1986). The effect of calcium sulphate concentration on the adsorption of a superplasticiser on a cement: methods, zeta potential and adsorption studies. *Cement and Concrete Composites*, *16*(1), 255–259.
- Andrew, R. M. (2017). Global CO<sub>2</sub> emissions from cement production. *Earth System Science Data*, 1–52.
- Arel, H. Ş., & Aydin, E. (2017). Effects of Ca-, Mg-, K-, and Na-lignosulfonates on the behavior of fresh concrete. *Construction and Building Materials*, *157*, 1084–1091.
- Assi, L. N., Deaver, E. (Eddie), & Ziehl, P. (2018). Using sucrose for improvement of initial and final setting times of silica fume-based activating solution of fly ash geopolymer concrete. *Construction and Building Materials*, *191*, 47–55.
- ASTM C109/109M-16a. (2016). Standard test method for compressive strength of hydraulic cement mortars (Using 2-in. or cube specimens). *ASTM International, West Conshohocken, PA*.
- ASTM C1679. (2017). ASTM C1679-14 Standard Practice for Measuring Hydration Kinetics of Hydraulic Cementitious Mixtures Using Isothermal Calorimetry. *ASTM International, West Conshohocken, PA*.
- ASTM C1749. (2017). Standard Guide for Measurement of the Rheological Properties of Hydraulic Cementitious Paste Using a Rotational Rheometer. *ASTM International, West Conshohocken, PA*.
- ASTM C191. (2019). Standard test methods for time of setting of hydraulic cement by Vicat needle. *ASTM International, West Conshohocken, PA*.
- Bakharev, T., Sanjayan, J. G., & Cheng, Y. B. (2000). Effect of admixtures on properties of alkali-activated slag concrete. *Cement and Concrete Research*, *30*(9), 1367–1374.
- Banfill, P. F.G. (2011). Additivity effects in the rheology of fresh concrete containing water-reducing admixtures. *Construction and Building Materials*, *25*(6), 2955–2960.
- Banfill, P.F.G. (2006). Rheology of fresh cement and concrete. *Rheology Reviews*, 61–130.
- Bernal, S. A, San Nicolas, R., van Deventer, J. S. J. & Provis, J. L. (2015). Water content modifies the structural development of sodium metasilicate-activated slag binders. *ALCONPAT Journal*, *5*(April), 30–41.
- Bernal, S.A., & Provis, J. L. (2014). Durability of alkali-activated materials: Progress and perspectives. *Journal of the American Ceramic Society*, *97*(4), 997–1008.
- Bernal, S.A., Rodríguez, E. D., Kirchheim, A. P., & Provis, J. L. (2016). Management and

- valorisation of wastes through use in producing alkali-activated cement materials. *Journal of Chemical Technology and Biotechnology*, 91(9), 2365–2388.
- Bessaies-Bey, H., Khayat, K. H., Palacios, M., Schmidt, W., & Roussel, N. (2022). Viscosity modifying agents: Key components of advanced cement-based materials with adapted rheology. *Cement and Concrete Research*, 152, 106646.
- Bilim, C., Karahan, O., Atiş, C. D., & Ilkentapar, S. (2013). Influence of admixtures on the properties of alkali-activated slag mortars subjected to different curing conditions. *Materials and Design*, 44, 540–547.
- Bishop, M., & Barron, A. R. (2006). Cement hydration inhibition with sucrose, tartaric acid, and lignosulfonate: Analytical and spectroscopic study. *Industrial and Engineering Chemistry Research*, 45(21), 7042–7049.
- Boeriu, C. G., Bravo, D., Gosselink, R. J. A., & Van Dam, J. E. G. (2004). Characterisation of structure-dependent functional properties of lignin with infrared spectroscopy. *Industrial Crops and Products*, 20(2), 205–218.
- Bolatbaev, K. N., Lugovitskaya, T. N., Kolosov, A. V., & Naboichenko, S. S. (2010). Fundamental aspects of the behavior of various lignosulfonates in solutions. *Russian Journal of Applied Chemistry*, 83(9), 1553–1557.
- Borukhov, I., Andelman, D., Borrega, R., Cloitre, M., Leibler, L., & Orland, H. (2000). Polyelectrolyte titration: Theory and experiment. *Journal of Physical Chemistry B*, 104(47), 11027–11034.
- Brookhaven, I. (2002). *Brookhaven ZetaPlus manual* (Issue 631). [http://www.vtpup.cz/common/manual/PrF\\_labpoakoch\\_Brookhaven\\_ZetaPlus\\_manual\\_EN.pdf](http://www.vtpup.cz/common/manual/PrF_labpoakoch_Brookhaven_ZetaPlus_manual_EN.pdf)
- Brough, A. R., & Atkinson, A. (2002). Sodium silicate-based, alkali-activated slag mortars - Part I. Strength, hydration and microstructure. *Cement and Concrete Research*, 32(6), 865–879.
- Burgos-Montes, O., Palacios, M., Rivilla, P., & Puertas, F. (2012). Compatibility between superplasticizer admixtures and cements with mineral additions. *Construction and Building Materials*, 31, 300–309.
- Carabba, L., Manzi, S., & Bignozzi, M. C. (2016). Superplasticizer addition to carbon fly ash geopolymers activated at room temperature. *Materials*, 9(7), 586.
- Češnovar, M., Traven, K., & Ducman, V. (2021). Deformation of Alkali-Activated Materials at an Early Age Under Different Curing Conditions. *Frontiers in Chemistry*, 9(June), 1–9.
- Chang, J. J. (2003). A study on the setting characteristics of sodium silicate-activated slag pastes. *Cement and Concrete Research*, 33(7), 1005–1011.
- Colombo, A., Geiker, M., Justnes, H., Lauten, R. A., & Weerdt, K. De. (2017). On the mechanisms of consumption of calcium lignosulfonate by cement paste. *Cement and Concrete Research*, 98, 1–9.
- Criado, M., Palomo, A., Fernández-Jiménez, A., & Banfill, P. F. G. (2009). Alkali activated fly ash: Effect of admixtures on paste rheology. *Rheologica Acta*, 48(4), 447–455.

- Criado, M., Walkley, B., Ke, X., Provis, J. L., & Bernal, S. A. (2018). Slag and activator chemistry control the reaction kinetics of sodium metasilicate-activated slag cements. *Sustainability*, *10*(12).
- Danner, T., Justnes, H., Geiker, M., & Andreas, R. (2015). Phase changes during the early hydration of Portland cement with. *Cement and Concrete Research*, *69*, 50–60.
- Deng, Y., Feng, X., Yang, D., Yi, C., & Qiu, X. (2012).  $\pi$ - $\pi$  Stacking of the aromatic groups in lignosulfonates. *BioResources*, *7*(1), 1145–1156.
- Deng, Y., Wu, Y., Qian, Y., Ouyang, X., Yang, D., & Qiu, X. (2010). Adsorption and desorption behaviors of lignosulfonate during the self-assembly of multilayers. *BioResources*, *5*(2), 1178–1196.
- Derkani, M. H., Bartlett, N. J., Koma, G., Carter, L. A., Geddes, D. A., Provis, J. L., & Walkley, B. (2022). Mechanisms of dispersion of metakaolin particles via adsorption of sodium naphthalene sulfonate formaldehyde polymer. *Journal of Colloid and Interface Science*, *628*, 745–757.
- Dilling, P., & Sarjeant, P. T. (1984). Reduction of lignin color. *U.S. Patent 4,454,066*.
- Douglas, E., & Brandstetr, J. (1990). A preliminary study on the alkali activation of ground granulated blast-furnace slag. *Cement and Concrete Research*, *20*, 746–756.
- Dunster, A. (2020, February). Low carbon cements. *Materials World*, 30–31.
- Elakneswaran, Y., Nawa, T., & Kurumisawa, K. (2009). Zeta potential study of paste blends with slag. *Cement and Concrete Composites*, *31*(1), 72–76.
- Elder, T., & Fort, R. (2010). Reactivity of Lignin-Correlation with Molecular Orbital Calculations. In C. Heiner, D. R. Dimmel, & J. A. Schmidt (Eds.), *Lignin and Lignans Advanced in Chemistry* (pp. 321–347). Taylor & Francis.
- Eraghi Kazzaz, A., Hosseinpour Feizi, Z., & Fatehi, P. (2019). Grafting strategies for hydroxy groups of lignin for producing materials. *Green Chemistry*, *21*(21), 5714–5752.
- Evstigneyev, E. I., Mazur, A. S., Kalugina, A. V., Pranovich, A. V., & Vasilyev, A. V. (2018). Solid-state  $^{13}\text{C}$  CP/MAS NMR for alkyl-O-aryl bond determination in lignin preparations. *Journal of Wood Chemistry and Technology*, *38*(2), 137–148.
- Fernández-Altable, V., & Casanova, I. (2006). Influence of mixing sequence and superplasticiser dosage on the rheological response of cement pastes at different temperatures. *Cement and Concrete Research*, *36*(7), 1222–1230.
- Fernández-Jiménez, A., & Palomo, A. (2003). Characterisation of fly ashes. Potential reactivity as alkaline cements. *Fuel*, *82*(18), 2259–2265.
- Fernández-Jiménez, A., Palomo, A., & Criado, M. (2005). Microstructure development of alkali-activated fly ash cement: A descriptive model. *Cement and Concrete Research*, *35*(6), 1204–1209.
- Fernández-Jiménez, A., Palomo, A., Sobrados, I., & Sanz, J. (2006). The role played by the reactive alumina content in the alkaline activation of fly ashes. *Microporous and Mesoporous Materials*, *91*(1–3), 111–119.
- Fernández-Jiménez, A., Palomo, J. G., & Puertas, F. (1999). Alkali-activated slag mortars. Mechanical strength behaviour. *Cement and Concrete Research*, *29*(8), 1313–1321.

- Fernandez-Jiménez, A., & Puertas, F. (1997). Alkali activated slag cements: Kinetic studies. *Cement and Concrete Research*, 27(3), 359–368.
- Fernandez-Jimenez, A., Puertas, F., & Arteaga, A. (1998). Determination of kinetic equations of alkaline activation of blast furnace slag by means of calorimetric data. *Journal of Thermal Analysis and Calorimetry* 52(3), 945–955.
- Feys, D. (2012). Understanding the pumping of conventional vibrated and self-compacting concrete. In *Understanding the Rheology of Concrete*. Woodhead Publishing Limited.
- Feys, Dimitri, Verhoeven, R., & De Schutter, G. (2009). Why is fresh self-compacting concrete shear thickening? *Cement and Concrete Research*, 39(6), 510–523.
- Flatt, R. J., & Ferraris, C. F. (2002). Acoustophoretic characterization of cement suspensions. *Materials and Structures/Materiaux et Constructions*, 35(253), 541–549.
- Flatt, Robert J., Schober, I., Raphael, E., Plassard, C., & Lesniewska, E. (2009). Conformation of adsorbed comb copolymer dispersants. *Langmuir*, 25, 845–855.
- Gardon, J. L., & Mason, S. G. (1955). Physicochemical studies of ligninsulphonates ii. Behavior as polyelectrolytes. *Canadian Journal of Chemistry*, 33, 1491–1501.
- Garg, N., & White, C. E. (2017). Mechanism of zinc oxide retardation in alkali-activated materials: an in situ X-ray pair distribution function investigation. *J. Mater. Chem. A*, 5(23), 11794–11804.
- Garside, M. (2022). Global cement production 1995 - 2021. *Statistica*.  
<https://www.statista.com/statistics/1087115/global-cement-production-volume/#statisticContainer>
- Gebregziabihier, B. S., Thomas, R., & Peethamparan, S. (2015). Very early-age reaction kinetics and microstructural development in alkali-activated slag. *Cement and Concrete Composites*, 55, 91–102.
- Gelardi, G., Mantellato, S., Marchon, D., Palacios, M., Eberhardt, A. B., & Flatt, R. J. (2015). Chemistry of chemical admixtures. In *Science and Technology of Concrete Admixtures*.
- Gierer, J. (1986). Chemistry of delignification. *Wood Science and Technology*, 20(1), 1–33.
- Goring, D. A. I., Vuong, R., Gancet, C., & Chanzy, H. (1979). The flatness of lignosulfonate macromolecules as demonstrated by electron microscopy. *Journal of Applied Polymer Science*, 24(4), 931–936.
- GreenAgroChem. (2022). Reducing sugar in calcium lignosulfonates. *GreenAgroChem*.  
[www.greenagrochem.com/reducing-sugar-in-calcium-lignosulfonates](http://www.greenagrochem.com/reducing-sugar-in-calcium-lignosulfonates)
- Gunasekara, C., Law, D. W., Setunge, S., & Sanjayan, J. G. (2015). Zeta potential, gel formation and compressive strength of low calcium fly ash geopolymers. *Construction and Building Materials*, 95, 592–599.
- Habbaba, A., & Plank, J. (2010). Interaction between polycarboxylate superplasticizers and amorphous ground granulated blast furnace slag. *Journal of the American Ceramic Society*, 93(9), 2857–2863.
- Habbaba, A., & Plank, J. (2012). Surface chemistry of ground granulated blast furnace slag in cement pore solution and its impact on the effectiveness of polycarboxylate superplasticizers. *Journal of the American Ceramic Society*, 95(2), 768–775.

- Han, D., & Ferron, R. D. (2015). Effect of mixing method on microstructure and rheology of cement paste. *Construction and Building Materials*, 93, 278–288.
- Hanehara, S., & Yamada, K. (1999). Interaction between cement and chemical admixture from the point of cement hydration, absorption behaviour of admixture, and paste rheology. *Cement and Concrete Research*, 29(8), 1159–1165.
- Hemmilä, V., Hosseinpourpia, R., Adamopoulos, S., & Eceiza, A. (2020). Characterization of Wood-based Industrial Biorefinery Lignosulfonates and Supercritical Water Hydrolysis Lignin. *Waste and Biomass Valorization*, 11(11), 5835–5845.
- Hill, R. L., Sarkar, S. L., Rathbone, R. F., & Hower, J. C. (1997). An examination of fly ash carbon and its interactions with air entraining agent. *Cement and Concrete Research*, 27(2), 193–204.
- Hofmann, A. (2010). Spectroscopic Techniques: I Spectrophotometric Techniques. In *Principles and Techniques of Biochemistry and Molecular Biology* (pp. 477–521). Cambridge University Press.
- Hommer, H. (2009). Interaction of polycarboxylate ether with silica fume. *Journal of the European Ceramic Society*, 29(10), 1847–1853.
- Houst, Y. F., Bowen, P., Perche, F., Kauppi, A., Borget, P., Galmiche, L., Le Meins, J. F., Lafuma, F., Flatt, R. J., Schober, I., Banfill, P. F. G., Swift, D. S., Myrvold, B. O., Petersen, B. G., & Reknes, K. (2008). Design and function of novel superplasticizers for more durable high performance concrete (superplast project). *Cement and Concrete Research*, 38(10), 1197–1209.
- Houst, Y. F., Bowen, P., & Siebold, A. (2002). Some basic aspects of the interaction between cement and superplasticizers. *Innovations and Developments In Concrete Materials And Construction*, 225–234.
- Huanhai, Z., Xuequan, W., Zhongzi, X., & Mingshu, T. (1993). Kinetic study on hydration of alkali-activated slag. *Cement and Concrete Research*, 23, 1253–1258.
- Ismail, I., Bernal, S. A., Provis, J. L., San Nicolas, R., Hamdan, S., & van Deventer, J. S. J. (2014). Modification of phase evolution in alkali activated blast furnace slag by the incorporation of fly ash. *Cement and Concrete Composites*, 45, 125–135.
- Jiang, S., Mutin, J., & Nonat, A. (1996). Studies on mechanism and physico-chemical parameters at the origin of the cement setting ii. Physico-chemical parameters determining the coagulation process. *Cement and Concrete Research*, 26(3), 491–500.
- Kalina, L., Bilek Jr, V., Hruby, P., Iliuschchenko, V., Kalina, M., & Smilek, J. (2022). On the action mechanism of lignosulfonate plasticizer in alkali-activated slag-based system. *Cement and Concrete Research*, 157, 106822.
- Kantro, D. (1980). Influence of Water-Reducing Admixtures on Properties of Cement Paste—A Miniature Slump Test. *Cement, Concrete and Aggregates*, 2(2), 95.
- Kashani, A., Provis, J. L., Qiao, G. G., & Van Deventer, J. S. J. (2014). The interrelationship between surface chemistry and rheology in alkali activated slag paste. *Construction and Building Materials*, 65, 583–591.
- Kashani, A., Provis, J. L., Xu, J., Kilcullen, A. R., Qiao, G. G., & Van Deventer, J. S. J. (2014). Effect of molecular architecture of polycarboxylate ethers on plasticizing

- performance in alkali-activated slag paste. *Journal of Materials Science*, 49(7), 2761–2772.
- Kauppi, A., Andersson, K. M., & Bergström, L. (2005). Probing the effect of superplasticizer adsorption on the surface forces using the colloidal probe AFM technique. *Cement and Concrete Research* 35, 133–140.
- Kocak, G., Tuncer, C., & Bütün, V. (2017). pH-responsive polymers. *Polymer Chemistry*, 144–176.
- Kovalchuk, G., Fernández-Jiménez, A., & Palomo, A. (2007). Alkali-activated fly ash: Effect of thermal curing conditions on mechanical and microstructural development - Part II. *Fuel*, 86(3), 315–322.
- Kusbiantoro, A., Ibrahim, M. S., Muthusamy, K., & Alias, A. (2013). Development of Sucrose and Citric Acid as the Natural based Admixture for Fly Ash based Geopolymer. *Procedia Environmental Sciences*, 17, 596–602.
- Lapierre, C., Pollet, B., & Rolando, C. (1995). New insights into the molecular architecture of hardwood lignins by chemical degradative methods. *Research on Chemical Intermediates*, 21(3–5), 397–412.
- Łażniewska-Piekarczyk, B. (2014). The methodology for assessing the impact of new generation superplasticizers on air content in self-compacting concrete. *Construction and Building Materials*, 53, 488–502.
- Le Bell, J. C. (1984). The relation between the structure of lignosulphonates and their effect as stabilizers for latex particulate dispersions. *Colloids and Surfaces*, 9(3), 237–251.
- Leary, G. J., & Newman, R. H. (1992). Cross Polarization/Magic Angle Spinning Nuclear Magnetic Resonance (CP/MAS NMR) Spectroscopy. In *Methods in Lignin Chemistry* (pp. 146–161). Springer-Verlag.
- Lei, L., & Chan, H. K. (2020). Investigation into the molecular design and plasticizing effectiveness of HPEG-based polycarboxylate superplasticizers in alkali-activated slag. *Cement and Concrete Research*, 136, 106150.
- Lei, L., Hirata, T., & Plank, J. (2022). 40 years of PCE superplasticizers - History, current state-of-the-art and an outlook. *Cement and Concrete Research*, 157, 106826.
- Lei, L., Palacios, M., Plank, J., & Jeknavorian, A. A. (2022). Interaction between polycarboxylate superplasticizers and non-calcined clays and calcined clays: A review. *Cement and Concrete Research*, 154, 106717.
- Li, H.-q., Huang, G.-h., An, C.-j., & Zhang, W.-x. (2012). Kinetic and equilibrium studies on the adsorption of calcium lignosulfonate from aqueous solution by coal fly ash. *Chemical Engineering Journal*, 200–202, 275–282.
- Li, R., Yang, D., Guo, W., & Qiu, X. (2013). The adsorption and dispersing mechanisms of sodium lignosulfonate on Al<sub>2</sub>O<sub>3</sub> particles in aqueous solution. *Holzforschung*, 67(4), 387–394.
- Liberto, T., Bellotto, M., & Robisson, A. (2022). Small oscillatory rheology and cementitious particle interactions. *Cement and Concrete Research*, 157, 106790.
- Lima, R. B., Raza, R., Qin, H., Li, J., Lindström, M. E., & Zhu, B. (2013). Direct lignin fuel

- cell for power generation. *RSC Advances*, 3(15), 5083–5089.
- Liu, S., Li, Q., Zuo, S., & Xia, H. (2022). Facile synthesis of lignosulfonate-derived sulfur-doped carbon materials for photocatalytic degradation of tetracycline under visible-light irradiation. *Microporous and Mesoporous Materials*, 336, 111876.
- Lowke, D., & Gehlen, C. (2017). The zeta potential of cement and additions in cementitious suspensions with high solid fraction. *Cement and Concrete Research*, 95, 195–204.
- Lu, Y., Lu, Y. C., Hu, H. Q., Xie, F. J., Wei, X. Y., & Fan, X. (2017). Structural characterization of lignin and its degradation products with spectroscopic methods. *Journal of Spectroscopy*, 2017, 8951658.
- Lutnaes, B. F., Myrvold, B. O., Lauten, R. A., & Endeshaw, M. M. (2008).  $^1\text{H}$  and  $^{13}\text{C}$  NMR data of benzylic sulfonic acids - Model compounds for lignosulfonate. *Magnetic Resonance in Chemistry*, 46(3), 299–305.
- Luukkonen, T., Abdollahnejad, Z., Ohenoja, K., Kinnunen, P., & Illikainen, M. (2019). Suitability of commercial superplasticizers for one-part alkali-activated blast-furnace slag mortar. *Journal of Sustainable Cement-Based Materials*, 8(4), 244–257.
- Madad, N., Chebil, L., Sanchez, C., & Ghoul, M. (2011). Effect of molecular weight distribution on chemical, structural and physicochemical properties of sodium lignosulfonates. *Rasayan Journal of Chemistry*, 4(1), 189–202.
- Malek, R. I. ., & Roy, D. . (1985). Electrokinetic phenomena and surface characteristics of fly ash particles. In *Materials Research Laboratory*.
- Malvern. (2000). Zeta potential: An Introduction in 30 minutes. In *Zetasizer Nano Serles Technical Note. MRK654-01* (Vol. 2).
- Malvern Instruments Limited. (2016). A Basic Introduction to Rheology Shear Flow. <https://cdn.technologynetworks.com/TN/Resources/PDF/WP160620BasicIntroRheology.pdf>
- Marchon, D., Sulser, U., Eberhardt, A., & Flatt, R. J. (2013). Molecular design of comb-shaped polycarboxylate dispersants for environmentally friendly concrete. *Soft Matter*, 9(45), 10719–10728.
- Maver, U., Maver, T., Persin, Z., Mozetic, M., Vesel, A., Gaberscek, M., & Stana-Kleinschek, K. (2013). Polymer characterisation with the Atomic Force Microscope. In F. Yilmaz (Ed.), *Polymer Science* (pp. 113–132). IntechOpen.
- Mbasha, W., Masalova, I., Haldenwang, R., & Malkin, A. (2015). The yield stress of cement pastes as obtained by different rheological approaches. *Applied Rheology*, 25(5), 1–11.
- Miller, S. A., John, V. M., Pacca, S. A., & Horvath, A. (2018). Carbon dioxide reduction potential in the global cement industry by 2050. *Cement and Concrete Research*, 114, 115–124.
- Mills, J., Mondal, P., & Wagner, N. (2022). Structure-property relationships and state behavior of alkali-activated aluminosilicate gels. *Cement and Concrete Research*, 151, 106618.
- Miyake, N., Ando, T., & Sakai, E. (1985). Superplasticized concrete using refined lignosulfonate and its action mechanism. *Cement and Concrete Research*, 15, 295–302.

- Myrvold, B. O. (2008). A new model for the structure of lignosulphonates. Part 1. Behaviour in dilute solutions. *Industrial Crops and Products*, 27(2), 214–219.
- Nachbaur, L., Mutin, J. C., Nonat, A., & Choplin, L. (2001). Dynamic mode rheology of cement and tricalcium silicate pastes from mixing to setting. *Cement and Concrete Research*, 31(2), 183–192.
- Nägele, E. (1986). The zeta potential of cement Part II: Effect of pH-value. *Cement and Concrete Research*, 16(6), 853–863.
- Nägele, E. (1985). The zeta-potential of cement. *Cement and Concrete Research*, 15(3), 453–462.
- Nägele, E., & Schneider, U. (1989). The zeta-potential of blast furnace slag and fly ash. *Cement and Concrete Research*, 19, 811–820.
- Nägele, E., & Schneider, U. (1987). The zeta - potential of cement. Part IV. Effect of simple salts. *Cement and Concrete Research*, 17(6), 977–982.
- Najimi, M., Ghafoori, N., & Sharbaf, M. (2020). Alkali-activated natural pozzolan/slag binders: Limitations and remediation. *Magazine of Concrete Research*, 72(18), 919–935.
- Nematollahi, B., & Sanjayan, J. (2014). Effect of different superplasticizers and activator combinations on workability and strength of fly ash based geopolymer. *Materials and Design*, 57, 667–672.
- Neville, A. M. (1995). *Properties of concrete* (4th ed.).
- Nimz, H., Robert, D., Faix, O., & Nemr, M. (1981). Carbon-13 NMR spectra of lignins, 8 \* Structural differences between lignins of hardwoods, softwoods, grasses and compression wood. *Holzforschung*, 35(1), 16–26.
- Nyman, V., Rose, G., & Ralston, J. (1986). The colloidal behaviour of kraft lignin and lignosulfonates. *Colloids and Surfaces*, 21(C), 125–147.
- Ocean Optics. (2009). *SpectraSuite Installation and Operation Manual*. In *Ocean Optics*.
- Ouyang, X., Deng, Y., Qian, Y., Zhang, P., & Qiu, X. (2011). Adsorption characteristics of lignosulfonates in salt-free and salt-added aqueous solutions. *Biomacromolecules*, 12(9), 3313–3320.
- Palacios, M., Houst, Y. F., Bowen, P., & Puertas, F. (2009). Adsorption of superplasticizer admixtures on alkali-activated slag pastes. *Cement and Concrete Research*, 39(8), 670–677.
- Palacios, M., & Puertas, F. (2005). Effect of superplasticizer and shrinkage-reducing admixtures on alkali-activated slag pastes and mortars. *Cement and Concrete Research*, 35(7), 1358–1367.
- Palacios, M., & Puertas, F. (2011). Effectiveness of mixing time on hardened properties of waterglass-activated slag pastes and mortars. *ACI Materials Journal*, 108(1), 73–78.
- Palacios, M., Puertas, F., & Banfill, P. F. G. (2008). Rheology and Setting of Alkali-Activated Slag Pastes and Mortars: Effect of Organic Admixture. *ACI Materials Journal*, 105(2), 140-148.
- Palomo, A., Banfill, P. F. G., Fernández-Jiménez, A., & Swift, D. S. (2005). Properties of

- alkali-activated fly ashes determined from rheological measurements. *Advances in Cement Research*, 17(4), 143–151.
- Palomo, A., Grutzeck, M. W., & Blanco, M. T. (1999). Alkali-activated fly ashes: A cement for the future. *Cement and Concrete Research*, 29(8), 1323–1329.
- Papo, A., & Piani, L. (2004). Effect of various superplasticizers on the rheological properties of Portland cement pastes. *Cement and Concrete Research*, 34(11), 2097–2101.
- Park, S.-J., & Seo, M.-K. (2011). Intermolecular Force. In *Interface Science and Composites* (1st ed., pp. 1–57). Elsevier.
- Perche, F., Houst, Y. F., Bowen, P., & Hofmann, H. (2003). Adsorption of lignosulfonates and polycarboxylates depletion and electroacoustic methods. *International Conference on Superplasticisers and Other Chemical Admixtures in Concrete*, 1–15.
- Plank, J., Sakai, E., Miao, C. W., Yu, C., & Hong, J. X. (2015). Chemical admixtures - Chemistry, applications and their impact on concrete microstructure and durability. *Cement and Concrete Research*, 78, 81–99.
- Plank, Johann, & Hirsch, C. (2007). Impact of zeta potential of early cement hydration phases on superplasticizer adsorption. *Cement and Concrete Research*, 37(4), 537–542.
- Provis, J. L. (2018). Alkali-activated materials. *Cement and Concrete Research*, 114, 40–48.
- Provis, J. L., Arbi, K., Bernal, S. A., Bondar, D., Buchwald, A., Castel, A., Chithiraputhiran, S., Cyr, M., Dehghan, A., Dombrowski-Daube, K., Dubey, A., Ducman, V., Gluth, G. J. G., Nanukuttan, S., Peterson, K., Puertas, F., van Riessen, A., Torres-Carrasco, M., Ye, G., & Zuo, Y. (2019). RILEM TC 247-DTA round robin test: mix design and reproducibility of compressive strength of alkali-activated concretes. *Materials and Structures*, 52(5), 1–13.
- Provis, J. L., & Bernal, S. A. (2014). Geopolymers and Related Alkali-Activated Materials. *Annual Review of Materials Research*, 44, 299–327.
- Provis, J. L., & van Deventer, J. S. J. (2014). Alkali Activated Materials: State-of-the-Art Report, RILEM TC 224-AAM. In *RILEM State-of-the-Art Reports*. Springer, Dordrecht
- Puertas, F., Alonso, M. M., Gismera, S., Lanzón, M., & Blanco-Varela, M. T. (2018). Rheology of Cementitious Materials: Alkali-Activated Materials or Geopolymers. *MATEC Web of Conferences*, 149.
- Puertas, F., Palacios, M., Manzano, H., Dolado, J. S., Rico, A., & Rodríguez, J. (2011). A model for the C-A-S-H gel formed in alkali-activated slag cements. *Journal of the European Ceramic Society*, 31(12), 2043–2056.
- Puertas, F., Palomo, A., Fernández-Jiménez, A., Izquierdo, J. D., & Granizo, M. L. (2003). Effect of superplasticisers on the behaviour and properties of alkaline cements. *Advances in Cement Research*, 15(1), 23–28.
- Puertas, F., Santos, H., Palacios, M., & Martínez-Ramírez, S. (2005). Polycarboxylate superplasticiser admixtures: effect on hydration, microstructure and rheological behaviour in cement pastes. *Advances in Cement Research*, 17(2), 77–89.
- Puertas, F., & Torres-Carrasco, M. (2014). Use of glass waste as an activator in the preparation of alkali-activated slag. Mechanical strength and paste characterisation.

*Cement and Concrete Research*, 57, 95–104.

- Puertas, F., Varga, C., & Alonso, M. M. (2014). Rheology of alkali-activated slag pastes. Effect of the nature and concentration of the activating solution. *Cement and Concrete Composites*, 53, 279–288.
- Qian, Y., Deng, Y., Yi, C., Yu, H., & Qiu, X. (2011). Solution behaviors and adsorption characteristics of sodium lignosulfonate under different pH conditions. *BioResources*, 6(4), 4686–4695.
- Qing-Hua, C., & Sarkar, S. L. (1994). A study of rheological and mechanical properties of mixed alkali activated slag pastes. *Advanced Cement Based Materials*, 1(4), 178–184.
- Qiu, X., Kong, Q., Zhou, M., & Yang, D. (2010). Aggregation behavior of sodium lignosulfonate in water solution. *Journal of Physical Chemistry B*, 114(48), 15857–15861.
- Rakngan, W., Williamson, T., Ferron, R. D., Sant, G., & Juenger, M. C. G. (2018). Controlling workability in alkali-activated Class C fly ash. *Construction and Building Materials*, 183, 226–233.
- Rashad, A. M., Bai, Y., Basheer, P. A. M., Collier, N. C., & Milestone, N. B. (2012). Chemical and mechanical stability of sodium sulfate activated slag after exposure to elevated temperature. *Cement and Concrete Research*, 42(2), 333–343.
- Ren, J. (2016). Superplasticiser for NaOH-activated slag: Competition and stability between superplasticiser and alkali-activator. University College London.
- Rintala, A., Havukainen, J., & Abdulkareem, M. (2021). Estimating the cost-competitiveness of recycling-based geopolymer concretes. *Recycling*, 6(3).
- Rodríguez-Lucena, P., Lucena, J. J., & Hernández-Apaolaza, L. (2009). Relationship between the structure of Fe-Lignosulfonate complexes determined by FTIR spectroscopy and their reduction by the leaf Fe reductase. *The Proceedings of the International Plant Nutrition Colloquium XVI*.
- Roussel, N., Ovarlez, G., Garrault, S., & Brumaud, C. (2012). The origins of thixotropy of fresh cement pastes. *Cement and Concrete Research*, 42(1), 148–157.
- Rouyer, J., & Poulesquen, A. (2015). Evidence of a Fractal Percolating Network During Geopolymerization. *Journal of the American Ceramic Society*, 98(5), 1580–1587.
- Ruwoldt, J. (2020). A Critical Review of the Physicochemical Properties of Lignosulfonates: Chemical Structure and Behavior in Aqueous Solution, at Surfaces and Interfaces. *Surfaces*, 3(4), 622–648.
- Ruwoldt, J., Simon, S., & Øye, G. (2020). Viscoelastic properties of interfacial lignosulfonate films and the effect of added electrolytes. *Colloids and Surfaces A: Physicochemical and Engineering Aspects*, 606(June), 125478.
- Shapley, P. (2022). Acid-Base Chemistry of Sugars. In *Chemistry 104* (pp. 1–11).
- Shi, C., & Day, R. L. (1995). A calorimetric study of early hydration of alkali-slag cements. *Cement and Concrete Research*, 25(6), 1333–1346.
- Shi, C., & Day, R. L. (1996). Some factors affecting early hydration of alkali-slag cements. *Cement and Concrete Research*, 26(3), 439–447.

- Shi, C., Qu, B., & Provis, J. L. (2019). Recent progress in low-carbon binders. *Cement and Concrete Research*, 122, 227–250.
- Shul'ga, N. V., Krut'ko, N. P., & Martynov, V. A. (2010). Complexation in aqueous solutions of lignosulfonates. *Russian Journal of Applied Chemistry*, 83(5), 906–910.
- Silverstein, R. M., Webster, F. X., & Kiemle, D. J. (2005). *Spectrometric Identification of Organic Compounds* (Seventh Edition). John Wiley & Sons, Inc.
- Stark, N. M., Yelle, D. J., & Agarwal, U. P. (2016). Techniques for Characterizing Lignin. *Lignin in Polymer Composites*, October, 49–66.
- Sun, Y., Zhang, S., Rahul, A. V., Tao, Y., Van Bockstaele, F., Dewettinck, K., Ye, G., & De Schutter, G. (2022). Rheology of alkali-activated slag pastes: New insight from microstructural investigations by cryo-SEM. *Cement and Concrete Research*, 157, 106806.
- Sun, Z., & Vollpracht, A. (2018). Isothermal calorimetry and in-situ XRD study of the NaOH activated fly ash, metakaolin and slag. *Cement and Concrete Research*, 103, 110–122.
- Tan, Z., Bernal, S. A., & Provis, J. L. (2017). Reproducible mini-slump test procedure for measuring the yield stress of cementitious pastes. *Materials and Structures*, 50(6), 1–12.
- Thomas, R., Ye, H., Radlinska, A., & Peethamparan, S. (2016). Alkali-Activated Slag Cement Concrete. *Concrete International*, 38(1), 33–39.
- Toledo, M. (2007). pH Theory Guide. Mettler Toledo.
- Tong, S., Yuqi, Z., & Qiang, W. (2021). Recent advances in chemical admixtures for improving the workability of alkali-activated slag-based material systems. *Construction and Building Materials*, 272, 121647.
- Uchikawa, H., Hanehara, S., & Sawaki, D. (1997). The role of steric repulsive force in the dispersion of cement particles in fresh paste prepared with organic admixture. *Cement and Concrete Research*, 27(1), 37–50.
- Uchikawa, H., Hanehara, S., Shirasaka, T., & Sawaki, D. (1992). Effect of admixture on hydration of cement, adsorptive behavior of admixture and fluidity and setting of fresh cement paste. *Cement and Concrete Research*, 22(6), 1115–1129.
- Uchikawa, H., Sawaki, D., & Hanehara, S. (1995). Influence of kind and added timing of organic admixture on the composition, structure and property of fresh cement paste. *Cement and Concrete Research*, 25(2), 353–364.
- Vainio, U., Lauten, R. A., Haas, S., Svedström, K., Veiga, L. S. I., Hoell, A., & Serimaa, R. (2012). Distribution of counterions around lignosulfonate macromolecules in different polar solvent mixtures. *Langmuir*, 28(5), 2465–2475.
- Viallis-Terrisse, H., Nonat, A., & Petit, J. C. (2001). Zeta-potential study of calcium silicate hydrates interacting with alkaline cations. *Journal of Colloid and Interface Science*, 244(1), 58–65.
- Vikan, H., Justnes, H., Winnefeld, F., & Figi, R. (2007). Correlating cement characteristics with rheology of paste. *Cement and Concrete Research*, 37(11), 1502–1511.
- Vyšvařil, M., Vejmelková, E., & Rovnaníková, P. (2018). Rheological and mechanical properties of alkali-activated brick powder based pastes: Effect of amount of alkali

- activator. *IOP Conference Series: Materials Science and Engineering*, 379(1).
- Walkley, B., Geddes, D. A., Matsuda, T., & Provis, J. L. (2022). Reversible Adsorption of Polycarboxylates on Silica Fume in high pH, High Ionic Strength Environments for Control of Concrete Fluidity. *Langmuir*, 38(5), 1662–1671.
- Wang, C., Kayali, O., & Liow, J. L. (2021). The effectiveness and mechanisms of superplasticisers in dispersing class F fly ash pastes. *Powder Technology*, 392, 81–92.
- Wang, S. D., Pu, X. C., Scrivener, K. L., & Pratt, P. L. (1995). Alkali-activated slag cement and concrete: A review of properties and problems. *Advances in Cement Research*, 7(27), 93–102.
- Wang, S. D., & Scrivener, K. L. (1995). Hydration products of alkali activated slag cement. *Cement and Concrete Research*, 25(3), 561–571.
- Wang, S., Scrivener, K. L., & Pratt, P. L. (1994). Factors affecting the strength of alkali-activated slag. *Cement and Concrete Research*, 24(6), 1033–1043.
- Wang, W., Zheng, B., Feng, Z., Deng, Z., & Fu, L. (2012). Adsorption of polycarboxylate-based superplasticizer onto natural bentonite. *Journal of Advanced Concrete Technology*, 10(10), 323–331.
- Winnefeld, F., Haha, M. Ben, Le Saout, G., Costoya, M., Ko, S.-C., & Lothenbach, B. (2015). Influence of slag composition on the hydration of alkali-activated slags. *Journal of Sustainable Cement-Based Materials*, 4(2), 85–100.
- Wren, A., Laffir, F., Mellot, N., & Towler, M. (2011). X-Ray Photoelectron Spectroscopy (J. M. Wagner (ed.)). *Nova Science Publishers, Incorporated*.
- Xie, J., & Kayali, O. (2016). Effect of superplasticiser on workability enhancement of Class F and Class C fly ash-based geopolymers. *Construction and Building Materials*, 122, 36–42.
- Yan, M., Yang, D., Deng, Y., Chen, P., Zhou, H., & Qiu, X. (2010). Colloids and Surfaces A : Physicochemical and Engineering Aspects Influence of pH on the behavior of lignosulfonate macromolecules in aqueous solution. *Colloids and Surfaces A: Physicochemical and Engineering Aspects*, 371(1–3), 50–58.
- Yan, Q., Li, J., Zhang, J., & Cai, Z. (2018). Thermal decomposition of Kraft lignin under gas atmospheres of argon, hydrogen, and carbon dioxide. *Polymers*, 10(7).
- Yang, D., Li, H., Qin, Y., Zhong, R., Bai, M., & Qiu, X. Q. (2015). Structure and Properties of Sodium Lignosulfonate with Different Molecular Weight Used as Dye Dispersant. *Journal of Dispersion Science and Technology*, 36(4), 532–539.
- Yilmaz, V. T., Odabaoğlu, M., İçbudak, H., & Ölmez, H. (1993). The degradation of cement superplasticizers in a high alkaline solution. *Cement and Concrete Research*, 23(1), 152–156.
- Yoshioka, K., Tazawa, E. I., Kawai, K., & Enohata, T. (2002). Adsorption characteristics of superplasticizers on cement component minerals. *Cement and Concrete Research*, 32(10), 1507–1513.
- Young, J. F. (1972). A review of the mechanisms of set-retardation in portland cement pastes containing organic admixtures. *Cement and Concrete Research*, 2(4), 415–433.

Yousuf, M., Mollah, A., Palta, P., Hess, T. R., Vempati, R. K., & Cocks, D. L. (1995). Chemical and physical effects of sodium lignosulfonate superplasticizer on the hydration of portland cement and solidification/stabilization consequences. *Cement and Concrete Research*, 25(3), 671–682.